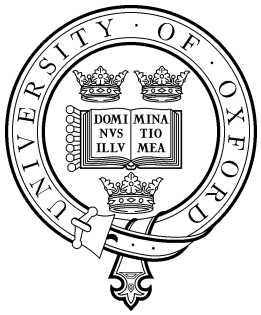
In Vivo Assessment of Substrate Utilisation in the Hypertrophied Heart; The Role of Glycolysis and Glucose Oxidation in Hypertrophic Progression

Submitted for the Degree of Doctor of Philosophy

Trinity Term 2016



Lucia F Giles

Department of Physiology, Anatomy and Genetics

Wadham College

University of Oxford

Supervisors:

Prof Damian Tyler

Prof Carolyn Carr

Dr Lisa Heather

Acknowledgements

I would like to thank everybody who has helped and supported me over the last 5 years, of which there are so many. Firstly, I would like to start by thanking my supervisors, Damian, Carolyn and Lisa. I would like thank Damian for giving me this opportunity at a time where I could only dream of having it and for his continued support over the last 5 years. I'd like to thank Carolyn for all the surgery which has been presented in this work (and there is a lot of it) but mostly all the great fun we had doing it and her unwavering support across the board. I'd like to thank Lisa for her continual support and interest throughout my time here, in particular for hanging a batch of hearts when I was injured. It was above and beyond. My thanks also Kieran for the opportunity to work here, her support and her love of the Archers and Professor David Greaves and the British Heart Foundation for my funding.

There are a range of people across the years who I have had the honour to work with. I would like to thank Lucy, Arne, Lydia, Angus, Jack, Andy, Rhys, Sophia, Filippo (my breakfast buddy), Beth, Kate, Latt, Luz, Dragana, Matt, Kerstin, Sophie and everybody in CMRG. The many dinners with Lucy, Arne and Roly is what I will remember of being a DPhil student and I will always think that breadsticks and humous as an appetiser is the height of sophistication, but I'm afraid there will be no more homemade humous. In addition, Lucy and Arne have supported me endlessly throughout in every way imaginable and long may the Aperol Spritz live on, that's if anyone other than Lucy can face them. I'd like to thank Jack for all those times he has averted my tears and also for a pretty horrendous hangover the day he invited me to sing in a Gaudy. I'd like to thank Angus for putting up with my incessant wittering about most things and continuously boosting my ego with relation to baking. The same goes for Andy who put up with every single cat story I have. I'd like to thank Sophia for all the trips to Maison Blanc and for inspiring my creativity both through her encouragement and her own art. This section would not have been complete without a mention of a Saturday morning DNP session with Lydia, my favourite being when Lydia turned up with a glass of water, some Olbas oil and a packet of Sudafed. It sums up how supportive you were across the time you were here. I

would also like to thank Nicola and my twin separated at birth, Yvonne, for all the fun, cake, knitting chat and support and I hope that I can remain an honorary occupant of your domain.

I would also like to thank the Gary, Andy, Lee, Kevin, Cathy and the team of porters in the department, who have definitely added a lot of laughs to my years as a DPhil student along with the team at the BSB in particular, Debbie, Carol, Beckie, Courtney, Ben, April and Russell, who have been of huge support and a pleasure to work with. Finally, I would like to thank the team up in Hull, Faisel, Rob, Shubhangi and Chris with whom I had a wonderful time.

Outside of the lab, there are so many people who have supported me over the years. To name just a few; Matthew, who has put up with me as a housemate for the last 3 years and has been endlessly supportive. Chris who has been particularly supportive over the write up period, Henry, who has supported throughout this whole process and Janek, my original breakfast buddy and who has supported me through the last 7 years.

As I come to the end, I would like to thank Vicky, who is the person without whom I could not have completed this. Vicky has seen me through every experiment, every high and every low and there has been an awful lot of fun along the way. I have learnt a huge amount, about a huge amount. Her day to day support has contributed a huge amount to this work and to me. I would also like to thank Anne-Marie, who I think of as a fourth supervisor. I was so lucky that Anne-Marie was on sabbatical when I was first a student in the lab and she is an amazing role model is so many ways. Finally, I would like to thank my parents, Stephen and Francesca, who have been an overwhelming support during my DPhil as they have been throughout my life. They have always inspired me to believe that I could achieve anything I put my mind to and taught me to never give up. Along side that, they have never let me give up, even when I'm sure it would have been a whole lot easier for them. I could not have wished for any more support.

Abstract

The work in this thesis investigates the role of glycolysis and glucose oxidation and the effects of metabolic modulation on the development of left ventricular hypertrophy (LVH) in the abdominal aortic constriction (AC) model.

Hypertrophy was induced via the surgical constriction of the abdominal aorta (AC) and through the combined use of cine MRI and dynamic nuclear polarization (DNP), hypertrophic development and progression was assessed. A 17 % increase in LV mass was observed within the AC group at 4, 9 and 14 weeks post-surgery accompanied by no evidence of functional decline. Increased incorporation into lactate was observed at 4 and 9 weeks post-surgery representative of enhanced glycolytic dependence. Increase glycolytic flux was confirmed in the isolated Langendorff-perfused heart at 10 weeks post-surgery. No metabolic changes were observed *in vivo* at 14 weeks post-surgery accompanied by no change in glycolytic flux in the perfused heart at 18 weeks post-surgery.

Treatment of the AC model with dichloroacetate (DCA; 0.75 g L^{-1}) was associated with an elevation in pyruvate dehydrogenase (PDH) flux as expected. When treatment was given immediately post-surgery, a significant increase in LV mass was observed at 4 (23 %), 9 (27 %) and 14 (24 %) weeks post-surgery accompanied by functional decline at 4 and 9 weeks post-surgery. However, treatment of the AC model with DCA at 5 weeks post-surgery, following the establishment of hypertrophy, was associated with no significant difference in LV mass (12 % increase) at 9 weeks post-surgery, however an elevation in LV mass was still present at 14 weeks post-surgery and no functional decline was observed. Treatment with either a low dose (0.1 mg kg^{-1} day^{-1}) or high dose (1 mg kg^{-1} day^{-1}) of Ramipril at 5 weeks post-surgery, following the development hypertrophy, was associated with a normalisation of LV mass in the treated groups but was not associated with any metabolic changes.

This work clarifies the structural, functional and metabolic changes which occur during hypertrophic development and progression as well as the effects of different metabolic therapies. It highlights the potential of the combined use of DNP and cine MRI to further understand hypertrophic progression in patients and the effects of different therapies.

Contents

1 General Introduction **15**

1.1 Overview 16

1.2 Myocardial Metabolism 17

1.2.1 An Overview of Cardiac Metabolism in the Healthy Heart 17

1.2.2 The Importance of ATP Production in Sustaining Cardiac Output . 17

1.2.3 Myocardial Glucose Metabolism 18

1.2.3.1 A Brief Overview of Glucose Metabolism within the Healthy Heart 18

1.2.3.2 The Regulation of Myocardial Glucose Utilisation 19

1.2.3.3 The Fates of Pyruvate 21

1.2.4 The Regulation of Pyruvate Dehydrogenase 22

1.2.5 Myocardial Fatty Acid Utilisation 23

1.2.5.1 A Brief Overview of Fatty Acid Oxdiation within the Heart 23

1.2.5.2 The Regulation of Fatty Acid Oxidation 24

1.2.6 The Glucose-Fatty Acid Cycle 27

1.3 Hypertrophic Remodelling of the Left Ventricle 28

1.4 Loss of Metabolic Flexibility in the Hypertrophied heart 29

1.4.1 Alterations in Metabolism within the Hypertrophied Heart 29

1.4.2 Metabolic Switching Within the Hypertrophied Heart 30

1.4.3 The Inability of the Heart to Adapt Following the Loss of Metabolic Flexibility 32

1.4.4 Does Metabolism within the Hypertrophied Heart Revert Back to the Foetal Phenotype? . . . 33
1.5 The Use of Magnetic Resonance Imaging to Assess Cardiac Structure and Function . . . 35
1.5.1 A Brief Overview of Nuclear Magnetic Resonance . . . 35
1.5.2 A Brief Overview of Magnetic Resonance Imaging . . . 36
1.5.3 The Cardiac Application of Magnetic Resonance Imaging . . . 37
1.6 The Principles and Application of Dynamic Nuclear Polarization . . . 40
1.6.1 An Overview of the Limitations of Magnetic Resonance Spectroscopy and Imaging . . . 40
1.6.2 A Brief Overview of the Principles of Dynamic Nuclear Polarization 40
1.6.3 The Use of Hyperpolarized Metabolites for Real-Time Metabolic Imaging . . . 42
1.7 Thesis Overview and Aims . . . 45

2 General Methods 47

2.1 Animal Work . . . 48
2.2 Surgical Induction of Left Ventricular Hypertrophy via Abdominal Aortic Constriction . . . 48
2.3 The Use of Cardiac Magnetic Resonance Spectroscopy and Magnetic Resonance Imaging to Assess Cardiac Structure, Function and Metabolism *In Vivo* . . . 49
2.3.1 The Preparation of Animals for Cardiac Magnetic Resonance Spectroscopy and Magnetic Resonance Imaging . . . 49
2.3.2 The Dynamic Nuclear Polarization of [^{13}C]-Labelled Substrates . . 49
2.3.3 The Use of [^{13}C]-Labelled Substrates to Assess Cardiac Metabolism 50
2.3.4 Analysis of ^{13}C Magnetic Resonance Spectroscopy . . . 50
2.3.4.1 Spectral Analysis following Injection of Hyperpolarized [1-13C]Pyruvate . . . 50
2.3.4.2 The Kinetic Model . . . 50

2.3.4.3 Spectral Analysis following Injection of Hyperpolarized [2-^{13}C]Pyruvate . . . 51
2.3.5 The Use of Cine Magnetic Resonance Imaging to Non-Invasively Assess Cardiac Structure and Function *In Vivo* . . . 52
2.3.5.1 Cine Magnetic Resonance Imaging Data Acquisition . . . 52
2.3.5.2 Cine Magnetic Resonance Imaging Data Analysis . . . 52
2.4 Preparation of Dichloroacetate and Ramipril Treatments . . . 53
2.4.1 Preparation and Use of Acute Dichloracetate Treatment . . . 53
2.4.2 Preparation and Use of Chronic Dichloroacetate Treatment . . . 53
2.4.3 Preparation and use of Ramipril Treatment . . . 54
2.5 Radiolabelled Isolated Langendorff Perfusion . . . 54
2.5.1 Preparation of Krebs-Heinseleit Buffer . . . 54
2.5.1.1 The Method of Preparation . . . 54
2.5.1.2 Preparation of 100 mM Palmitate Stock . . . 55
2.5.2 Heart Isolation . . . 55
2.5.3 Assessment of Cardiac Function in the Isolated Langendorff Perfused Heart . . . 55
2.5.4 The Use of Radio-labelled Substrates and Perfusion Protocols . . . 56
2.5.4.1 Assessment of Basal and Insulin-Stimulated Metabolism . 56
2.5.4.2 Assessment of Ischemia Reperfusion Recovery in the Isolated Langendorff Perfused Heart . . . 57
2.5.5 The Measurement of Myocardial Glycolytic Flux . . . 58
2.5.6 The Measurement of Myocardial Fatty Acid Oxidation . . . 59
2.5.7 Measurement of the Rate of Lactate Efflux from the Perfused Heart 59
2.6 Blood Sampling and Plasma Analysis . . . 60
2.7 Tissue Collection . . . 60
2.8 Biochemical Analysis . . . 61
2.8.1 Measurement of Myocardial Glycogen . . . 61
2.8.2 Myocardial Intracellular Lactate Extraction . . . 61

2.9 Statistical Analysis 62
2.9.0.1 Chapter 3 62
2.9.0.2 Chapter 4 62
2.9.0.3 Chapter 5 62
2.9.0.4 Chapter 6 63

3 Structural, Functional and Metabolic Characterisation of Hypertrophic Development following Abdominal Aortic Constriction 64

3.1 Chapter Overview 65
3.2 Introduction 66
3.2.1 An Overview of the Abdominal Aortic Constriction Model 66
3.2.2 Structural and Functional Changes with the Development of Hypertrophy in the Aortic Constriction Model 66
3.2.3 Metabolic Remodelling with the Development of Hypertrophy in the Abdominal Aortic Constriction Model 68
3.2.4 Chapter Aims 69
3.3 Methods 71
3.3.1 Study Overview 71
3.3.2 Animal Work 71
3.3.3 Surgical Induction of Left Ventricular Hypertrophy 72
3.3.4 *In Vivo* Assessment of Cardiac Structure and Function 72
3.3.5 *In vivo* Assessment of Metabolic Parameters using Dynamic Nuclear Polarization 72
3.3.6 *Ex vivo* Assessment of Glycolytic Flux in the Isolated Langendorff Perfused Heart 73
3.3.6.1 The Assessment of Ischemia Reperfusion Recovery in the Hypertrophied Heart 73
3.3.6.2 The Assessment of Basal and Insulin-Stimulated Glycolytic Flux in the Hypertrophied Heart at 18 Weeks Post-Surgery 73

3.3.7 Measurement of the Rate of Lactate Efflux from the Langendorff Perfused Heart . . . 74
3.3.8 Statistical Analysis . . . 74
3.4 Results . . . 75
3.4.1 Structural Remodelling at 4, 9 and 14 Weeks Post-Surgery . . . 75
3.4.2 Functional Remodelling following the Induction of Hypertrophy at 4, 9 and 14 Weeks Post-Surgery . . . 77
3.4.3 Metabolic Adaptation with the Development and Progression of Hypertrophy *in vivo* . . . 81
3.4.4 Alterations in Glycolytic Flux in the Hypertrophied Heart at 10 Weeks Post-Surgery and the Ability of the Hypertrophied Heart to Recover from Ischemia . . . 86
3.4.4.1 Metabolic Changes and Cardiac Function in the Hypertrophied Heart Following Ischemia Reperfusion . . . 86
3.4.4.2 The Ability of the Hypertrophied Heart to Recover from Cardiac Hypertrophy . . . 92
3.4.4.3 Alterations in Glycolytic Flux in the Hypertrophied Heart at 18 Weeks Post-Surgery . . . 96
3.5 Discussion . . . 99
3.5.1 A Summary of Findings . . . 99
3.5.2 The Initial Stages of Hypertrophic Remodelling is Associated with an Enhanced Glycolytic Dependence . . . 100
3.5.3 No Change in Glyolytic Flux is Observed with Stabilisation of Cardiac Hypertrophy . . . 102
3.5.4 Conclusions and Future Perspectives . . . 103

4 The Effects of Acute and Chronic Up-Regulation of Pyruvate Dehydrogenase Activity on Cardiac Metabolism 105

4.1 Chapter Overview . . . 106
4.2 Introduction . . . 107

4.2.1 The Mechanism and Pharmacology of Dichloroacetate 107
4.2.2 The Physiological Effects of Dichloroacetate 108
4.2.3 The Effects of Dichloroacetate Treatment on Metabolism 109
4.2.3.1 The Effects of Dichloroacetate on Glucose Metabolism . . 110
4.2.3.2 The Effects of Dichloroacetate on Fatty Acid Metabolism . 112
4.2.3.3 The Effects of Dichloroacetate on Metabolism 113
4.2.4 Chapter Aims 113
4.3 Methods 115
4.3.1 Study Overview 115
4.3.2 Animal Work 115
4.3.3 Preparation and Administration of Dichloroacetate 116
4.3.3.1 Preparation of Dichloroacetate for Acute Administration . 116
4.3.3.2 Preparation of Dichloroacetate for Chronic Treatment . . 116
4.3.4 *In vivo* Assessment of PDH Flux and Flux into the TCA cycle . . . 116
4.3.5 *Ex vivo* Assessment of Glycolytic Flux and Fatty Acid Oxidation in the Isolated Langendorff Perfused Heart 117
4.3.6 Blood Sampling and Plasma Analysis 118
4.3.7 Biochemical Analysis 118
4.3.7.1 Myocardial Glycogen Content 118
4.3.7.2 Myocardial Intracellular Lactate Content 118
4.3.8 Statistical Analysis 118
4.4 Results 119
4.4.1 The *in vivo* Effects of Acute Dichloroacetate Treatment on Myocardial Metabolism 119
4.4.2 The Effects of Acute Dichloroacetate Treatment on Glycolysis, Lactate Efflux and Fatty Acid Oxidation in the Perfused Heart 121
4.4.3 The Effects of Acute Dichloroacetate Treatment on Cardiac Function in the Perfused Heart 123

4.4.4 The *in vivo* Effects of Chronic Dichloroacetate Treatment on Myocardial Metabolism . . . 125
4.4.5 The Effects of Chronic Dichloroacetate Treatment on Pyruvate Dehydrogenase Flux and TCA Cycle Intermediates . . . 125
4.4.6 The Effects Chronic Dichloroacetate Treatment on Glycolysis, Lactate Efflux and Fatty Acid Oxidation in the Perfused Heart . . . 127
4.4.7 The Effect of Chronic Dichloroacetate Treatment on Cardiac Function in the Perfused Heart . . . 129
4.4.8 The Biochemical Effects of Chronic Dichloroacetate Treatment . . . 131
4.4.9 The Systemic Effects of Chronic Dichloroacetate Treatment . . . 131
4.5 Discussion . . . 134
4.5.1 Summary of Results . . . 134
4.5.2 Dichloroacetate Treatment Alters the Metabolic Profile of the Heart 135
4.5.3 Chronic Dichloroacetate Treatment leads to Long-Term Metabolic Adaptation within the Heart . . . 136
4.5.4 The Mechanism of Dichloroacetate in the Heart . . . 138
4.6 Conclusions and Future Perspectives . . . 140

5 The Effect of Chronic Up-regulation of Pyruvate Dehydrogenase Activity on Hypertrophic Development and Progression 141
5.1 Chapter Overview . . . 142
5.2 Introduction . . . 144
5.2.1 Metabolic Remodelling with the Development of Left Ventricular Hypertrophy - A Brief Overview . . . 144
5.2.2 Metabolic-based Therapies as a Treatment for Hypertrophy and Heart Failure . . . 145
5.2.3 Dichloroacetate as a Treatment for Cardiac Hypertrophy . . . 146
5.2.4 Chapter Aims . . . 147
5.3 Methods . . . 149
5.3.1 Study Overview . . . 149

5.3.2 Animal Work . . . 150
5.3.3 Surgical Induction of Left Ventricular Hypertrophy . . . 150
5.3.4 Dichloroacetate Preparation and Treatment . . . 150
5.3.5 *In Vivo* Assessment of Cardiac Structure and Function . . . 151
5.3.6 *In vivo* Assessment of Metabolic Parameters using Dynamic Nuclear Polarization . . . 151
5.3.7 *Ex vivo* Assessment of Glycolytic Flux in the Isolated Langendorff Perfused Heart . . . 151
5.3.8 Measurement of the Rate of Lactate Efflux from the Langendorff Perfused Heart . . . 152
5.3.9 Statistical Analysis . . . 152
5.4 Results . . . 153
5.4.1 The Effect of Early and Late Dichloroacetate Treatment on Structural Remodelling in the Hypertrophic Heart . . . 153
5.4.2 The Effect of Early and Late Dichloroacetate Treatment on Functional Remodelling in the Hypertrophic Heart . . . 155
5.4.3 The Effect of Early and Late Dichloroacetate Treatment on Myocardial Metabolism *in vivo* . . . 160
5.4.4 The Effect of Early and Late Dichloroacetate Treatment on Myocardial Metabolism in the Langendorff-Perfused Heart . . . 164
5.5 Discussion . . . 168
5.5.1 Summary of Findings . . . 168
5.5.1.1 The Effect of Early Dichloroacetate Treatment on Hypertrophic Function and Progression . . . 168
5.5.1.2 The Effect of Late Dichloroacetate Treatment on Hypertrophic Function and Progression . . . 169
5.5.2 Dichloroacetate Treatment During the Initial Stages of Hypertrophic Remodelling Induces Functional Decline . . . 170

5.5.3 Dichloroacetate Treatment During the Later Stages of Hypertrophic Remodelling May Attenuate Hypertrophy . . . 173
5.5.4 The Effect of Dichloroacetate Treatment has a Differential Effect Dependent on the Stage of Hypertrophy . . . 174
5.6 Conclusions and Future Perspectives . . . 176

6 The Effects of Ramipril Treatment on Myocardial Metabolism 177
6.1 Chapter Overview . . . 178
6.2 Introduction . . . 179
6.2.1 The Renin-Angiotensin-Aldosternone System and its Role in the Development of Cardiac Hypertrophy . . . 179
6.2.1.1 The Classic Renin-Angiotensin-Aldosterone System . . . 179
6.2.1.2 The Alternative Aspects of the Renin-Angiotensin-Aldosterone System . . . 181
6.2.2 The Effects of Ramipril, an Angiotensin-Converting Enzyme Inhibitor 183
6.2.3 The Alternative Routes via which Ramipril May Act to Improve Myocardial Viability during Hypertension and Hypertrophy . . . 185
6.2.3.1 Ramipril Treatment Increases Bradykinin Release Improving Ischemia Reperfusion Recovery . . . 186
6.2.3.2 Ramipril Promotes Calcium Handling within the Hypertrophied Myocardium . . . 186
6.2.4 Chapter Aims . . . 188
6.3 Methods . . . 189
6.3.1 Study Overview . . . 189
6.3.2 Animal Work . . . 190
6.3.3 Surgical Induction of Left Ventricular Hypertrophy . . . 190
6.3.4 Preparation and Administration of Ramipril Treatment . . . 190
6.3.5 *In Vivo* Assessment of Cardiac Structure and Function . . . 191
6.3.6 *In vivo* Assessment of Metabolic Parameters using Dynamic Nuclear Polarization . . . 192

6.3.7 Assessment of Glycolytic Flux and Ischemia Reperfusion Injury the Isolated Langendorff Perfused Heart . . . 192
6.3.8 Blood Sampling and Plasma Analysis . . . 192
6.3.9 Statistical Analysis . . . 193
6.4 Results . . . 194
6.4.1 Characterisation of Hypertrophic Development at 4 Weeks Post-Surgery . . . 194
6.4.2 Metabolic Characterisation of the Heart with the Development of Hypertrophy at 4 Weeks Post-Surgery . . . 195
6.4.3 The Effect of Ramipril Treatment on Hypertrophic Progression . . 197
6.4.4 The Effects of Ramipril Treatment on Myocardial Metabolism . . . 203
6.4.4.1 The Effects of Ramipril Treatment on Glycolytic Flux in the Langendorff-Perfused Heart . . . 207
6.4.5 The Impact of Ramipril Treatment on Ischemia Reperfusion Recovery in the Treated and Untreated Hypertrophied Heart . . . 209
6.4.6 Further Biochemical Analysis . . . 217
6.4.6.1 Plasma Analysis following Ramipril Treatment . . . 217
6.5 Discussion . . . 218
6.5.1 Summary of Findings . . . 218
6.5.2 Ramipril Treatment Induces Hypertrophic Regression Independent of Dosage . . . 219
6.6 Conclusions and Future Perspectives . . . 220

7 General Discussion 221

7.1 A Brief Overview . . . 222
7.2 Metabolic Changes with Hypertrophic Development in the Abdominal Aortic Constriction Model . . . 224
7.3 The Use of Dichloroacetate Treatment and Ramipril Treatment in the Hypertrophied Heart in Elucidating the Role of Metabolism in Hypertrophied Development and Progression . . . 227

7.4 Final Conclusions and Future Perspectives 231

Bibliography **232**

AppendixA *In Vivo* Assessment of Cardiac Metabolism and Function in the Abdominal Aortic Banding Model of Compensated Cardiac Hypertrophy **253**

Abbreviations

α-KG: α-ketoglutarate

AC: aortic constriction

ACE: angiotensin converting enzyme

ACEI: angiotensin converting enzyme inhibitor

ADP: adenosine diphosphate

ALT: alanine aminotransferase

AMP: adenine monophosphate

AMPK: AMP-dependent kinase

Ang: Angiotensin

ATP: adenosine triphosphate

AT-R_1: Angiotensin Receptor 1

AT-R_2: Angiotensin Receptor 2

BSA: bovine serum albumin

Ca^{2+}: calcium ions

CoA: coenzyme A

$CaCl_2$: calcium chloride

CK: creatine kinase

cpm: counts per minute

CPT: carnitine palmitoyl transferase

CO: cardiac output

dH_2O: deionised H_2O

DCA: dichloroacetate

DNP: dynamic nuclear polarization

ECG: electrocardiogram

EDTA: ethylenediaminetetraacetic acid

EDP: end diastolic pressure

EDV: end diastolic volume

EPR: electron paramagnetic resonance

ESP: end systolic pressure

ESV: end systolic volume

ETC: electron transport chain

EtOH: ethanol

F6P: fructose 6-phosphate

F1,6BP: fructose 1,6-bisphosphate

F2,6BP: fructose 2,6-bisphosphate

F2,6BPase: fructose 2,6-bisphosphatase

FA: fatty acid

FAD^+: flavin adenine dinucleotide

FADH: reduced flavin adenine dinucleotide

FAO: fatty acid oxidation

FAT: fatty acid transporter

FLASH: fast low-angle shot

γ: gyromagnetic ratio

GLUT: glucose transporter

HCl: hydrochloric acid

HDL: high density lipoprotein

HK: hexokinase

HR: heart rate

I: nuclear spins

i/c: subcutaneous

i/p: intraperitoneal

KCl: potassium chloride

KH: Krebs-Heinseleit

$\mathbf{KH_2PO_4}$: potassium phosphate

KO: knockout

KOH: potassium hydroxide

LCAD: long-chain fatty acyl dehydrogenase

LDH: lactate dehydrogenase

LDL: low density lipoprotein

LV: left ventricular

LVDP: left ventricular developed pressure

LVH: left ventricular hypertrophy

$\mathbf{MgSO_4}$: magnesium sulphate

MCAD: medium-chain fatty acyl dehydrogenase

MRI: magnetic resonance imaging

MRS: magnetic resonance spectroscopy

mRNA: messenger RNA

NaCl: sodium chloride

$\mathbf{NAD^+}$: nicotinamide adenine dinucleoside

NADH: reduced nicotinamide adenine dinucleoside

$\mathbf{NaHCO_3}$: sodium bicarbonate

NaOH: sodium hydroxide

$\mathbf{NaSO_3}$: sodium sulphate

NEFA: non-esterified fatty acid

NMR: nuclear magnetic resonance

PC: pyruvate carboxylase

PCA: perchloric acid

PCr: phosphocreatine

PDH: pyruvate dehydrogenase

$\mathbf{PDH}_a$: active pyruvate dehydrogenase

$\mathbf{PDH}_b$: total pyruvate dehydrogenase

$\mathbf{PDH}_t$: total pyruvate dehydrogenase

PDK: pyruvate dehydrogenase kinase

PDP: pyruvate dehydrogenase phosphatase

PET: positron emission tomography

PFK: phosphofructokinase

PK: pyruvate kinase

PLB: phospholambin B

PPARα: peroxisome proliferator-activated receptor α

P/O: phosphate-to-oxygen

RAA: renin-angiotensin-aldosterone

RCR: respiratory control ratio

RF: radiofrequency

RPP: rate pressure product

S: electronic spins

SEM: standard error of the mean

siRNA: small interfering RNA

SR: sarcoplasmic reticulum

SV: stroke volume

TAC: thoracic aortic constriction

TAG: triacylglyceride

TCA: tricarboxylic

Chapter 1

General Introduction

1.1 Overview

The development and progression of hypertension-induced left ventricular hypertrophy is underpinned by a number of biochemical and physiological changes. Although hypertrophy is initially a compensatory response to a systemic increase in blood pressure, it eventually leads to functional decline and the onset of heart failure. The factors which underpin this switch from compensation to de-compensation are unknown and are likely to be associated with the remodelling process. One aspect of this remodelling is the change in metabolism that occurs during hypertrophic development, on which this work is focused. This chapter provides an overview of metabolism in the healthy heart as well as in the hypertrophied and failing heart and the ways it can be assessed *in vivo*.

1.2 Myocardial Metabolism

1.2.1 An Overview of Cardiac Metabolism in the Healthy Heart

Fatty acid oxidation contributes approximately 60-90 % of ATP generation within the myocardium with the remaining energy derived from the metabolism of glucose [1]. Endogenous energy stores are limited within the heart, therefore under healthy conditions, myocardial substrate selection is largely dependent on the concentration of circulating metabolites in the plasma [2]. ATP is required by the cardiac muscle to promote contraction of the cardiac muscle, therefore the oxidation of endogenous substrates is directly coupled to maintaining a sufficient cardiac output. Disruption or impairment of substrate availability or selection in the heart is suggested to underpin several major diseases such as diabetes, ischemic heart disease, hypertrophic progression and heart failure [3, 4, 5].

1.2.2 The Importance of ATP Production in Sustaining Cardiac Output

ATP is synthesised in the mitochondria following the oxidation of respiratory substrates, which in the healthy heart are predominately fatty acids [6]. Approximately 60-70 % of the ATP produced is used in myofibrillar contraction and the remaining 30-40 % is required to maintain the myocardial calcium stores via the sarcoplasmic reticulum (SR) Ca^{2+} ATPase [1]. Following synthesis in the mitochondria, the ATP used in contraction requires transportation to the myofibrils. This is facilited by the phosphocreatine (PCr) shuttle which transfers ATP across the mitochondrial membranes, which are otherwise impermeable to ATP, to the myofibrils. This involves the reversible phosphorylation of creatine catalysed by mitochondrial and myofibril isoforms of creatine kinase (CK) as described in Figure 1.1 [7].

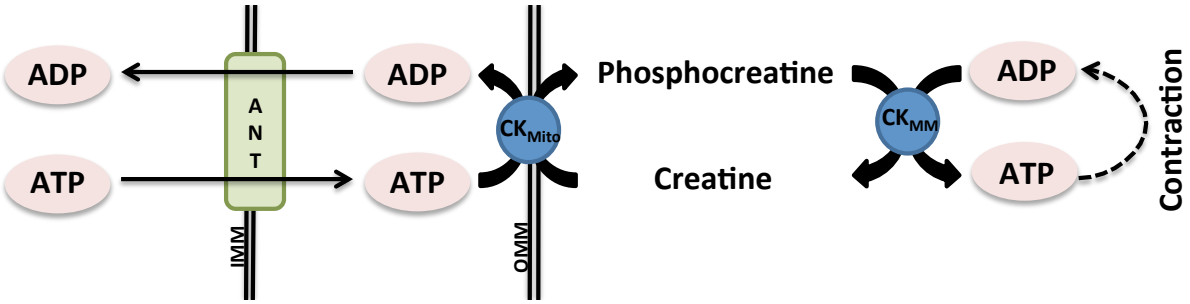


Figure 1.1: The Phosphocreatine Shuttle. ANT: Adenine Nucleotide Transporter; CK_{Mito}: Mitochondiral Creatine Kinase; CK_{MM}: Myofibrillar Creatine Kinase Isozyme; IMM: Inner Mitochondrial Membrane; OMM: Outer Mitochondrial Membrane. Adapted from Neubauer *et al*, 2007 and Sorokina *et al*, 2007. [8, 9]

The availability of creatine both in its phosphorylated and dephosphorylated forms is essential for sustained myocardial contraction and maintenance of the cardiac output [10]. Within the healthy myocardium, approximately only one third of the creatine pool is phosphorylated at any specific point suggesting that the system acts to buffer ATP synthesis and availability ensuring that there is sufficient capacity to maintain cardiac output during periods of high stress when additional ATP is required [8].

A reduction in ATP production is observed in the later stages of heart failure and is estimated to be at most a reduction of 30-40 % [11]. This may occur as a result of disruption within the interfibrillar mitochondria which is associated with hypertrophic development within the cardiomyocyte and is associated with defects in the electron transport chain (ETC), a decreased capacity for oxidative phosphorylation as well as impaired ATP production [12, 13]. Furthermore, a 30-70 % decrease in creatine and PCr is observed in the early stages of heart failure accompanied by a 20 % decrease in CK activity [14]. This may account for energy depletion within the heart which contributes to the decline in cardiac function associated with the later stages of hypertrophy and heart failure [15].

1.2.3 Myocardial Glucose Metabolism

1.2.3.1 A Brief Overview of Glucose Metabolism within the Healthy Heart

In the healthy heart, fatty acids provide approximately 70-90 % of the ATP required to maintain normal cardiac output with the remaining 10-30 % derived from glycolytic

origin [16, 1]. Despite this, glucose provides an invaluable source of energy for myocardial contraction. The metabolic profile of the foetal heart is characteristically glucose dependent and there is an argument that under situations of chronic stress such as sustained hypertension and heart failure, the heart reverts back to the foetal phenotype shifting specifically towards enhanced levels of glycolytic dependence [17, 12, 1, 18, 19]. Fatty acids produce considerably more ATP per mole of carbon consumed making them both more energy dense and efficient as a respiratory fuel, however, given the initial stages of glucose oxidation via glycolysis can occur in the absence of oxygen, glucose is more energy efficient with relation to the number of oxygen molecules consumed [20, 21, 22].

Glycolysis, the pathway through which glucose is metabolised to pyruvate, only produces a limited number of ATP molecules and reducing equivalents in the form of NADH, however, it provides a rapid source of energy under stress conditions such as exercise, chronic hypertension and where oxygen is limiting (Fig 1.2) [1, 23]. The subsequent metabolism of pyruvate to lactate also serves to regenerate the oxidising agent NAD^+ required for sustained glycolytic flux [23].

1.2.3.2 The Regulation of Myocardial Glucose Utilisation

Glycolysis is a tightly regulated pathway controlled at both an allosteric level and globally by the effects of insulin, adrenaline and glucagon (Fig 1.2) [24]. With many reactions shared with the gluconeogenic pathway, the key regulatory steps within glycolysis are non-reversible defining the directionality of the pathway. Hexokinase, phosphofructokinase-1 (PFK-1) and pyruvate kinase (PK) form the key regulatory enzymes within glycolysis with their activity determined largely by allosteric effectors from within the pathway itself (Fig 1.2) [24, 25]. Myocardial hexokinase is inhibited by the product of its reaction, glucose 6-phosphate, self-limiting the concentration of glucose which enters the pathway [23]. Conversely, in the presence of high concentrations of fructose 6-phosphate (F6P), PFK-1 is stimulated by the allosteric effector,fructose 2,6-bisphosphate (F2,6BP). F2,6BP is the alternate product of F6P metabolism catalysed by the bifunctional enzyme, phosphofructokinase-2/fructose 2,6-bisphosphatase (PFK-2/F2,6BP; Fig 1.2) [26].

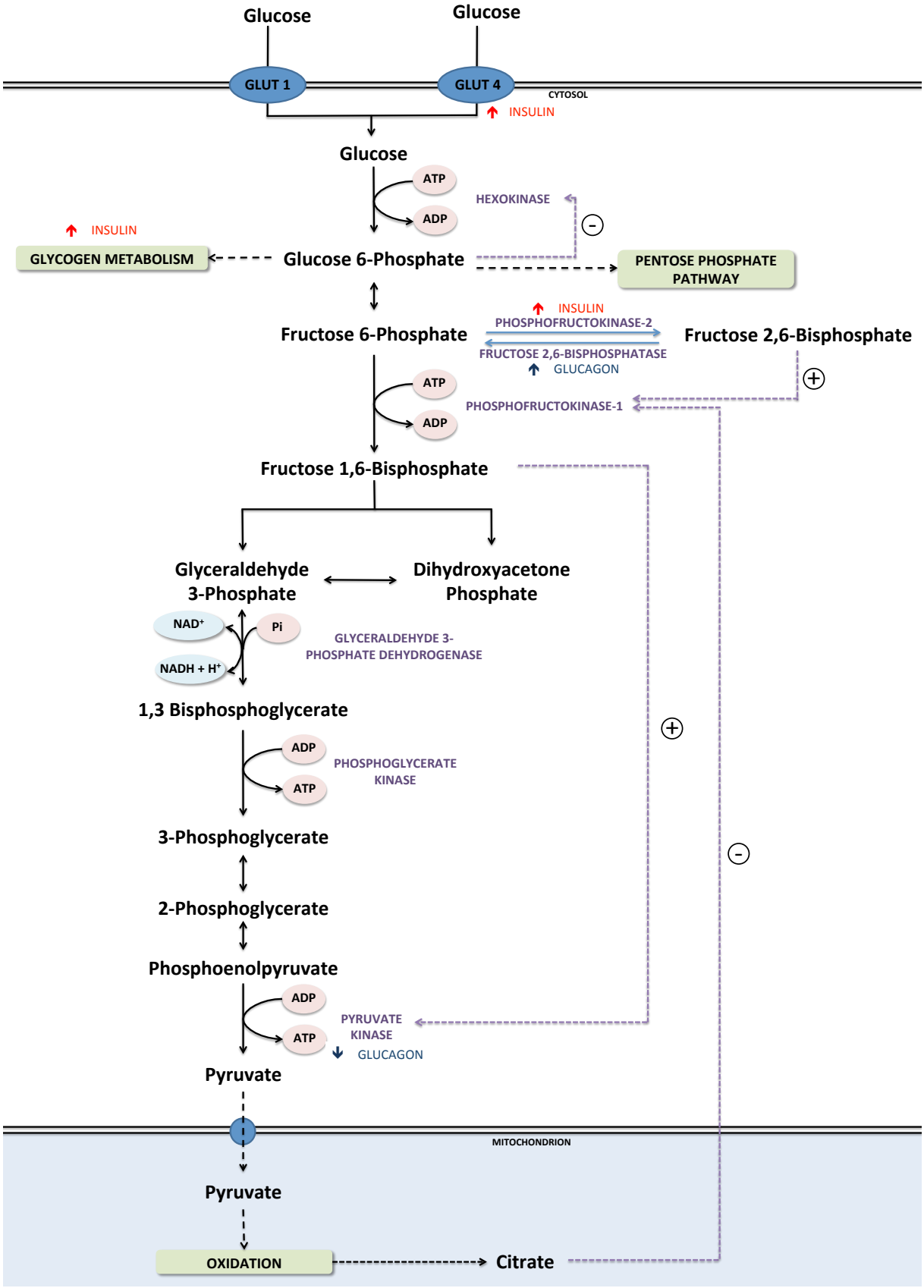


Figure 1.2: Allosteric and Hormonal Regulation of the Glycolytic Pathway

Insulin promotes PFK-2 activity through phosphatase 2A mediated dephosphorylation of the PFK-2/F2,6BPase complex with the simultaneous inhibition of F2,6BPase activity [27]. This signals an abundance of glucose within the system and a subsequent increase in glucose uptake mediated by the insulin-dependent translocation of GLUT4 [28]. Enhanced PFK-2/F2,6BPase promotes the conversion of F6P to F2,6BP by PFK2 directing flux through PFK-1 along the glycolytic pathway [27]. Fructose 1,6-bisphosphate (F1,6BP), the product of the reaction catalysed by PFK-1, also acts as an allosteric activator of PK, which catalyses the final reaction within the glycolytic pathway promoting the formation of pyruvate, the end-product of glycolysis (Fig 1.2) [24, 23].

1.2.3.3 The Fates of Pyruvate

Pyruvate plays a key role within three major metabolic pathways and its metabolism is tightly linked to the energy status of the cell [29, 30]. Pyruvate can undergo three fates; (i) complete oxidation via the tricarboxylic acid (TCA) cycle via pyruvate dehydrogenase (PDH), (ii) reduction to lactate via lactate dehydrogenase (LDH) or (iii) conversion to alanine via alanine aminotransferase (ALT; Fig 1.3) [31]. The flexibility of the metabolic fates of pyruvate is a useful resource within glucose metabolism. Energetically, the complete oxidation of pyruvate is favourable, however, under conditions of high demand such as during exercise or stress, glucose provides a ready source of energy through the partial oxidation during glycolysis. The reduction of pyruvate to lactate via LDH allows regeneration of NAD^+ to facilitate an enhanced rate of glycolytic flux [18]. Furthermore substrate cycling between alanine and pyruvate provides precursors for gluconeogenesis and the link between the cardiac muscle and liver [32].

Alternatively, pyruvate can enter the TCA cycle through carboxylation to oxaloacetate catalysed by the mitochondrial enzyme, pyruvate carboxylase. This anaplerotic mechanism acts to ensure that the pool size of TCA cycle intermediates remains sufficient for the cycle to function effectively. Within the heart, pyruvate carboxylation accounts for approximately 2-6 % of flux into the TCA cycle and acts to replaces intermediates lost to other anaplerotic processes [1].

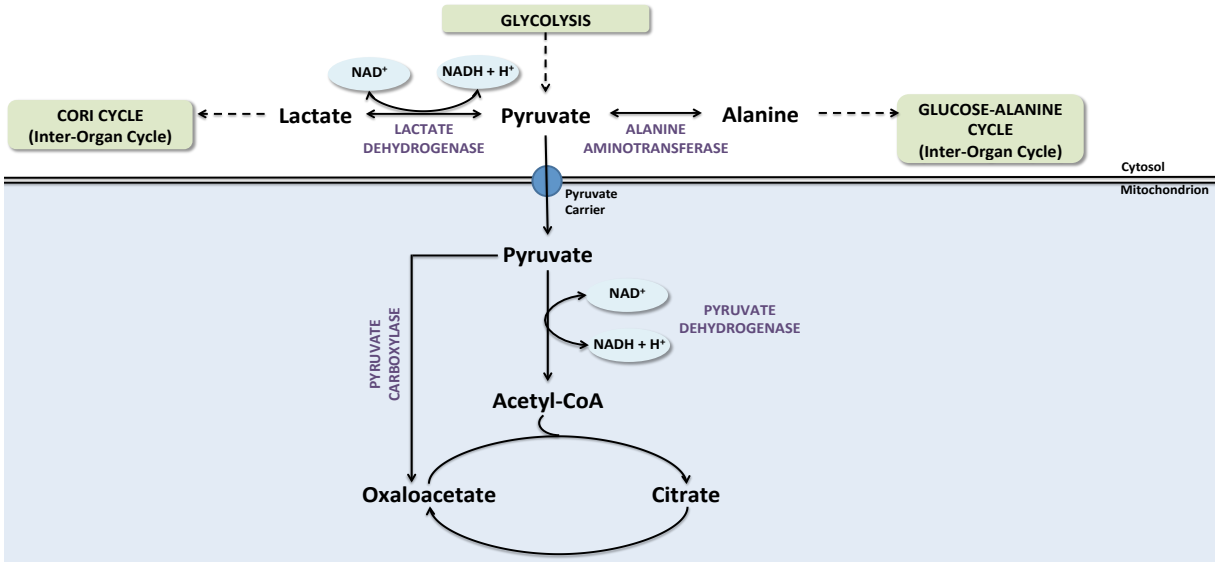


Figure 1.3: The Alternative Fates of Pyruvate Metabolism

1.2.4 The Regulation of Pyruvate Dehydrogenase

Pyruvate dehydrogeanse (PDH) is a tightly regulated multi-enzyme complex located in the mitochondrial matrix, the regulation of which is tightly coupled to the energy state of the cell and provides the link between reciprocal regulation of glucose and fatty acid (FA) oxidation [30]. The complex consists of three enzymes; pyruvate dehydrogenase (E1), which catalyses the decarboxylation of pyruvate; dihydrolipoate acetyl transferase (E2), which catalyses the formation of acetyl-CoA; and dihydrolipoyl dehydrogenase (E3), which catalyses the reduction of NAD^+ to NADH [33].

The E1 complex is reversibly phosphorylated by pyruvate dehydrogenase kinase (PDK), which is bound tightly within the complex suppressing PDH activity. Dephosphorylation and subsequent activation of PDH is catalysed by the mitochondrial phosphatase, pyruvate dehydrogenase phosphatase (PDP) [23]. The relative activities of the cardiac isoforms of the PDH regulatory enzymes, PDP-1 and -2 and PDK-1, -2 and -4, determine the ratio of active PDH (PDH_a) to inactive PDH (PDH_b), and hence the flux through PDH within the heart [33].

High concentrations of ADP and pyruvate suppress PDK-4 activity promoting PDH flux and glucose oxidation via a feed-forward mechanism [34]. Conversely PDK-4 activity is enhanced by elevated concentrations of NADH relative to NAD^+ ([NADH]:[NAD^+])

and acetyl-CoA to coenzyme A (CoA) ([Acetyl-CoA]:[CoA]), acting via end-product inhibition, reducing flux through PDH and promoting flux through fatty acid oxidation [35]. PDP is regulated by calcium (Ca^{2+}) flux within the cell allowing tight coupling between contractile function and PDH flux, without disrupting the balance of regulatory metabolites within the mitochondria [36].

1.2.5 Myocardial Fatty Acid Utilisation

1.2.5.1 A Brief Overview of Fatty Acid Oxdiation within the Heart

Fatty acid oxidation provides the majority (70-90%) of ATP within the healthy heart [1]. Myocardial lipid stores are limited, therefore the majority of fatty acids used in oxidation are obtained from the blood [21]. Oxidation of long-chain fatty acids occurs within the mitochondrial matrix via the β-oxidation pathway. This involves a series of oxidation and hydration reactions followed by the removal of a two-carbon molecule in the form of acetyl-coA. The key enzymes involved in β-oxidation are acyl-CoA dehydrogenase, enoyl-CoA hydratase, L-3 hydroxyacyl CoA and 3-ketoacyl CoA thiolase [21]. NAD^+ and FAD^+ acts as electron acceptors during the oxidation reactions and are reduced to NADH and FADH respectively prior to oxidation within the electron transport chain and the release of ATP. The acetyl-CoA released from fatty acid oxidation subsequently enters the TCA cycle for complete oxidation and the further production of the reduced cofactors; FADH and NADH [1].

The oxidation of fatty acids is far more energy efficient than the oxidation of glucose with one molecule of palmitate generating 103 molecules of ATP compared with 31 molecules of ATP from the complete oxidation of glucose [21]. However, the oxidation of fatty acids requires a higher concentration of oxygen reducing its phosphate-to-oxygen (P/O) ratio relative to glucose [21]. The P/O value of an oxidative substrate determines the amount of ATP produced for each molecule of oxygen consumed by the mitochondria and is one measure of substrate efficiency [37]. Furthermore, glycolysis enables the rapid production of ATP via substrate level phosphorylation in the absence of oxygen. This limits the use of fatty acids under conditions of high demand and the rapid acquisition of

ATP via the glycolytic pathway is favoured. The oxidation of fatty acids appears to play a role in maintaining sustained cardiac function and long term shifts in the balance between fatty acid oxidation and glucose utilisation are thought to underpin cardiac dysfunction in the hypertrophied, diabetic and ischemic heart.

1.2.5.2 The Regulation of Fatty Acid Oxidation

An overview of the regulation of fatty acid oxidation, synthesis and storage is summarised in Figure 1.4. The rate of fatty acid oxidation is largely dependent on the availability of fatty acids for oxidation. In the heart this is determined by both fatty uptake into the cell and uptake of fatty acids into the mitochondrion for oxidation [38]. Given myocardial lipid stores are limited, the uptake of fatty acids into the cardiomyocytes is determined by the activity of the fatty acid transporters and the circulating levels of fatty acids. CD36/fatty acid translocase (FAT), one of the main fatty acid transporters within the heart, is regulated by insulin, promoting fatty acid uptake into the heart within the post-priandial state (Fig 1.4) [39]. Secondary to uptake into the cell, fatty acids which are committed to oxidation require transport into the mitochondrion. The β-oxidation pathway is compartmentalised within the mitochondria meaning the uptake of free fatty acids into the mitochondrion provides one of the main regulatory steps within fatty acid metabolism (Fig 1.4)

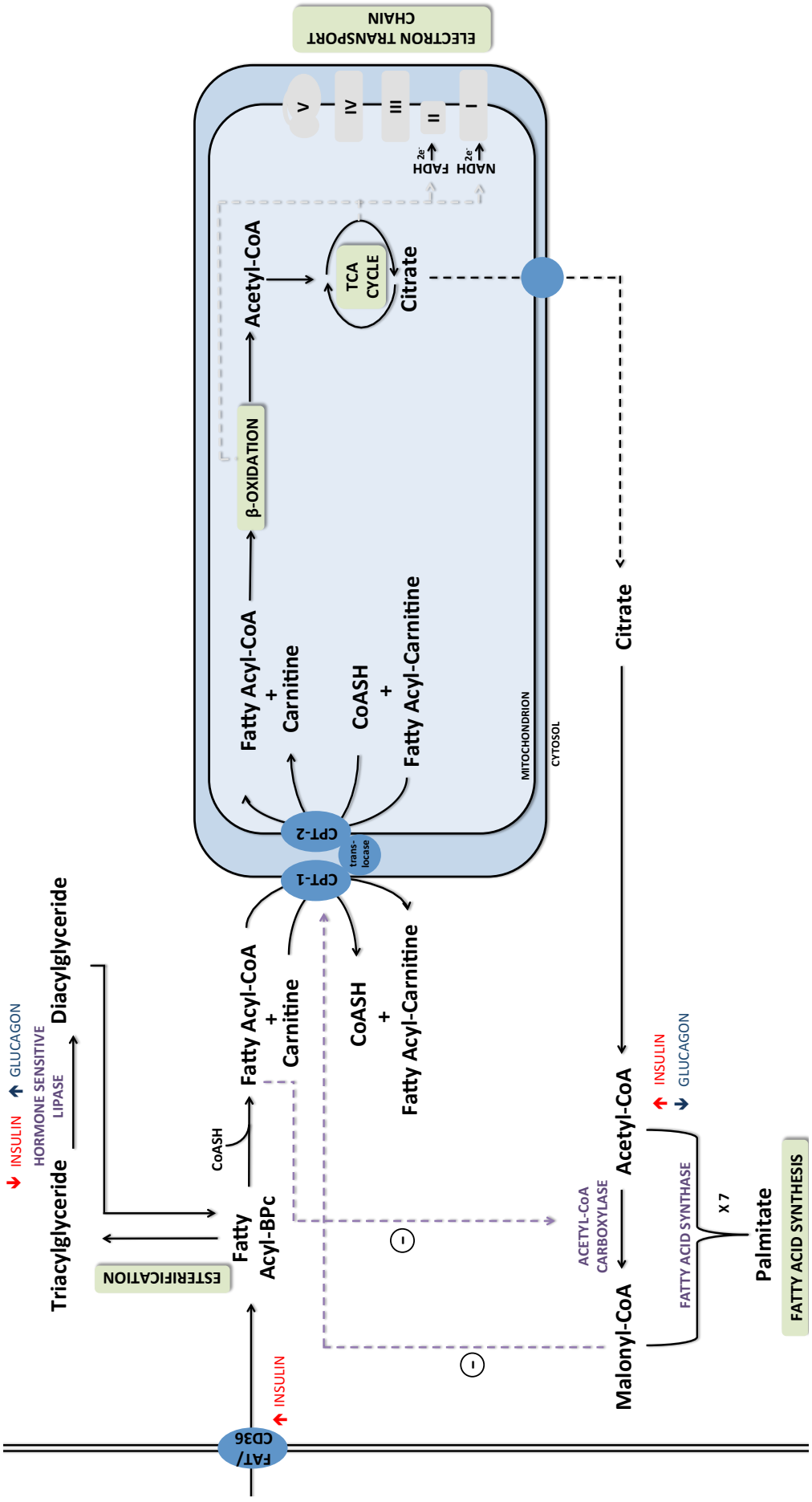


Figure 1.4: The Regulation of Fatty Acid Oxidation

Carnitine palmitoyl transferase (CPT)-1, located on the inside of the outer mitochondiral membrane, is responsible for the initial uptake of the fatty acid across the outer mitochondrial membrane [40]. On uptake into the cell, free fatty acids are conjugated with Coenzyme A (CoA) to form fatty acyl-CoA. The fatty acid moiety is subsequently transferred to carnitine by CPT-1 to form fatty acyl-carnitine suitable for transfer across the inter-mitochondrial membrane cavity via carnitine:acylcarntine translocase and the inner mitochondrial membrane by CPT-2. CPT-2 subsequently catalyses the transfer of the fatty acid moiety to CoA to re-form fatty acyl-CoA for subsequent oxidation via the β oxdiation pathway (Fig 1.4) [38]. The enzymes involved in β-oxidation are sensitive to the energy status within the mitochondrion. Both acyl-CoA dehydrogenase and L3-hydroxyacyl CoA are affected by the relative concentrations of NAD^+ to NADH and FAD^+ to FADH and 3-ketoacyl-CoA thiolase is regulated by the relative concentrations of mitochondrial acetyl-CoA to CoA [21].

The availability of fatty acids, which are largely derived from the circulating plasma is also a limiting factor in fatty acid oxidation, as are the levels of carnitine under conditions of high fatty acid oxidation [21, 41]. Reduced carnitine levels have also been implicated in the decline in cardiac function associated with hypertrophic development [42]. CPT-1 is inhibited by L-carnitine and also inhibited by malonyl-CoA, which is the product of the first committed step of fatty acid sythesis preventing the simultaneous oxidation and synthesis of fatty acids and formation of a futile cycle [23, 40]. Via a reciprocal mechanism, palmitoyl-CoA inhibits acetyl-CoA carboxylase (ACC), the key regulatory enzyme in fatty acid synthesis of which there are two isoforms [21]. Through this mechanism fatty acid oxidation is indirectly regulated via glucagon and insulin [21].

Both isoforms of ACC catalyse the conversion of acetyl-CoA to malonyl-CoA however, the malonyl-CoA produced by ACC-1 is committed to fatty acid synthesis whilst ACC-2, which is located in the mitochondrial membrane, produces a distinct pool of malonyl-CoA which is involved in the regulation of CPT-1. ACC-1 is expressed across most tissues, whereas ACC-2 is highly expressed in the heart and skeletal muscle. [43]. Glucagon inhibits the activity of both acetyl-CoA carboxylase isoforms via the activation of AMP-

dependent kinase (AMPK), reducing fatty acid synthesis and the synthesis of malonyl-CoA promoting fatty acid uptake and oxidation [44, 22, 43]. However, insulin promotes fatty acid synthesis via activation of acetyl-CoA carboxylase with the subsequent increase in malonyl-CoA levels, increased inhibition of CPT-1 and the reduction of uptake of fatty acids into the mitochondrion for oxidation [45]. Interestingly, although this mechanism occurs both in the heart and the liver, the specificity of these tissue-specific isoforms of CPT-1 for malonyl-CoA are in the region of 10-fold less than is present in other organs suggesting that this mechanism acts less acutely within the heart than in other organs [44].

1.2.6 The Glucose-Fatty Acid Cycle

The glucose-fatty acid cycle (or Randle Cycle) was first described by Randle in 1963 as the mechanism by which circulating concentrations of fatty acids and glucose are maintained at homeostatic levels [6]. The glucose-fatty acid cycle operates at an inter-organ level and is an important mechanism in ensuring metabolic homoeostasis mediated by the liver. At both the organ and cellular level, pyruvate dehydrogenase (PDH) plays an important role in mediating the relative oxidation of glucose and fatty acids. As previously described in Chapter 1.2.4, flux through PDH is reduced under high concentrations of acetyl-CoA, which is both the product of the metabolism of pyruvate by PDH and the end product of the β-oxidation pathway [35]. Conversely, PDH is up-regulated by high concentrations of pyruvate, signalling high levels of glycolytic flux. This acts to reduce flux through the glycolytic pathway when fatty acid oxidation is elevated but promotes glycolytic flux when levels of fatty acid oxidation are reduced. This ensures an appropriate balance between glucose and fatty acid oxidation at the cellular level [46]. Furthermore, the alternative metabolism of pyruvate into lactate and alanine which can be released from the cell into the circulation for inter-organ consumption means that the activity of PDH plays an integral role in maintaining metabolic homoeostasis [6].

1.3 Hypertrophic Remodelling of the Left Ventricle

Left ventricular hypertrophy (LVH) is an independent risk factor in the development of heart failure [4]. Despite acting as an initially compensatory response to normalise ventricular pressure and wall tension in response to a chronic increase in systemic blood pressure, sustained stress eventually becomes detrimental leading to cardiomyocyte disruption and heart failure [47, 8, 48, 49].

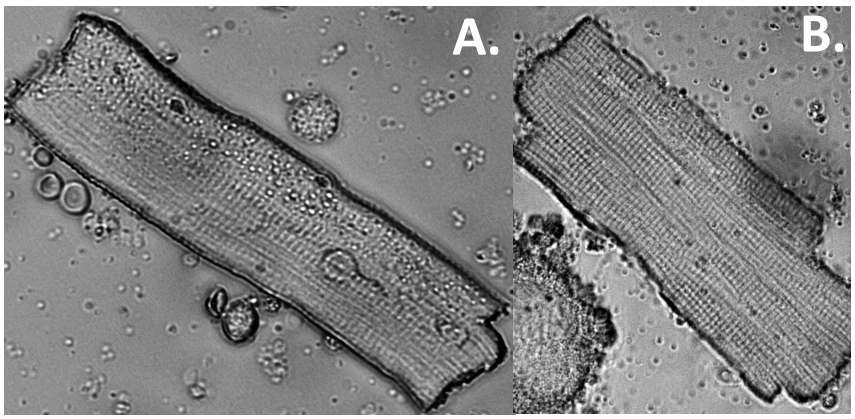


Figure 1.5: Isolated Cardiomyocytes. A. A Normal Cardiomyocyte. B. A Hypertrophied Cardiomyocyte Isolated from the Abdominal Aortic Constriction Model of Left Ventricular Hypertrophy. *Courtesy of Dr Anne-Marie Seymour.*

A sustained increase in blood pressure acts as a bio-mechanical stimulus leading to the release of a cascade of signalling molecules including hormones, cytokines, and growth factors which stimulate myocardial reorganisation and growth [48]. Pathological hypertrophy is characterised by an increase in myocardial width relative to length where sarcomeres are added in parallel leading to widening of the cell compared to physiological hypertrophy where the sarcomeres are added in succession increasing the length relative to width as shown in Figure 1.5 [48, 47]. Compared with physiological hypertrophy where the addition of sarcomeres in series increases the tensor strength of the cell, the parallel addition of sarcomeres and expansion of the extracellular matrix results in cellular disruption specifically localised to the interfibrillar mitochondria with associated defects in the electron transport chain (ETC), decreased oxidative phosphorylation and impaired ATP production with evidence of cellular death via both apoptosis and necrosis [47, 1, 12]. This may provide some insight into why a mechanism, which is initially compensatory, is

such a high risk factor in the development of heart failure.

1.4 Loss of Metabolic Flexibility in the Hypertrophied heart

1.4.1 Alterations in Metabolism within the Hypertrophied Heart

Changes in metabolism are concomitant with the development of hypertrophy. However, due to the stage-specific nature of hypertrophic progression combined with the limitations in the way in which we study hypertrophic development and progression, the changes which occur during hypertrophic remodelling are in general, poorly characterised and often conflicting [42].

A switch from predominatly fatty acid oxidation to enhanced glucose utilisation with the development of hypertrophy is well characterised and is particularly evident in the early stages of hypertrophy [1, 42, 4, 50, 51]. The driving force for this switch remains unknown as does its impact on the heart as hypertrophy progresses. It has been proposed that it is this switch in metabolism which underpins energy depletion in the heart. Glycolysis is substantially less energetically favourable than fatty acid oxidation and cardiac glycogen stores are limited, potentially leading to energy depletion within the myocardium [15]. However, whether the hypertrophied myocardium is associated with energy depletion remains unclear. Neubauer *et al* identified that the ratio of PCr to ATP can be used as a predictor of mortality in patients with dilated cardiomyopathy [11, 51]. This has been mirrored in animal models but measurement of the PCr:ATP ratio is limited within animal models due to the low signal to noise ratio associated with *in vivo* spectroscopy and the rapid hydrolysis of ATP within isolated tissue *post-mortem* [51]. This may account for the differing reports on the energy status of the myocardium from different animal models of left ventricular hypertrophy. Interestingly, Doenst *et al* identified a reduction in the ratio of cardiac power to ATP from the initial stages of hypertrophic development in the thoracic aortic constriction (TAC) model of LVH. In conjunction with the identification of a reduction in both fatty acid oxidation and glucose oxidation with the development

of hypertrophy, this suggests that the impairment in substrate utilisation is associated with a reduction in the ability of the heart to maintain a sustained output. Although this correlation did exist in the work presented by Doenst *et al*, they saw no reduction in mitochondrial oxidation capacity until functional impairment was observed [52]. This supports a role of impaired substrate selection in the development of hypertrophy and although these findings are interesting, it should also be noted that the TAC model is an accelerated and aggressive model of LVH limiting its physiological relevance [53]. However, it may still represent changes within the hypertrophied heart which occur at the later stages of the remodelling process.

1.4.2 Metabolic Switching Within the Hypertrophied Heart

The driving force behind the switch towards enhanced glycolysis and reduced fatty acid oxidation in the hypertrophied heart is unknown. One theory is that the increase in glycolysis is driven by the pressure-induced increase in demand associated with hypertension and a reduction in fatty acid oxidation comes as a secondary mechanism according to the glucose-fatty acid (Randle) cycle [51, 6]. However, work presented by Doenst *et al* reports a depression in both fatty acid oxidation and glucose oxidation in the hypertrophied mouse heart isolated from the thoracic aortic constriction (TAC) model of left ventricular hypertrophy (LVH) [52]. This is interesting as work by Seymour *et al in vivo* demonstrate an increased glycolytic dependence but no change in glucose oxidation suggesting an uncoupling between glycolysis and glucose oxidation in the abdominal aortic constriction model (AC) of LVH [50]. This is supported by work by Pereira *et al* in the more severe TAC mouse model [54]. In the light of these studies, it seems unlikely that the reduction in fatty acid oxidation observed is driven by the shift towards increased glucose utilisation via the glucose-fatty acid cycle alone.

One suggestion for impaired fatty acid utilisation is a reduction in carnitine which has been observed within the hypertrophied heart and is largely dependent on the stage and severity of hypertrophy [42]. Carnitine is required for the successful transport of fatty acids

into the mitochondria for oxidation [21]. Work by Broderick *et al* suggests that the role of carnitine has an indirect effect on glucose metabolism. In hearts perfused in the presence of glucose and palmitate, the presence of palmitate results in reduced glucose oxidation, whereas when perfused with glucose, fatty acids and carnitine, this depression in glucose oxidation was not observed. Broderick *et al* suggest that this occurs due to an enhanced capacity for the transfer of acetyl groups from CoA to carnitine following glycolysis [55]. The role of carnitine as an acceptor of acetyl groups within the mitochondrion prevents the accumulation of acetyl-CoA during high rates of substrate oxidation and the subsequent inhibition of pyruvate dehydrogenase (PDH) which may account for the enhanced glucose oxidation observed in the absence of fatty acid oxidation [56]. It could be suggested that a reduction in carnitine levels may account for the depression in both glucose and fatty acid oxidation observed. This is supported by work by Schonekess *et al*, which reported an increase in glucose oxidation within the hypertrophied heart when perfused with carnitine. The hearts, which were isolated from the rats at 8 weeks following abdominal aortic constriction (AC) surgery, exhibited enhanced glycolytic rates which were unchanged in the presence of carnitine, but glucose oxidation was promoted [57].

In terms of the role of the glucose-fatty acid cycle in the development of hypertrophy and heart failure, the hypertrophied heart is associated with enhanced glycolysis represented by increased lactate production but no change in PDH. Therefore, it appears unlikely that the metabolic profile associated with the AC model is driven purely by either the glucose-fatty acid cycle or carnitine. Mitochondrial disruption may also play a role in impaired substrate utilisation as both long-chain fatty acid oxidation and the final stages of glucose oxidation occur within the mitochondrial matrix [8, 58]. In addition, disruption of the mitochondria is associated with impaired calcium handling and poor cardiac function [59].

1.4.3 The Inability of the Heart to Adapt Following the Loss of Metabolic Flexibility

Metabolic flexibility is key to sustained cardiac function. Under normal conditions, the heart only produces ATP at between 15-35 % of its oxidative capacity compared with 80-90 % during maximum exertion [1]. The ability of the heart to compensate for such a large change in function is dependent on being able to switch from one substrate to another [20]. Under stress situations, the heart favours glucose utilisation due to the rapid acquisition of ATP via the glycolytic pathway [16, 23] which is perhaps why glucose is favoured during hypertrophy and heart failure. A sustained glycolytic dependence within the heart may impair the ability of the heart to compensate for a change in functional demand. However, work conducted by Allard *et al* in the perfused heart identified a 47 % reduction in fatty acid oxidation in the hypertrophied heart accompanied by a 12 % increase in glycolytic flux when compaired with the Sham group at a low work load. Following the induction of a high work load, fatty acid oxidation was normalised in the hypertrophied heart and glycolysis was accelarated in the Sham hearts to the levels seen in the hypertrophied hearts suggesting that the hypertrophied heart was still able to meet the increased functional demands [42]. The hypertrophied hearts within this study were isolated from rats at 8 weeks following abdominal aortic constriction (AC) surgery. The AC model is a slow-onset model of hypertrophy therefore this evidence may represent a phase of hypertrophy during which the heart is still able to cope with an increase in demand [19].

The foetal heart also favours glycolysis as a substrate presumably to allow rapid growth [12, 18]. Within the foetal heart, high glycolytic dependence is supported by the activity of the malate/aspartate and α-glycerophosphate shuttles, which is a mechanism by which NAD^+ is regenerated ensuring the high level of glycolytic flux demanded can be sustained [60]. However, work by Rupert *et al* identified that neither the malate/aspartate or α-glycerophosphate shuttle are re-activated within the hypertrophied myocardium [18]. However, the absence of a mechanism to cope with a sustained elevation in glycolytic flux, may be a contributing factor to the finite benefits of hypertrophic development.

1.4.4 Does Metabolism within the Hypertrophied Heart Revert Back to the Foetal Phenotype?

In conjunction with enhanced glycolytic flux, an elevation in GLUT 1 levels have been observed within the hypertrophied heart and are proposed to aid cardiac adaptation during hypertrophy [21, 54]. Enhanced GLUT 1 levels are also observed within the foetal myocardial metabolic profile supporting a reversion to the foetal profile within the hypertrophied heart [54]. However, studies in GLUT 1 KO mice identified no enhanced onset of heart failure in mice which had undergone thoracic aortic constrition (TAC). Interestingly, following the knockout of GLUT 1, Periria *et al* observed a compensatory increase in fatty acid oxidation. This was not sufficient to prevent mitochondrial dysfunction or hypertrophic remodelling, however, it may have compensated for the loss of GLUT 1 [54]. Based on this study, the role of GLUT 1 in the onset of hypertrophic progression remains unclear. However, studies conducted in mice with a cardiac specific GLUT 4 KO experienced cardiac hypertrophy with compensated function and, death was accelerated within the KO hearts where the ability of the heart to deal with an increased workload was reduced. Interesting, GLUT1 expression was increased 3-fold within the heart following the GLUT4 KO and the serum composition remained the same [61]. However, the absence of insulin-stimulated glucose uptake suggests that GLUT 4 plays a role in the development of cardiac hypertrophy. Interestingly, in the later stages of hypertrophy, during the transition to heart failure, a reduction in GLUT1 and GLUT 4 mRNA levels has been observed in patients [62]. Although mRNA levels are not fully conclusive, it suggests that glucose transport plays a role in the development of heart failure. Furthermore, it supports that the metabolic profile of the heart differs during hypertrophy and heart failure.

Peroxisome proliferator-activated receptor α (PPARα) is also proposed to play a role in the development of heart failure. The α- isoform of the peroxisome proliferator-activated receptor is expressed specifically within the heart and liver and has been shown to have a differential effect on hypertrophic development. Furthermore, alteration in PPARα has been linked to the foetal metabolic profile [21]. As a transcription factor, PPARα regulates the expression of regulatory enzymes and transporters associated with fatty acid uptake

and oxidation including, CD36/FAT, carnitine palmitoyl transferase-1 (CPT-1) as well as medium chain and long chain fatty acyl dehydrogenase (MCAD and LCAD) as well pyruvate dehydrogenase kinase (PDK)-2 and -4 [1, 63]. Akki *et al* identified a reduction in palmitate oxidation within the Langendorff-perfused heart at 9 weeks post-abdominal aortic constriction (AC) surgery accompanied by a reduction in PPARα suggesting that the transcription factor may play a role in substrate switching within the hypertrophied heart. Interestingly, this was accompanied by no change in PDH flux *in vitro* which was later supported by further *in vivo* work by Seymour *et al* [64, 50]. Furthermore, Seymour *et al* reported no change in levels of PDK-4 which is inconsistent with a reduction in PPARα [50]. Conversely, Degens *et al* identified no change in fatty acid oxidation or the associated enzymes within the AC model, however, this was in hearts isolated at 4 weeks post-surgery, which is earlier than the changes reported by Akki *et al* [65].

It is likely that a number of aspects, expanding beyond metabolism, contribute to the transition from compensatory hypertrophy to heart failure. In terms of metabolism, the conflicting evidence with relation to what underpins this switch from fatty acid oxidation to enhanced glucose utilisation suggests that metabolism within the heart lies under the Goldilocks principle where any alterations outside the "normal" metabolic constraints has a detrimental effect in the longer term. Many of these studies have been conducted on whole hearts, tissue, and cells isolated from models of hypertrophy, however, the difficulty in clarifying the stage of hypertrophy adds ambiguity to the work produced. The use of *in vivo* techniques such as cardiac magnetic resonance imaging (MRI) and the novel technique of dynamic nuclear polarisation (DNP) allows more sensitive clarification of hypertrophic progression. In addition, both techniques are associated with minimal invasion lending themselves to longitudinal studies where the development and progression of hypertrophy can be clarified over time.

1.5 The Use of Magnetic Resonance Imaging to Assess Cardiac Structure and Function

1.5.1 A Brief Overview of Nuclear Magnetic Resonance

The principle of nuclear magnetic resonance (NMR) is dependent on individual nuclei within a system or material possessing spin, examples include ^{13}C, ^{31}P, ^{23}Na and ^{1}H [66, 67]. The spin of a nuclei, such as a proton is considered a quantum mechanic phenomenon related to its intrinsic angular momentum and in combination with charge, the atom exhibits a magnetic property similar to that of a small bar magnet [66]. An individual nucleus is characterised by its gyromagnetic ratio (γ) which is the ratio of its angular momentum, which can be defined as the ability of the proton to continue along its path of rotation if otherwise undisturbed, to its molecular momentum [66]. If the proton is subsequently placed within a magnetic field, B_0, the atom aligns along the direction of the field and its altered processional frequency is defined by the Larmour Frequency, the product of the gyromagnetic ratio and the magnetic field as described in equation 1.1 [67, 66].

$$\omega = \gamma B_0 \tag{1.1}$$

Physiologically relevant isotopes such as ^{1}H, ^{13}C, ^{31}P and ^{23}Na are found naturally, however, their application to medical imaging is largely dependent on both their natural abundance and tissue concentration. ^{13}C has a very low natural abundance, whereas, ^{31}P, ^{23}Na and ^{1}H have a very high natural abundance but conversely the tissue concentrations of ^{31}P and ^{23}Na are very low, making them less suitable for medical imaging. ^{1}H, or protons, however are both very abundant and present in very high concentrations within the body in water and fat. Furthermore ^{1}H has a high gyromagnetic ratio and therefore a high resonance frequency making it suitable for nuclear magnetic resonance imaging [66].

Protons exhibit a spin of 1/2 meaning they can exist in one of two possible conformations. On the application of a magnetic field (B_0), a higher proportion, in the order of one per million extra protons will align in the direction of the magnetic field opposed to

against the direction of the field creating a net magnetic moment within the sample. At this point, the protons or nuclei with a spin of 1/2 will resonate at the Larmour frequency (typically within the radiofrequency megahertz range) and the nuclei are sensitive to energy at this frequency. Within NMR, the application of a magnetic field (B_1), also known as a radiofrequency (RF) pulse, at the Lamour frequency deposits energy into the spin system and decay of this energy can be detected via magnetic induction in loops of wire placed adjacent to the sample. The signals produced are related to the concentration and chemical environment of the nucleus and provide information about the environment in which the molecule is located [66, 67].

1.5.2 A Brief Overview of Magnetic Resonance Imaging

Magnetic resonance imaging (MRI) is an extension of nuclear magnetic resonance where the signal emitted from hydrogen atoms located in different chemical environments within the body are used to generate an image. As described in the previous section, the application of an radiofrequency (RF) pulse is sufficient to excite hydrogen nuclei within a given region and the energy emitted during relaxation provides information about the chemical environment of the system [67]. Within MRI, the signals obtained are reconstructed using a complex mathematical operator known as Fourier Transform which is used to the obtain the frequency and phase of the signals emitted [68].

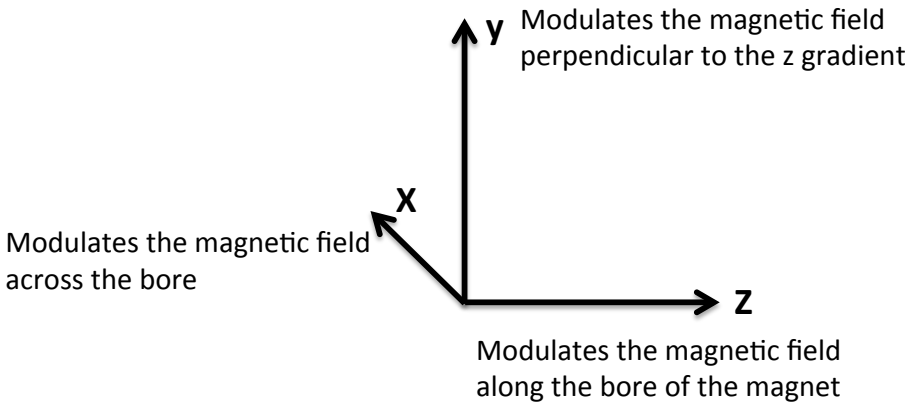


Figure 1.6: The Direction of Magnetic Field Gradients. Adapted from Cardiovascular Magnetic Resonance, Oxford Specialist Handbook in Cardiology [68]

MR images are usually obtained within a slice-wise manner and only the spins within the region of interest are excited. This is achieved by the application of gradients at the same time as the RF pulse. Physically, gradients are coils placed around the magnetic field. The application of energy through these coils varies the magnetic field in different directions as shown in Figure 1.6 [68]. The application of the gradient leads to a change in the Larmor frequency of the spins located within the direction of the gradient. Application of a modified RF pulse at a frequency equal to the Lamour frequency of the spins within the slice of interest leads to selective excitation of those nuclei and an image corresponding to that region alone [68].

1.5.3 The Cardiac Application of Magnetic Resonance Imaging

Cardiac magnetic resonance imaging (MRI) is a non-invasive technique which can be used for the *in vivo* assessment of left ventricular structure and function. Cine MRI involves acquisition of a series of consecutive images during the cardiac cycle, from which a range of functional and structural parameters can be derived [69, 68].

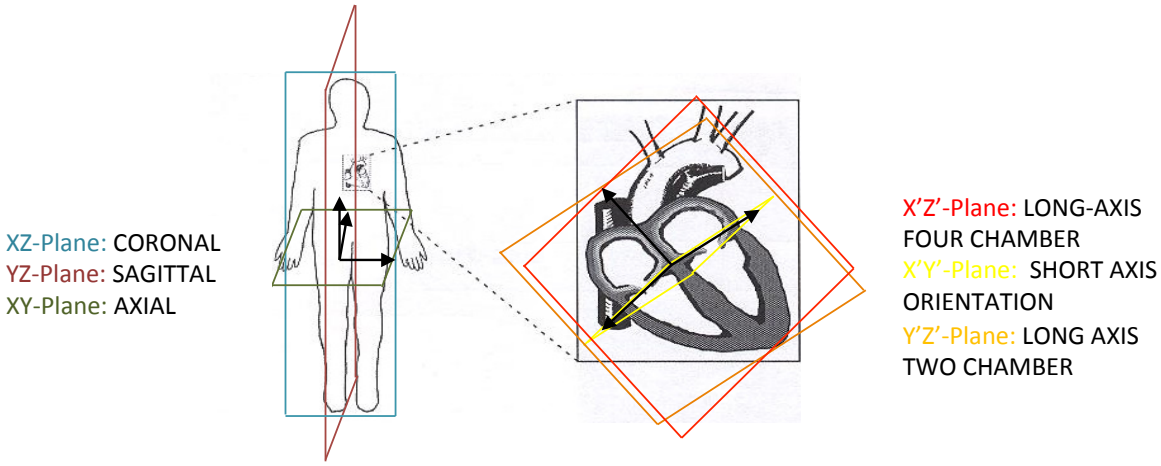


Figure 1.7: Defining the Cardiac Axis. Adapted from Schneider *et al* 2006 [70]

Images are acquired in contiguous slices (Fig 1.8) from the apex of the heart to the base through selective excitation of slices across the axis of the heart [70]. Given the oblique orientation of the heart within the thoracic cavity shown in Figure 1.7, the cardiac axis differs from defined planes of the body. Images are typically acquired in the short-axis orientation depicting the left-ventricle with circular appearance with the right ventricle taking on a crescent formation as shown in Figure 1.8 [70].

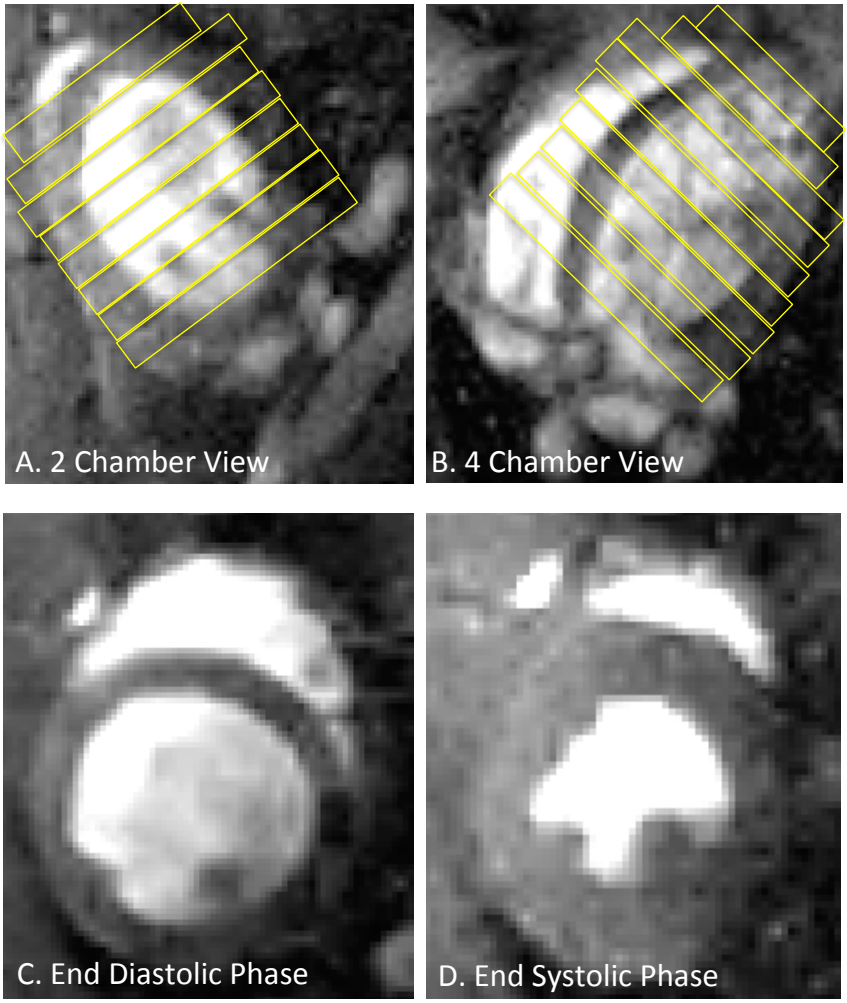


Figure 1.8: The Acquistion of Cine MRI Images. A. Long-Axis 2 Chamber View. B. Long-Axis 4 Chamber View. C. Short-Axis Mid Ventricular Slice - Diastolic Phase. D. Short-Axis Mid Ventricular Slice - Systolic Phase.

The determination of structural parameters such as end-diastolic and end-systolic volumes (EDV and ESV) and left ventricular (LV) mass can be calculated directly from pixel analysis of the LV wall following segmentation of the epi- and endo-cardial borders. Functional parameters such as stroke volume (SV), and cardiac output (CO), within the heart can also be calculated and used to characterise cardiac function [70, 69].

1.6 The Principles and Application of Dynamic Nuclear Polarization

1.6.1 An Overview of the Limitations of Magnetic Resonance Spectroscopy and Imaging

Sensitivity is an inherent limitation of MR imaging and spectroscopy (MRS). Nuclei such as ^{1}H, ^{23}Na and ^{31}P have a high natural abundance. However, whereas ^{1}H is present in high concentrations in tissue making it a prime candidate for medical imaging, the tissue concentrations of ^{23}Na and ^{31}P are much lower [66, 71]. ^{31}P spectroscopy was used by Conway *et al* to identify a reduction in the ratio of phosphocreatine to ATP (PCr:ATP) in patients undergoing treatment for heart failure [72]. It continues to be used both clinically and pre-clinically for research purposes [11], but due to the low tissue abundance of ^{31}P combined with its relatively low gyromagnetic ratio [66], phosphorus imaging is not currently used routinely in clinical practice due to sensitivity issues.

In terms of biological and medical imaging, ^{13}C would be an ideal nucleus for imaging, however, ^{13}C has a very low natural abundance of approximately 1 % combined with a gyromagnetic ratio which is around a quarter of the gyromagnetic ratio of ^{1}H [73]. However, this can be overcome through the use of a novel technique known as dissolution dynamic nuclear polarization (DNP) which results in sensitivity improvements of greater than 10,000 fold [74]. DNP has been applied to ^{13}C-based molecules including pyruvate [75], lactate [76, 77], butyrate [78] and acetate [79]. They can be used to image metabolism both *in vivo* and in real time. The pre-clinical use of this technique for metabolic imaging [75] is increasing and its application has extended to use in humans following the first in human study produced by Nelson *et al* in 2013, in patients with prostate cancer [80].

1.6.2 A Brief Overview of the Principles of Dynamic Nuclear Polarization

Dynamic nucelar polarization (DNP) combines NMR spectroscopy with electron paramagnetic resonance (EPR) to induce hyperpolarisation by temporarily forcing spin alignment in the same direction. At thermal equilibrium, nuclei which align with the magnetic field

(B_0) have a slightly lower energy than those aligned against the magnetic field, driving a weak net polarization within the direction of the magnetic field (Fig 1.9) [75]. Forcing net polarization of one direction via dynamic nuclear polarization leads to up to 10,000 fold increases in signal as depicted in Figure 1.9 [75, 74].

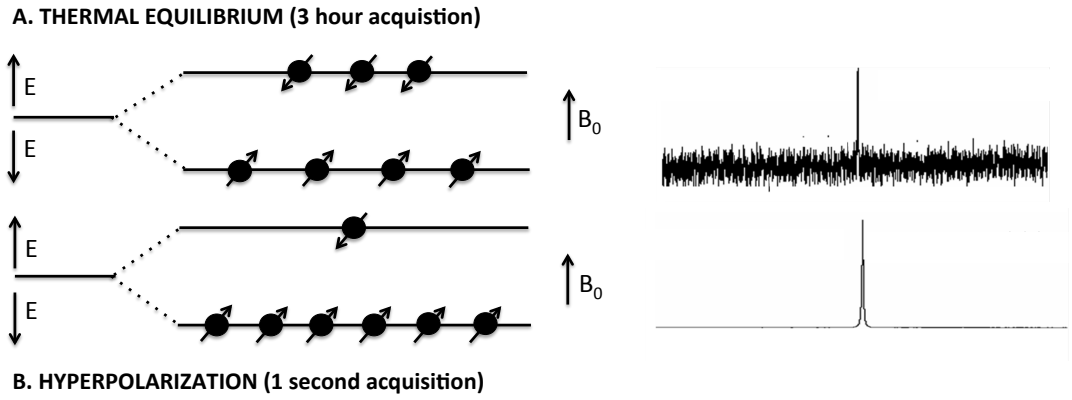


Figure 1.9: Thermal Equilibrium vs. Hyperpolarization. Adapted from Schroeder *et al* (2011) [75].

Practically, an isotopically-enriched solution such as ^{13}C-labelled pyruvate, is mixed with a free radical and cooled to temperatures of 1K in the bore of a super-conducting magnet bringing it into the solid state [81, 74].

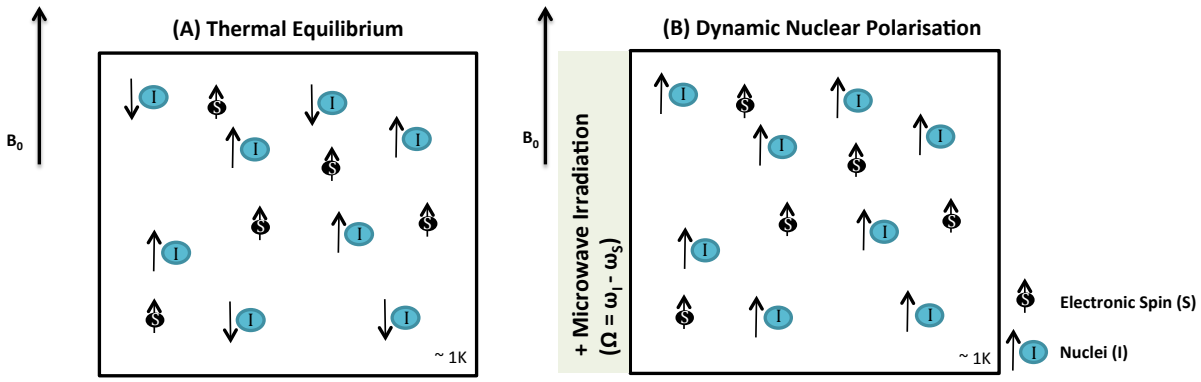


Figure 1.10: A Schematic Overview of Dynamic Nuclear Polarization. Adapted from Schroeder *et al* (2011) [75].

Under these conditions, the electronic spins (S) of the radical align with the direction of the magnetic field whereas the nuclear spins (I) of the [^{13}C] labelled sample remain poorly polarised as shown in Figure 1.10. Application of a microwave source set at the frequency of the electronic spins (ω_S) minus the frequency of the nuclear spins (ω_I) or $\Omega = \omega_S$ - ω_I, is

sufficient to induce simultaneous reversal of S and I in opposite direction, a phenomenon known as flip-flop transitions. Assuming that 50 % of I are aligned along the magnetic field and 50 % against the magnetic field, a close-unity polarisation can be reached if the flip-flops are forced at a greater rate than the rate of relaxation (Fig 1.10) [82]. The time period during which the irradiated sample remains in the solid state is proportional to the percentage polarisation, which is rapidly lost on return to the liquid state. The use of a specially designed ejection system has been developed to rapidly dissolve the sample in solution, a process referred to as dissolution DNP whilst maintaining the hyperpolarised state for a period seconds to minutes. The solution can either be injected *in vivo* or used *in vitro* to track the isotopic label in real time using MRS [81, 74].

1.6.3 The Use of Hyperpolarized Metabolites for Real-Time Metabolic Imaging

Real-time tracking of hyperpolarized ^{13}C-labelled metabolites has been demonstrated both *ex vivo* in the perfused heart [78], *in vivo* in small animal models [83, 3, 84, 78, 85, 77, 30] and pigs [86, 79, 30] and more recently to assess metabolic changes in patients with prostate cancer [80]. The use of hyperpolarized substrates conveys an advantage over positron emission tomography (PET) imaging, currently the gold standard in *in vivo* metabolic imaging, as metabolites downstream of the initial probe can be determined compared with PET which mainly provides information on fluxes and is also associated with a radiation dose [29, 87]. [1-^{13}C]labelled pyruvate (Fig 1.11) remains the most widely used substrate in metabolic imaging owing both to its suitability for dynamic nuclear polarisation (DNP) and the dissolution process due to its natural glassing properties and long T1 relaxation time.

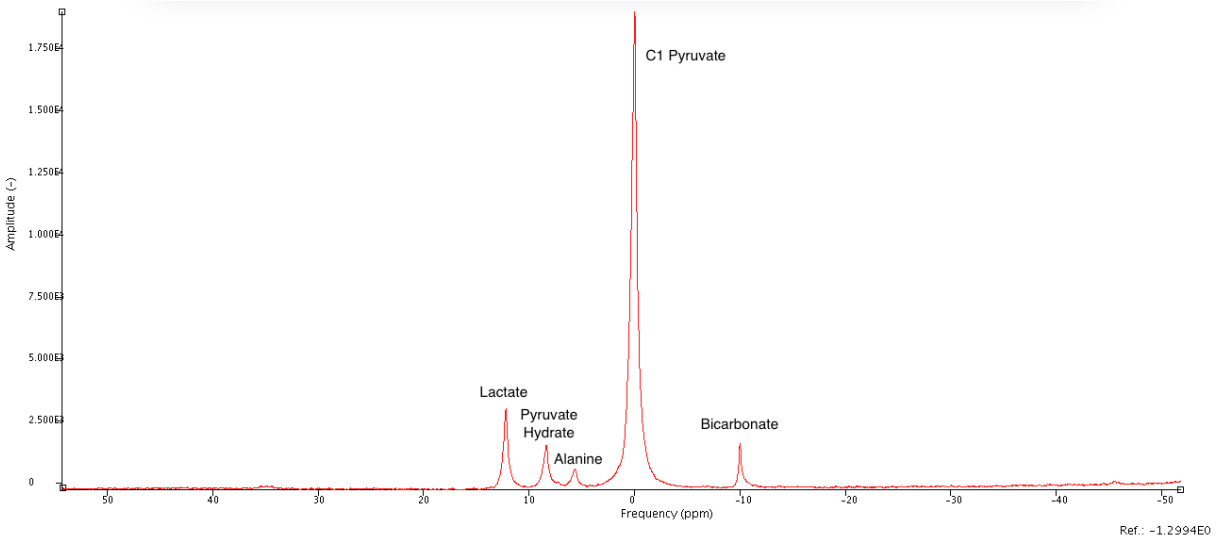


Figure 1.11: The Metabolism of [1-^{13}C]Pyruvate

Furthermore, the catabolism of pyruvate metabolism marks one of the key integrative steps within the direction of its metabolism directly linked to the energy-status of the cell [29, 30]. [2-^{13}C]pyruvate (Fig 1.12) is also used to probe TCA cycle intermediates, however, its polarization and T1 relaxation times are less favourable than [1-^{13}C]pyruvate due to its lower polarization and shorter T1 relaxation time [88, 29]. The metabolism of [1-^{13}C] and [2-^{13}C]pyruvate is shown in Figure 1.13.

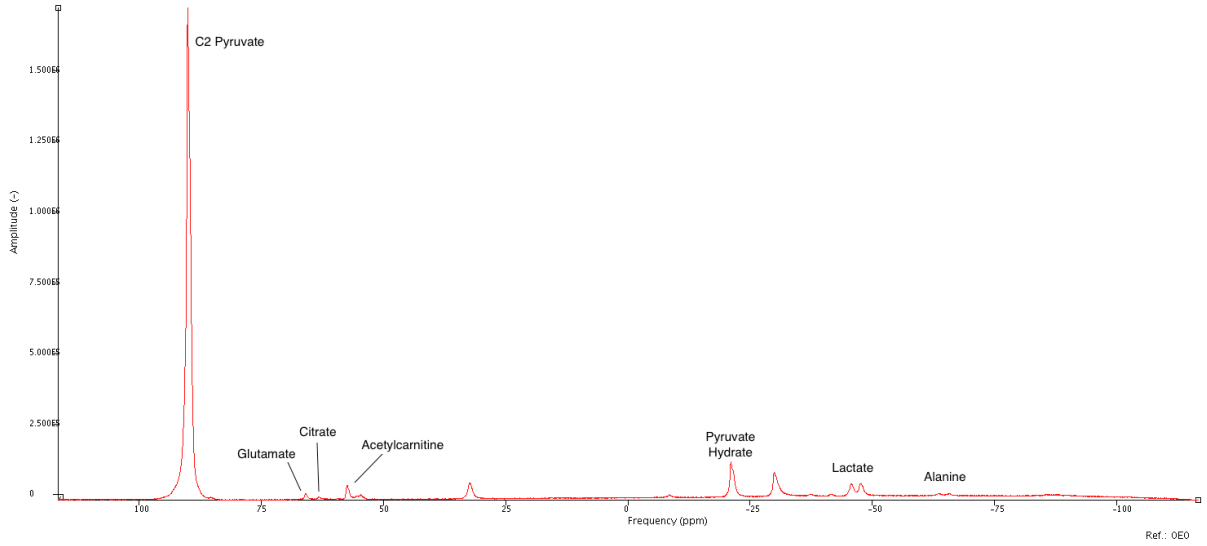


Figure 1.12: The Metabolism of [2-^{13}C]Pyruvate.

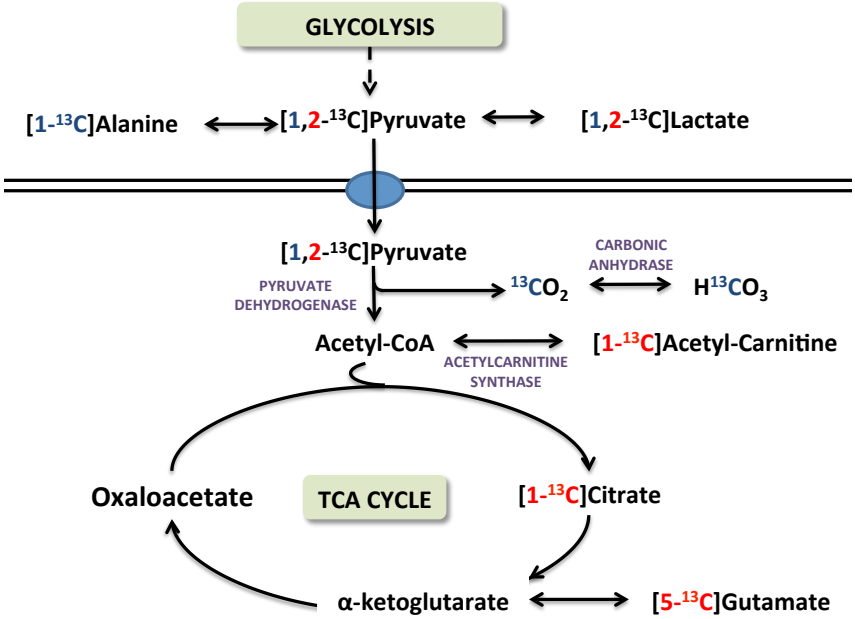


Figure 1.13: The Metabolism of [1-^{13}C]- and [2-^{13}C]-labelled Pyruvate

The development of probes for *in vivo* imaging is attractive and aside from pyruvate, acetate and butyrate have been used to probe fatty acid metabolism *in vivo* in the pig heart and the isolated perfused rat heart respectively [79, 78]. The use of hyperpolarized glucose has also been used to probe glycolysis and the pentose phosphate pathway within T cell lymphoma (EL4) and Lewis lung carcinoma (LL2) induced tumours as well as yeast cell lines [89, 90]. However, the application of hyperpolarized glucose to cardiac studies either *ex vivo* or *in vivo* does not appear suitable. No evidence of downstream metabolites were observed either *in vivo* or in the perfused heart, possibly due to the low rates of the pentose phosphate pathway within the heart (Giles L and Tyler D J, *Unpublished Data*).

Metabolic changes with the development of heart disease have been well documented making the use of hyperpolarized [^{13}C]pyruvate a useful tool in both elucidating metabolic changes which occur with disease onset and the management and treatment of disease progression [29, 87]. This has been demonstrated in various studies by Schroeder *et al* [88], Atherton *et al* [91], Seymour *et al* [50] and Dodd *et al* [85], which examined metabolic changes and treatment response following ischemia reperfusion and hypertrophy. As well as providing a useful tool for pre-clinical research, Rider and Tyler outline the translational

potential of DNP and the clinical application of hyperpolarized [1-^{13}C]pyruvate to patients with heart disease [92].

1.7 Thesis Overview and Aims

The work in this thesis addresses the role of metabolic remodelling in the development and progression of hypertrophy within the abdominal aortic constriction (AC) model with the aim of identifying targets which could be of therapeutic benefit.

Initially the relationship between hypertrophic remodelling and glucose metabolism was clarified within the AC model in a novel longitudinal *in vivo* study. This confirmed the presence of an increased glycolytic dependence during hypertrophic development representative of uncoupling between glycolysis and glucose oxidation. To address the energetic imbalance within the heart, the metabolic modulator, dichlorocactate (DCA), a known positive effector of pyruvate dehydrogenase (PDH) was used to modulate restore coupling between glycolysis and glucose oxidation correcting the myocardial energy balance and inducing cardiac regression. Although, no regression of hypertrophy was observed within the hypertrophied heart following chronic DCA treatment, as originally hypothesised, when DCA was given immediately post-surgery, a functional decline was observed within the treated heart marked by a reduction in ejection fraction. This suggests that contrary to what has previously been hypothesised within the literature [11, 15, 52], enhanced glycolytic dependence in the initial stages of hypertrophic development is an essential part of the remodelling process.

Finally, using a different perspective, metabolism was assessed within the hypertrophied heart following treatment with either a sub-antihypertensive or antihypertensive dose of Ramipril, a widely used and highly regarded antihypertensive. This work aimed to identify whether the positive effects of Ramipril treatment extended past that of its antihypertensive properties and also had a metabolic effect. This work remains inconclusive and would benefit from an increased sample size. However, it suggests that an anti-hypertensive dose of Ramipril may promote glycolytic flux within the hypertrophied heart.

The combination of these different avenues of investigation has resulted in the further clarification of the role of metabolic remodelling within hypertrophic development.

Chapter 2

General Methods

This chapter summarises the general methods used throughout this work. More specific methods are described within the individual experimental chapters.

2.1 Animal Work

All animals were housed in animal facilities at the University of Oxford and all related experiments were conducted by a licensed individual in accordance with the Home Office Guidance on the Operation of the Animals (Scientific Procedures) Act of 1986 and to University of Oxford Institutional Guidelines.

Animals were housed in a dedicated facility (Biomedical Sciences Services, University of Oxford, UK) under a 12 hr light-dark cycle and maintained on standard laboratory chow (Harlan Laboratories, Kent, UK) and standard laboratory water given *ad libtum* unless otherwise stated. All *in vivo* metabolic experiments were performed whilst animals were in the fed state (taken as between 6 am and 1 pm) unless otherwise stated.

2.2 Surgical Induction of Left Ventricular Hypertrophy via Abdominal Aortic Constriction

Left ventricular hypertrophy (LVH) was surgically induced in male Sprague-Dawley rats (Harlan Laboratories, Kent, UK) via abdominal aortic constriction (AC) [93, 50]. Animals underwent food restriction from the evening prior to surgery. A laparotomy was performed under anaesthesia induced using 3% isoflurane in 3 L min^{-1} O_2 and maintained at 2.5% isoflurane at 1 L min^{-1} O_2 prior to placement of a reproducible constriction between the left and right renal arteries. Initially a 0.7 mm OD blunted needle (Sterican, B. Braun Medical Ltd, UK) was placed along the abdominal aorta and a non-absorbable suture (Persel, US 0, UK Ph 3.5) was passed under the aorta and secured tightly around the needle . The needle was subsequently removed leaving a reproducible constriction around the abdominal aorta. Sham animals underwent the same procedure without constriction of the abdominal aorta. Animals received a pre-operative *i/c* dose of rimayl to prevent post-operative pain and a post-operative *i/p* dose of amphiphen to prevent infection and

were closely monitored for the following 24 hours.

2.3 The Use of Cardiac Magnetic Resonance Spectroscopy and Magnetic Resonance Imaging to Assess Cardiac Structure, Function and Metabolism *In Vivo*

2.3.1 The Preparation of Animals for Cardiac Magnetic Resonance Spectroscopy and Magnetic Resonance Imaging

Anaesthesia was induced using 4% Isoflurane in O_2 (2 L min[1]) and anaesthesia maintained at 2% Isoflurane. For magnetic resonance spectroscopy studies, a cannula was subsequently placed in the tail vein of the rat for *i/v* infusion of hyperpolarized [^{13}C]labelled substrates (Sigma, Dorset, UK). Rats were placed in a custom-built cradle with anaesthesia and temperature maintained via an in-built nose-cone and warm air-flow system respectively [69]. Electrodes were placed and secured subcutaneously in the forelimbs of the rat to obtain an electrocardiogram (ECG) for the monitoring of the heart rate (HR) [94].

2.3.2 The Dynamic Nuclear Polarization of [^{13}C]-Labelled Substrates

Approximately 40 mg of either [1-^{13}C] or [2-^{13}C]labelled pyruvic acid (Sigma, Dorset, UK) doped with 15 mM triyl radical (OXO63, GE Healthcare, UK) and 3 μl of Dotarem (1:50 dilution; Guerbet, Birmingham, UK) was hyperpolarized in a custom-built manually operated polarizer as previously described [74]. Following 45 minutes of microwave irradiation (94 GHz) at 1 K, the sample was rapidly dissolved in 100 mg L^{-1} NaOH solution (31 mM Tris-base, 60 mM sodium hydroxide, 0.25 mM dipotassium salt of ethylenediaminetetraacetic acid (EDTA)) heated to 180 °C and pressurised to 10 Bar yielding an 80 mM solution of hyperpolarized sodium [1-^{13}C]pyruvate or [2-^{13}C]pyruvate at physiological temperature and a pH of 7.2.

2.3.3 The Use of [^{13}C]-Labelled Substrates to Assess Cardiac Metabolism

A home-built ^{1}H/^{13}C butterfly coil (coil diameter: 65 mm) was centred over the rat heart to localise the signal received from the heart. Localisation of the heart was confirmed following placement of the cradle in a 7 T horizontal bore magnetic resonance (MR) scanner (Varian Medical Systems, Yarnton, Oxford) through acquisition of a proton fast low-angle shot (FLASH) image in the axial orientation. An electrocardiogram (ECG)-gated shim was used to reduce the proton linewidth to <150 Hz. Immediately prior to injection of hyperpolarized [^{13}C]-labelled substrates, an ECG-gated ^{13}C magnetic resonance pulse-acquire spectroscopy sequence was initiated. Approximately 1 ml of hyperpolarized [^{13}C]-labelled substrate was infused over 10 seconds and 60 single scan spectra were acquired over a period of 60 seconds ([1-^{13}C]pyruvate: TR = 1 s; excitation flip angle: 5°; sweep width: 13593 Hz; acquired points: 2048; [2-^{13}C]pyruvate: TR = 1 s; excitation flip angle: 30°; sweep width: 17606 Hz; acquired points: 2048) [84, 88].

2.3.4 Analysis of ^{13}C Magnetic Resonance Spectroscopy

2.3.4.1 Spectral Analysis following Injection of Hyperpolarized [1-13C]Pyruvate

^{13}C spectra were analysed using the AMARES algoritum in the jMRUI software package [95]. Spectra were DC-offset corrected, based on the last half of data points acquired and peaks corresponding to [1-^{13}C]pyruvate, [1-^{13}C]lactate, [1-^{13}C]alanine, $^{13}CO_2$ and [^{13}C]bicarbonate were assigned at each time point with prior knowledge and used as input data for the kinetic model described below [94].

2.3.4.2 The Kinetic Model

The kinetic model used was based on a model (Equation 2.1) originally developed by Zierhut *et al*, 2010 [96] for the analysis of hyperpolarized magnetic resonance spectroscopy (MRS) data and was further developed by Atherton *et al*, 2011 (Equation 2.2) [97] .

The initial set of equations was used to calculate the change in pyruvate signal over the acquisition time through integrating the area under the [^{13}C]pyruvate peak ($S^{\mathrm{Pyr}}(t)$). Equation 2.1 fits: k_{Pyr}, the rate constant for the decay of the pyruvate signal (s^{-1}); R_i the rate of pyruvate arrival (a.u.s^{-1})and t_a, the time of pyruvate arrival. t_e is taken as the sum of the time of arrival (t_a) and the known injection time which in this case was 10 s [91].

$$S^{\mathrm{Pyr}}(t) = \begin{cases} 0 & t < t_a \\ \frac{R_i}{k_{\mathrm{Pyr}}}\left(1 - e^{-k_{\mathrm{Pyr}}(t-t_a)}\right) & t \in [t_a,\, t_e] \\ M_{\mathrm{Pyr}} e^{-k_{\mathrm{Pyr}}(t-te)} & t > t_e \end{cases} \tag{2.1}$$

$$S^{X\neq\mathrm{Pyr}} = \begin{cases} 0 & t < t_a \\ \frac{k_{\mathrm{Pyr}X}\cdot R_i}{k_{\mathrm{Pyr}}-k_X}\left[\frac{1-e^{-k_X(t-t_a)}}{k_X} - \frac{1-e^{k_{\mathrm{Pyr}}(t-t_a)}}{k_{\mathrm{Pyr}}}\right] & t \in [t_a,\, t_e] \\ \frac{M_{\mathrm{Pyr}}\cdot k_{\mathrm{Pyr}\,X}}{k_{\mathrm{Pyr}}-k_X}\left[e^{-k_X(t-t_e)} - e^{-k_{\mathrm{Pyr}}(t-t_e)}\right] + M_X e^{-k_X(t-te)} & t > t_e \end{cases} \tag{2.2}$$

The parameters obtained from Equation 2.1 were subsequently used in equation 2.2 which uses dynamic ^{13}C-metabolite data to calculate the rate constant for pyruvate to bicarbonate, $k_{pyr\rightarrow bicarb}$, the flux through pyruvate dehydrogenase (PDH; s^{-1}), the rate constant for pyruvate to lactate, $k_{pyr\rightarrow lac}$, representative of the flux through lactate dehydrogenase (LDH) and the rate constant from pyruvate to alanine, $k_{pyr\rightarrow ala}$, taken as the flux through alanine aminotransferase (ALT) [91].

2.3.4.3 Spectral Analysis following Injection of Hyperpolarized [2-^{13}C]Pyruvate

In order to increase the signal-to-noise ratio of the spectra acquired following injection of [2-^{13}C]pyrvate, spectra from 30 individual timepoints were summed prior to analysis, and the peaks assigned to [2-^{13}C]pyrvate, [1-^{13}C]acetylcarnitine, [1-^{13}C]citrate and [5-^{13}C]glutamate. Incorporation of ^{13}C label into each of the metabolites was quantified as the ratio of metabolite peak intensities to the peak intensity of [2-^{13}C]pyruvate. Peaks were subsequently normalised to average pyruvate dehydrogenase (PDH) flux acquired as

described in Section 2.3.4.1 to determine the any differences in TCA metabolites independently of the flux through PDH.

2.3.5 The Use of Cine Magnetic Resonance Imaging to Non-Invasively Assess Cardiac Structure and Function *In Vivo*

2.3.5.1 Cine Magnetic Resonance Imaging Data Acquisition

Cardiac structure and function was assessed *in vivo* using cine magnetic resonance imaging (MRI) on a 7 T MR scanner (Varian Medical Systems, Yarnton, UK) using either a quadrature high pass birdcage coil with a 72 mm internal diameter (RAPID Biomedical GmbH, Germany) or a phase array 4-channel surface receive volume transmit coil (RAPID Biomedical GmbH, Germany). A series of sagittal and axial scout electrocardiogram (ECG)-gated fast low-angle shot (FLASH) cardiac-localised images were acquired and used to define the axes of the heart [70] following global shimming. Betweeen 10 and 11 contiguous cine-MR images (28-35 frames per cardiac cycle) were acquired of the heart in the short-axis orientation covering the entire heart [69]. Imaging parameters were as given; field of view: 51.2 x 51.2 mm, matrix size: 256 x 256, slice thickness: 1.6 mm, TE/TR: 1.43/4.6 ms, Gaussian RF excitation pulse: 0.5 ms/17.5°and either 6 averages (quadrature birdcage coil) or 4 averages (4-channel surface receive coil).

2.3.5.2 Cine Magnetic Resonance Imaging Data Analysis

End-diastolic and end-systolic frames of each slice were selected according to the maximum and minimum volimes of the left ventricle respectively. Freehand selection of the epi- and endocardial borders of the left ventricle were used to quantify the end-systolic volume (ESV) and end-diastolic volume (EDV) using the ImageJ software package [98]. The cardiac mass was taken as the product of the area between the endo- and epi-cardial boarders, the thickness of the slice acquired (1.6 mm) and the specific muscle tissue density (1.06 g cm^{-3}). *In vivo* cardiac functional parameters *in vivo* were subsequently calculated including stroke volume (SV = EDV - ESV), ejection fraction (EF = SV/EDV)

and cardiac output (CO = SV X heart rate (HR)) [69].

2.4 Preparation of Dichloroacetate and Ramipril Treatments

2.4.1 Preparation and Use of Acute Dichloracetate Treatment

A concentration of 30 mg ml^{-1} dichloroacetate (DCA) was selected for the acute up-regulation of pyruvate dehydrogenase as previously described by Atherton *et al* in the T3 hyperthyroid model of left ventricular hypertrophy. A bolus infusion of DCA was sufficient to induce a 33 % increase in PDH flux in the T3 model relative to the control and a 4-fold increase in flux relative to the untreated T3 model [91].

A 30 mg ml^{-1} DCA (Sigma, Dorset, UK) solution was prepared and neutralised to pH 7.2 using NaOH 12-24 hours prior to use. Anaesthetised rats were infused with an initial *i/v* bolus dose of DCA (1 ml, 30 mg ml^{-1}) via a cannula placed in the tail vein followed by continuous infusion (0.5 ml, 30 mg ml^{-1}) over 15 minutes immediately prior to measurement of pyruvate dehydrogenase (PDH) flux using hyperpolarized [1-^{13}C]pyruvate as previously described in Section 2.3.4.1 [91].

2.4.2 Preparation and Use of Chronic Dichloroacetate Treatment

A concentration of 0.75 g L^{-1} was selected for chronic up-regulation of PDH as previously described by Atherton *et al*. Chronic treatment with 0.75 g L^{-1} DCA for one week was sufficient to induce an 83 % increase in PDH flux in the DCA treated T3 model and 5.5-fold increase in PDH flux when compared with the untreated T3 model [91].

DCA (0.75 g L^{-1}, Sigma, Dorset, UK) was prepared in drinking water and neutralised to pH 7.2 using NaOH and administered *ad libitum* to rats in place of standard drinking water. DCA treatment was prepared freshly and replaced every 72 hrs [91].

2.4.3 Preparation and use of Ramipril Treatment

The high, antihypertensive and low sub-antihypertensive doses of Ramipril used where selected based on the work by Unger *et al.* Following a dose response study in which peridonpril (0.1, 1, 3, and 10 mg kg^{-1} day^{-1}) was given orally to spontaneously hypertensive rats over a four week period, Unger *et al* identified that blood pressure was normalised at a dose between 1-3 mg kg^{-1} day^{-1} and threshold value lay at 0.1 mg kg^{-1} day^{-1}. Based on this evidence, a high dose, antihypertensive dose of Ramipril was taken at 1 mg kg^{-1} day^{-1} and a low antihypertensive dose taken at 0.1 mg kg^{-1} day^{-1} [99].

Ramipril treatment (High Dose: 1 mg kg^{-1} day^{-1}; Low Dose: 0.1 mg kg^{-1} day^{-1}; Sigma Aldrich, Dorset, UK) was prepared in drinking water and administered to rats in place of standard drinking water. Drinking water was monitored a minimum of every two days and the treatment adjusted accordingly based on the average weight of the cage of rats.

2.5 Radiolabelled Isolated Langendorff Perfusion

2.5.1 Preparation of Krebs-Heinseleit Buffer

2.5.1.1 The Method of Preparation

Krebs-Heinseleit (KH) buffer was prepared using 118 mM NaCl, 4.7 mM KCl, 12 mM $MgSO_4$, 1.3 mM $CaCl_2$, 0.5 mM EDTA, 25 mM $NaHCO_3$, 1.2 mM KH_2PO_4 and 11 mM glucose. Following filtration, bovine serum albumin (BSA; 1.5 %; Lampire, USA) was added to the buffer and allowed to dissolve completely. The buffer was subsequently heated to 30 °C and a concentration of 0.4 mM palmitate was added to the solution using a heated tip from a 100 mM stock. Palmitate stock was heated to 70 °C within a water bath prior to addition to the KH-palmitate buffer. The KH-albumin-palmitate buffer was placed in dialysis tubing and left over night in KH buffer free of palmitate and BSA to allow chelation of free calcium by albumin. The free calcium concentration was checked immediately prior to use using a radiometer blood gas analyser and adjusted to a final concentration of 1.35 mM.

2.5.1.2 Preparation of 100 mM Palmitate Stock

A stock of 100 mM palmitate was prepared through dissolving 2.56 g of palmitic acid (Sigma Aldrich, Dorset, UK) in 2 ml of ethanol (Sigma Aldrich, Dorset, UK) in a water bath set to 70 °C. Potassium carbonate (K_2CO_3) was dissolved the minimum volume of deionised water (dH_2O) required and slowly added to the palmitic acid solution. Following precipitation, the solution was left to dry within the water bath (70 °C) and the dried salt dissolved in 100 ml of fresh saline.

2.5.2 Heart Isolation

Male Sprague-Dawley rats were terminally anaesthetised with an *i/p* injection of sodium pentobarbital (400 mg kg^{-1}; Euthatal, Merial, Woking, UK). Hearts were rapidly excised following cessation of both the pedal and corneal reflexes and placed in ice-cold Krebs-Henseleit (KH) buffer prior to cannulation of the aorta and perfusion via the Langendorff mode at a constant pressure of 100 mmHg at 37 °C. Hearts were perfused with 200 ml recirculating KH buffer (118 mM NaCl, 4.7 mM KCl, 12 mM $MgSO_4$, 1.3 mM $CaCl_2$, 0.5 mM EDTA, 25 mM $NaHCO_3$, 1.2 mM KH_2PO_4, pH 7.4) containing 11 mM glucose, 0.4 mM palmitate (0.4 mM palmitate, 0.1 M K_2CO_3,2% EtOH, 0.9% saline) bound to 1.5 % fatty acid-free bovine serum albumin (BSA; Lanvin, USA) gassed with 95 % oxygen and 5 % carbon dioxide (Carbogen).

2.5.3 Assessment of Cardiac Function in the Isolated Langendorff Perfused Heart

A fluid filled PVC balloon, attached via a polythene tube to a bridge amplifier and a PowerLab data acquisition system (AD Instruments, Oxfordshire, UK) was inserted into the left ventricle and inflated to achieve an end-diastolic pressure of 4 mmHg and used to assess functional changes within the isolated perfused heart.

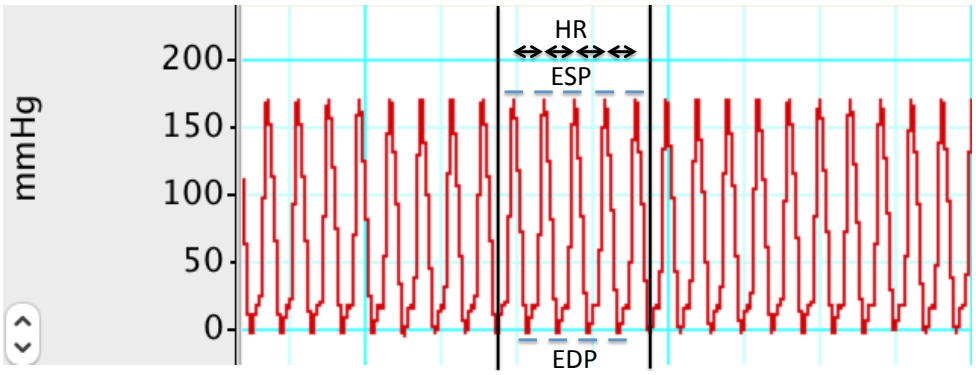


Figure 2.1: A Representative Functional Trace of the Langendorff Perfused Heart. HR: Heart Rate; ESP: End Systolic Pressure; EDP: End Diastolic Pressure

A pressure waveform as shown in Figure 2.1 was recorded and a direct read out of end systolic pressure (ESP) and end diastolic pressure (EDP) was obtained from the peak and trough of the waveform respectively (Fig 2.1). Heart rate (HR) was taken as the frequency at which the peak of the waveform occured. The left ventricular developed pressure (LVDP) was calculated as the difference between the ESP and EDP and the rate pressure product (RPP), which is taken as the measure of cardiac function, is described as the product of the LVDP and the HR.

2.5.4 The Use of Radio-labelled Substrates and Perfusion Protocols

To assess either glycolytic flux or fatty acid oxidation, 0.5 μCi of [5-^{3}H]Glucose or [9,10-^{3}H]Palmitate respectively was added to the circulating volume of KH buffer containing 11 mM glucose and 0.4 mM palmitate bound to albumin (1.5 %) as previously described in Section 2.5.2. A sample volume of 1 ml of perfusate was taken every four minutes during the assessment of glycolytic flux and 1.5 ml taken every four minutes during the assessment of fatty acid oxidation.

2.5.4.1 Assessment of Basal and Insulin-Stimulated Metabolism

Basal metabolism was measured for the first 20 minutes following a 10 minute acclimatisation prior to the addition of insulin (2084 pmol L^{-1}; Novorapid, Novo Nordisk, Denmark) into 200 ml of circulating perfusion buffer after which samples were taken for a further

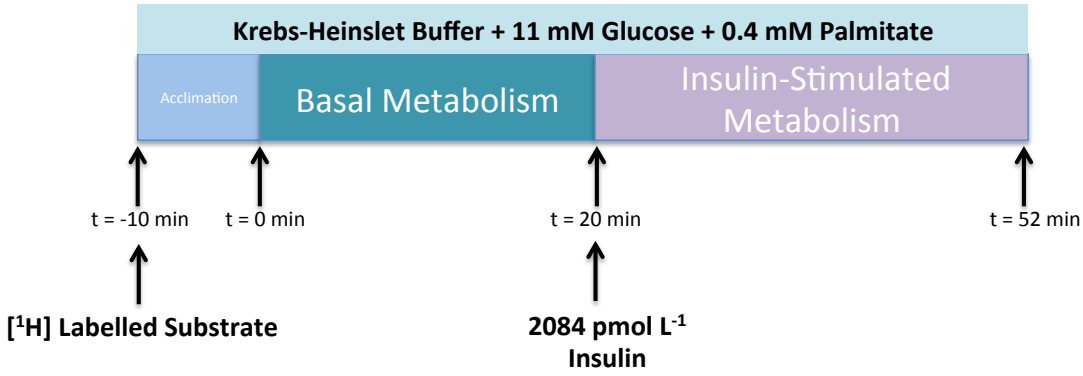


Figure 2.2: Assessment of Basal and Insulin-Stimulated Metabolism in the Isolated Langendorff-Perfused Heart.

32 minutes. Hearts were washed for 4 minutes with fresh Krebs-Heinsleit (KH) buffer in the absence of radiotracer and rapidly freeze-clamped whilst on the cannula with liquid nitrogen-cooled Wollenberg tongs. Frozen tissue was stored at -80 °C and the aliquots of perfusate taken were stored at -20 °C for subsequent analysis.

2.5.4.2 Assessment of Ischemia Reperfusion Recovery in the Isolated Langendorff Perfused Heart

Insulin (2084 pmol L^{-1}) was added to the 200 ml recirculating buffer at the beginning of a 10 minute (t = -10 minutes) acclimatisation period following the addition of a radio-labelled tracer as previously described in Section 2.5.4.

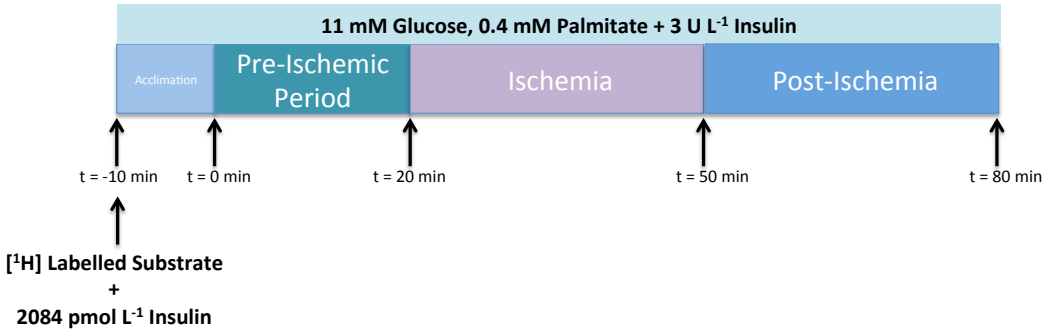


Figure 2.3: Ischemia Reperfusion Protocol

Pre-ischemic measurements of cardiac function and metabolism was assessed for the first 20 minutes (t = 0 minutes to t = 20 minutes) following which the heart was placed

into low flow ischemia for a total of 30 mins (t = 21 minutes to t = 50 minutes; Fig 2.3). During the ischemic period, flow was adjusted according to the weight of the heart to achieve a final flow rate of 0.3 ml min^{-1} gww^{-1}. Normal flow was resumed at t = 50 minutes and the post-ischemic function and metabolism assessed for a further 30 minutes (t = 80; Fig 2.3). Hearts were washed in fresh Krebs-Heinsleit (KH) buffer in the absence of radiotracer for 4 minutes and were rapidly freeze-clamped whilst on the cannula using liquid nitrogen-cooled Wollenberg tongs. Frozen tissue was stored at -80 °C for further analysis.

2.5.5 The Measurement of Myocardial Glycolytic Flux

The rate of glycolysis was determined from the production of water at the enolase stage of the glycolytic pathway. Radiolabelled glucose and water were separated via ion-exchange chromatography using Dowex© (1x4 chloride form, 100-200 mesh, Sigma, Dorset, UK) as previously described by Lopaschuk *et al* [100]. Dowex© was prepared in 1.35 M NaOH and 1.62 M boric Acid and repeatedly washed with dH_2O until a pH less than 7.5 was achieved. A total of 200 μl of perfusate was passed through a short nose glass Pasteur pipette containing Dowex©. Columns were washed with 2 ml of dH_2O at 15 minutes following the addition of perfusate and the efflux collected in scintillation vials. The sample preparation was mixed with 10 ml of Ecolite scintillation cocktail (MP Biomedicals, USA) and the levels of ^3H_2O counted on a scintillation counter. The specific activity was measured directly from 200 μl perfusate taken at t = 0 following the 10 minute acclimatisation period.

The cumulative glucose consumption within each sample was calculated as follows:

$$\frac{(\text{sample } (t = x) \text{ cpm} - \text{sample } (t = 0) \text{ cpm}) \times \text{recirculating buffer (ml)}}{(\text{specific activity per ml} - \text{sample } (t = 0)) \text{ cpm}) \times \text{glucose (11 mM)}}$$

The glycolytic consumption for each individual sample was plotted as a function of time to give the rate of glycolysis (μmol min^{-1}) and normalised to heart weight given in gram of wet weight of tissue (gww).

2.5.6 The Measurement of Myocardial Fatty Acid Oxidation

The rate of palmitate oxidation was determined from the production of ^3H_2O as previously described by Lopashuk *et al* [100]. [^{3}H]palmitate was extracted from individual aliquots of perfusate via the Folch method leaving ^3H_2O. A 0.5 ml sample of perfusate was added to 1.88 ml of Folch solution (1:2 chloroform:methanol) and mixed. A volume of 0.625 ml chloroform and 0.625 ml 2 M potassium chloride (KCl) prepared in 0.4 M hydrochloric acid (HCl; KCl-HCL) was added to the initial reaction mixture and rotated for 15 minutes at 40 rpm (Stuart Laboratory Rotor SB3) and left to stand for 1 hour allowing separation of the aqueous and organic layers. The aqueous layer was removed and placed in a fresh tube whist the organic layer was discarded. A further 1 ml of chloroform was added to the reaction mixture followed 1 ml of methanol and 0.9 ml of KCL-HCL. The reaction mixture was rotated as previously described for a total of 15 minutes and allowed to stand for a further hour. The aqueous layer was removed from the reaction mixture and retained. A volume of 0.5 ml of the aqueous layer was mixed with 10 ml of Ecolite liquid scintillation cocktail (BP Medical, USA) and read on a scintillation counter. Specific activity was measured in 0.5 ml of perfusate taken at t = 0 minutes

The cumulative palmitate consumption within each sample was calculated as follows:

$$\frac{(\text{sample } (t = x) \text{ cpm} - \text{sample } (t = 0) \text{ cpm}) \times 8.26 \times 2 \times \text{recirculating buffer (ml)}}{(\text{specific activity per ml} - \text{sample } (t = 0)) \text{ cpm}) \times (2 \text{ / palmitate (0.4 mM)})}$$

The palmitate consumption for each individual sample was plotted as a function of time to give the rate of palmitate oxidation (μmol min^{-1}) and normalised to the heart weight given in gram of wet weight tissue (gww).

2.5.7 Measurement of the Rate of Lactate Efflux from the Perfused Heart

The concentration of lactate in the perfusate was measured via a standard photometric method. The concentration of lactate was measured in a sample volume of 100 μl perfusate assayed in 1 ml of assay buffer (0.2 M Tris Base (Sigma Aldrich, Dorset, UK), 10

mM K^+ EDTA, 5 % Hydrazine Hydrate (Sigma Aldrich, Dorset, UK), 0.88 mM NAD^+ (Sigma Aldrich, Dorset, UK) adjusted to pH 9.5 using HCl and 0.9 ml of dH_2O. Baseline absorbance was measured at 340 nm immediately prior to the addition of 10 μl bovine heart lactate dehydrogenase (LDH, 10 U, Sigma Aldrich, Dorset, UK) to the assay buffer. Following a 20 minute incubation period at room temperature, absorbance was re-read and recorded. The concentration of lactate samples was calculated from a standard curve of absorbances from lactate of known concentrations and used to calculate the rate of lactate efflux.

2.6 Blood Sampling and Plasma Analysis

Terminal blood samples where obtained from the chest cavity immediately following removal of the heart. Whole blood samples were microcentrifuged (Eppendorff Centrifuge 5415R, Eppendorff, Hamburg, Germany) at 3000 rpm for 10 minutes at 4 °C and the plasma isolated and rapidly frozen in liquid nitrogen and stored at -80 °C.

Samples were run for a range of metabolites including glucose, lactate, triacylglycerides (TAG), non-esterified fatty acids (NEFA), cholesterol, low-density lipoprotein (LDL), high-density lipoprotein (HDL) and β-hydroxybutyrate using a ABX Pentra 400 (Horiba ABX Diagnostics, Irvine, CA, USA).

2.7 Tissue Collection

Heart, liver and skeletal muscle was extracted and rapidly freeze-clamped using liquid nitrogen-cooled Wollenberg tongs, unless otherwise described, following the induction of terminal anaesthesia with either 5% Isoflurane in 2 L min_{-1} O_2 or an *i/p* injection of sodium pentobarbital (150 mg kg^{-1}). Frozen heart and liver tissue was ground into a fine powder using a liquid nitrogen-cooled pestle and mortar and stored at -80 °C.

2.8 Biochemical Analysis

2.8.1 Measurement of Myocardial Glycogen

A volume of 100 μl of 30 % potassium hydroxide (KOH) solution was added to approximately 50 mg of freeze-clamped powered cardiac tissue and heated to 105 °C for 1 hour. A total of 50 μl of 2 % sodium sulphate ($NaSO_3$) solution and 600 μl ethanol was subsequently added and samples incubated overnight at 4 °C. Following the incubation stage, samples were centrifuged in a refrigerated Eppendorff Centrifuge 5415R (4 °C, 16000 g; Eppendorff, Hamburg, Germany) for 5 minutes. The resultant pellet, which contained glycogen, was resuspended in 500 μl of 80 % ethanol using sonication and the ethanol left to evaporate overnight. Following the second overnight incubation, 375 μl of deionised water (dH_2O) was added to the glycogen pellet followed by 125 μl of amyloglucosidase containing buffer (5 mg of amyloglycosidase (Sigma Aldrich, Dorset, UK) in 10 ml of 1 M sodium acetate). The reaction mixture was incubated for 1 hour at 37 °C prior to the addition of a further 100 μl of dH_2O and a final centrifugation for 5 minutes (16000 g, 4 °C Eppendorff Centrifuge 5415R, Eppendorff, Hamburg, Germany). The result supernatant was assayed for glucose on an ABX Pentra 400 autoanalyser (Horiba ABX Diagnostics, California, USA).

2.8.2 Myocardial Intracellular Lactate Extraction

A volume of 0.5 ml of ice-cold 6 % perchloric acid (PCA) was added to approximately 100 mg of freeze-clamped, finely powdered cardiac tissue and incubated for 10 minutes on ice. Following a centrifugation in a refrigerated Eppendorff Centrifuge 5415R for 10 minutes (4 °C, 16000 g; Eppendorff, Hamburg, Germany), the resultant supernatant was extracted and neutralised following the addition of 100 μl of 1 M Tris base. An ice-cold, 6 M potassium hydroxide (KOH) solution was added in 5 μl increments and the pH measured following each addition until a pH of 7 was achieved. Following a final 10 minute centrifugation (4 °C, 16000 g; Eppendorff Centrifuge 5415R, Eppendorff, Hamburg, Germany), the resultant supernatant was assayed for lacate using an ABX Pentra 400 (Horiba ABX Diagnostics, California, USA).

2.9 Statistical Analysis

All data are reported as Mean ± Standard Error of the Mean (SEM). The specific statistical analysis used under different situations is further broken down according to chapter.

2.9.0.1 Chapter 3

In vivo structural, functional and metabolic data was analysed using an unpaired, two-tailed Student's t test given only two experimental groups were compared. The glycolytic and cardiac functional data obtained form the perfused heart at 10 weeks post-surgery was also analysed using the same statistical parameters. Perfusion data acquired at 18 weeks post-surgery was analysed using a two-way ANOVA with repeated measures as different experimental conditions were tested within the same sample group. Insulin and hypertrophy as independent variables.

2.9.0.2 Chapter 4

The *in vivo* metabolic data in Chapter 4 was analysed using an unpaired, two-tailed Student's t test given only two experimental groups were compared. All perfusion data within this chapter was analysed using a two-way ANOVA with repeated measures as different experimental conditions were tested within the same sample group. DCA and insulin were taken as independent variables.

2.9.0.3 Chapter 5

All *in vivo* metabolic and structural data was assessed using a one-way ANOVA with a Sidak correction for multiple comparisons taking into account the presence of four experimental groups. Perfusion data was analysed using a two-way ANOVA with repeated measures as different experimental conditions were tested within the same sample group. Hypertrophy and insulin were taken as independent variables.

2.9.0.4 Chapter 6

Structural and metabolic data obtained at 4 weeks post-surgery was analysed using an unpaired two-tailed t-test given only two experimental groups were compared. Both data obtained at 9 weeks post-surgery and all perfusion data was analysed using a one-way ANOVA with Sidak correction for multiple corrections given four experimental groups were considered.

Statistical analysis was performed using the GraphPad Prism 7 Software Package (GraphPad Software, California, USA)

Chapter 3

Structural, Functional and Metabolic Characterisation of Hypertrophic Development following Abdominal Aortic Constriction

3.1 Chapter Overview

This chapter investigates the development and progression of hypertrophy following abdominal aortic constriction (AC) surgery. The data summarised in this chapter is taken from the subsequent experimental chapters where the effects of different therapeutic approaches on hypertrophy have been assessed. This chapter characterises the structural, functional and metabolic changes associated with hypertrophic remodelling aside from any metabolic modulation discussed in future chapters.

Our previous work in the AC model, summarised in Appendix A, focused on the effects of a "Western" diet, defined as a diet high in both fat and simple sugars, on the development and progression of cardiac hypertrophy [50]. That study highlighted a role for metabolic remodelling within the heart during hypertrophic remodelling characterised by an enhanced flux into lactate, consistent with elevated glycolysis. This chapter aims to further characterise the structural, functional and metabolic changes which occur with the development and progression of cardiac hypertrophy within the AC model. Cardiac hypertrophy was induced via the surgical constriction of the abdominal aorta representative of an aortic stenosis. The gradual increase in blood pressure following constriction of the aorta is sufficient to induce a slow-onset model of hypertrophy [101, 102]. The development of hypertrophy and any metabolic changes associated with structural and functional remodelling were assessed *in vivo* at 4, 9 and 14 weeks post-surgery using cine MRI and hyperpolarized [^{13}C]pyruvate. Glycolytic flux and the ability of the heart to recover from ischemia was further assessed in a subset of hypertrophic rats perfused via the Langendorff mode at 10 weeks post-surgery and basal and insulin-stimulated glycolytic flux assessed in a further subset of rats at 18 weeks post-surgery.

3.2 Introduction

3.2.1 An Overview of the Abdominal Aortic Constriction Model

Abdominal aortic constriction (AC) is a widely accepted model for the induction of hypertension and left ventricular hypertrophy (LVH) [101]. The model is similar to the trans-thoracic aortic constriction (TAC) model of heart failure, but involves the isolation and constriction of the abdominal aorta between the two renal arteries as shown in Figure 3.1 [103].

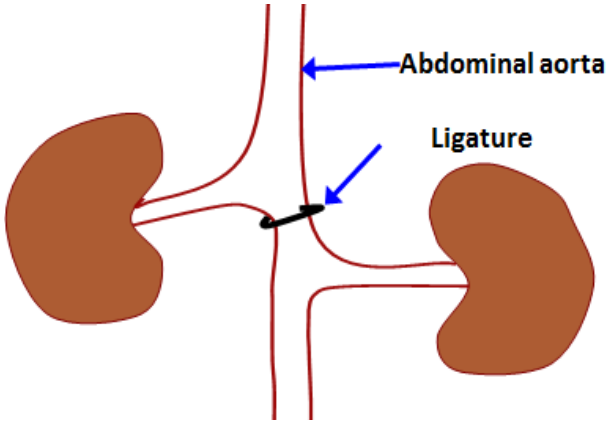


Figure 3.1: The Abdominal Aortic Constriction Model of Left Ventricular Hypertrophy. *(Courtesy of Dr Ashwin Akki)*

Constriction of the abdominal aorta provides a less severe but more physiologically relevant model of cardiac hypertrophy compared with the TAC model of LVH, which is characterised by its rapid progression into heart failure [104]. The gradual progression of LVH which occurs with abdominal aortic constriction lends the model to the longitudinal assessment of metabolic, structural and functional changes which occur with hypertrophic development and progression.

3.2.2 Structural and Functional Changes with the Development of Hypertrophy in the Aortic Constriction Model

Morphological measurements from the *ex vivo* studies conducted by Akki *et al* report the development of LVH at 9 week post-surgery with no evidence of heart failure, characterised

by the absence of fluid in the lungs [4]. The development of hypertrophy, was further confirmed by our previous work *in vivo* at 4, 9 and 14 weeks using cine MRI and by Rupert *et al* who report evidence of hypertrophy following echocardiography by 1 week post-surgery and subsequently 4 weeks and 12 weeks post-surgery [50, 18].

Studies conducted by Miyamoto *et al* extended the duration of hypertrophy to 10-23 weeks post-surgery and confirmed the presence of hypertrophy using echocardiography. Prior to the 18 weeks post-surgery, Miyamoto *et al report* an increase in fractional shortening within the hypertrophied heart, consistent with an elevation in function following hypertrophic development and compensated hypertrophy [105]. Our previous work identified no change in cardiac output or ejection fraction despite the presence of hypertrophic remodelling at 4, 9 or 14 weeks post-surgery (Appendix A) [50]. Furthermore, Rupert *et al* reported no change in the respiratory control ratio (RCR), a marker of the ability of the mitochondria to produce ATP, in mitochondria isolated from hearts which had experienced 1 week, 1 month or 3 months of aortic constriction. This suggests no evidence of mitochondrial dysfunction between 4 and 12 weeks post-surgery [18].

However, from 18 weeks post-surgery, Miyamoto *et al* report a reduction in fractional shortening within the hypertrophied myocardium indicating that the hearts may be starting to transition into a different stage of hypertrophy [105]. Work by Boateng *et al* also shows a reduction in the protein levels and activity of sarcoplasmic reticulum Ca^{2+} ATPase (SERCA)-2A between 1 and 14 weeks post-surgery suggestive of impaired calcium handling irrespective of any evidence in functional decline [105, 103]. Impaired calcium handling has also been identified in patients presenting with end-stage heart failure suggesting that mechanisms which underpin functional decline are initiated in the early stages of hypertrophic remodelling prior to any phenotypic evidence of functional impairment. It also further confirms the suitability of the abdominal aortic constriction model as a representation of slow-onset hypertrophy [106, 105].

3.2.3 Metabolic Remodelling with the Development of Hypertrophy in the Abdominal Aortic Constriction Model

Despite no evidence of functional decline at 9 weeks post-surgery within this model, the initial stages of metabolic adaptation have been observed with hypertrophic development. *Ex vivo* studies performed by Akki *et al* in the isolated Langendorff-perfused heart revealed a significant reduction in palmitate oxidation in the hypertrophied heart at 9 weeks post-surgery perfused via the Langendorff mode [4]. Our previous *in vivo* work identified a increase in flux into lactate in the abdominal aortic constriction (AC) model at 9 and 14 weeks post-surgery, representative of increased glycolytic dependence which suggests that the hypertrophied heart is undergoing metabolic switiching from fatty acid oxidation to increased glycolytic dependence as widely described in the literature (Appendix A) [50, 107, 1]. As previously described in Chapter 1.4, Allard *et al* also identified a reduction in fatty acid oxidation within the AC model at 8 weeks post-surgery accompanied by an increase in glycolytic flux. However, myocardial metabolism was normalised at higher workloads suggesting that the heart still has the capacity to adapt at this stage [42].

The mechanisms by which this switch away from fatty acid oxidation towards enhanced glycolytic dependence occurs are unclear. Consistent with a reduction in palmitate oxidation, Akki *et al* report a reduction in the expression of the transcription factor, peroxisome proliferator-activated receptor-α (PPARα), a key regulator of the expression of the genes involved in long chain fatty acid uptake and oxidation in the AC model at 9 weeks post-surgery. Decreased expression of PPARα was accompanied by a decrease in the expression of mitochondrial carnitine palmitate transferase-1 (mCPT-1) and medium-chain acyl-CoA dehydrogenase (MCAD) consistent with a reduction in fatty acid uptake and oxidation in mitochondria [4]. Interestingly, Akki *et al* also a report a reduction in the expression of pyruvate dehydrogenase (PDH) regulatory enzymes, pyruvate dehydrogenase kinase (PDK)-1 and 4 which suppress PDH activity. However, no alteration in the ratio of active to total PDH (PDH_a:PDH_t) was reported by Akki *et al in vitro*. This

was supported by our previous work where no change in the PDH_a:PDH_t was observed *in vitro* and no change in PDH flux was identified *in vivo* despite evidence of hypertrophy and enhanced glycolytic dependence (Appendix A) [50].

These observations support the presence of metabolic switching within the hypertrophic heart from fatty acid oxidation towards an increase glycolytic dependence. Given glycolysis is substantially less energetically favourable than fatty acid oxidation, this switch may underpin the tipping point between compensated and de-compensated hypertrophy. Furthermore, damage to the heart during the early stages of hypertrophy may contribute to the onset of heart failure [19].

3.2.4 Chapter Aims

The work in this chapter is focused on the clarification of the structural, functional and metabolic changes which occurs with the development and progression of hypertrophy. A number of studies, which have previously been discussed in Chapters 3.2.3 and 1.4, have been conducted on the role of metabolic remodelling in hypertrophy both within the abdominal aortic constriction (AC) model and other models of left ventricular hypertrophy (LVH), however, the stage of hypertrophy discussed is often poorly clarified. The work presented here aims to link the stage of hypertrophy to the metabolic changes associated with the remodelling process aided through the use of the novel combination of *in vivo* techniques of dynamic nuclear polarization and cine MRI. The effects of hypertrophic remodelling on glycolytic flux was further assessed in a subset of hypertrophied hearts perfused via the Langendorff mode at 10 and 18 weeks post-surgery.

Within this study, cardiac structure, function and metabolism was assessed in the AC model of LVH at 4, 9 and 14 weeks post-surgery. The presence of hypertrophy within the AC model has previously been confirmed from 1 week by Rupert *et al* and *ex vivo* at 9 weeks by Akki *et al* [18, 4]. Based on these reports; assessment was taken at 4 weeks to characterise the effects of early hypertrophic development whilst ensuring that hypertrophy was present; the 9 week assessment was aimed at assessing compensated hypertrophy and extension to 14 weeks post-surgery was aimed at induce the intial stages

of functional decline within the model, however, the heart remained compensated at this point.

3.3 Methods

3.3.1 Study Overview

Structural, functional and metabolic remodelling was assessed at 4, 9 and 14 weeks following abdominal aortic constriction using cine MRI and hyperpolarized [^{13}C]labelled pyruvate as shown in Figure 3.2. Glycolytic flux and the ability of the heart to recover from ischemia in the Langendorff-perfused heart was assessed in subset of animals at 10 weeks post-surgery.

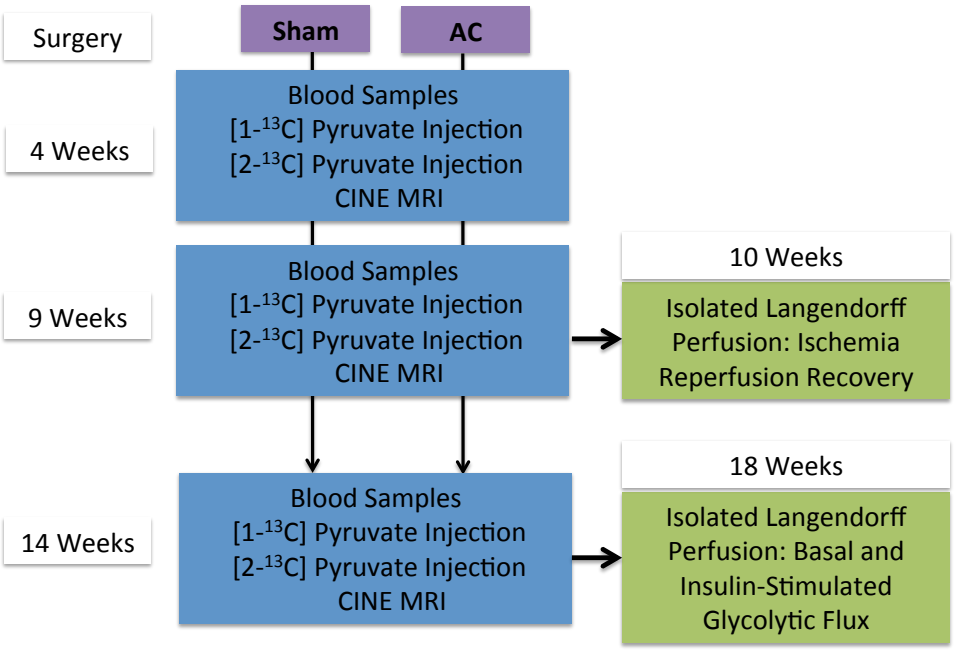


Figure 3.2: The Assessment of Structural, Functional and Metabolic Changes with the Development of Hypertrophy Following Abdominal Aortic Constriction

Basal and insulin-stimulated glycolytic flux was further assessed in the Langendorff-perfused heart in a second subset of animals at 18 weeks post-surgery.

3.3.2 Animal Work

All animal experiments were conducted by a licensed individual in accordance with the Home Office Guidance on the Operation of Animals (Scienctific Procedures) Act of 1986 and to University of Oxford institutional guidelines.

Animals were housed in a dedicated facility (Biomedical Sciences Services, University of Oxford, UK) under a 12 hr light-dark cycle and maintained on a standard laboratory

chow (Harlan Laboratories, Kent, UK) and standard laboratory water given *ad libtum* unless otherwise stated. All *in vivo* metabolic experiments were performed whilst animals were in the fed state (taken as between 6 am and 1 pm) unless otherwise stated.

3.3.3 Surgical Induction of Left Ventricular Hypertrophy

Male Sprague-Dawley rats (200-250 g; Harlan Laboratories, Kent, UK) underwent constriction of the abdominal aorta (AC; n = 32) between the two renal arteries under aseptic conditions as previously described in Section 2.2. Following a laparotomy whereby the abdominal aorta was exposed, a reproducible constriction was placed around the aorta between the two renal arteries. Sham (n = 29) animals received the same procedure but without constriction of the aorta as described in Section 2.2.

3.3.4 *In Vivo* Assessment of Cardiac Structure and Function

Cardiac structure and function was assessed at 4, 9 and 14 weeks post-surgery using cine MRI as previously described in Section 2.3.5. Male Sprague-Dawley rats were anaesthetised and placed in a custom-built cradle within a 7 T magnetic resonance scanner (Varian Biomedical, Yarnton, UK) as described in Section 2.3.1. Betweeen 10 and 11 contiguous cine-MR images (28-35 frames per cardiac cycle) were acquired of the heart in the short-axis orientation covering the entire heart [69] using either a quadrature high pass birdcage coil (RAPID Biomedical GmhB, Germany), or a phase array 4-channel surface receive volume transmit coil (RAPID Biomedical GmhB, Germany) as previously described in Section 2.3.5.

3.3.5 *In vivo* Assessment of Metabolic Parameters using Dynamic Nuclear Polarization

Pyruvate dehydrogenase (PDH) flux and flux into the TCA cycle were also assessed *in vivo* at 4, 9 and 14 weeks post-surgical induction of left ventricular hypertrophy using [^{13}C]pyruvate labelled on the first or second prime carbon respectively as previously de-

scribed in Section 2.3. Male Sprague-Dawley rats were prepared as described in Section 2.3.1 following which approximately 1 ml of either hyperpolarized [1-^{13}C]- or [2-^{13}C]-pyruvate was infused over 10 seconds and 60 single scan spectra were acquired over a period of 60 seconds as previously described in Section 2.3.

3.3.6 *Ex vivo* Assessment of Glycolytic Flux in the Isolated Langendorff Perfused Heart

3.3.6.1 The Assessment of Ischemia Reperfusion Recovery in the Hypertrophied Heart

At 10 weeks post-surgery, hearts from a subset of animals (Sham: n = 8; AC: n = 9) were isolated and perfused with Krebs-Heinsleit (KH) buffer containing 11 mM glucose, 0.4 mM palmitate, 2048 pmol L^{-1} insulin and 0.5 μCi [5-^{1}H]glucose as previously described in Section 2.5. Following a 10 minute acclimatisation period, pre-ischemic function and metabolism were assessed for a total of 20 minutes following which hearts received low flow ischemia (0.3 ml min^{-1} gww^{-1}) for a period of 30 minutes as previously described in Section 2.5.4.2. Normal flow was resumed for a further 20 minutes as described in Section 2.5.4.2. Hearts were washed for 4 minutes with fresh KH free of radiotracer at the end of the perfusion protocol and rapidly freeze-clamped on the cannula and stored at -80 °C for subsequent analysis as previously described in Section 2.5.4.2. A sample of perfusate (1 ml in volume) was taken every 4 minutes over the 80 minute perfusion period and used to calculate myocardial glycolytic flux as previously described Section 2.5.5.

3.3.6.2 The Assessment of Basal and Insulin-Stimulated Glycolytic Flux in the Hypertrophied Heart at 18 Weeks Post-Surgery

At 18 weeks post-surgery a further subset of hearts (Sham: n = 14; AC: n = 12) were isolated and perfused with Krebs-Heinsleit (KH) buffer containing 11 mM glucose, 0.4 mM palmitate and 0.5 μCi [5-^{1}H]glucose as previously described in Section 2.5.4.1. Following a 10 minute acclimation period, hearts were perfused for 20 minutes to obtain basal glycolytic rates prior to the addition of insulin (2048 pmol L^{-1}). Hearts were perfused

for a further 32 minutes to determine the insulin-stimulated glycolytic flux as previously described in Section 2.5.4.1. Hearts were washed for 4 minutes with fresh KH buffer free of radiotracer at the end of the perfusion protocol and rapidly freeze-clamped on the cannula and stored at -80 °C for subsequent analysis as previously described in Section 2.5.4.1. A sample (1 ml) of perfusate was taken every 4 minutes across the 52 minute perfusion period and stored at -20 °C as previously described in Section 2.5.4.1.

3.3.7 Measurement of the Rate of Lactate Efflux from the Langendorff Perfused Heart

The rate of lactate efflux was measured from aliquots of perfusate from hearts perfused via the Langendorff mode as previously described in Section 2.5.7.

3.3.8 Statistical Analysis

All data is presented as mean ± standard error of the mean (SEM). *In vivo* structural, functional and metabolic data was analysed using an unpaired, two-tailed Student's t test as was glycolytic and cardiac functional data obtained from the perfused heart at 10 weeks post-surgery. Perfusion data acquired at 18 weeks post-surgery was analysed using two-way ANOVA with repeated measures taking insulin and hypertrophy as independent variables.

All data was analysed using the GraphPad Prism 7 Software Package (GraphPad Softwares, California, USA).

3.4 Results

3.4.1 Structural Remodelling at 4, 9 and 14 Weeks Post-Surgery

Structural and functional parameters were assessed in rats which had undergone the surgical induction of hypertrophy at 4, 9 and 14 weeks post-surgery using cine MRI. As previously discussed, the points at which hypertrophic remodelling was assessed were selected based on previous *ex vivo* work conducted within the model. The presence of compensated left ventricular hypertrophy was confirmed in the perfused heart by Akki *et al* at 9 weeks post-surgery [4]. Assessment of cardiac structure and function at 4 weeks was selected to provide an early assessment of hypertrophic development which is in line with work by Rupert *et al* [18]. The extension of the study to 14 weeks post-surgery was aimed to induce function decline, however, this was not observed.

Consistent with the development of hypertrophy, a 15 % increase in left ventricular (LV) mass was observed in the AC group vs. the Sham group at 4 weeks post-surgery (Sham: 834 ± 15 mg; AC: 963 ± 32 mg; Fig 3.3A; $p < 0.001$ *vs. Sham*) . This was sustained at 9 weeks post-surgery with a 16 % increase in LV mass observed in the AC group vs. the Sham group (Sham: 934 ± 13 mg; AC: 1085 ± 33 mg; Fig 3.3D; $p < 0.001$ *vs. Sham*) and at 14 weeks post-surgery with an 18 % increase in LV mass observed in the AC group vs. the Sham group (Sham: 961 ± 29 mg; AC: 1131 ± 59 mg; Fig 3.3G; $p < 0.01$ *vs. Sham*). This was accompanied by a 16 % increase in LV mass to body weight ratio in the AC group vs. the Sham group at 4 weeks post-surgery (Sham: 2.31 ± 0.04; AC: 2.69 ± 0.08; Fig 3.3C; *p 0.001 vs. Sham*), a 15 % increase in the AC group vs. the Sham group at 9 weeks a post-surgery (Sham: 2.25 ± 0.03; AC: 2.58 ± 0.07; Fig 3.3F; $p < 0.001$ *vs. Sham*) and a 14 % increase in the AC group vs. the Sham group at 14 weeks post-surgery (Sham: 2.12 ± 0.04; AC: 2.42 ± 0.13; Fig 3.3I; $p < 0.05$ *vs. Sham*). No change in body weight was observed between the Sham and AC groups at 4, 9 and 14 weeks post-surgery (4 weeks: Fig 3.3B; $p = 0.56$ *vs. Sham*; 9 weeks: Fig 3.3E; $p = 0.75$ *vs. Sham*; 14 weeks: Fig 3.3H; $p = 0.35$ *vs. Sham*).

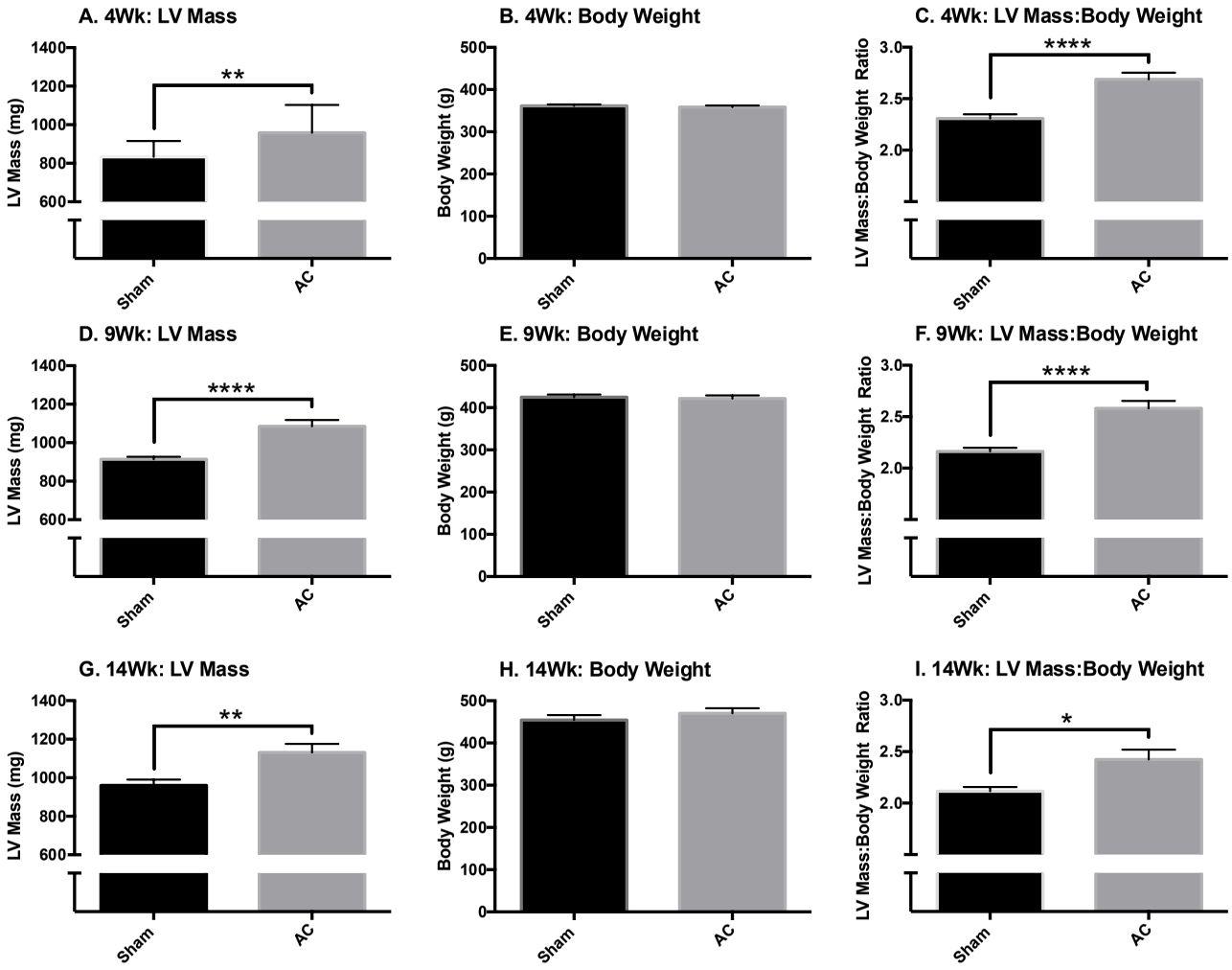


Figure 3.3: Structural Changes at 4, 9 and 14 weeks Post- the Surgical Induction of Hypertrophy. A. Left Ventricular (LV) Mass at 4 Weeks Post-Surgery. B. Body Weight at 4 Weeks Post-Surgery; C. LV Mass to Body Weight Ratio at 4 Weeks Post-Surgery; D. LV Mass at 9 Weeks Post-Surgery. E. Body Weight at 9 Weeks Post-Surgery; F. LV Mass to Body Weight Ratio at 9 Weeks Post-Surgery; G. LV Mass at 14 Weeks Post-Surgery. H. Body Weight at 14 Weeks Post-Surgery; I. LV Mass to Body Weight Ratio at 14 Weeks Post-Surgery. 4 Weeks: Sham: n = 29; AC: n = 22; 9 Weeks: Sham: n = 29; AC: n = 32; 14 Weeks: Sham: n = 18; AC: n = 23. * $p < 0.05$ *vs. Sham* ** $p < 0.01$ *vs. Sham* **** $p < 0.001$ *vs. Sham.* $Mean \pm SEM$ Unpaired Two-Tailed Student's t test. AC: Aortic Constriction.

3.4.2 Functional Remodelling following the Induction of Hypertrophy at 4, 9 and 14 Weeks Post-Surgery

A trend towards an increase in cardiac output was observed in the AC group vs. the Sham group at 4 weeks post-surgery (7 %; Fig 3.4A; *p = 0.11 vs. Sham*) and at 9 weeks post-surgery in the AC group relative to the Sham group (3 %; Fig 3.4D; *p = 0.10 vs. Sham*) but this failed to reach statistical significance. No change in cardiac output was observed in the AC group vs. the Sham group at 14 weeks post-surgery (Fig 3.4G; *p = 0.83 vs. Sham*). No change in ejection fraction was observed in the AC group vs. the Sham group at 4, 9 or 14 weeks post-surgery (4 weeks: Fig 3.4B; *p = 0.79 vs. Sham*; 9 weeks: Fig 3.4E; *p = 0.67 vs. Sham*; 14 weeks: Fig 3.4H; *p = 0.31 vs. Sham*). Heart rate remained unchanged in the AC group vs. the Sham group at 4 or 9 weeks post-surgery (4 weeks: Fig 3.4C; *p = 0.39 vs. Sham*; 9 weeks: Fig 3.4F; *p = 0.62 vs. Sham*). However, a trend towards a decrease in heart rate was observed in the AC group vs. the Sham at 14 weeks post-surgery but this did not reach statistical significance (Fig 3.4I; *p = 0.08 vs. Sham*).

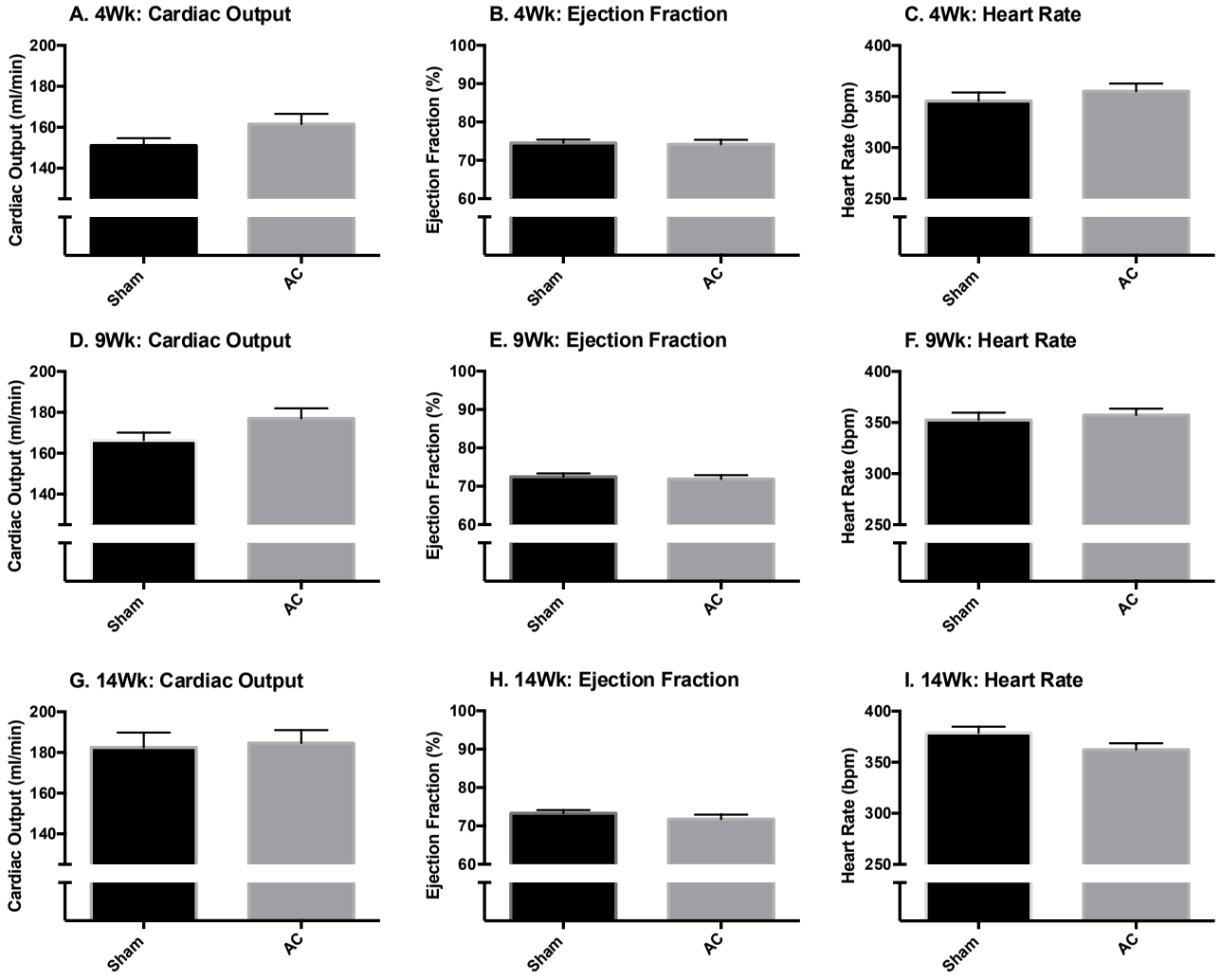


Figure 3.4: Changes in Functional Parameters at 4, 9 and 14 Weeks Post- the Surgical Induction of Hypertrophy. A. Cardiac Output at 4 Weeks Post-Surgery; B. Ejection Fraction at 4 Weeks Post-Surgery; C. Heart Rate at 4 Weeks Post-Surgery; D. Cardiac Output at 9 Weeks Post-Surgery; E. Ejection Fraction at 9 Weeks Post-Surgery; F. Heart Rate at 9 Weeks Post-Surgery; G. Cardiac Output at 14 Weeks Post-Surgery; H. Ejection Fraction at 14 Weeks Post-Surgery; I. Heart Rate at 14 Weeks Post-Surgery. 4 Weeks: Sham: n = 29; AC: n = 22; 9 Weeks: Sham: n = 29; AC: n = 32; 14 Weeks: Sham: n = 18; AC: n = 23. $Mean \pm SEM$ Unpaired two-tailed Student's t test. AC: Aortic Constriction

No change in stroke volume was observed in the AC group vs. the Sham group at 4, 9 or 14 weeks post-surgery (4 weeks: Fig 3.5A; $p = 0.28$ *vs. Sham*; 9 weeks: Fig 3.5D; $p = 0.13$ *vs. Sham*; 14 weeks: Fig 3.5D; $p = 0.31$ *vs. Sham*). This was accompanied by a trend towards an increase in end diastolic volume (EDV) in the AC group vs. the Sham at 4 weeks post-surgery (Fig 3.5B; $p = 0.10$ *vs. Sham*) but this failed to reach statistical significance. An 8 % increase in EDV was observed at 9 weeks post-surgery in the AC group vs. the Sham group (Fig 3.5E; $p < 0.05$ *vs. Sham*). No change in EDV was observed in the AC group vs. the Sham group at 14 weeks post-surgery (Fig 3.5H; $p < 0.16$ *vs. Sham*).

No change in the end systolic volume (ESV) was observed in the AC group vs. the Sham group at 4, 9 or 14 weeks post-surgery (4 weeks: Fig 3.5C; $p = 0.24$ *vs. Sham*; 9 weeks: Fig 3.5F; $p = 0.13$ *vs. Sham*; 14 weeks: Fig 3.5I; $p = 0.10$ *vs. Sham*).

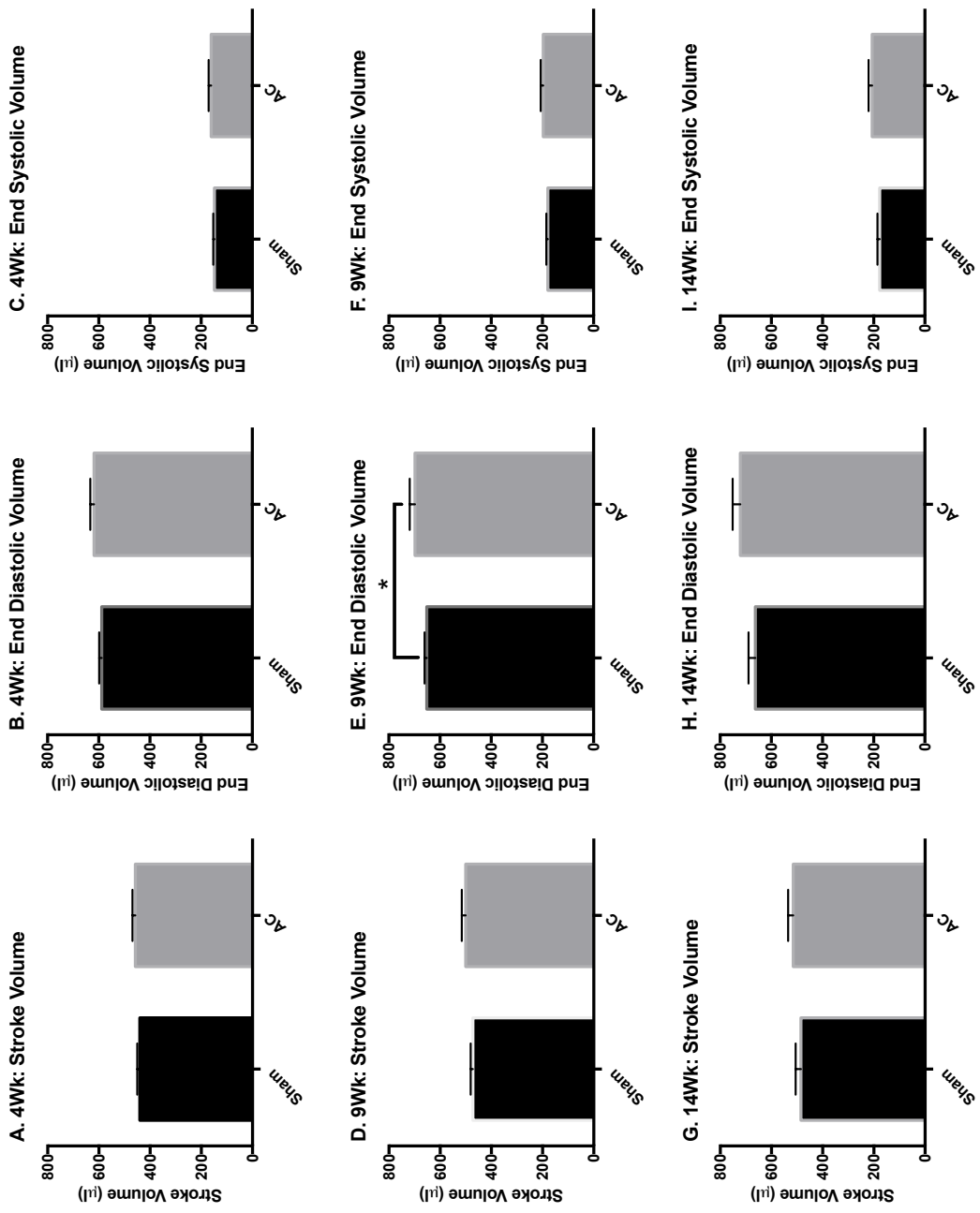


Figure 3.5: Further Changes in Functional Parameters at 4, 9 and 14 Weeks Post- the Surgical Induction of Hypertrophy. A. Stroke Volume at 4 Weeks Post-Surgery; B. End Diastolic Volume at 4 Weeks Post-Surgery; C. End Systolic Volume at 4 Weeks Post-Surgery; D. Stroke Volume at 9 Weeks Post-Surgery; E. End Diastolic Volume at 9 Weeks Post-Surgery; F. End Systolic Volume at 9 Weeks Post-Surgery; G. Stroke Volume at 14 Weeks Post-Surgery; G. End Diastolic Volume at 14 Weeks Post-Surgery; H. End Systolic Volume at 14 Weeks Post-Surgery. 4 Weeks: Sham: n = 29; AC: n = 22; 9 Weeks: Sham: n = 29; AC: n = 32; 14 Weeks: Sham: n = 18; AC: n = 23. * $p < 0.05$ *vs. Sham* $Mean \pm SEM$ Unpaired Two-Tailed Student's t test. AC: Aortic Constriction.

3.4.3 Metabolic Adaptation with the Development and Progression of Hypertrophy *in vivo*

Pyruvate dehydrogenase (PDH) flux and ^{13}C label incorporation into lactate, alanine, acetylcarnitine, citrate and glutamate were assessed in the hypertrophic heart *in vivo* at 4, 9 and 14 weeks post-surgery following the injection of either hyperpolarised [1-^{13}C]pyruvate or [2-^{13}C]pyruvate.

No change in PDH flux was identified in the AC group vs. the Control group at 4, 9 or 14 weeks post-surgery (4 weeks: Fig 5.5A; $p = 0.22$ *vs. Sham*; 9 weeks: Fig 5.5D; $p = 0.28$ *vs. Sham*; 14 weeks: Fig 5.5G; $p = 0.73$ *vs. Sham*). A 19 % increase in label incorporation into lactate was observed in the AC group vs. the Sham group at 4 weeks post-surgery (Sham: 0.0143 ± 0.008 s^{-1}; AC: 0.0170 ± 0.0009 s^{-1}; Fig 5.5B; $p < 0.05$ *vs. Sham*) and a 23 % increase in label incorporation into lactate in the AC group vs. the Sham group was observed at 9 weeks post-surgery (Sham: 0.0133 ± 0.0008 s^{-1}; AC: 0.0163 ± 0.0010 s^{-1}; Fig 5.5E; $p < 0.05$ *vs. Sham*). No change in label incorporation into lactate was observed in the AC group vs. the Sham group at 14 weeks post-surgery (Fig 5.5H; $p = 0.67$ *vs. Sham*). No change in label incorporation into alanine was observed in the AC group vs. the Sham group at 4, 9 or 14 weeks post-surgery (4 weeks: Fig 5.5C; $p = 0.56$ *vs. Sham*; 9 weeks: Fig 5.5F; $p = 0.94$ *vs. Sham*; 14 weeks: Fig 5.5I; $p = 0.29$ *vs. Sham*).

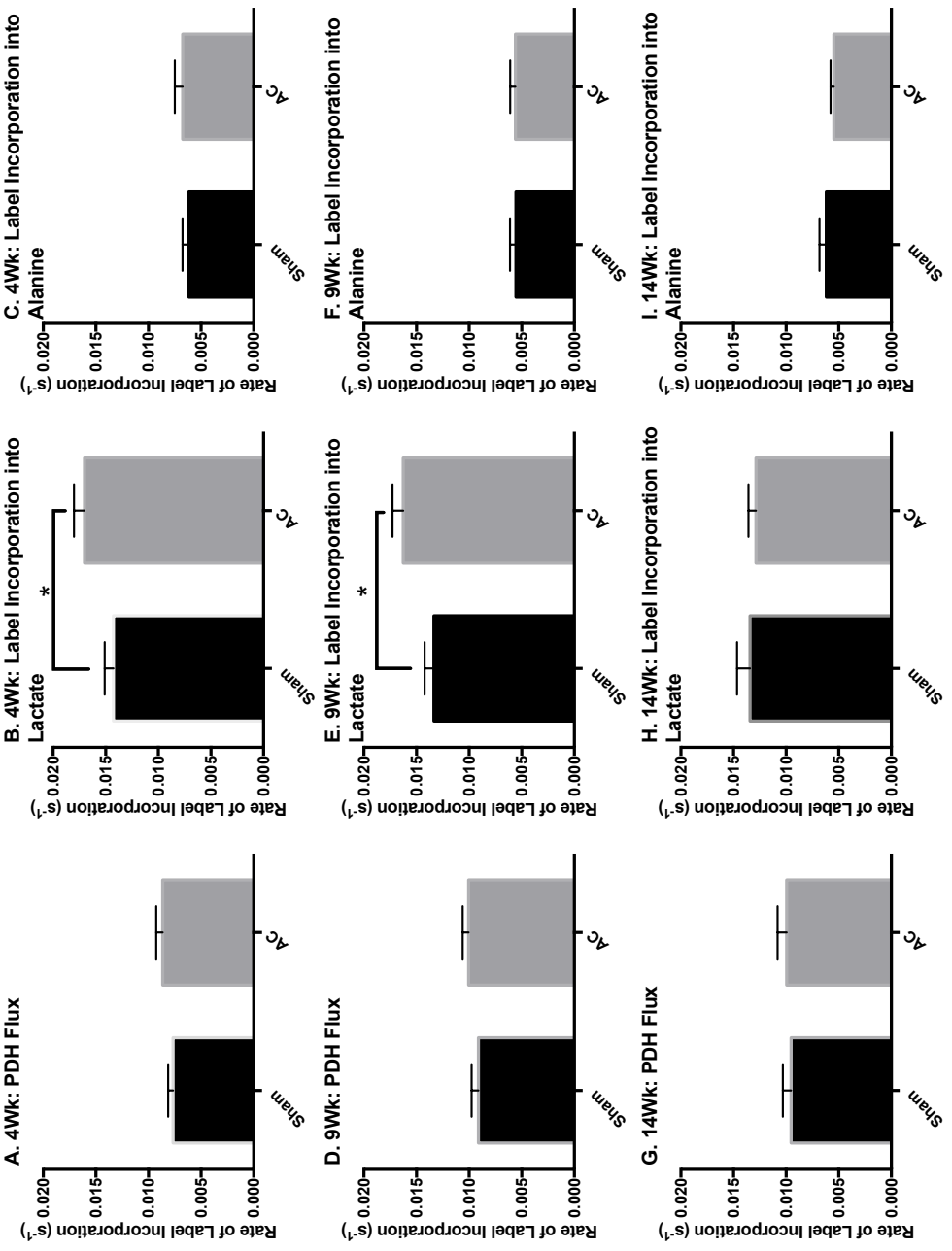


Figure 3.6: Flux through PDH and Label Incorporation into Lactate and Alanine at 4, 9 and 14 Weeks Post- the Surgical Induction of Hypertrophy. A. Pyruvate Dehydrogenase (PDH) Flux at 4 Weeks Post-Surgery; B. Lactate Production at 4 Weeks Post-Surgery; C. Alanine Production at 4 Weeks Post-Surgery; D. Pyruvate Dehydrogenase (PDH) Flux at 9 Weeks Post-Surgery; E. Lactate Production at 9 Weeks Post-Surgery; F. Alanine Production at 9 Weeks Post-Surgery; G. Pyruvate Dehydrogenase (PDH) Flux at 14 Weeks Post-Surgery; H. Lactate Production at 14 Weeks Post-Surgery; I. Alanine Production at 14 Weeks Post-Surgery. 4 Weeks: Sham: n = 29; AC: n = 32; 9 Weeks: Sham: n = 24; AC: n = 29; 14 Weeks: Sham: n = 18; AC: n = 23. * $p < 0.05$ *vs. Sham.* $Mean \pm SEM$. Unpaired Two-Tailed Student's t test; AC: Aortic Constriction.

No change in label incorporation into acetylcarnitine, citrate or glutamate was observed in the AC group vs. the Sham group at 4, 9 or 14 weeks post-surgery (4 weeks: acetylcarnitine: Fig 3.7A; $p = 0.28$ *vs. Sham*; citrate: Fig 3.7B; $p = 0.69$ *vs. Sham*; glutamate: Fig 3.7C; $p = 0.33$ *vs. Sham*; 9 weeks: acetylcarnitine: Fig 3.7D; $p = 0.86$ *vs. Sham*; citrate: Fig 3.7E; $p = 0.88$ *vs. Sham*; glutamate: Fig 3.7F; $p = 0.96$ *vs. Sham*; 14 weeks: acetylcarnitine: Fig 3.7D; $p = 0.99$ *vs. Sham*; citrate: Fig 3.7E; $p = 0.66$ *vs. Sham*; glutamate: Fig 3.7F; $p = 0.58$ *vs. Sham*).

No further change in label incorporation into acetylcarnitine, citrate or glutamate was observed following the normalisation to average PDH flux in the AC group vs. the Sham group at 4, 9 or 14 weeks post-surgery (4 weeks: acetylcarnitine: Fig 3.8A; $p = 0.94$ *vs. Sham*; citrate: Fig 3.8B; $p = 0.69$ *vs. Sham*; glutamate: Fig 3.8C; $p = 0.33$ *vs. Sham*; 9 weeks: acetylcarnitine: Fig 3.8D; $p = 0.18$ *vs. Sham*; citrate: Fig 3.8E; $p = 0.79$ *vs. Sham*; glutamate: Fig 3.8F; $p = 0.25$ *vs. Sham*; 14 weeks: acetylcarnitine: Fig 3.8G; $p = 0.79$ *vs. Sham*; citrate: Fig 3.8H; $p = 0.66$ *vs. Sham*; glutamate: Fig 3.8I; $p = 0.42$ *vs. Sham*).

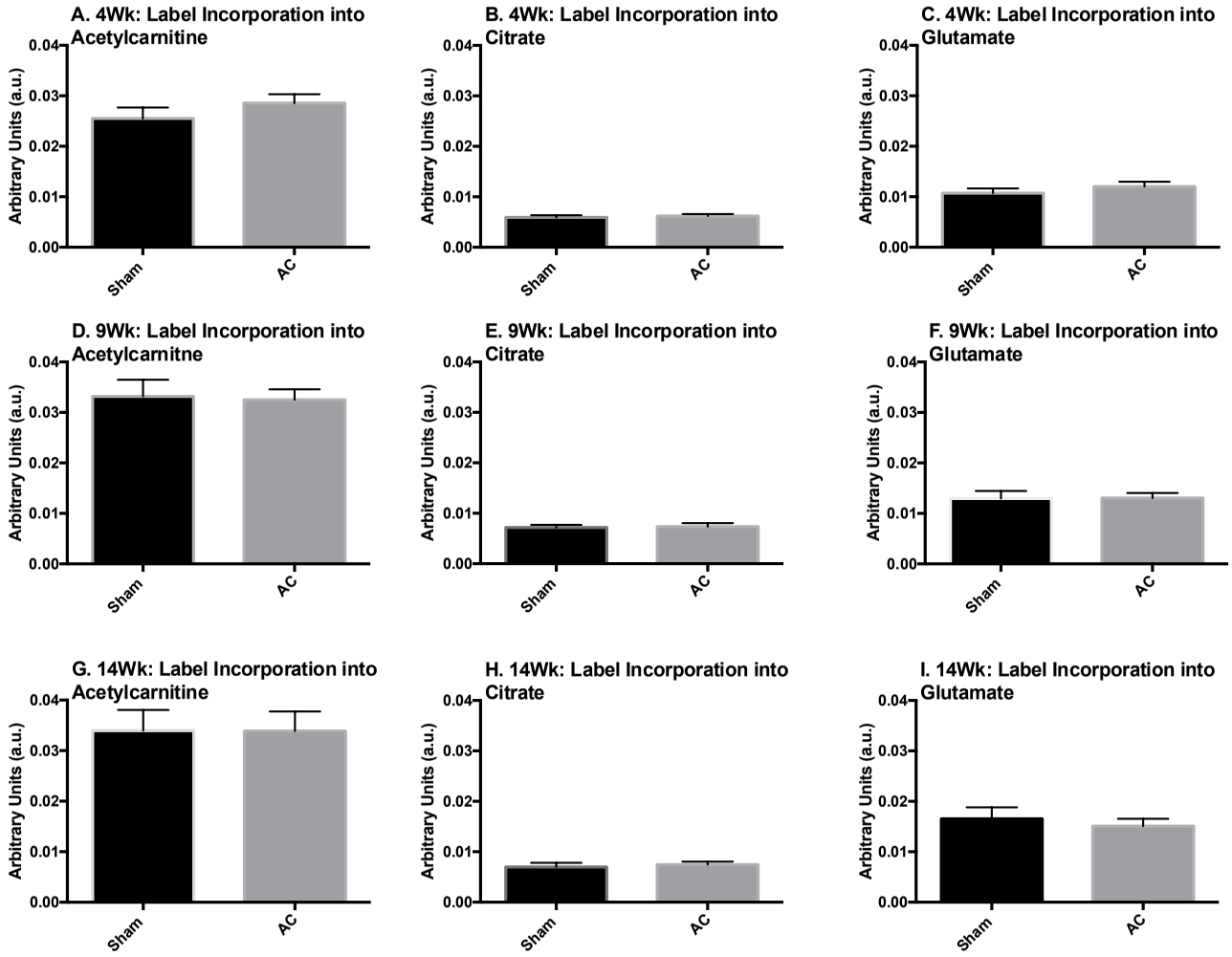


Figure 3.7: Label Incorporation into Acetylcarnitine, Citrate and Glutamate at 4, 9 and 14 Weeks Post- the Surgical Induction of Hypertrophy. A. Label Incorporation into Acetylcarnitine at 4 Weeks Post-Surgery; B. Label Incorporation into Citrate at 4 Weeks Post-Surgery; C. Label Incorporation into Glutamate at 4 Weeks Post-Surgery; D. Label Incorporation into Acetylcarnitine at 9 Weeks Post-Surgery; E. Label Incorporation into Citrate at 9 Weeks Post-Surgery; F. Label Incorporation into Glutamate at 9 Weeks Post-Surgery; G. Label Incorporation into Acetylcarnitine at 14 Weeks Post-Surgery; H. Label Incorporation into Citrate at 14 Weeks Post-Surgery; I. Label Incorporation into Glutamate at 14 Weeks Post-Surgery. 4 Weeks: Sham: n = 18; AC: n = 21. 9 Weeks: Sham: n = 12; AC: n = 17; 14 Weeks: Sham: n = 10; AC: n = 14. $Mean \pm SEM$ Unpaired Two-Tailed Student's t test. AC: Aortic Constriction

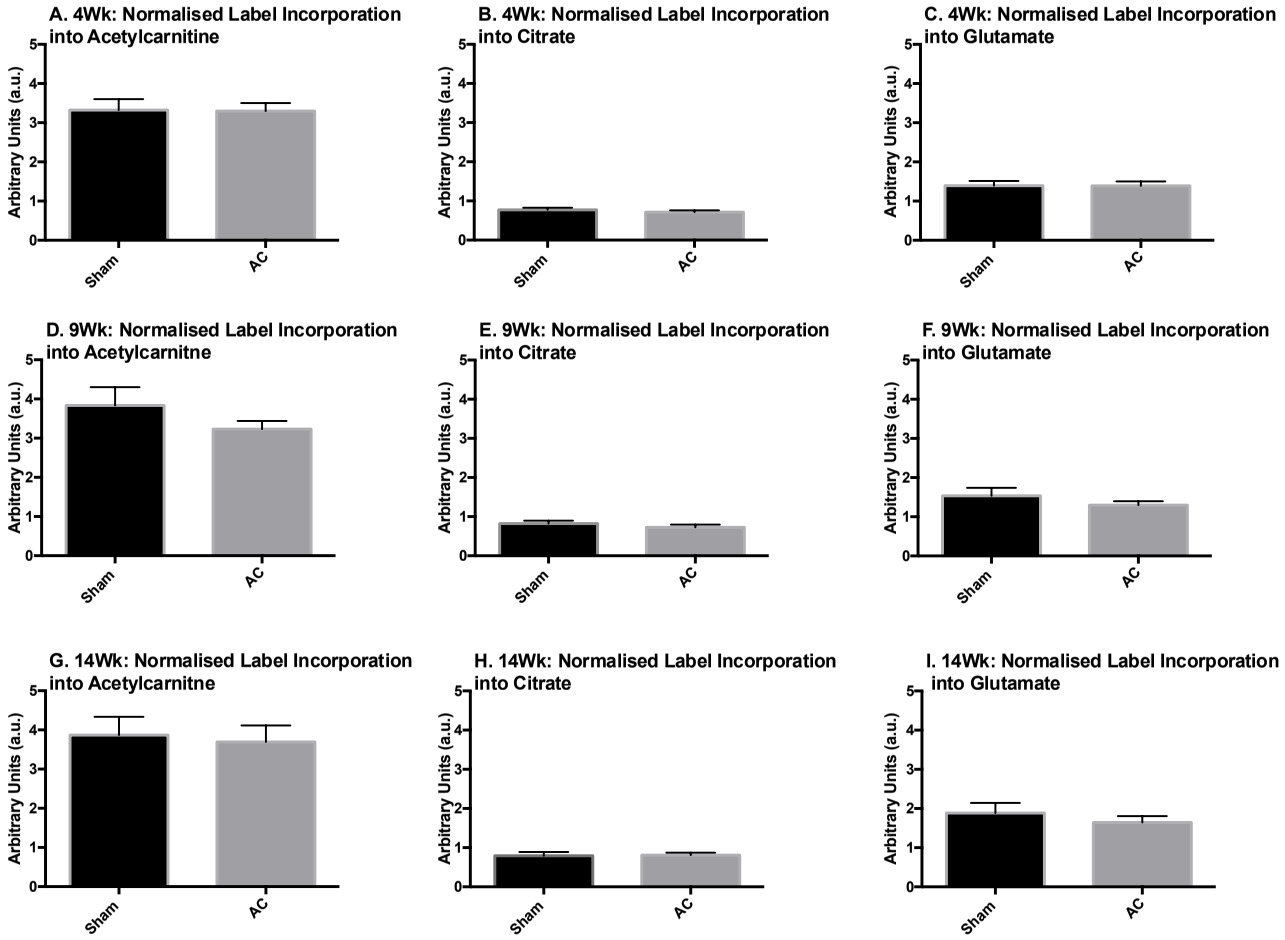


Figure 3.8: Label Incorporation into Acetylcarnitine, Citrate and Glutamate at 4, 9 and 14 Weeks Post- the Surgical Induction of Hypertrophy Normalised to Average Pyruvate Dehydrogenase (PDH) Flux. A. Normalised Label Incorporation into Acetylcarnitine at 4 Weeks Post-Surgery; B. Normalised Label Incorporation into Citrate at 4 Weeks Post-Surgery; C. Normalised Label Incorporation into Glutamate at 4 Weeks Post-Surgery; D. Normalised Label Incorporation into Acetylcarnitine at 9 Weeks Post-Surgery; E. Normalised Label Incorporation into Citrate at 9 Weeks Post-Surgery; F. Normalised Label Incorporation into Glutamate at 9 Weeks Post-Surgery; G. Normalised Label Incorporation into Acetylcarnitine at 14 Weeks Post-Surgery; H. Normalised Label Incorporation into Citrate at 14 Weeks Post-Surgery; I. Normalised Label Incorporation into Glutamate at 14 Weeks Post-Surgery. 4 Weeks: Sham: n = 18; AC: n = 21. 9 Weeks: Sham: n = 12; AC: n = 17; 14 Weeks: Sham: n = 10; AC: n = 14. $Mean \pm SEM$ Unpaired Two Tailed Student's t test. AC: Aortic Constriction.

3.4.4 Alterations in Glycolytic Flux in the Hypertrophied Heart at 10 Weeks Post-Surgery and the Ability of the Hypertrophied Heart to Recover from Ischemia

3.4.4.1 Metabolic Changes and Cardiac Function in the Hypertrophied Heart Following Ischemia Reperfusion

A 21 % increase in pre-ischemic glycolytic flux was observed in the AC group relative to the Sham group at 10 weeks post-surgery (Sham: 0.7741 ± 0.054 s^{-1}; AC: 0.9346 ± 0.045 s^{-1}; Fig 3.9A; $p < 0.05$ *vs. Sham*). No change in ischemic or post ischemic glycolytic flux was observed in the AC group vs. the Sham group (ischemia: Fig 3.9B; $p = 0.31$ *vs. Sham*; post-ischemia: Fig 3.9C; $p = 0.76$ *vs. Sham*).

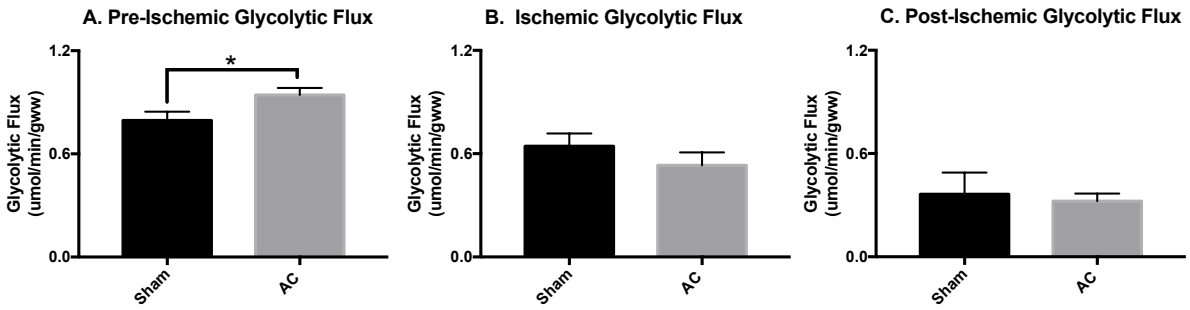


Figure 3.9: Insulin-Stimulated Glycolytic Flux in the Hypertrophied Heart at 10 Weeks Post- the Surgical Induction of Hypertrophy. A. Pre-Ischemic Glycolytic Flux. B. Ischemic Glycolytic Flux. C. Post-Ischemic Glycolytic Flux. Sham: n = 8; AC: n = 9; * $p < 0.05$ *vs. Sham*; Unpaired Two-Tailed Student's t test. $Mean \pm SEM$. AC: Aortic Constriction.

No change in average pre-ischemic or post-ischemic function represented by rate pressure product (RPP; Fig 3.10A) was observed in the AC group vs. the Sham group (pre-ischemic: Fig 3.10B; $p = 0.23$ *vs. Sham*; post-ischemic: Fig 3.10C; $p = 0.7$ *vs. Sham*). This was accompanied by no change in average pre-ischemic or post-ischemic left ventricular developed pressure (pre-ischemic: Fig 3.11B; $p = 0.34$ *vs. Sham*; post-ischemic: Fig 3.11C; $p = 0.78$ *vs. Sham*) or heart rate (pre-ischemic: Fig 3.12C; $p = 0.65$ *vs. Sham*; post-ischemic: Fig 3.12C; $p = 0.13$ *vs. Sham*) in the AC group vs. the Sham group.

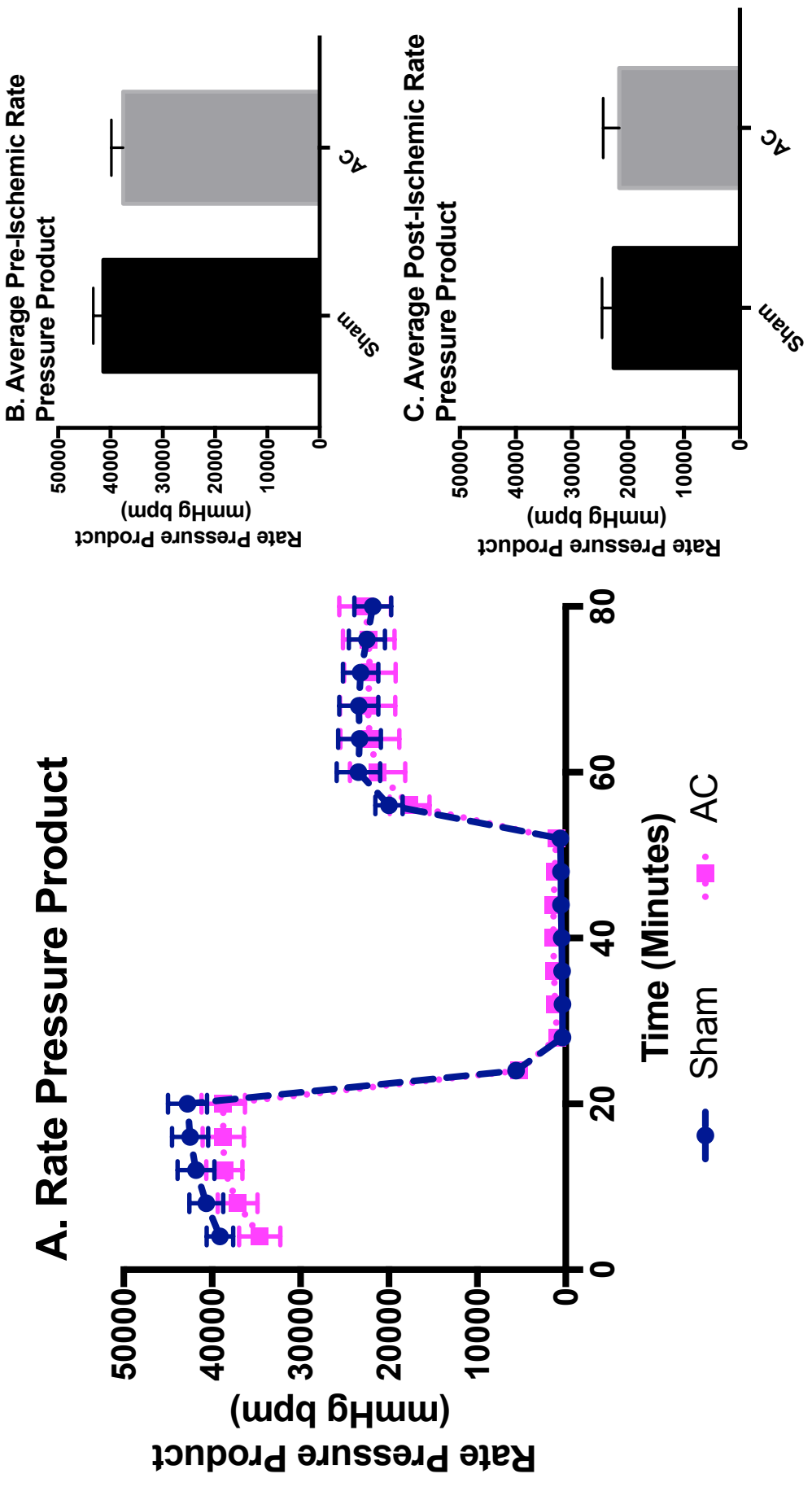


Figure 3.10: The Recovery of Cardiac Function Following Ischemia in the Hypertrophied Heart at 10 Weeks Post- the Surgical Induction of Hypertrophy. A. Rate Pressure Product. B. Average Pre-Ischemic Rate Pressure Product. C. Average Post-Ischemic Rate Pressure Product. Sham: n = 8; AC: n = 9. Unpaired Two Tailed Student's t-test. $Mean \pm SEM$. Aortic Constriction.

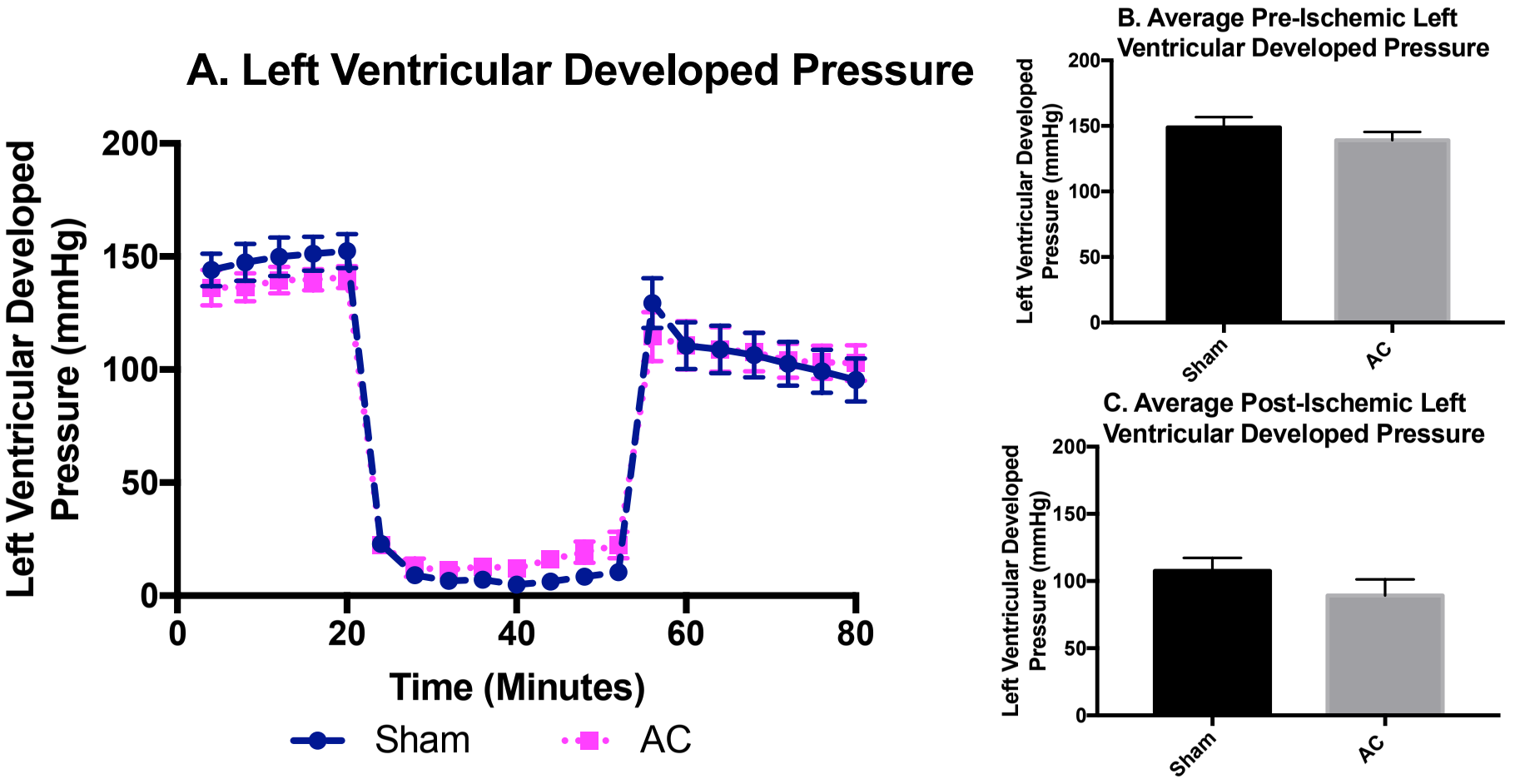


Figure 3.11: The Recovert of Left Ventricular Pressure Following Ischemia in the Hypertrophied Heart at 10 Weeks Post- the Surgical Induction of Ischemia. A. Left Ventricular Developed Pressure. B. Average Pre-Ischemic Left Ventricular Developed Pressure. C. Average Post-Ischemic Left Ventricular Developed Pressure. Sham: n = 8; AC: n = 9. Unpaired Two-Tailed Student's t test. $Mean \pm SEM$. AC: Aortic Constriction.

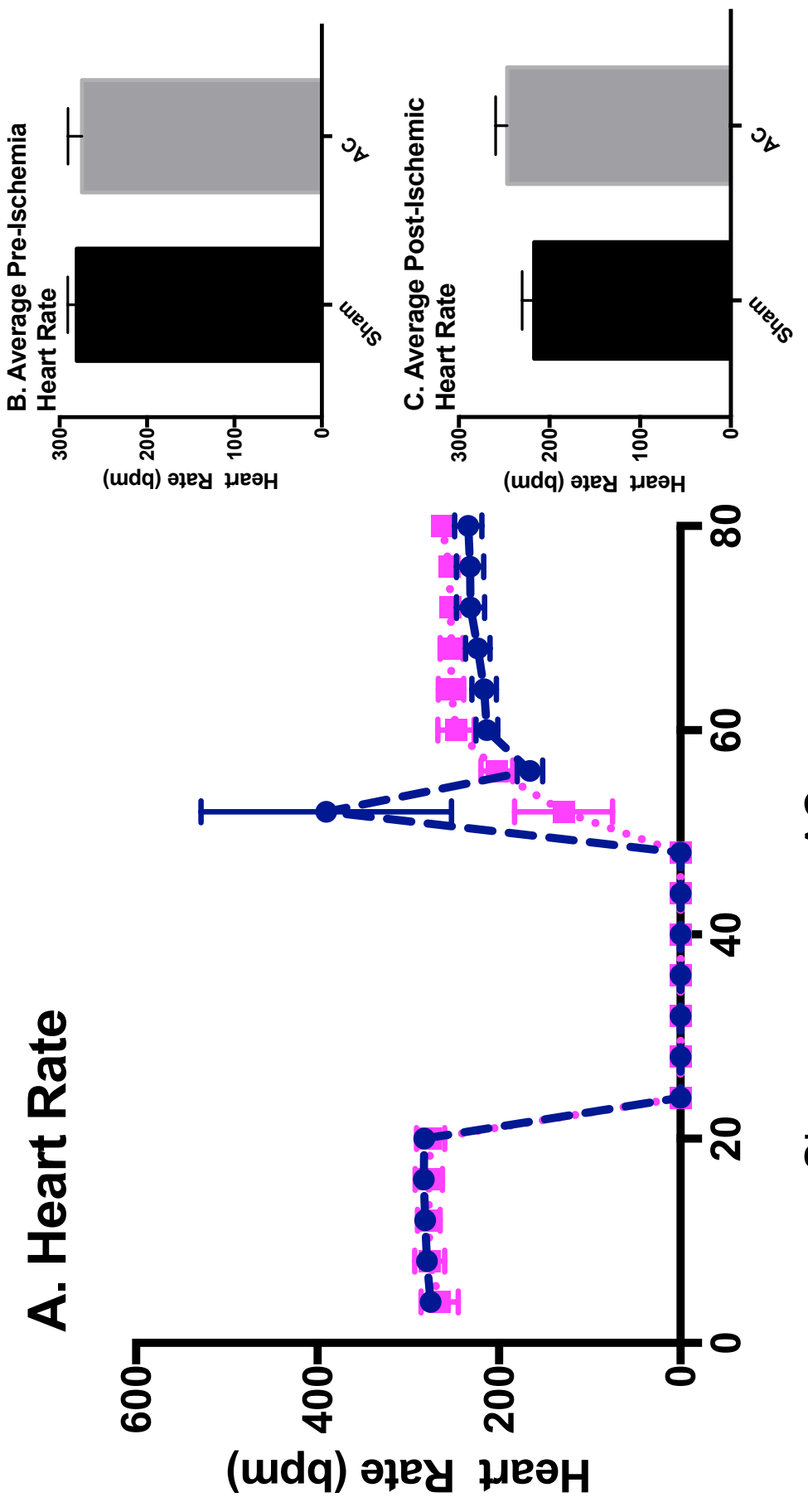


Figure 3.12: The Recovery of Heart Rate following Ischemia in the Hypertrophied Heart at 10 Weeks Post- the Surgical Induction of Hypertrophy. A. Heart Rate. B. Average Pre-Ischemic Heart Rate. C. Average Post-Ischemic Heart Rate. Sham: n = 8; AC: n = 9; Unpaired, Two-Tailed Student's t test. $Mean \pm SEM$. AC: Aortic Constriction.

No change in average pre-ischemic end disatolic pressure (EDP) was observed in the AC group vs. the Sham group (Fig 3.13B; $p = 0.28$ *vs. Sham*). A significant increase in EDP was observed in the AC group relative to the Sham group from 24 minutes post-the induction of ischemia (Fig 3.13A). A 31 % increase in average EDP was observed during ischemia in the AC group accompanied a 72% increase in average post-ischemic EDP relative to the Sham group (ischemic: Sham: 23 ± 4 mmHg; AC: 42 ± 6 mmHg; Fig 3.13C; $p < 0.05$ *vs. Sham*; post-ischemic: Sham: 47 ± 5 mmHg; AC: 81 ± 10 mmHg; Fig 3.13D; $p < 0.05$ *vs. Sham*).

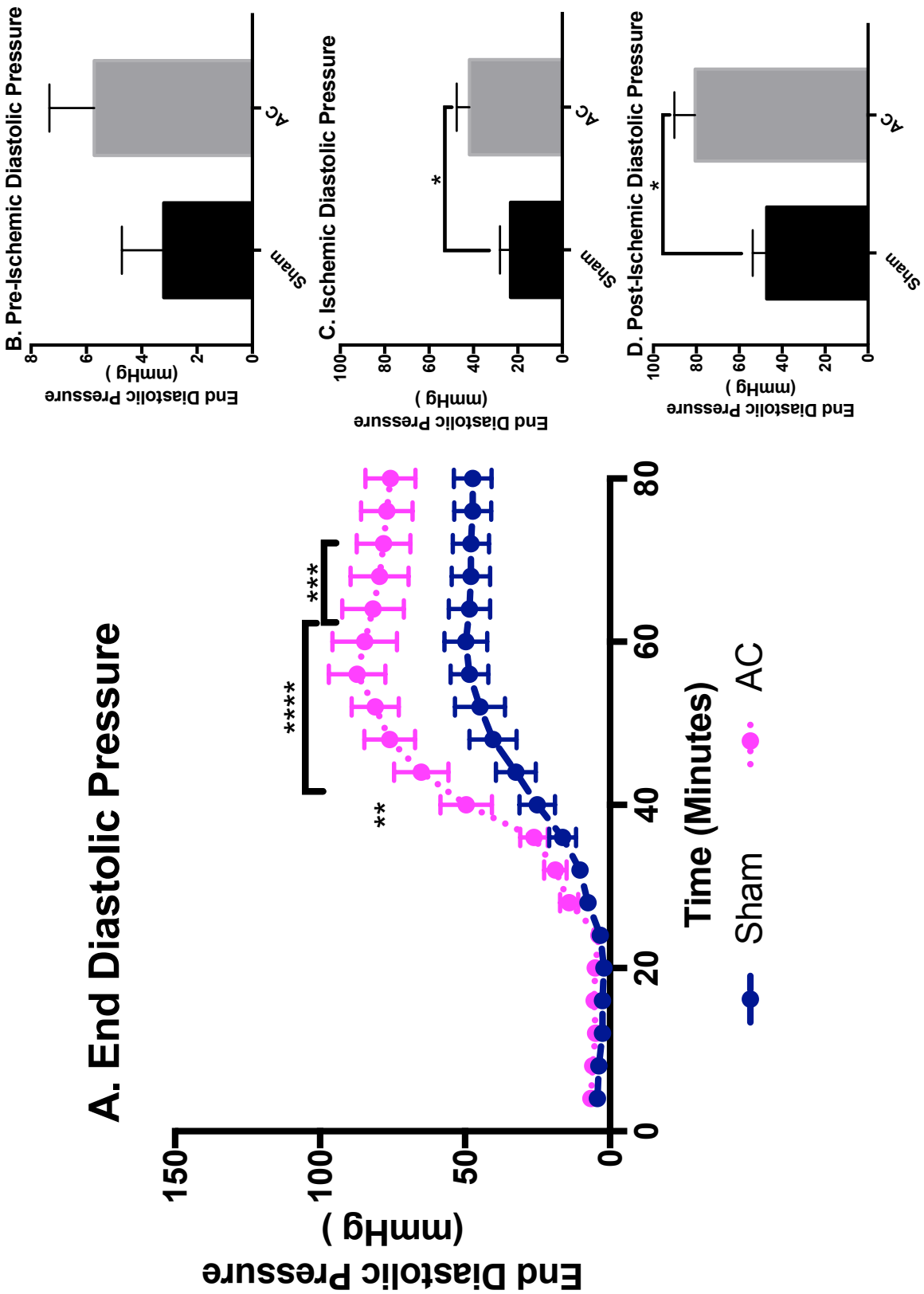


Figure 3.13: The Recovery of End Distolic Pressure Following Ischemia in the Hypertrophied Heart at 10 Weeks Post- the Surgical Induction of Hypertrophy. A. End Diastolic Pressure. B. Average Pre-Ischemic End Diastolic Pressure. C. Average Post-Ischemic Diastolic Pressure. Sham: n = 8; AC: n = 9. * $p < 0.05$ *vs. Sham*; ** $p < 0.01$ *vs. Sham* *** $p < 0.005$ *vs. Sham*; **** $p < 0.001$ *vs. Sham*. Unpaired Two-Tailed Student's t test. $Mean \pm SEM$. AC: Aortic Constriction.

3.4.4.2 The Ability of the Hypertrophied Heart to Recover from Cardiac Hypertrophy

To better understand the ability of the heart to recover from ischemia, the functional paramaters were investigated at 1 minute (immediately post-recovery), 3 minutes (initial stages of recovery) and 30 minutes post-surgery (at the end of the recovery period).

No change in rate pressure product (RPP) was observed in the AC group vs. the Sham group at 1 minute, 3 minutes or 30 minutes post-ischemia (1 minute: Fig 3.14A; $p = 0.51$ *vs. Sham*; 3 minutes: Fig 3.14D; $p = 0.49$ *vs. Sham*; 30 minutes: Fig 3.14G; $p = 0.70$ *vs. Sham*). A 33 % reduction in left ventricular developed pressure (LVDP) was observed in the AC group vs. the Sham group at 1 minute post-ischemia accompanied by a 66 % increase in heart rate in the AC group vs. the Sham, but this failed to reach statistical significance (LVDP: Sham: 150 ± 13 mmHg; AC: 100 ± 14 mmHg; Fig 3.14B; $p < 0.05$ *vs. Sham*; HR: Fig 3.14C; $p = 0.06$ *vs. Sham*).

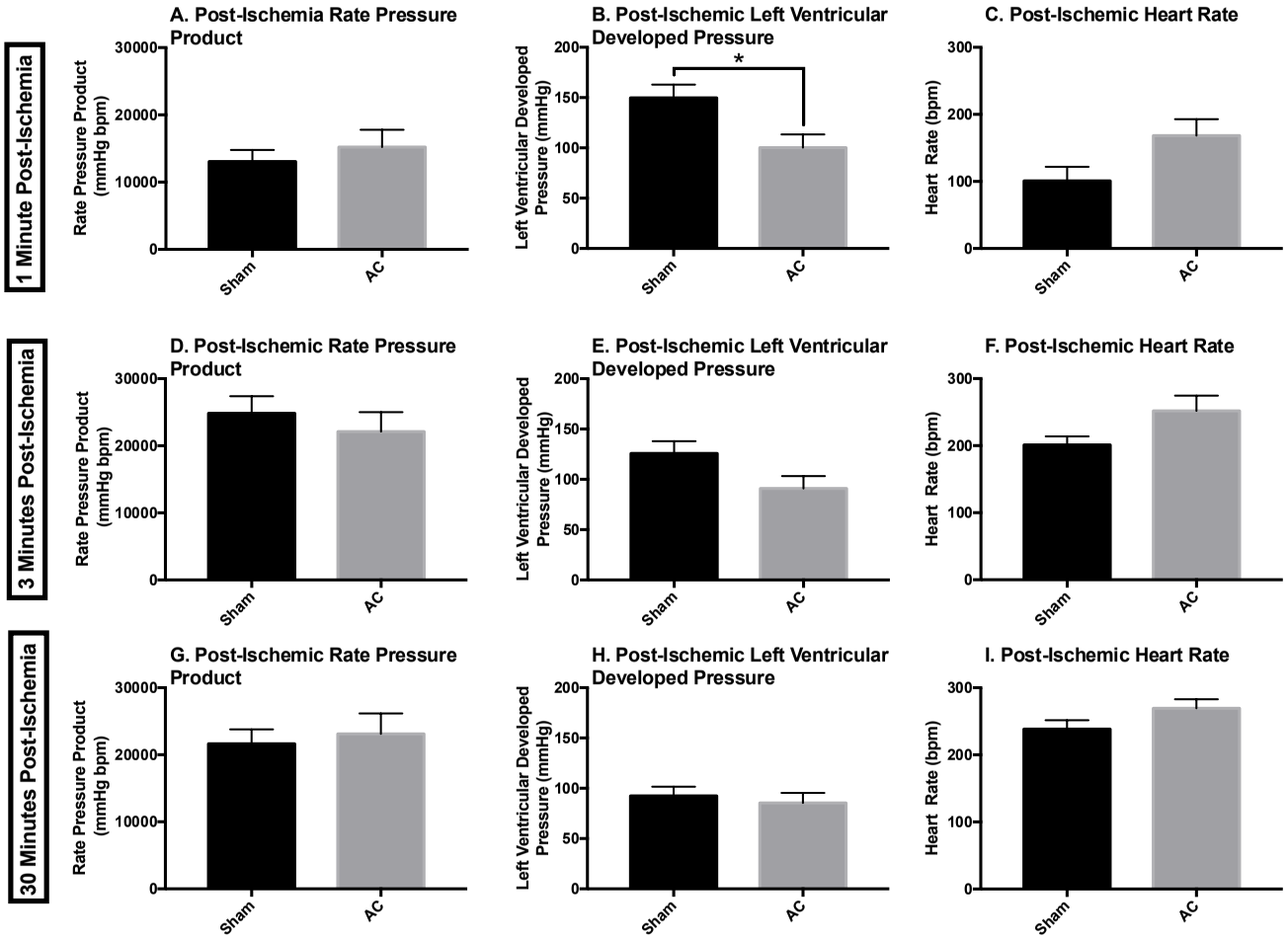


Figure 3.14: The Ability of the Hypertrophied Heart to Recover from Ischemia at 10 Weeks Post- the Surgical Induction of Hypertrophy. A. Rate Pressure Product at 1 Minute Post-Ischemia. B. Left Ventricular Developed Pressure at 1 Minute Post-Ischemia. C. Heart Rate at 1 Minute Post-Ischemia. D. Rate Pressure Product at 3 Minutes Post-Ischemia. E. Left Ventricular Developed Pressure at 3 Minutes Post-Ischemia. F. Heart Rate at 30 Minutes Post-Ischemia. G. Rate Pressure Product at 30 Minutes Post-Ischemia. H. Left Ventricular Developed Pressure at 30 Minutes Post-Ischemia. I. Heart Rate at 30 Minutes Post-Ischemia. Sham: n = 8; AC: n = 9; * $p < 0.05$ *vs. Sham*; Unpaired Two-Tailed Student's t-test. $Mean \pm SEM$. AC: Aortic Constriction.

A 28 % reduction in LVDP was sustained in the AC group vs. the Sham at 3 minutes post-ischemia accompanied by a 25 % increase in heart rate but both failed to reach statistical significance (LVDP: Fig 3.14E; $p = 0.06$ *vs. Sham*; HR: Fig 3.14F; $p = 0.07$ *vs. Sham*). No change in either LVDP or HR was observed in the AC group vs. the Sham group at 30 minutes post-ischemia (LVDP: Fig 3.14H; $p = 0.62$ *vs. Sham*; HR: Fig 3.14I; $p = 0.13$ *vs. Sham*).

The percentage recovery of individual functional parameters was calculated relative to the pre-ischemic function taken at one minute prior to ischemia. The percentage recovery of the cardiac function, represented by RPP, was unchanged the AC group when compared to the Sham group at 1, 3 and 30 minutes post-surgery (1 minute: Fig 3.15A; $p = 0.31$ *vs. Sham*; 3 minutes: Fig 3.15D; $p = 0.82$ *vs. Sham*; 30 minutes: Fig 3.15G; $p = 0.33$ *vs. Sham*). A 31 % reduction in the recovery of LVDP was observed in the AC group relative to the Sham group at 1 minute post-surgery accompanied by a 75 % elevation in the percentage recovery of heart rate within the AC group vs. the Sham group (LVDP: Sham: 100 ± 10 %; AC: 69 ± 9 %; Fig 3.15B; $p < 0.05$ *vs. Sham*; HR: Sham: 36 ± 8 %; AC: 62 ± 8 %; Fig 3.15C; $p < 0.05$ *vs. Sham*). No further differences in the recovery of LVDP was observed in the AC group relative to the Sham group at 3 minutes or 30 minutes post-ischemia (3 minutes: Fig 3.15E; $p = 0.14$ *vs. Sham*; 30 minutes: Fig 3.15H; $p = 0.98$ *vs. Sham*). However, a 31 % increase in the recovery of heart rate was observed in the AC group vs. the Sham group at 3 minutes post-ischemia (Sham: 71 ± 4 %; AC: 93 ± 4 %; Fig 3.15F; $p < 0.01$ *vs. Sham*) and an 18 % increase in percentage heart rate recovery in the AC group vs. Sham group at 30 minutes post-ischemia (Sham: 85 ± 5 %; AC: 100 ± 4 %; Fig 3.15I; $p < 0.05$ *vs. Sham*).

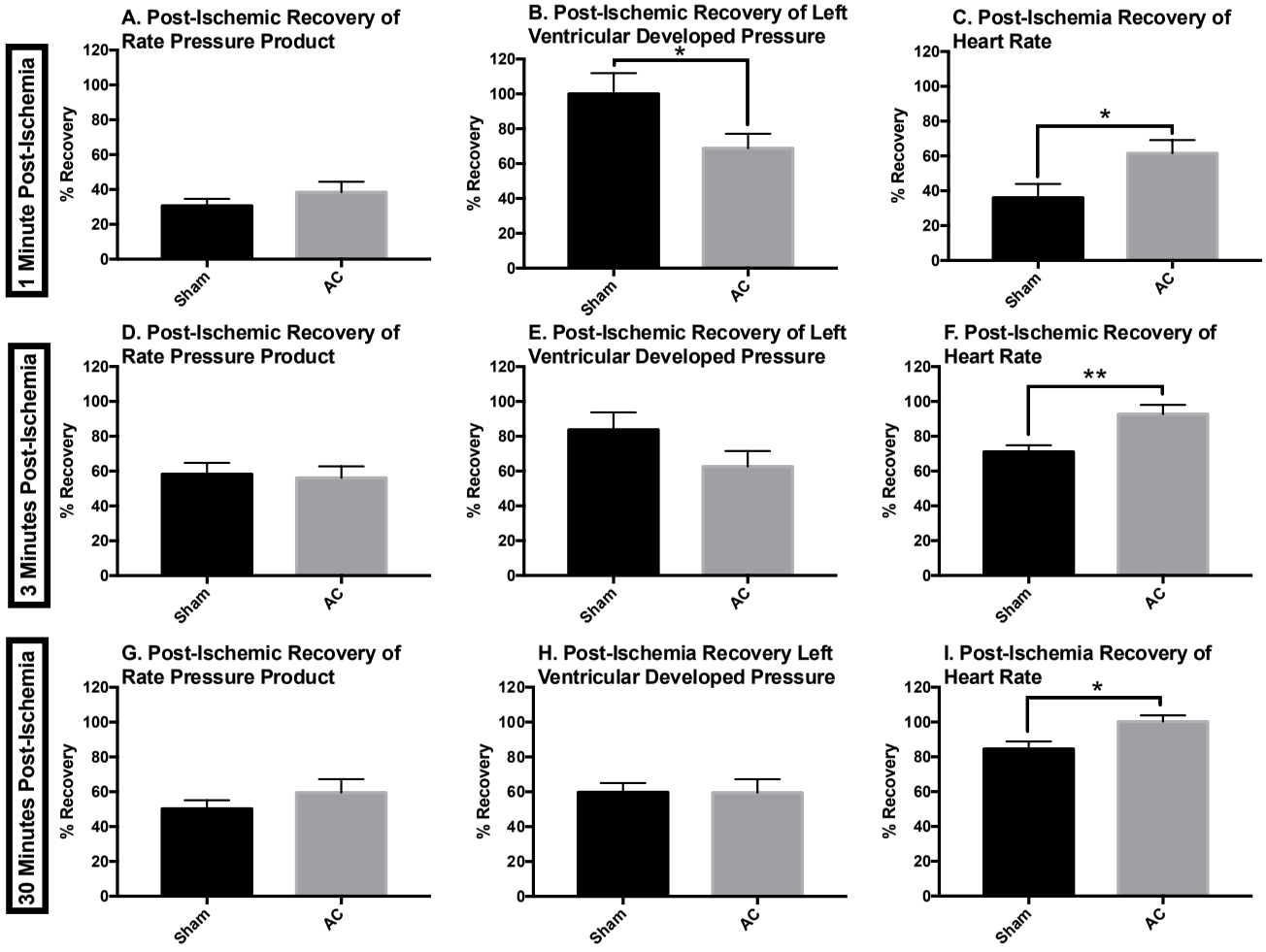


Figure 3.15: The Percentage Recovery of the Hypertrophied Heart Following Ischemia Re-perfusion at 10 Weeks Post-Surgery. A. Percentage Recovery of Rate Pressure Product at 1 Minute Post-Ischemia. B. Percentage Recovery of Left Ventricular Developed Pressure at 1 Minute Post-Surgery. C. Percentage Recovery of Heart Rate at 1 Minute Post-Surgery. D. Percentage Recovery of Rate Pressure Product at 3 Minutes Post-Ischemia. E. Percentage Recovery of Left Ventricular Developed Pressure at 3 Minutes Post-Surgery. F. Percentage Recovery of Heart Rate at 3 Minutes Post-Surgery. G. Percentage Recovery of Rate Pressure Product at 30 Minutes Post-Ischemia. H. Percentage Recovery of Left Ventricular Developed Pressure at 30 Minutes Post-Surgery. I Percentage Recovery of Heart Rate at 30 Minutes Post-Surgery. Sham: n = 8; AC: n = 9; * $p < 0.05$ *vs. Sham*; ** $p < 0.01$ *vs. Sham*. Unpaired Two-Tailed Student's t test. $Mean \pm SEM$. AC: Aortic Constriction.

3.4.4.3 Alterations in Glycolytic Flux in the Hypertrophied Heart at 18 Weeks Post-Surgery

The presence of hypertrophy at 18 weeks post-surgery had no effect on glycolytic flux in the AC group vs. the Sham group (Fig 3.16A; $p = 0.53$ *vs. Sham*). The presence of insulin stimulated glycolytic flux in both the Sham and AC group (Fig 3.16A; $p < 0.05$ *vs. Basal*).

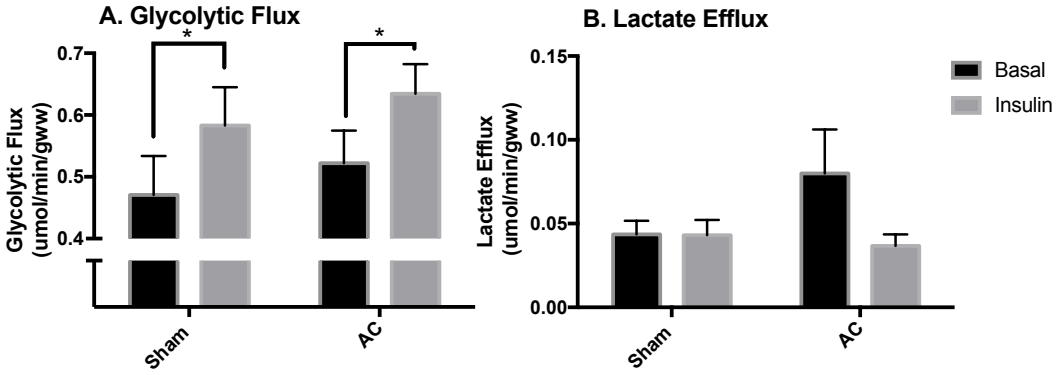


Figure 3.16: Changes in Glyolytic Flux in the Isolated Langendorff Perfused Heart at 18 Weeks Post- the Surgical Induction of Hypertrophy. A. Glycolytic Flux; B. Lactate Efflux. Glycolytic Data: Sham: n = 15; AC: n = 12. Lactate Efflux: Sham: n = 10; AC = 6. * $p < 0.05$ *vs. Sham* $Mean \pm SEM$ Two-Way ANOVA with Repeated Measures. AC: Aortic Constriction

A 23 % increase in glycolytic flux was observed within the Sham group following the addition of insulin (Basal: 0.4788 ± 0.0582 μmol min^{-1} gww^{-1}; Insulin: 0.5908 ± 0.0060 μmol min^{-1} gww^{-1}; Fig 3.16A) and a 26 % increase in glycolytic flux within the AC group in the presence of insulin (Basal: 0.5025 ± 0.0522 μmol min^{-1} gww^{-1}; Insulin: 0.6344 ± 0.0479 μmol min^{-1} gww^{-1}; Fig 3.16A). The presence of insulin had a near significant effect on lactate production ($p = 0.08$ *vs. Basal*; Fig 3.16B) whereas the presence of hypertrophy failed to reach significant on lactate efflux however, the sample size presented here is very small (Fig 3.16B; $p = 0.32$ *vs. Sham*). Increasing the sample size may provide a better understanding of the relationship between effects of hypertrophy and insulin.

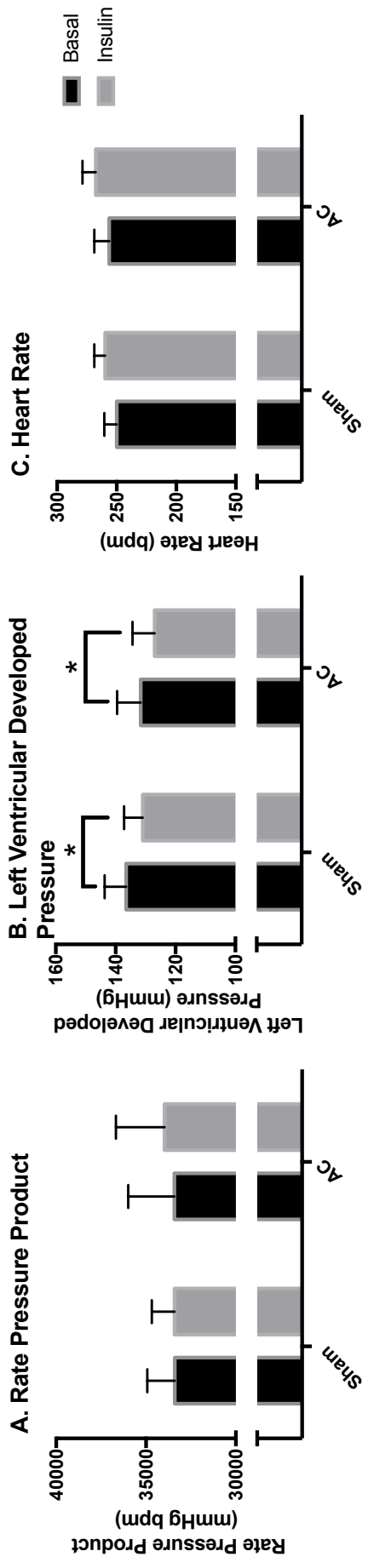


Figure 3.17: Functional Parameters in the Isolated Langendorff Perfused Heart at 18 Weeks Post- the Surgical Induction of Hypertrophy. A. Rate Pressure Product (RPP); B. Left Ventricular Developed Pressure (LVDP); C. Heart Rate (HR). Sham: n = 14; AC: n = 12. * $p < 0.05$ *vs. Sham*. $Mean \pm SEM$ Two-Way ANOVA with Repeated Measures. AC: Aortic Constriction

No change in either basal rate pressure product (RPP) or insulin-stimulated RPP was observed in the AC group vs. the Sham group at 18 weeks post-surgery (Fig 3.17A; $p = 0.92$ *vs. Sham*). Insulin had no effect on RPP irrespective of hypertrophic development (Fig 3.17A; $p = 0.68$ *vs. Basal*). The addition of insulin induced a significant change in left ventricular developed pressure (LVDP; $p < 0.05$ *vs. Basal*; Fig 3.17B) and was associated with a 4 % reduction in LVDP within the Sham group (Basal: 136 ± 7 mmHg; Insulin: 131 ± 6 mmHg; Fig 3.17B) and a 3 % reduction in LVDP in the AC group (Basal: 131 ± 8 mmHg vs. Insulin: 127 ± 7 mmHg; Fig 3.17B). This was accompanied by a 4 % increase in heart rate within the Sham group following the addition of insulin and a 5 % increase in insulin-stimulated heart rate in the AC group but this failed to reach statistical significance (Fig 3.17C; $p = 0.06$ *vs. Basal*). Cardiac function was compensated overall.

3.5 Discussion

3.5.1 A Summary of Findings

Consistent with the development of hypertrophy, a significant increase in left ventricular (LV) mass and LV mass to body weight ratio was observed following aortic constriction at 4, 9 and 14 weeks post-surgery. End diastolic volume (EDV), end systolic volume (ESV) and stroke volume remained largely unchanged at 4, 9 and 14 weeks post-surgery, however, a significant increase in end diastolic volume was observed at 9 weeks post-surgery likely due to changes in myocardial structure such as hypertrophy of the cardiomyocytes and the development of fibrosis within the ventricular wall.

A slight increase in cardiac output, which failed to reach statistical significance was observed in the AC group at 4 and 9 weeks post-surgery suggesting a compensatory response to increased systemic pressure. No change in ejection fraction was observed in the AC group despite evidence of hypertrophic development at 4, 9 and 14 weeks and heart rate remained unchanged at 4 and 9 weeks post-surgery. A decrease in heart rate was observed in the AC group at 14 weeks post-surgery.

Metabolically, a significant increase in lactate production was observed in the hypertrophic heart at 4 and 9 weeks post-surgery. This was accompanied by no change in PDH flux at either 4 or 9 weeks and no increase in label incorporation into acetylcarnitine, citrate or glutamate suggesting an increase in glycolytic flux during hypertrophic development. This was confirmed by a significant increase in pre-ischemic insulin-stimulated glycolytic flux in the perfused heart at 10 weeks post-surgery. No change in glycolytic flux was observed in the hypertrophied heart during or post-ischemia. Overall post-ischemic function, characterised by rate pressure product remained the same in the hypertrophied heart when compared to the Sham hearts, however, the way in which the heart recovered from the ischemic period differed. Recovery within the hypertrophied heart was marked by a significant increase in heart rate to compensate for a reduction in left ventricular developed pressure (LVDP). This reduction in LVDP may result from damage to the cardiac tissue during the ischemic period represented by a significant increase in end diastolic pressure during the ischemic and post-ischemic period which is representative of contrac-

ture within the left ventricle. LVDP was restored by the end of the post-ischemic period, however, heart rate remained at a higher level than that observed in the Sham group.

Interestingly, no change in lactate production or label incorporation into any other metabolites was observed in the AC group at 14 weeks post-surgery suggesting that hypertrophic development may have stabilised by 14 weeks post-surgery. This was accompanied by no change in both basal and insulin-stimulated glycolytic flux in the AC group at 18 weeks post-surgery.

3.5.2 The Initial Stages of Hypertrophic Remodelling is Associated with an Enhanced Glycolytic Dependence

Consistent with the studies previously conducted in the abdominal aorta constriction model (AC) of left ventricular hypertrophy [50, 108, 18], this study confirms an increase in left ventricular mass and heart weight to body weight ratio at 4 and 9 weeks post-surgery consistent with hypertrophic remodelling. Furthermore, the development of hypertrophy was associated with a slight increase in cardiac output at 4 and 9 weeks post-surgery representative of compensated hypertrophy. This differs considerable from the thoraic aortic constriction (TAC) model of LVH which leads to the rapid onset of heart failure with only a acute period where the heart is compensated [101].

Metabolically within the AC model, the initial stages of hypertrophic remodelling was associated with an increase in myocardial lactate production representative of an increase in glycolytic dependence, as described in our previous work summarised in Appendix A and has been widely reported both in the AC model and different models of left ventricular hypertrophy [52, 57, 42, 54]. Enhanced pre-ischemic glycolytic flux was subsequently confirmed at 10 weeks post-surgery in the perfused heart suggesting that enhanced glycolytic dependence both plays a role in remodelling the left ventricle and may aid compensation within the heart. Following ischemia, the hypertrophic heart recovered to a similar functional level to the Sham heart accompanied by a similar pattern in glycolytic flux. This is in support of the work by Allard *et al* which reported a normalisation of metabolism following increased work loads, here, glycolytic flux is normalised during the stress of

ischemia [42].

The mechanism by which the hypertrophied heart recovered functionally from the ischemic period differed from the Sham hearts. This was marked by a compensatory increase in heart rate, which allowed maintenance of cardiac function despite a reduction in left ventricular developed pressure (LVDP). The hypertrophied heart also sustained substantially more damage than the Sham heart represented by a significantly enhanced end distolic pressure (EDP). Work by Cunningham *et al* in the dioxycorticosterone-salt model of LVH reported a higher EDP within the hypertrophied heart following 15 minutes of hypoxia which they attribute to the presence of metabolic remodelling with the hypertrophied heart. Perfusion with high levels of glucose and insulin lowered the final EDP in both the control and hypertrophied heart suggesting that glucose handling plays a role in preventing damage to the left ventricle when oxygen is limiting [109]. However, within the work presented here, despite evidence of damage to the left ventricle, LVDP was restored by the end of the ischemic period, this suggests that the hypertrophied heart remains compensated at this stage but may take a longer period of time to recover from ischemia. This may be due to the development of fibrosis within the hypertrophied heart at this stage which is particularly evident in the angiotensin II (AngII) induced model of left ventricular hypertrophy [110]. Given the placement of the band between the two kidneys within the AC model, there is likely an additional stimulation of AngII within this model which may accelerate fibrosis within the myocardium leading to the effects observed here.

This work suggests that up until 10 weeks post-surgery, the heart is undergoing metabolic and functional remodelling to meet the increased demand on the heart following the induction of hypertension but is still able to cope with external stress such as ischemia.

3.5.3 No Change in Glyolytic Flux is Observed with Stabilisation of Cardiac Hypertrophy

Cardiac output is maintained at 14 weeks post-surgery but a reduction in heart rate was observed within the hypertrophied heart. This suggests that the heart is starting to stabilise and adapt to the chronic increase in systemic blood pressure. This was accompanied by no evidence of enhanced glycolytic flux, represented by no change in label incorporation into lactate *in vivo* at 14 weeks post-surgery. As there was no apparent change in function at 14 weeks post-surgery, it is possible an increased glycolytic dependence is no longer required as the heart has transitioned fully into compensation. In support of this, no change in glycolytic flux was observed at 18 weeks post-surgery. This differs from our previous work where an increased glycolytic dependence was not evident at 4 weeks post-surgery but was sustained at 14 weeks post-surgery [50]. No difference in the severity of hypertrophy was evident between this study and our previous study (Appendix A) and it may highlight the complexity and stage-specific variation in the remodelling process.

This is interesting as within the literature, increased glycolytic dependence is proposed to underpin energetic disruption within the hypertrophied heart, however, the link between altered substrate selection and impaired energetics has yet to be clarified [19]. Within the data presented here, glycolytic flux has been restored between 14 and 18 weeks post-surgery with hypertrophied hearts functioning similarly to their control during perfusion at 18 weeks post-surgery. Studies in knock-out models of GLUT 1 [54] and GLUT 4 [62] may provide further information into the mechanism by which altered substrate selection plays a role in hypertrophic remodelling. As previously discussed in Chapter 1.4.4 loss of GLUT 1, the basal glucose transporter in the heart had no effect on hypertrophic progression in the mouse model of TAC whereas the loss of GLUT 4 lead to the onset of LVH in the absence of any other factors suggesting that the insulin-induced modified substrate utilisation provides an important role in hypertrophic development [54, 62].

Within the work presented here, the addition of insulin, which globally stimulates glucose uptake, glucose oxidation and fatty acid storage, leads to an alteration in how the heart maintains a constant functional output further supporting a role of insulin in

modulating cardiac function. A reduction in left ventricular developed pressure (LVDP) was observed on the addition of insulin, accompanied by an increase in heart rate and normalisation of rate pressure product or cardiac function. Although the presence of insulin is physiologically more relevant, it suggests that inducing a different metabolic profile within the hypertrophied heart is significant in how the heart maintains functional output.

3.5.4 Conclusions and Future Perspectives

This study has focused on the glycolytic changes which coincide with structural and functional remodelling with the progression of cardiac hypertrophy. We previously hypothesised that the switch away from fatty acid oxidation towards glycolytic dependence was a key contributor to functional decline within the heart. However, this work suggests that enhanced glycolytic flux aids the initial stages of cardiac remodelling within the heart, meeting the increased energy demand to compensate for an increased workload. This appears to stabilise between 10 and 14 weeks post-surgery, with this work suggesting that the increase in glycolytic dependence is not sustained.

Outside of the role of glycolysis in hypertrophic remodelling the additional contributors to hypertrophic development have not been considered. As previously stated in Section 3.2.3, both Akki *et al* and Allard *et al* report a reduction in palmitate oxidation in the aortic constriction model at low work loads in support of a wide body of literature which hypothesis that enhanced glucose utilisation is accompanied by reduced fatty acid oxidation [107, 1, 4, 42]. No evidence of functional decline was apparent within this study, however, the mechanism by which the hypertrophied heart recovers from ischemia where shifted. Furthermore, this does not mean that the metabolic changes which occur during the developmental stages of hypertrophy do not contribute to the the onset of heart failure as hypertrophy progresses. This suggests that the progression of hypertrophy and the onset of functional decline is associated with a series of contributing factors of which metabolic remodelling is one aspect.

Following the model past 18 weeks to a minimum of 23 weeks, where Miyamoto *et*

al report the initial stages of functional decline [105], would provide an indication as to whether the hearts start to fail and what metabolic changes occur during this period. Further identification of the role of fatty acid oxidation would also provide an interesting avenue due to the tight coupling of the oxidation of fatty acids to glucose utilisation.

Chapter 4

The Effects of Acute and Chronic Up-Regulation of Pyruvate Dehydrogenase Activity on Cardiac Metabolism

4.1 Chapter Overview

This chapter investigates the metabolic effects of acute and chronic dichloroacetate (DCA) treatment on cardiac metabolism to explore the potential of DCA as a treatment for heart disease.

The role of DCA as a stimulant of pyruvate dehydrogenase (PDH) was first demonstrated in 1973 [111] since when it has been considered a promising drug for the treatment of a variety of diseases such as ischemia reperfusion injury [112], congenital hyperlactatemia [113] [114], hypertrophy [91], diabetes [115], hypercholesteremia [116, 117] and cancer [118]. DCA treatment remains widely used pre-clinically both as a tool to modulate metabolism and as a potential treatment in disease models. The effects of DCA treatment on PDH flux are well characterised, however the wider effects of DCA on the metabolic profile of the heart are poorly understood. This study aims to further clarify the effects of DCA treatment on cardiac metabolism widening the potential for its use in the treatment of heart disease.

4.2 Introduction

4.2.1 The Mechanism and Pharmacology of Dichloroacetate

Dichloroacetate (DCA) is a pyruvate mimetic which indirectly up-regulates pyruvate dehydrogenase (PDH) activity via the inhibition of the PDH regulatory enzyme pyruvate dehydrogenase kinase (PDK) [119, 120, 35]. The relative structures of pyruvate and DCA are summarised in Figure 4.1.

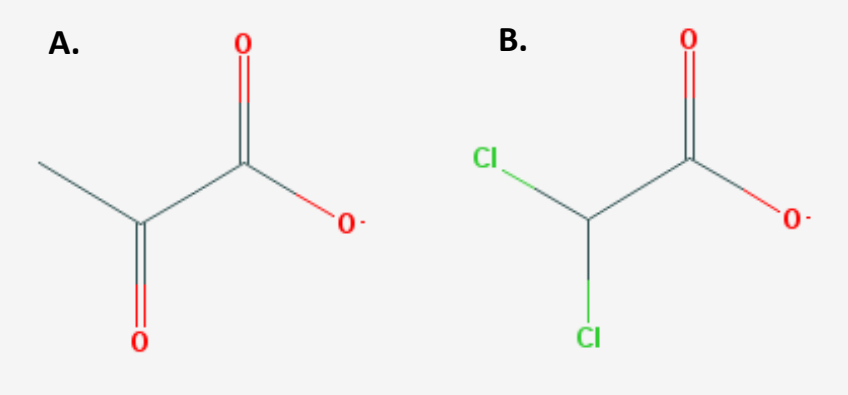


Figure 4.1: The Relative Structures of Pyruvate and DCA. A. Pyruvate. B. DCA.

Within the structure of DCA, two chloride ions replace the methyl group and the carbonyl group at the 2' position whilst the 3' carboxyl group remains intact.

The effect of DCA as a stimulant of pyruvate dehydrogenase (PDH) was discovered by Randle and Whitehouse in 1973 [111] and whilst other halogenated carboxylic analogs and DCA derivatives have also been shown to upregulate PDH flux, none are as potent as DCA. This is due in part to the rapid uptake of DCA, which strongly resembles pyruvate (Fig 4.1), into the mitochondria via the pyruvate translocator, where it accumulates resulting in rapid and effective activation of PDH via the inactivation of PDK [120]. Whitehouse *et al* propose that a concentration of 1 mmol L^{-1} is required to stimulate maximal activity of PDH [119].

The mechanism by which DCA inhibits PDK remains unknown. However, the combined use of mutation, siRNA and the elucidation of crystal structures of PDK1 and PDK3 bound to DCA has provided some insight into how DCA may act. The E1 regulatory subunit of PDH contains three different phosphorylation sites; Ser 264 (Site 1),

Ser 271 (Site 2) and Ser 203 (Site 3) and phosphorylation at any one of these sites is sufficient to inactivate PDH. The various isoforms of PDK have differing affinities for the individual phosphorylation sites and given that different isoforms are specific to different tissues and upregulated under different conditions, this may affect the tissue and situation-specific effectiveness of DCA [121, 122]. The relative affinites of PDK for the individual E1 phosphorylation sites and their locations are summarised in Figure 4.2 and Figure 4.3.

E1 Subunit Phosphorylation Sites	Order of PDK Affinity
Ser 264	PDK 2 > PDK 4 ≈ PDK 1 > PDK3
Ser 271	PDK 3 > PDK 4 > PDK 2 > PDK1
Ser 203	PDK1

Figure 4.2: A Summary of the Affinity for PDK Isoforms for Individual Phosphorylation Sites within the E1 Complex. [121]

PDK Isoform	Apparent Ki for DCA (mM)	Location	Affected By
PDK 1	1.0 ± 0.2	heart, pancreas, skeletal muscle	hypoxia
PDK 2	0.20 ± 0.05	ubiquitous	starvation, diabetes
PDK 3	8.0 ± 1.0	testes, kidney, brain	
PDK 4	0.5 ± 0.2	heart, pancreas, skeletal muscle, kidney	starvation, diabetes

Figure 4.3: A Summary of the Apparent Ki of PDK Isoforms for DCA. [122, 121]

Through mutation studies, DCA was shown to bind to the N terminus of PDK2 and inhibition of PDK2 via siRNA mimicked that of DCA treatment supporting the proposition that DCA acts through a PDK-mediated mechanism [121, 118]. A shielded binding pocket for DCA was further identified within the N terminal domain of PDK1 from the crystal structure of PDK1 in the DCA-bound conformation but no mechanism for inhibition was identified. The degree of shielding of the DCA binding site may account for the differing affinities of DCA as an inhibitor of the different isoforms of PDK. The apparent Ki for DCA of each of the PDK isoforms are summarised in Figure 4.3 [121].

4.2.2 The Physiological Effects of Dichloroacetate

A wide range of studies have assessed the physiological effects of DCA. However, the concentrations, length of treatment and organs they are assessed in vary. Although, this provides insight into the potential targets and mechanisms by which DCA acts,

the metabolic profile of different organs varies significantly. Pyruvate dehydrogenase (PDH) remains the most studied target of DCA although additional targets of DCA such as thiamine-containing enzymes [123] and hydroxymethylglutatyl coenzyme A (HMG-CoA) reductase [124] in the liver have been proposed. Given the integrative nature of metabolism both within individual organs and systemically it is difficult to determine what is a direct target of DCA and what is a secondary effect. This section provides a comprehensive review of the effects of DCA treatment on PDH but the different variables, and often conflicting results should be noted.

Physiologically, the relative states of the PDH regulatory enzymes, PDK and pyruvate dehydrogenase phophatase (PDP) are dependent on the relative concentrations of [ATP]:[ADP], [NADH]:[NAD^+], [acetyl-CoA]:[CoA] and pyruvate [34, 35]. High concentrations of ATP relative to ADP promote PDK's inhibition of PDH flux whilst enhanced ADP concentrations inhibit PDK and promote PDH flux [34]. ATP has been shown to be noncompetative with DCA in terms of PDK inhibition whereas the concentration of ADP appears to have a synergistic effect with DCA on PDK inhibition by DCA [119, 125]. Work by Pratt *et al* proposed that DCA associates with the ADP-bound conformation of PDH rather than the free enzyme itself supported by no evidence of competitive inhibition with ATP in the presence of DCA [125]. This suggests that DCA-related inhibition of PDK would be enhanced in a low energy state where ADP concentrations are dominant such as fasting or post-exercise. However, Evans *et al* report that chronic dosing with DCA appears to increase the half-life of DCA activation possibly through inhibition of its own metabolism [126, 120]. This is supported by a sustained decrease in plasma lactate and alanine concentrations for up to 2 weeks following termination of DCA treatment in both diabetic animals and humans [127, 126, 114].

4.2.3 The Effects of Dichloroacetate Treatment on Metabolism

The global mechanism by which dichloroacetate (DCA) affects cellular metabolism is poorly clarified and aside from its effects on pyruvate dehydrogeanse (PDH) up-regulation,

which are well characterised, DCA treatment has been reported to broadly alter the metabolic state of the cell affecting fatty acid, glucose, chlolesterol and glycogen metabolism [128]. It is unclear whether DCA directly affects the enzymes involved in these pathways or whether it is a key example of the integrated nature of metabolism where alteration in the activity of PDH, a key regulatory enzyme in metabolism, impacts cardiac metabolism as a whole. It has been proposed that DCA acts on enzymes containing thiamine including α-ketoglutarate (α-KG) dehydrogenase, a key regulatory enzyme in the tricarboxylic (TCA) cycle [123] and extended DCA treatment in humans is associated with a thiamine deficiency [113]. In support, α-KG dehydrogenase inhibition has been associated with the onset of neurodegenerative disease [129] whilst perpherial neuropathy is reported as a side effect of DCA treatment [116, 130, 120].

4.2.3.1 The Effects of Dichloroacetate on Glucose Metabolism

Dichloroacetate (DCA) treatment has been reported to have a range of effects on glycolytic flux, in some cases it has been shown to be increased, others it has been shown to decrease or stay the same. This may be due to the length and concentration of treatment as previously described. It appears most likely that DCA treatment is associated with a decrease in glycolytic flux, lactate and alanine production. The effects of DCA treatment is further reviewed and the different experimental conditions noted.

Following an increase in PDH flux, DCA treatment has been shown to enhance glucose oxidation *in vitro* in tissue isolated from rat heart and diaphragm [119]. Despite this, observations by Lorni *et al* that diisopropylammonium dichloroacetate treatment had no effect on glucose uptake in rat diaphragmatic muscle with no change in muscle or hepatic glycogen content [120, 131]. Conversely, studies by Clark *et al* supported an increase in glucose storage reporting a greater than 25 % increase in glycogen content within the rat muscle in the fed state when incubated with of 1 mM DCA accompanied by enhanced levels of glucose-6-phosphate, which is an allosteric enhancer of glycogen synthase [132]. Enhanced muscle glycogen content was accompanied by a decrease in glycolytic flux irrespective of insulin concentration with enhanced substrate cycling between fructose-1,6

bisphospate and fructose-6-phosphate, a key regulatory reaction within glycolysis catalysed by phosphofructokinase-1 (PFK-1) [120]. PFK-1 activity is allosterically regulated by citrate, an intermediate within the tricarboxylic acid (TCA) cycle [120, 1]. At high concentrations of citrate, such as during enhanced levels of glucose oxidation which was observed in cellular extracts incubated with DCA, both Clark *et al* and Sobrino *et al* report a repression in PFK-1 activity and repressed glycolytic flux in muscles cells and adipose cells respectively [132, 133]. Sobrino *et al* also show an increase in the levels of fructose-2,6-bisphosphate, an allosteric inhibitor of PFK-1, in adipose cells incubated with DCA whereas Clark *et al* note no change in either intracellular citrate or ATP levels suggesting this doesn't account for the reduction in glycolytic flux observed [132, 133].

Wambolt *et al* also report a decrease in glycolytic flux in hypertension-induced hypertrophied hearts perfused via the Langendorff mode with 1 mM DCA during nonischemic perfusion and reperfusion [112] and work by Anderson *et al* in both normal and diabetic rat liver observed a reduction in the activity of hepatic hexokinase and pyruvate kinase, also key enzymes in glycolytic regulation [134]. Glucose-6-phosphate is an allosteric inhibitor of hexokinase in the liver, the levels of which are shown to be enhanced in isolated muscle preparations by Clark *et al* suggesting that if glucose uptake is unchanged as described by Lorni *et al* and Clark *et al* with the exception of supraphysiological insulin levels, that in the presence of DCA, excess glucose is directed into glycogen storage and glycolytic flux is reduced [132, 120].

DCA also acts to reduce lactate production which has promoted its use as a treatment for both acquired and inherent lactic acidosis [116, 113]. Clark *et al* report a decrease in lactate production in muscle preparations incubated with DCA, 80 % of which is attributed to the reduction in glycolytic flux previously discussed [132]. Alanine levels are also reduced in the presence of DCA reducing the availability of precursors for gluconeogenesis. The Cori and glucose-alanine cycles act between the muscle and liver as the muscle cannot directly release glucose to the circulation, therefore, the release of alanine and lactate from the muscle provides gluconeogenic precursors which can be transported via the circulation to the liver for glucose synthesis [1]. Disruption of these cycles, reducing

hepatic gluconeogenesis, may account in part for the glucose lowering effects of DCA seen in diabetic animals [128].

Demaugue *et al* suggest that DCA is metabolised via glyoxalate, an inhibitor of hydroxymethylglutaryl coenzyme A (HMG-CoA) reductase, to oxalate, an inhibitor of the gluconeogenic enzyme pyruvate carboxylase (PC), in the liver. Incubation with DCA was shown to significantly reduce gluconeogenesis from lactate, pyruvate and alanine in isolated hepatocytes from fasted rats [124]. When examined in isolated mitochondria, the inhibitory effect of DCA on PC appears to be dependent on the length of incubation with DCA. The concentration of DCA has been shown to increase within the mitochondrion and is linked to the ADP concentration within the mitochondrial matrix [120, 125]. This is supported by a 40 % decrease in ATP observed by Demaugre *et al* within the hepatic mitchondria following the addition of DCA to the preparation. Oxalate concentrations measured by Demaugre *et al* after a 40 minute incubation period of hepatocytes with 1 mM DCA were also sufficient to inhibit PC suggesting that the product of DCA degradation may at least be partially responsible for decreases in gluconeogenesis observed in the liver [124].

4.2.3.2 The Effects of Dichloroacetate on Fatty Acid Metabolism

Dichloroacetate (DCA) has been shown by Whitehouse and Randle to up-regulate pyruvate dehydrogenase (PDH) supported by the inhibition of ^{32}P label incorporation into PDH in the perfused heart following treatment with 1 mM DCA indicative of reduced phosphorylation of PDH [111]. Increased PDH up-regulation following DCA treatment is proposed to promote glucose oxidation through increased coupling between glycolysis and the TCA cycle and has been shown to reduce short and medium-chain fatty acid oxidation in both the heart and skeletal muscle [128, 120]. This is supported by a 52 % reduction in $^{3}H_2O$ incorporation into fatty acids in isolated hepatocytes following chronic incubation with DCA accompanied by a 38 % reduction in label incorporation into cholesterol [135].

4.2.3.3 The Effects of Dichloroacetate on Metabolism

As noted at the beginning of this review, a range of metabolic changes have reported following dichloroacetate (DCA) treatment. From the literature presented, it would suggest that DCA treatment acts to decrease glycolytic flux, lactate production, alanine production, fatty acid oxidation and chloesterol synthesis whilst promoting pyruvate dehydrogenase flux and glycogen storage. The work in this chapter focuses purely on the effect of DCA treatment on metabolism within the heart. DCA treatment is administered both acutely and chronically and the metabolic effects assessed both *in vivo* and in the perfused heart.

4.2.4 Chapter Aims

The work in this chapter acts to further clarify the metabolic effects of dichloroacetate (DCA) on cardiac metabolism. The role of DCA as a positive effector pyruvate dehydrogenase (DCA) is well characterised [119], however, its effect on other areas of metabolism are poorly characterised. Given the integrative nature of metabolism and the effect of metabolic disruption in diseases such as diabetes, ischemic heart disease and hypertrophy, the wider effects of DCA on myocardial metabolism is an important consideration when assessing the potential of DCA as a treatment.

Within this work, the acute and chronic effects of DCA treatment are assessed both *in vivo* and in the perfused heart. The use of a combination of *in vivo* and *ex vivo* techniques provides a complementary assessment of the same question. An *in vivo* study of the effect of acute and chronic DCA treatment on myocardial metabolism in many ways is a gold standard analysis of the therapeutic effects of a specific compound. In addition, the systemic effects of DCA are also taken into consideration when looking *in vivo*. However, the work here is limited to looking at the effects of DCA treatment on PDH flux and the label incorporation into lactate and alanine. Furthermore, it is possible that a true analysis of label incorporation into lactate in particular may be limited by the sensitivity of dynamic nuclear polarisation, the technique used to assess metabolism *in vivo* as previously discussed in Chapter 1.6.3. However, the results obtained correlate with

those obtained in the Langendorff perfused heart which is a well-established technique for metabolic analysis.

Metabolic assessment in the perfused heart is in many ways more versatile as many more labelled compounds are available and the conditions under which the experiment can often be varied to a greater extent. Within this study, the effects of acute and chronic DCA treatment on glycolytic flux, lactate efflux and fatty acid oxidation were further assessed providing complementary information to the question posed. However, perfusion via the Langendorff is not without it limitations as a technique particularly as the is placed heart within an isolated system without any of the *in vivo* humoral and systemic effects which is a particular drawback when looking at non-cardiac specific drug such as DCA. The use of these two techniques therefore provides a wider dimension to the study than relying on an individual technique alone. However, it would be prudent to acknowledge the assets and limitations of both techniques when considering the results presented.

4.3 Methods

4.3.1 Study Overview

The effects of acute and chronic pyruvate dehydrogenase (PDH) up-regulation on cardiac metabolism were assessed both *in vivo* and in the isolated heart perfused via the Langendorff mode using either hyperpolarized [^{13}C]pyruvate or [^{3}H]glucose and [^{3}H]palmitate respectively. Complimentary biochemical work was performed on cardiac tissue to assess the molecular changes associated with PDH up-regulation. An outline of the study is detailed in Figure 4.4.

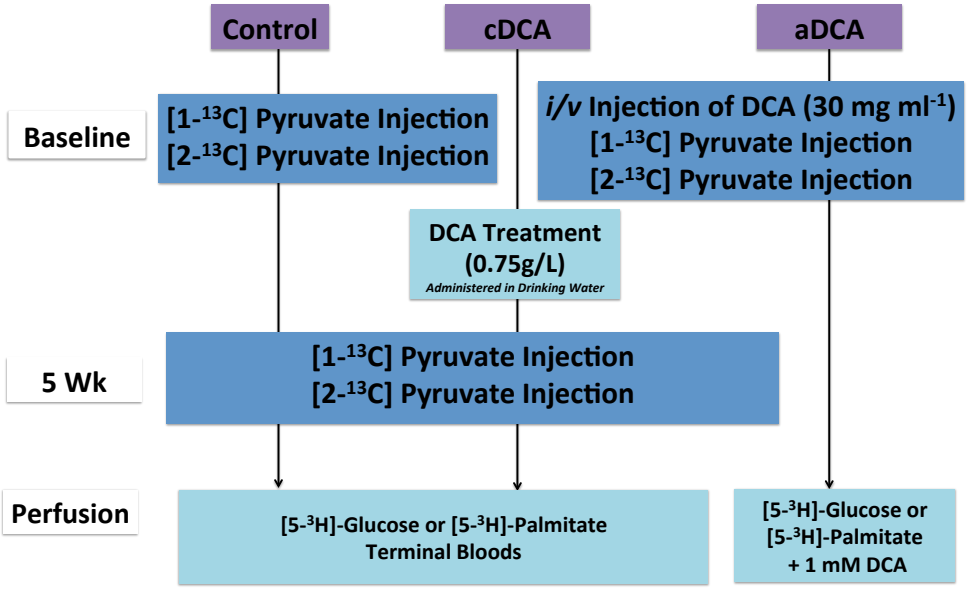


Figure 4.4: Assessment of the Effects of Acute and Chronic Pyruvate Dehydrogenase Up-Reguation on Cardiac Metabolism - A Study Overview. aDCA: Acute DCA Treatment; cDCA: Chronic DCA Treatment

4.3.2 Animal Work

All animal experiments were conducted by a licensed individual in accordance with the Home Office Guidance on the Operation of Animals (Scienctific Procedures) Act of 1986 and to University of Oxford institutional guidelines.

Animals were housed in a dedicated facility (Biomedical Sciences Services, University of Oxford, UK) under a 12 hr light-dark cycle and maintained on a standard laboratory chow (Harlan Laboratories, Kent, UK) and standard laboratory water given *ad libitum*

unless otherwise stated. All *in vivo* metabolic experiments were performed whilst animals were in the fed state (taken as between 6 am and 1 pm) unless otherwise stated

4.3.3 Preparation and Administration of Dichloroacetate

4.3.3.1 Preparation of Dichloroacetate for Acute Administration

A solution of dichloroacetate (DCA; 30 mg ml^{-1}) was prepared as previously described in Section 4.3.3.1 for *i/v* infusion through neutralisation of dichloroacetic acid (1.56 g L^{-1}; Sigma-Aldrich, Dorset, UK) with sodium hydroxide to a pH of 7.2, suitable for injection.

4.3.3.2 Preparation of Dichloroacetate for Chronic Treatment

Dichloroacetate (0.75 g L^{-1}) treatment was prepared through neutralisation of dichloroacetic acid (1.56 g L^{-1}; Sigma-Aldrich, Dorset, UK) using sodium hydroxide to a pH of 7.2 as previously described in Section 4.3.3.1 and administered in drinking water for 5 weeks. Fresh treatment was prepared a minimum of every 3 days. Control rats were maintained on standard laboratory water.

4.3.4 *In vivo* Assessment of PDH Flux and Flux into the TCA cycle

The effect of DCA treatment on cardiac metabolism was assessed *in vivo* in male Sprague-Dawley rats following acute and chronic treatment with dichloroacetate (DCA) using hyperpolarized [1-^{13}C] and [2-^{13}C]labelled pyruvate as previously described in Section 2.3. Acute measurements were taken immediately following a bolus *i/v* infusion of DCA (30 mg ml^{-1}) as previously described in Section 4.3.3.1 and chronic measurements taken at 5 weeks following continuous treatment with DCA (0.75 g L^{-1}) administered in drinking water. Rats (Acute: Control: n = 5; DCA: n = 5; Chronic: Control: n = 5; DCA: n = 5) were prepared as described in 2.3.1 following which approximately 1 ml of either hyperpolarized [1-^{13}C]- or [2-^{13}C]-pyruvate was infused over 10 seconds and 60 single

scan spectra were acquired over a period of 60 seconds as previously described in Section 2.3.4.1.

4.3.5 *Ex vivo* Assessment of Glycolytic Flux and Fatty Acid Oxidation in the Isolated Langendorff Perfused Heart

Glycolytic flux and fatty acid oxidation was assessed in the isolated Langendorff perfused heart following acute and chronic treatment with dichloroacetate (DCA) as previously described in Section 2.5. Hearts were isolated and perfused for 52 minutes as described in Section 2.5.2 during which the effects of DCA treatment on basal and insulin-stimulated metabolism were assessed as described in Section 2.5.4.1.

For the assessment of the effect of acute DCA treatment on either glycolytic flux (Control: n = 7; DCA: n = 6) or fatty acid oxidation (Control: n = 6; DCA: n = 7), 1 mM of DCA (1.56 g L^{-1} Sigma-Aldrich, Dorset, UK) [111] was added to the perfusion buffer at t = -10 minutes at the same time as the addition of either [5-^{3}H]glucose or [9,10-^{3}H]palmitate as previously described in Section 2.5.4. In hearts which had experienced chronic treatment with DCA, animals had been dosed with DCA (0.75 g L^{-1}) given *ad libitum* in drinking water for 5 weeks as previously described in Section 2.4.2 but no DCA was added to the perfusion buffer (glycolytic flux: Control: n = 7; DCA: n = 7; fatty acid oxidation: Control: n = 6; DCA: n = 5).

Hearts were given a 10 minute acclimatisation period as previously described in Section 2.5.4.1 after which basal glycolytic flux was assessed for 20 minutes following which insulin (2048 pmol L^{-1}; Novo Nordisk, Denmark) was added and insulin-stimulated glycolytic flux was assessed for a further 32 minutes. Hearts were washed in fresh Krebs-Heinsleit (KH) buffer for 4 minutes in the absence of radio tracers and rapidly freeze clamped on the cannula using liquid nitrogen cooled Wollenberg tongs as previously described in Section 2.5.4.1. Samples of 1 ml were taken in the assessment of glycolytic flux and samples of 1.5 ml taken in the assessment of fatty acid oxidation, were taken every 4 minutes for a period of 52 minutes and subsequently stored at -20 °C for further analysis. Glycolytic flux and fatty acid oxidation was assessed via the methods described in Sections 2.5.5 and

2.5.6 respectively.

4.3.6 Blood Sampling and Plasma Analysis

Terminal bloods were obtained as previously described in Section 2.6 and the plasma concentrations of glucose, lactate, triacylglycerides (TAG), low-density lipoprotein (LDL), cholesterol, high-density lipoprotein (HDL), and β-hydroxybutyrate were assessed using an ABX Pentra 400 (Horiba ABX Diagnostics, California, USA) as previously described in Section 2.6.

4.3.7 Biochemical Analysis

4.3.7.1 Myocardial Glycogen Content

Myocardial glycogen content was assessed in freeze clamped powdered cardiac tissue from Control rats and rats which had undergone 5 weeks of chronic DCA treatment as previously described in 2.8.1.

4.3.7.2 Myocardial Intracellular Lactate Content

Myocardial intracellular lactate content was assessed in freeze clamped powdered cardiac tissue from Control rats and rats which had undergone 5 weeks of chronic DCA treatment as previously described in Section 2.8.2.

4.3.8 Statistical Analysis

All data presented is present as mean ± standard error of the mean. *In vivo* metabolic data was analysed using a unpaired, two-tailed Student's t test whereas all perfusion data was analysed using a two-way ANOVA with repeated measures taking insulin and DCA treatment as independent variables. All data was analysed using the GraphPad Prism 7 software package (GraphPad Softwares, California, USA).

4.4 Results

4.4.1 The *in vivo* Effects of Acute Dichloroacetate Treatment on Myocardial Metabolism

Following an acute infusion with dichloroacetate (DCA), pyruvate dehydrogenase (PDH) flux was increased by 45% in the DCA group when compared with the Control group (Control: 0.0064 ± 0.0011 s^{-1}; DCA: 0.0138 ± 0.0014 s^{-1}; Fig 4.5A; *p <0.005 vs. Control*). This is consistent with PDH up-regulation. No change in label incorporation into either lactate (Fig 4.5B; *p = 0.20 vs. Control*) or alanine (Fig 4.5C; *p = 0.36 vs. Control*) was observed in the DCA-treated vs. Control group following an acute infusion with DCA.

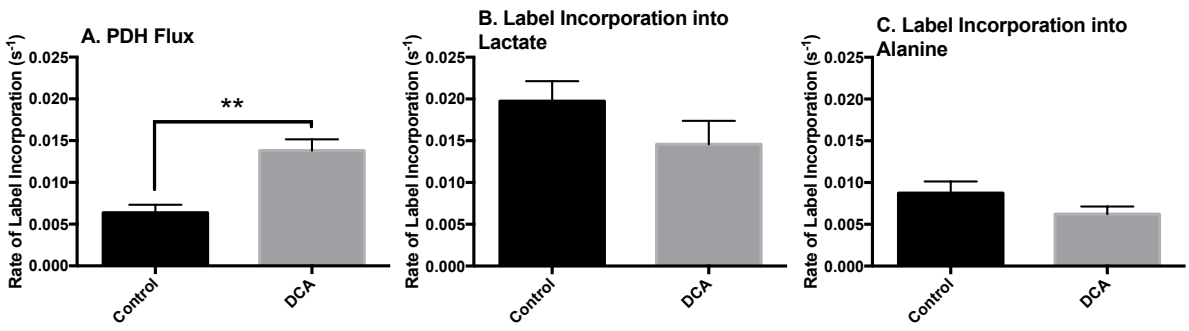


Figure 4.5: Pyruvate Dehydrogenase (PDH) Flux following an Acute Infusion with DCA. A. PDH Flux; B. Label Incorporation into Lactate; C. Label Incorporation into Alanine. Control: n = 5; DCA: n = 5. ** *p <0.01 vs. Control*. $Mean \pm SEM$. Unpaired Two-Tailed Student's t test. DCA: DCA Treatment.

Following an acute infusion with DCA, flux into acetylcarnitine, citrate or glutamate remained unchanged (acetylcarnitine: Fig 4.6A; $p = 0.27$ *vs. Control*; citrate: Fig 4.6B; $p = 0.93$ *vs. Control*; glutamate: Fig 4.6C; $p = 0.94$ *vs. Control*).

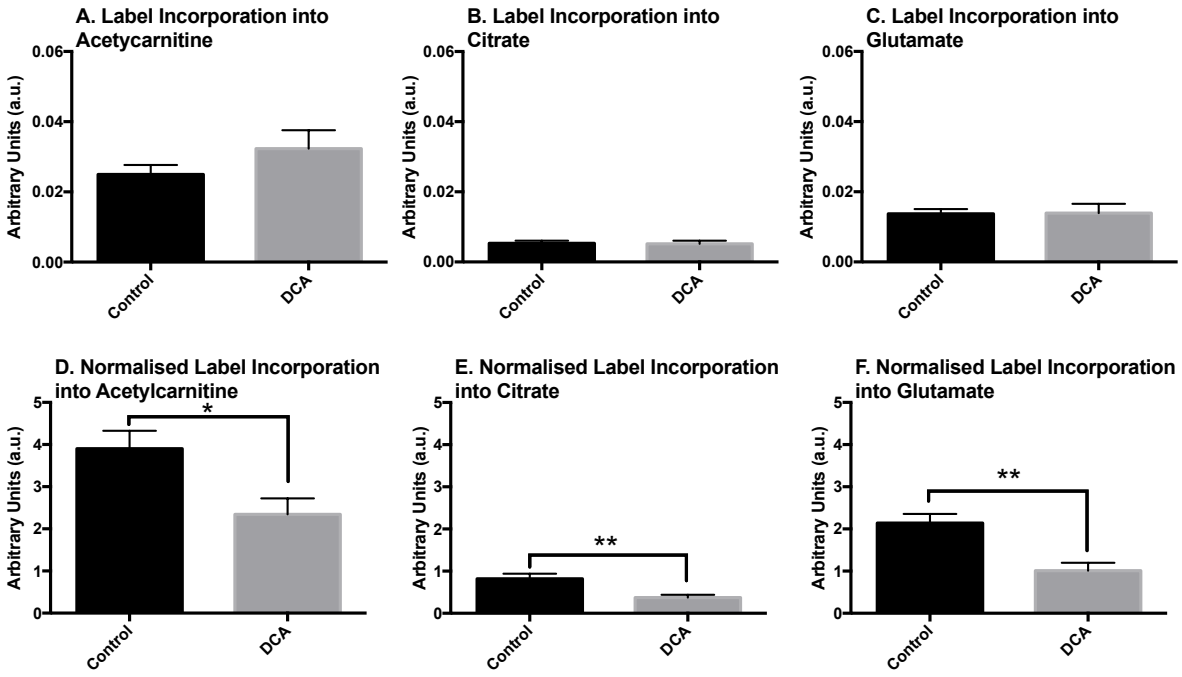


Figure 4.6: The Effects of an Acute DCA Infusion on Label Incorporation into TCA Intermediates. A. Label Incorporation into Acetylcarnitine; B. Label Incorporation into Citrate; C. Label Incorporation into Glutamate; D. Normalised Label Incorporation into Acetylcarnitine. E. Normalised Label Incorporation into Citrate; F. Normalised Label Incorporation into Glutamate. Control: n = 5; DCA: n =5. * $p < 0.05$ *vs. Control*; ** $p < 0.01$ *vs. Control*. Unpaired Two-Tailed Student's t test. DCA: DCA Treatment

However, when normalised to the average PDH flux, a significant reduction in label incorporation in acetylcarntine, citrate and glutmate was observed in the DCA group vs. the Control group (acetylcarnitine: Control: 3.9032 ± 0.4246 a.u.; DCA: 2.3423 ± 0.7111 a.u.; Fig 4.6D; $p < 0.05$ *vs. Control*; citrate; Control: 0.8207 ± 0.1207 a.u.; DCA: 0.3732 ± 0.1387 a.u.; Fig 4.6E; $p < 0.01$ *vs. Control*; glutamate: Control: 2.1401 ± 0.2159 a.u.; DCA: 1.0088 ± 0.3545 a.u.; Fig 4.6F; $p < 0.01$ *vs. Control*)

4.4.2 The Effects of Acute Dichloroacetate Treatment on Glycolysis, Lactate Efflux and Fatty Acid Oxidation in the Perfused Heart

Basal glycolytic flux was reduced by 25 % in the DCA treatment group vs. the Control group (Control: 0.5676 ± 0.0341 μmol min^{-1} gww^{-1}; DCA: 0.4528 ± 0.0460 μmol min^{-1} gww^{-1}; Fig 4.7A; *p <0.05 vs. Control*). Similarly, a 37 % reduction in insulin-stimulated glycolytic flux was observed in the DCA treatment group vs. the Control group (Control: 0.7740 ± 0.0392 μmol min^{-1} gww^{-1}; DCA: 0.5629 ± 0.0357 μmol min^{-1} gww^{-1}; Fig 4.7A; *p <0.05 vs. Control*).

The presence of insulin was associated with a 36 % increase in glycolytic flux in the Control group (Basal: 0.5676 ± 0.0341 μmol min^{-1} gww^{-1}; Insulin: 0.7740 ± 0.0392 μmol min^{-1} gww^{-1}; Fig 4.7A; *p <0.01 vs. Basal*) and a 24 % increase in the DCA Treatment group (Basal: 0.4258 ± 0.0460 μmol min^{-1} gww^{-1} vs. Insulin: 0.5629 ± 0.0357 μmol min^{-1} gww^{-1}; Fig 4.7A; *p <0.01 vs. Basal*).

A reduction in glycolytic flux in the DCA Treatment group was accompanied by a 64 % decrease in basal lactate efflux (Control: 0.0703 ± 0.0122 μmol min^{-1} gww^{-1}; DCA: 0.0252 ± 0.0058 μmol min^{-1} gww^{-1}; Fig 4.7C; *p <0.001 vs. Control*) and a 67 % decrease in insulin-stimulated lactate efflux (Control: 0.0664 ± 0.0085 μmol min^{-1} gww^{-1}; DCA: 0.0221 ± 0.0081 μmol min^{-1} gww^{-1}; Fig 4.7C; *p <0.001 vs. Control*). Insulin had no effect on lactate efflux (*p = 0.6025 vs. Basal*; Fig 4.7C).

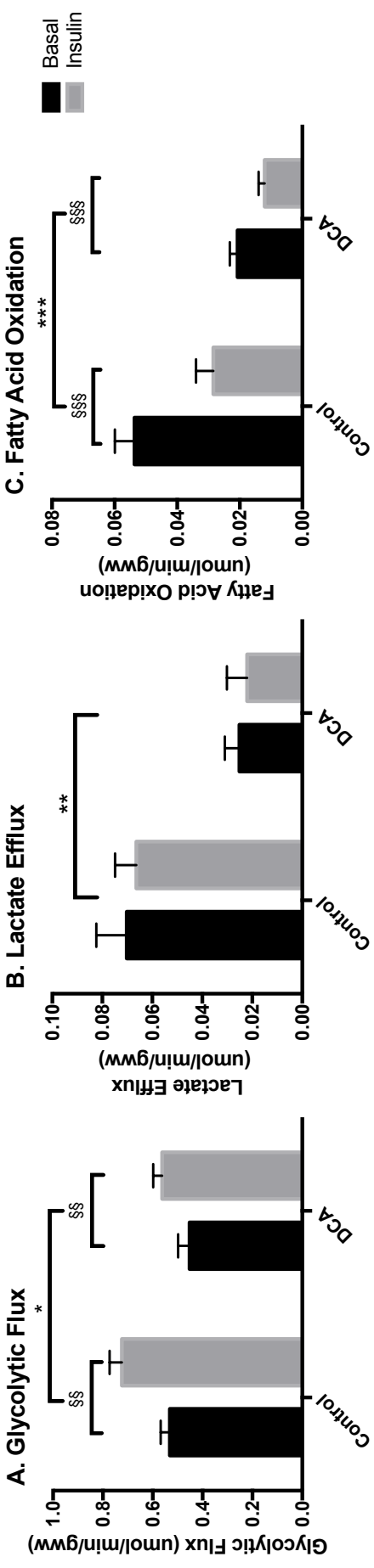


Figure 4.7: The Metabolic Effects of Acute Dichloroacetate (DCA) Treatment (1 mM DCA) in the Isolated Langendorff Perfused Heart. A. Glycolytic Flux; B. Lactate Efflux; C. Fatty Acid Oxidation. Glycolytic Flux: Control: n = 7; DCA: n = 6; Lactate Efflux: Control: n = 7; DCA: n = 6; Fatty Acid Oxidation: Control: n = 6; DCA: n = 7. * $p < 0.05$ *vs. Control* ** $p < 0.01$ *vs. Control* *** $p < 0.005$ *vs. Control* §§ $p < 0.01$ *vs. Basal* §§§ $p < 0.005$ *vs. Basal.* $Mean \pm SEM$ Two-Way ANOVA with Repeated Measures. DCA: DCA Treatment.

An acute DCA infusion was associated with a significant reduction in fatty acid oxidation (Fig 4.7B; *p <0.005 vs. Control*). A 61 % decrease in basal fatty acid oxidation (Control: 0.0537 ± 0.0058 μmol min^{-1} gww^{-1}; DCA: 0.0208 ± 0.0025 μmol min^{-1} gww^{-1}; Fig 4.7B) and a 57 % decrease in insulin-stimulated fatty acid oxidation (Control: 0.02852 ± 0.0051 μmol min^{-1} gww^{-1} vs. DCA: 0.0121 ± 0.0019 μmol min^{-1} gww^{-1}; Fig 4.7B) was observed in the DCA Treatment group vs. the Sham group.

The addition of insulin also resulted in a significant reduction in fatty acid oxidation (Fig 4.7B; *p <0.005 vs. Basal*). A 47 % decrease in fatty acid oxidation was observed in the Control group in the presence of insulin (Basal: 0.0537 ± 0.0058 μmol min^{-1} gww^{-1}; Insulin: 0.0285 ± 0.0051 μmol min^{-1} gww^{-1}; Fig 4.7B). This was accompanied by a 41 % decrease in the DCA Treatment group (Basal: 0.0208 ± 0.0025 μmol min^{-1} gww^{-1}; Insulin: 0.0121 ± 0.0019 μmol min^{-1} gww^{-1}; Fig 4.7B).

4.4.3 The Effects of Acute Dichloroacetate Treatment on Cardiac Function in the Perfused Heart

DCA treatment was associated with no change in either basal rate pressure product (RPP) or insulin-stimulated RPP (Fig 4.8A; *p = 0.26 vs. Control*). Insulin also had no effect on RPP (Fig 4.8A; *p= 0.12 vs. Basal*). Neither insulin nor DCA treatment had an effect on left ventricular developed pressure (LVDP; Fig 4.8B; *p = 0.54 vs. Control*) or heart rate (HR; Fig 4.8C; *p = 0.40 vs. Control*)

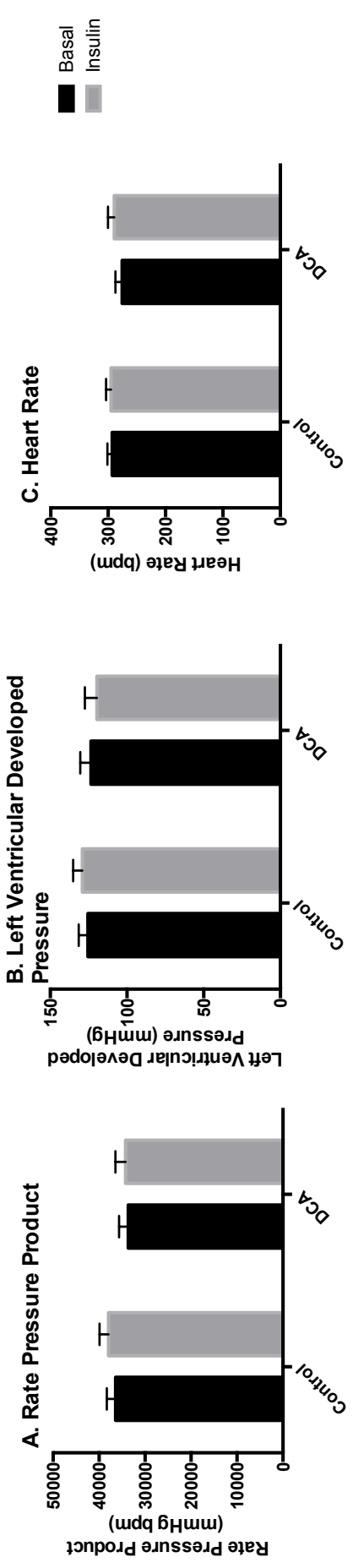


Figure 4.8: Cardiac Function following Acute Perfusion with 1 mM Dichloroacetate (DCA). A. Rate Pressure Product (RPP); B. Left ventricular Developed Pressure (LVDP); C. Heart Rate. Control: n = 13; DCA: n = 13. $Mean \pm SEM$ Two-Way ANOVA with Repeated Measures. DCA: DCA Treatment.

4.4.4 The *in vivo* Effects of Chronic Dichloroacetate Treatment on Myocardial Metabolism

The effects of chronic dichloroacetate (DCA) treatment was assessed *in vivo* and in hearts perfused via the Langendorff mode. DCA was administered in drinking water given *ad libitum* for a total of 5 weeks following which the effects of treatment on pyruvate dehydrogenase (PDH) and flux into the TCA cycle was assessed *in vivo* following the injection of either hyperpolarized [1-^{13}C]- or [2-^{13}C]-labelled pyruvate respectively. The effects of chronic DCA treatment on the rates of myocardial glycolysis and fatty acid oxidation was further assessed in the perfused heart using [5-^{3}H]glucose and [5-^{3}H]palmitate respectively.

4.4.5 The Effects of Chronic Dichloroacetate Treatment on Pyruvate Dehydrogenase Flux and TCA Cycle Intermediates

A 49 % increase in pyruvate dehydrogenase (PDH) flux was observed in the DCA Treatment vs. the Control group following 5 weeks of DCA treatment consistent with chronic PDH up-regulation (Control: 0.0077 ± 0.0009 s^{-1}; DCA: 0.0114 ± 0.0012 s^{-1}; Fig 4.9A; *$p < 0.01$ vs. Control*).

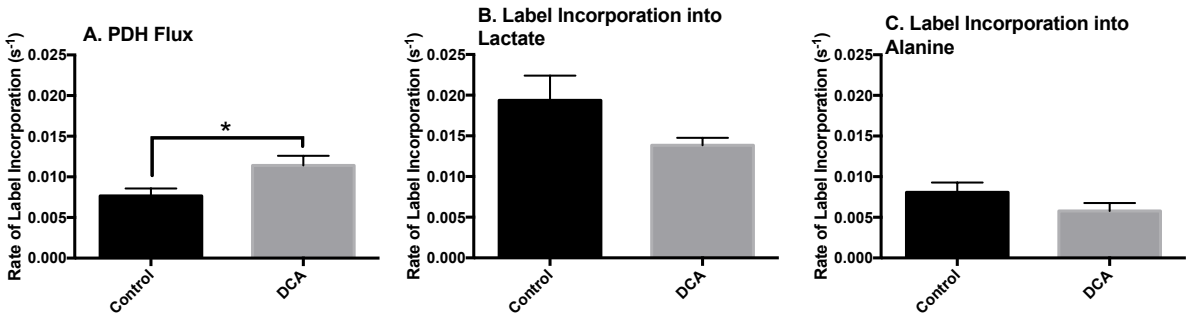


Figure 4.9: Pyruvate Dehydrogenase (PDH) Flux following 5 Weeks of DCA Treatment. A. PDH Flux; B. Label Incorporation into Lactate; C. Label Incorporation into Alanine. * *$p < 0.05$ vs. Control* $Mean \pm SEM$. Unpaired Two-Tailed Student's t Test. DCA: DCA Treatment.

This was associated with no change in label incorporation into either lactate or alanine in the DCA Treatment group vs. the Control group (lactate: Fig 4.9B; *$p = 0.15$ vs. Control*; alanine: Fig 4.9C; *$p = 0.22$ vs. Control*).

A 64% increase in label incorporation into acetylcarnitine was observed in the DCA Treatment group vs. the Control group (Control: 0.0320 ± 0.0056 a.u.; DCA: 0.0525 ± 0.0034 a.u.; Fig 4.10A; *p <0.05 vs. Control*). However, when normalised to the average PDH flux , no change was observed in the DCA Treatment group vs. the Control group (Fig 4.10D; *p = 0.70 vs. Control*) suggesting the increase in label incorporation in acetylcarnitine prior to normalisation was a result of enhanced PDH flux following DCA treatment.

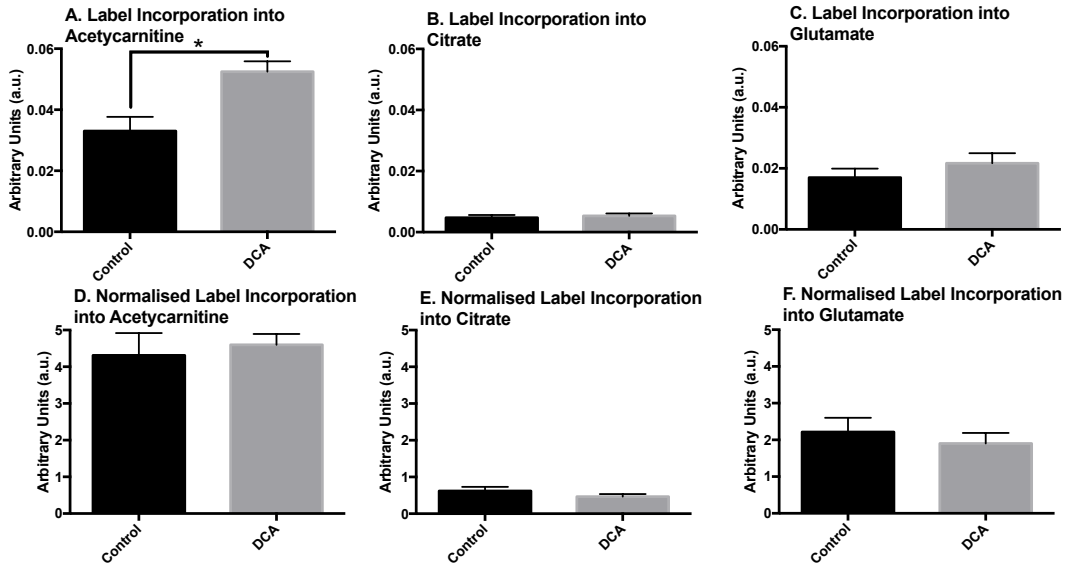


Figure 4.10: Altered Flux into the TCA Cycle following 5 Weeks of DCA Treatment. A. Label Incorporation into Lactate; B. Label Incorporation into Glutamate; C. Label Incorporation into Acetylcarnitine. Control: n = 5; DCA: n = 5 * *p <0.05 vs. Control* $Mean \pm SEM$. Unpaired Two-Tailed Student's t Test. DCA: DCA Treatment.

No change in label incorporation into citrate or glutamate was observed (citrate: Fig 4.10B; *p = 0.64 vs. Control*; glutamate: Fig 4.10C; *p = 0.31 vs. Control*). This was sustained following normalisation of citrate and glutamate with PDH flux (normalised citrate: Fig 4.10E; *p = 0.31 vs. Control*; normalised glutamate: Fig 4.10F; *p = 0.55 vs. Control*).

4.4.6 The Effects Chronic Dichloroacetate Treatment on Glycolysis, Lactate Efflux and Fatty Acid Oxidation in the Perfused Heart

Chronic dichloroacetate (DCA) treatment induced a significant reduction in glycolytic flux (Fig 4.11A; $p < 0.05$ *vs. Control*). DCA treatment was associated with a 26 % decrease in basal glycolytic flux in the DCA Treatment group vs. the Control group (Control: 0.5679 ± 0.0341 μmol min^{-1} gww^{-1}; DCA: 0.4213 ± 0.0299 μmol min^{-1} gww^{-1}; Fig 4.11A) and a 24 % decrease in insulin-stimulated glycolytic flux (Control: 0.7740 ± 0.0392 μmol min^{-1} gww^{-1}; DCA: 0.5863 ± 0.0347 μmol min^{-1} gww^{-1}; Fig 4.11A).

The addition of insulin induced a significant increase in glycolytic flux (Fig 4.11A; $p < 0.001$ *vs. Basal*). Within the Control group, the presence of insulin led to a 36 % increase in glycolytic flux (Basal: 0.05676 ± 0.0341 μmol min^{-1} gww^{-1} Insulin: 0.7740 ± 0.0392 μmol min^{-1} gww^{-1}; Fig 4.11A) and a 39 % increase in glycolytic flux in the DCA Treatment group (Basal: 0.4213 ± 0.0299 μmol min^{-1} gww^{-1}; Insulin: 0.5863 ± 0.0357 μmol min^{-1} gww^{-1}; Fig 4.11A).

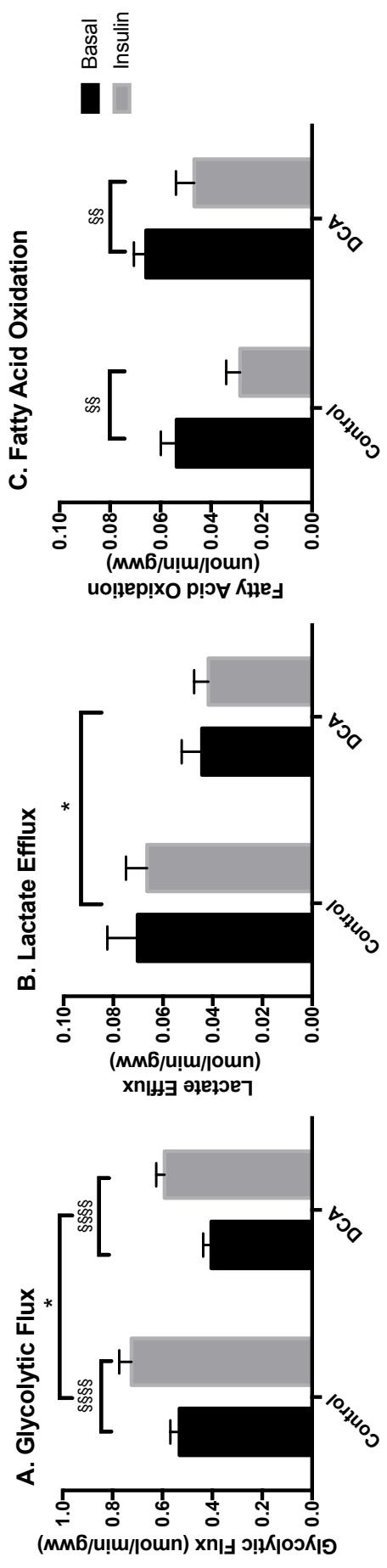


Figure 4.11: The Effects of Chronic Dichloroacetate (DCA; 0.75 g L^{-1}) Treatment in the Isolated Langendorff Perfused Heart. A. Glycolytic Flux; B. Lactate Efflux; C. Fatty Acid Oxidation. Glycolytic Flux: Control: n = 7; DCA: n = 7; Lactate Efflux: Control: n = 7; DCA: n = 6; Fatty Acid Oxidation: Control: n = 6; DCA: n = 5. * $p < 0.05$ *vs. Control* §§ $p < 0.01$ *vs. Basal* §§§§ $p < 0.001$ *vs. Basal.* $Mean \pm SEM$ Two-Way ANOVA with Repeated Measures. DCA: DCA Treatment.

DCA treatment induced a significant reduction in lactate efflux (Fig 4.11B; $p < 0.05$ *vs. Control*). Consistent with a reduction in glycolytic flux, a 37 % decrease in both basal and insulin-stimulated lactate efflux was observed in the DCA Treatment group vs. the Control group (Control: Basal: 0.0703 ± 0.0122 μmol min^{-1} gww^{-1}; Insulin: 0.0634 ± 0.0085 μmol min^{-1} gww^{-1}; DCA: Basal: 0.0443 ± 0.0882 μmol min^{-1} gww^{-1}; Insulin: 0.0418 ± 0.0057 μmol min^{-1} gww^{-1}; Fig 4.11B). Insulin had no effect on lactate efflux (Fig 4.11B; $p = 0.64$ *vs. Control*).

DCA treatment induced an increase in fatty acid oxidation, however, this failed to reach statistical significance (Fig 4.11B; $p = 0.07$ *vs. Control*). A 23 % increase in basal fatty acid oxidation was observed in the DCA Treatment group vs. the Control group (Fig 4.11B) accompanied by a 63 % increase in insulin-stimulated fatty acid oxidation in the DCA treatment group vs. the Control group (Fig 4.11B).

This was accompanied by a significant reduction in fatty acid oxidation following the addition of insulin (Fig 4.11B; $p < 0.01$ *vs. Basal*). A 47 % decrease in fatty acid oxidation was observed in the Control group (Basal: 0.0537 ± 0.0058 μmol min^{-1} gww^{-1}; Insulin: 0.0285 ± 0.0051 μmol min^{-1} gww^{-1}; Fig 4.11B) and a 29 % reduction in the DCA Treatment group following the addition of insulin (Basal: 0.0658 ± 0.0048 μmol min^{-1} gww^{-1}; Insulin: 0.0467 ± 0.0072 μmol min^{-1} gww^{-1}; Fig 4.11B).

4.4.7 The Effect of Chronic Dichloroacetate Treatment on Cardiac Function in the Perfused Heart

Dichloroacetate (DCA) treatment induced no change in cardiac function measured by rate pressure product (RPP; Fig 4.12A; $p = 0.99$ vs. Control).

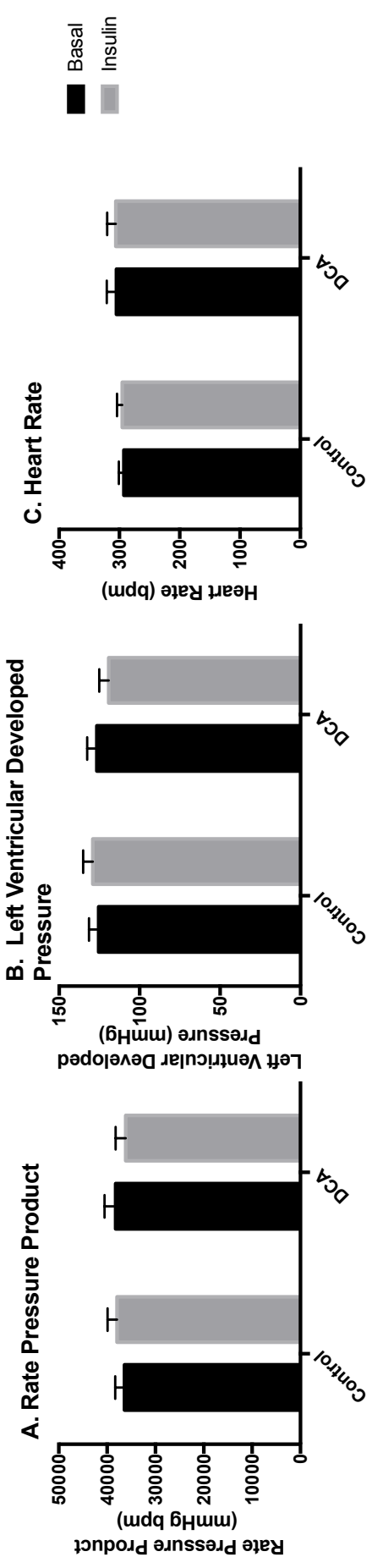


Figure 4.12: The Effect of Chronic DCA Treatment on Cardiac Function in the Langendorff Perfused Heart. A. Rate Pressure Product (RPP); B. Left Ventricular Developed Pressure (LVDP); C. Heart Rate (HR). Control: n = 5; DCA: n = 5. $Mean \pm SEM$ Two-Way ANOVA with Repeated Measures. DCA: DCA Treatment

No further change in left ventricular developed pressure (LVDP) or heart rate (HR) was observed following DCA treatment or the addition of insulin (DCA: LVDP: Fig 4.12B; $p = 0.60$ *vs. Control*; HR: Fig 4.12C; $p = 0.49$ *vs. Control*; Insulin: RPP: Fig 4.12A; $p = 0.69$ *vs. Basal*; LVDP: Fig 4.12B; $p = 0.62$ *vs. Basal*; HR: Fig 4.12C; $p = 0.42$ *vs. Basal*).

4.4.8 The Biochemical Effects of Chronic Dichloroacetate Treatment

No change in myocardial glycogen content (Fig 4.13A; $p = 0.98$ *vs. Control*) or intracellular lactate content (Fig 4.13B; $p = 0.96$ *vs. Control*) was observed in the DCA Treatment group vs. the Sham group.

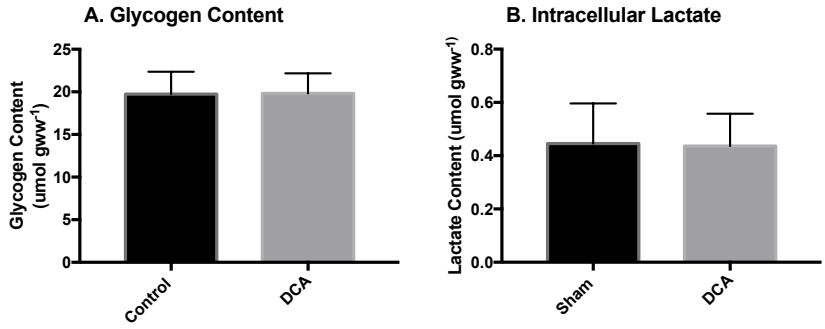


Figure 4.13: The Effect of Chronic DCA Treatment on Myocardial Glycogen and Intracellular Lactate Content. A. Myocardial Glycogen Content. B. Intracellular Lactate Content. Glycogen Content: Control: n = 7; DCA: n = 6; Intracellular Lactate: Control: n = 4; DCA: n = 5; $Mean \pm SEM$ Unpaired Two-Tailed Student's t test. DCA: DCA Treatment

4.4.9 The Systemic Effects of Chronic Dichloroacetate Treatment

No change in plasma concentrations of glucose, cholesterol or high density lipoprotein (HDL) was observed in the DCA Treatment group vs. the Control group (glucose: Fig 4.14A; $p = 0.94$ *vs. Control*; cholesterol: Fig 4.14E; $p = 0.20$ *vs. Control*; HDL: Fig 4.14G; $p = 0.52$ *vs. Control*). A 33 % reduction in plasma lactate concentration and a 19 % reduction in the concentration of low density lipoprotein (LDL) was observed in the

DCA Treatment vs. the Control group (lactate: Control: 5.32 ± 0.66 mmol; DCA: 3.55 ± 0.43 mmol; Fig 4.14B; $p < 0.05$ *vs. Control*; LDL: Control: 0.36 ± 0.01 mmol; DCA: 0.29 ± 0.01 mmol). A 22 % reduction in plasma triacylglyceride levels was also observed, however, this failed to reach statistical significance (Control: 0.70 ± 0.07 mmol; DCA: 0.54 ± 0.05 mmol; Fig 4.14C; $p = 0.07$ *vs. Control*). A 23 % increase in 3-hydroxybutyrate was observed in the DCA Treatment group vs. the Control group (Control: 0.2726 ± 0.018 mmol; DCA: 0.3881 ± 0.0204 mmol; $p < 0.001$ *vs. Control*).

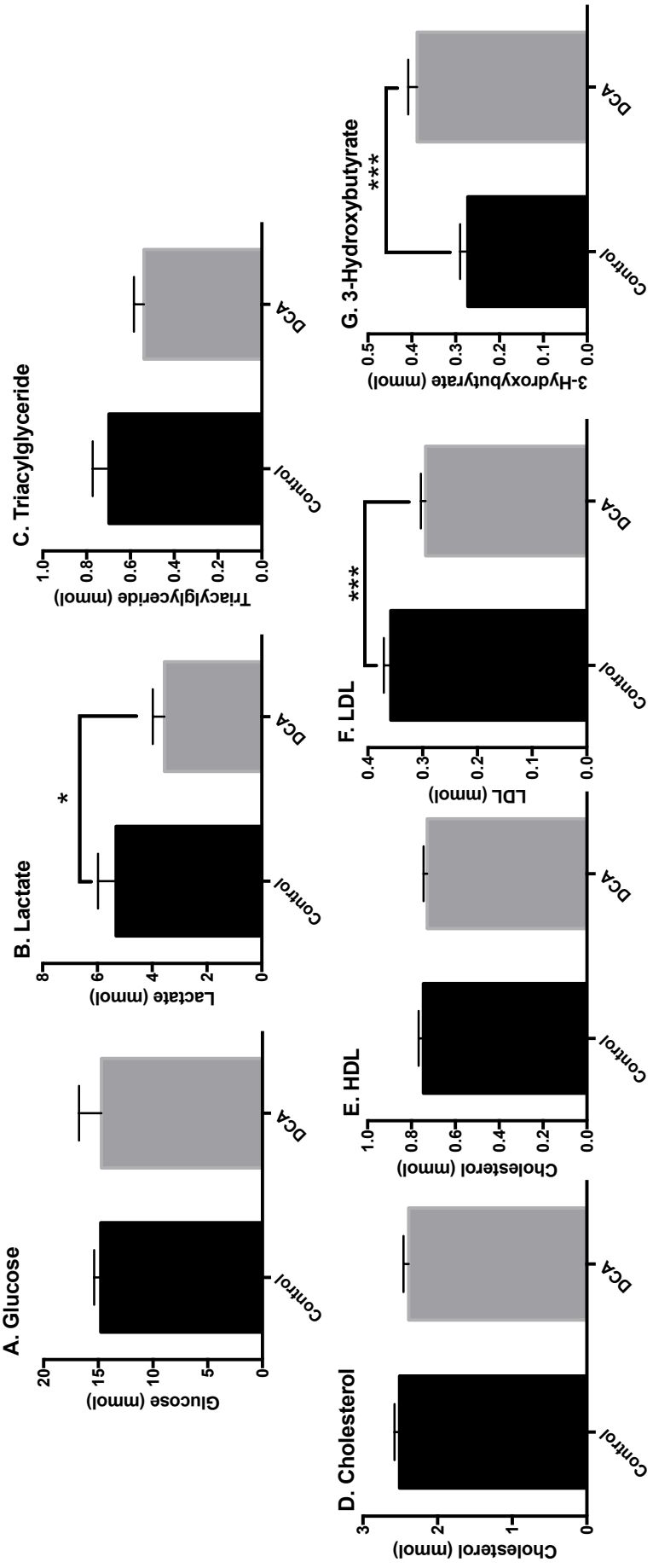


Figure 4.14: Serum Metabolite Concentrations Following 5 Weeks of Chronic DCA Treatment with DCA. A. Glucose. B. Lactate. C. Triacylglyceride. D. Cholesterol. E. High-Density Lipoprotein (HDL). F. Low-Density Lipoprotein (LDL). G. 3-Hydroxybutyrate. Control: n = 14; DCA: n = 16. * $p < 0.05$ *vs. Control*; *** $p < 0.005$ *vs. Control*; Unpaired Two-Tailed Student's t test. $Mean \pm SEM$. DCA: DCA Treatment.

4.5 Discussion

4.5.1 Summary of Results

The effects of acute and chronic dichloroacetate (DCA) treatment on myocardial metabolism were assessed both *in vivo* and in the perfused heart. Pyruvate dehydrogenase (PDH) flux was shown to be enhanced *in vivo* following both acute and chronic DCA treatment.

Glycolytic flux was significantly reduced in the perfused heart following both acute and chronic DCA treatment accompanied by a significant reduction in lactate effux. Fatty acid oxidation was reduced following acute treatment with DCA. When normalised to PDH flux, a reduction in flux into citrate and the anapleoretic products, acetylcarnitine and glutamate suggesting a reduced flux into the TCA cycle, which may be plausible given that both glycolytic flux and fatty acid oxidation is reduced. However, without the normalisation, no change in TCA cycle intermediates is observed, suggesting that further clarification is required before drawing a definite conclusion. If a reduction in flux into TCA cycle is present, this metabolic profile may be suggestive of an energy depleted state within the heart following acute DCA treatment although no change in function was observed following perfusion with DCA.

Chronic DCA treatment was associated with a similar metabolic profile. Enhanced PDH flux was accompanied by a decrease in glycolytic flux and lactate efflux as previously described, however, a significant increase in fatty acid oxidation was observed following chronic treatment suggesting that the heart is adapting to chronic DCA treatment in some capacity. This was accompanied by no change in label incorporation into citrate, acetylcarnitine and glutamate when normalised to PDH flux. However, without normalisation to PDH flux, a significant increase in label incorporation into acetylcarnitine which is consistent with enhanced PDH flux.

Systemically, DCA treatment is associated with a reduction in circulating concentrations of triacylglycerides, low-density lipoprotein and lactate. This was accompanied by no change in plasma concentrations of glucose, cholesterol or high-density lipoprotein but a significant increase in 3-hydroxybutyrate concentrations.

4.5.2 Dichloroacetate Treatment Alters the Metabolic Profile of the Heart

This study identified alterations in the metabolic profile of the heart following acute and chronic dichloroacetate (DCA) treatment. Pyruvate dehydrogenase (PDH) flux was enhanced following both acute and chronic treatment with DCA as previously described by Whitehouse *et al* [111].

This study has identified that following acute treatment with DCA, enhanced myocardial PDH flux is accompanied by a decrease in glycolytic flux, lactate efflux, fatty acid oxidation and a possible reduction in flux into the TCA cycle and its anapleorotic intermediates. Based on these observations, acute DCA treatment does not appear to convey a beneficial metabolic profile for the heart and is more representative of a situation where the heart is energy depleted. Despite an increase in PDH flux, a reduction in glycolytic flux may mean that less pyruvate available to enter TCA cycle coupled with a reduction in the acetyl-CoA available from fatty acid oxidation. Further clarification of DCA treatment on the TCA cycle would add to this work. Metabolomics would provide an insight into the absolute concentrations of the TCA intermediates, which when combined with the *in vivo* data may provide a clearer picture. Applying a stress to the heart such as dobutamine or ischemia may also further clarify whether acute treatment of the heart with DCA is inducing a negative profile.

These findings are supported by reports by Wambolt *et al* within the hypertrophied heart that perfusion with 1 mM DCA is sufficient to reduce glycolytic flux in hypertrophied hearts [112]. Furthermore Stacpoole *et al* report a reduction in the oxidation of short and medium fatty acids in both preparations of heart and skeletal muscle incubated with DCA [120] and the use of DCA to treat lactic acidosis has been well characterised [113, 114, 120].

4.5.3 Chronic Dichloroacetate Treatment leads to Long-Term Metabolic Adaptation within the Heart

Chronic dichloroacetate (DCA) treatment induces a carbohydrate metabolic profile within the heart similar to that of acute DCA treatment characterised by enhanced pyruvate dehydrogenase (PDH) flux and a significant reduction in glycolytic flux and lactate efflux as previously described in Section 4.5.2. The role of DCA in reducing blood glucise and hyperglycaemia has previously been described by Stacpoole *et al* in diabetic patients and chemically-induced models of diabetes. They propose that a reduced in blood glucose is induced by a DCA-mediated inhibition of glucose synthesis in the liver combined with stimulation of the peripheral tissues to use glucose [128]. It is therefore possible that the reduction of glycolysis within the heart is also aided by the systemic effects of DCA treatment. However, a reduction in glycolysis is observed in the perfused heart acutely treated with DCA therefore it suggests that DCA is inducing a tissue specific effect.

Contrary to what was observed in the acutely treated heart, an increase in fatty acid oxidation was observed following chronic DCA treatment accompanied by no change in flux into citrate or glutamate. Stacpoole *et al* report a 52 % reduction in $^{3}H_2O$ label incorporation into fatty acids following chronic DCA treatment in patients suggesting a shift towards fatty acid oxidation and reduced fatty acid storage [135]. This was accompanied by no change in label incorporation into acetylcarnitine was observed within this study with chronic DCA treatment when normalised to PDH flux, however, a significant increase in label incorporation into acetylcarnitine was observed prior to normalisation to PDH flux. This suggests that acetyl-CoA groups may be sequestered as acetylcarntine to maintain an elevated level of PDH activity [56]. As previously discussed, metabolomic analysis may help to further clarify the effects of chronic DCA treatment on cardiac metabolism. Acute DCA treatment is associated with a reduction in fatty acid oxidation as previously described in Section 4.5.2. This suggests that chronic DCA treatment is inducing an adaptive response where the energy deficit induced during acute DCA treatment is met by an upregulation of fatty acid oxidation.

Despite a reduction in glycolytic flux following DCA treatment, no change in myocardial glycogen content was observed and circulating glucose concentrations remained constant. It would therefore be interesting to look at whether glucose uptake is altered following DCA treatment, work by Lorni *et al* suggested that DCA had no effect on glucose uptake in the heart and liver along with no change in glycogen content as described in this study supportive of the work presented here [131]. Intracellular lactate content also remained unchanged suggesting that DCA reduces flux from pyruvate to lactate rather than the lactate pool itself.

In terms of the effect of DCA treatment on fatty acid metabolism, Stacpoole *et al* have previously shown that chronic incubation with DCA is associated with decreased fatty acid storage within isolated hepatocytes [135]. It would be interesting to look at myocardial fatty acid content especially given fatty acid oxidation is upregulated within the heart following chronic DCA treatment and systemic triacylglyceride levels are reduced. This suggests that fatty acid mobilisation may be favoured over fatty acid storage following chronic DCA treatment in order to meet the increased demand for fatty acid oxidation.

Interestingly, chronic DCA treatment is associated with a substantial increase in circulating levels of 3-hydroxybutyrate. DCA and glyoxylate, a metabolite of DCA are proposed to inhibit HMG-CoA reductase, the first committed step of cholesterol synthesis which has previously been described by Demaugre *et al* in hepatic mitchondria [120, 124]. Acetoacetyl-CoA, which results from the thiolation of two molecules of acetyl-CoA, is the substrate for both the cholesterol synthesis and ketogenic pathways [136]. Inhibition of HMG-CoA reductase via oxalate as described by Demaugre *et al* may increase the substrate availability for the ketogenic pathway leading to enhanced production of β-hydroxybutyrate and an elevated levels within the serum as described within this study and is an example of how the systemic effects of DCA treatment may also be contributing to the myocardial metabolic profile [124].

4.5.4 The Mechanism of Dichloroacetate in the Heart

The differing metabolic profiles observed following either acute or chronic treatment provides some insight into which pathways dichloroacetate (DCA) may target, however, the specific points which DCA targets still remain unclear. Previous work by Sobrino *et al* and Clark *et al* suggests that DCA may suppress the glycolytic enzyme, phosphofructokinase-1 (PFK-1) in adipose and muscle cells respectively, although the mechanism by which this is thought to occur is not known [133, 137]. Anderson *et al* report a reduction in the hepatic hexokinase and pyruvate kinase (PK) activity following DCA treatment [134]. Our findings support a reduction in glycolytic flux is directly impacted by DCA treatment but provides no insight into the mechanism through which this occurs. A reduction in glycolytic flux is sustained following chronic treatment with DCA whilst an adaptive response is induced within the fatty acid oxidation pathway. This suggests an additional target of DCA, aside from PDH, lies within the glycolytic pathway. PFK-1 is inhibited by high levels of citrate, which is a potential mechanism through which glycolysis may be reduced [1]. However, this study suggests that citrate is unlikely to play a role as no elevation in citrate is observed. Furthermore, flux into the TCA cycle is normalised following chronic DCA treatment. This is supported by the findings of Clark *et al* who report no change in citrate levels despite evidence of reduced glycolytic flux in muscle cells incubated with DCA [137].

In the light of these findings of this study, it also appears unlikely that α-ketoglutarate (α-KG) dehydrogenase is targeted by DCA as suggested by Tretter and Adam-Vizi [123]. α-KG dehydrogenase is a thiamine containing dehyhydrogenase similar to PDH which is why it has been proposed as a target for DCA [123]. These findings show that the reduction in flux into the TCA cycle following acute DCA treatment was normalised during chronic treatment with DCA, it therefore seems unlikely that α-KG dehydrogenase is a target of DCA otherwise a reduction in TCA cycle flux would be sustained with chronic DCA treatment.

This study supplements the work previously conducted focusing largely on the metabolic

profile of the heart following acute DCA treatment. This is advantageous when examining the use of DCA to treat cardiac disease, however, the effects of DCA treatment on other organs hasn't been clarified here. Given DCA is a non-specific inhibitor of PDK, isoforms of which are present in all tissues, this needs to be taken into consideration when considering the use of DCA as treatment.

4.6 Conclusions and Future Perspectives

Within this study, we have shown that an acute infusion with DCA induces a reduction in glycolytic flux and fatty acid oxidation aside from the up-regulation of PDH flux. When given chronically however, an increase in fatty acid oxidation is observed accompanied by a normalisation of flux into the TCA cycle, suggesting there are some compensatory adaptation to DCA treatment when given long-term but PDH activity remains up-regulated. This differs from the metabolic profile most commonly described in the literature, however, it is likely that this due to the organ specific nature of this study and the duration of the treatment used. It would therefore be interesting to further clarify the molecular effects of DCA treatment which underpin the metabolic changes observed in the heart including the effects of chronic DCA treatment on the myocardial fatty content and both fatty acid and glucose uptake.

The findings presented here suggest that DCA would be a suitable treatment for cardiac hypertrophy [50, 4, 42]. The development of hypertrophy is associated with a switch away from fatty acid oxidation towards increased glycolytic dependence. Given that chronic DCA treatment is associated with a reduction in glycolytic flux and an enhanced dependence on fatty acid oxidation, it may have a beneficial influence on the heart. This is further discussed in Chapter 5.

Chapter 5

The Effect of Chronic Up-regulation of Pyruvate Dehydrogenase Activity on Hypertrophic Development and Progression

5.1 Chapter Overview

The structural, functional and metabolic changes which occur during hypertrophic development have previously been investigated in Chapter 3. This work highlighted that the heart undergoes a phase of compensatory hypertrophy for up to 10 weeks following the induction of hypertension via constriction of the abdominal aorta. The induction of hypertension is associated with a compensatory increase in left ventricular mass, which is supported by an increase in glycolytic flux. By 14 weeks post-surgery, the heart appeared to have adapted to the sustained increase in blood pressure with no further evidence of altered glucose handling observed at 18 weeks post-surgery. This finding is well supported within the literature and it is widely hypothesised that during hypertrophic development, the heart undergoes metabolic switching away from fatty acid oxidation in favour of increased glycolytic dependence [4, 5, 91, 1, 12, 138, 50, 42, 51]. Glycolysis is significantly less energetically favourable than fatty acid oxidation and although a normalisation of glycolytic flux was observed within the abdominal aortic constriction model of hypertrophy, this extended period of glycolytic dependence may have caused irreversible damage to the heart which acts as a precursor to functional decline.

The restoration of coupling between glycolysis and glucose oxidation, is therefore an attractive therapeutic avenue. Dichloroacetate (DCA) was identified as a potent indirect activator of pyruvate dehydrogenase (PDH) making it a suitable therapy to restore the coupling between glycolysis and glucose oxidation. Furthermore, the work summarised in Chapter 4 suggests that chronic DCA treatment may also act to reduce glycolytic flux and promote fatty acid oxidation. When applied to the hypertrophied heart, it may act to restore a positive metabolic profile within the heart preventing the negative aspects of left ventricular hypertrophy.

This chapter investigates the effects of DCA treatment on hypertrophic development in the abdominal aortic banding model of hypertrophy immediately post-surgery (Early Treatment) and the effects of treatment following the establishment of hypertrophy (Late Treatment). Cardiac structure, function and metabolism were assessed *in vivo* at 4, 9 and 14 weeks post-surgery using cine MRI and hyperpolarized [^{13}C]labelled pyruvate.

DCA treatment was given freely in drinking water either immediately post-surgery (Early Treatment) or at 5 weeks post-surgery (Late Treatment) following the characterisation of hypertrophy. The effects of DCA treatment on glycolytic flux were assessed in the Langendorff-perfused heart at 18 weeks post-surgery.

5.2 Introduction

5.2.1 Metabolic Remodelling with the Development of Left Ventricular Hypertrophy - A Brief Overview

The presence of metabolic remodelling with the development of hypertrophy is well-accepted, however, the role it plays in the development and progression of hypertrophy and heart failure is less well understood. Metabolic switching away from fatty acid oxidation towards enhanced glucose utilisation is thought to underpin energy depletion within the heart eventually leading to the development of heart failure [4, 5, 91, 1, 12, 138, 50, 42, 51]. The work described in Chapter 3.2.3 suggests that these metabolic changes are largely dependent on the stage of hypertrophy [51].

A number of mechanisms are proposed to underpin the metabolic remodelling. Work by Broderick *et al* propose that carnitine plays a role in both the reduction in fatty acid oxidation observed within the hypertrophied heart and the alteration in glucose utilisation via disruption of the acetyl-CoA/CoA pool [55]. It has also been proposed that the heart reverts back to a metabolic profile observed in the foetus, which is highly glycolytic [139]. A more comprehensive review of the metabolic changes with the development of hypertrophy is described in Chapter 1.4 but one consistency is the potentially negative role of an increased glycolytic dependency with the development of hypertrophy. A number of metabolic therapies have been developed to target the alteration in metabolic profile within the heart.

The modulation of fatty acid oxidation within the hypertrophied heart is particularly attractive and is focused on reducing fatty acid oxidation within the heart in order to force coupling between glycolysis and glucose oxidation via the glucose-fatty acid cycle. Several therapies have been developed and trialled with moderate success [139]. Dicholoracetate (DCA) is also an attractive treatment for hypertrophy and heart failure. Traditionally, DCA was thought to simply enhance flux through pyruvate dehydrogenase (PDH), however, the work described in Chapter 4 indicates that DCA acts beyond that of PDH, reducing glycolytic flux and promoting fatty acid oxidation suggesting it may be an ideal

drug for the treatment of left ventricular hypertrophy.

5.2.2 Metabolic-based Therapies as a Treatment for Hypertrophy and Heart Failure

A number of metabolic treatments for hypertrophy and heart failure have been developed. A range of metabolic targets exist and the promotion of glucose oxidation is one of the key areas following the evidence of an increased glycolytic dependence with the development of hypertrophy and heart failure. A brief summary is presented below of the areas targeted and some of the drugs used in the treatment of hypertrophy and heart failure.

Etomoxir, ethyl-2-tetradecyl glycidate, oxfenicine and perhexilline target carnitine-palmitoyl transferase (CPT)-1 inhibiting the uptake of fatty acids into the mitochondria for oxidation [139, 21]. CPT-1 provides a natural regulatory point within fatty acid oxidation which has previously been described in Chapter 1.2.5.2. Inhibition of CPT-1 prevents the oxidation of fatty acids forcing enhanced glucose utilisation via a glucose-fatty acid cycle mediated mechanism. Both Etomoxir and Perhexilline received moderate success when used clinically. Treatment with Etomoxir was associated with an improved ejection fraction, exercise-induced cardiac output and improved clinical status when adiministered to patients with NYHA class II heart failure and Perhexilline was used clinically in France to treat angina. However, both drugs were associated with liver toxicity in direct relation to inhibition of CPT-1 [21]. Interestingly, Etomoxir is proposed to also improve calcium handling as is Ramipril, a widely-perscribed angiotensin converting enzyme inhibitor (ACEI) fully described in Chapter 6, which may also have a metabolic basis [21, 93].

The inhibition of fatty acid oxidation is also an attractive therapeutic target in promoting glucose oxidation. Trimetazidine inhibits 3-ketoacyl-CoA thiolase which catalyses the final step of fatty acid oxidation during which one molecule of acetyl-CoA is cleaved from the fatty acyl chain resulting in the partial oxidation of the fatty acid. Trimetazidine is sucessfully used as a treatment for angina and as well as reducing fatty acid oxidation,

it has also been shown to enhance glucose oxidation via re-establishing coupling between glycolysis and glucose oxidation. Ranolazine is another partial inhibitor of fatty acid oxidation, which also successfully promotes glucose oxidation via the glucose-fatty acid cycle. However, the partial oxidation of fatty acids was associated with negative side effects due to the role of partially-oxidised fatty acids and lipid accumulation on lipotoxicity in the heart [139].

Within these treatments, the emphasis is largely placed on reducing fatty acid oxidation within the hypertrophied myocardium and enhancing glucose oxidation to modulate the metabolic profile already present within the hypertrophied heart. There is evidence that fatty acid oxidation is detrimental to the hypertrophied and failing myocardium leading to the accumulation of lipids and reactive oxygen species (ROS) which are associated with lipotoxicity [140, 51]. Both Trimetazidine and Ranolazine, which successfully inhibit fatty acid oxidation and promote increased coupling between glycolysis and glucose oxidation, have been shown to have a beneficial effect within the diseased myocardium [139, 21]. Given the problems associated with the incomplete oxidation of fatty acids, a treatment which acts to increase coupling between glycolysis and glucose oxidation mediated via carbohydrate metabolism may be a more viable option [21]. Dichloroacetate (DCA) upregulates pyruvate dehydrogenase (PDH) activity, increasing coupling between glycolysis and glucose oxidation and may provide a more suitable treatment for hypertrophy, heart failure and ischemic heart disease [111].

5.2.3 Dichloroacetate as a Treatment for Cardiac Hypertrophy

The work summarised in Chapter 3 identified the presence of an increased glycolytic dependence in the hypertension induced, hypertrophied heart at 4 and 9 weeks post-abdominal aortic constriction surgery. This is supported by previous work by Seymour *et al* and Allard *et al* who also report increased glycolytic dependence within the abdominal aortic constriction (AC) model [50, 42]. Furthermore, the work summarised in Chapter 4 examined the metabolic changes associated with chronic dichloroacetate (DCA) treat-

ment. The effect of DCA on enhancing PDH flux is well-documented, however, the wider effects of DCA treatment were previously poorly characterised. The work in Chapter 4 provided a heart-specific analysis of the metabolic changes associated with both acute and chronic DCA treatment. Interestingly, it identified that although DCA acts to enhance PDH flux, this is associated with a reduction in glycolytic flux and an increased dependence on fatty acid oxidation when administered chronically. The mechanism by which this occurs is unclear and it may represent the increased efficiency of enhanced coupling between glucose and glucose oxidation or alternatively DCA may target one or more of the enzymes within glycolysis. An increase in fatty acid oxidation was also observed within the heart following chronic treatment with DCA. This differed from the metabolic profile observed following acute treatment with DCA where glycolytic flux and fatty acid oxidation were reduced following an acute infusion with DCA leading to a reduction in flux into the TCA cycle. Therefore it would appear that chronic DCA treatment induces an adaptive shift to fatty acid oxidation within the heart. Given that the development of hypertrophy is associated with a shift from fatty acid oxidation to enhanced glycolytic flux, treatment with DCA, which reduces glycolytic flux and promotes fatty acid oxidation may act to restore the energy balance within the hypertrophied heart.

5.2.4 Chapter Aims

The work presented in this chapter aimed to assess the effect of chronic dichloroacetate (DCA) treatment on hypertrophic development and progression. Clarification of the role of glycolysis in the process of hypertrophic remodelling in Chapter 3 identified an increased glycolytic dependence in the initial stages of hypertrophy representative of uncoupling between glycolysis and glucose oxidation. The impact of this energy imbalance within the heart was discussed in more detail in Chapter 1.4 and is widely considered to be negative. The effects of DCA on PDH is well-characterised with enhanced PDH activity leading to increased coupling between glycolysis and glucose oxidation leadjng to restoration of the energy balance within the hypertrophied heart. Work conducted by Atherton *et al* reported a hypertrophic regression in the T3 hyperthyroid model of left ventricular

hypertrophy following DCA treatment which may translate to the AC model of LVH Furthermore, the work presented in Chapter 4 identified an increased dependence on myocardial fatty acid oxidation in addition to restored coupling between glycolysis and glucose oxidation which would potentially be of benefit in the hypertrophied heart.

5.3 Methods

5.3.1 Study Overview

An overview of the study is summarised in Figure 5.1. Left ventricular hypertrophy (LVH) was induced in male Sprague-Dawley rats via abdominal aortic constriction (AC; n = 58; 200-250 g) as previously described [4]. Control (Sham; n = 20; 200-250 g) rats underwent the same process but without constriction of the aorta. Structural and functional analysis of the heart was performed using cine MRI and metabolic changes were assessed following injection of hyperpolarized [^{13}C]-labelled pyruvate at 4, 9 and 14 weeks post-surgery. A subset of AC rats (Early DCA Treatment) were treated with DCA (0.75 g $L^{(-1)}$) administered *ad libitum* in the drinking water two days post-surgery. A further subset of AC rats (Late DCA Treatment) were treated from 5 weeks post-surgery following the initial characterisation of LVH in the AC group. Hearts were rapidly excised at 18 weeks post-surgery and perfused via the Langendorff mode with ^{3}H-labelled glucose and used to assess the effects of chronic DCA treatment on basal and insulin-stimulated glycolytic flux.

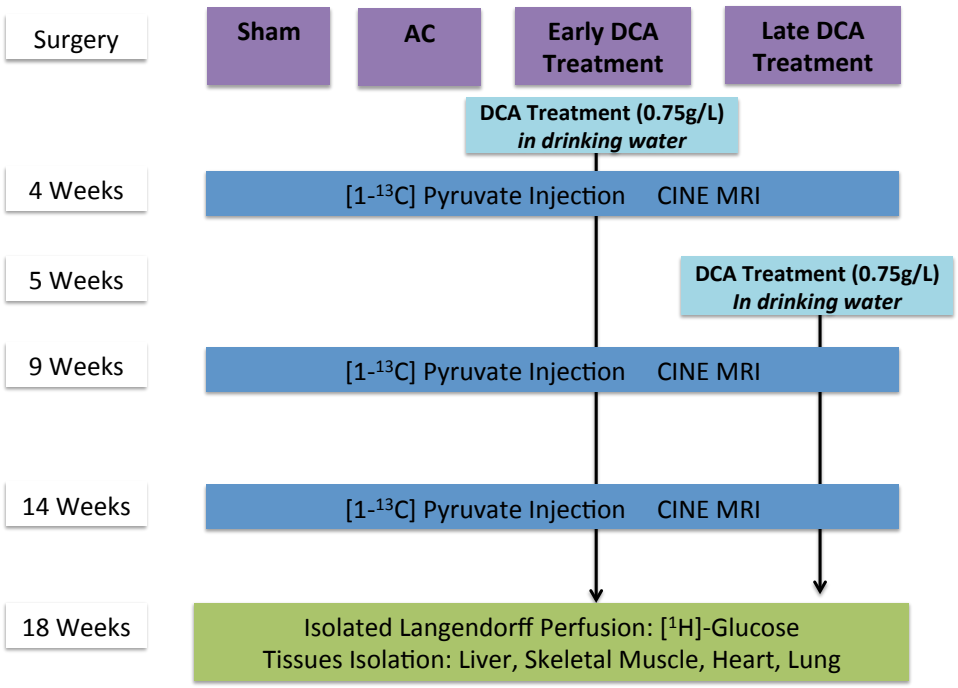


Figure 5.1: The Effects of Chronic Pyruvate Dehydrogenase Up-Regulation on Hypertrophic Development and Progression - A Study Overview

5.3.2 Animal Work

All animal experiments were conducted by a licensed individual in accordance with the Home Office Guidance on the Operation of Animals (Scienctific Procedures) Act of 1986 and to University of Oxford institutional guidelines.

Animals were housed in a dedicated facility (Biomedical Sciences Services, University of Oxford, UK) under a 12 hr light-dark cycle and maintained on a standard laboratory chow (Harlan Laboratories, Kent, UK) and standard laboratory water given *ad libitum* unless otherwise stated. All *in vivo* metabolic experiments were performed whilst animals were in the fed state (taken as between 6 am and 1 pm) unless otherwise stated

5.3.3 Surgical Induction of Left Ventricular Hypertrophy

Male Sprague-Dawley rats (200-250 g; Harlan Laboratories, Kent, UK) underwent constriction of the abdominal aorta (AC; n = 58) between the two renal arteries under aseptic conditions as previously described in Section 2.2. Following a laparotomy whereby the abdominal aorta was exposed, a reproducible constriction was placed around the aorta between the two renal arteries. Sham (n = 20) animals received the same procedure but without constriction of the aorta.

5.3.4 Dichloroacetate Preparation and Treatment

Dichloroacetate (DCA) treatment (0.75 g L^{-1}) was prepared from dichloroactic acid (1.563 g ml^{-1}; Sigma Aldrich, Dorset, UK) added to standard laboratory water neutralised to a pH of approximately 7.2 with sodium hydroxide solution (Fisher Scientific Laboritories, New Hampshire, USA) as previously described in Section 2.4.2.

Treated groups received chronic treatment with dichloroacetate (DCA; 0.75 g L^{-1}) administered in drinking water *ad libitum* at either two days post-surgery (Early DCA Treatment; n = 13) or from 5 weeks post-surgery (Late DCA Treatment; n = 19) following the development of left ventricular hypertrophy (LVH). DCA treatment was maintained in the treated groups until 18 weeks post-surgery whilst control rats were maintained on

standard laboratory water. Fresh DCA treatment was made up and replaced a minimum of every three days

5.3.5 *In Vivo* Assessment of Cardiac Structure and Function

Cardiac structure and function was assessed at 4, 9 and 14 weeks post-surgery using cine MRI as previously described in Section 2.3.5. Male Sprague-Dawley rats were anaesthetised as described in Section 2.3.1 and placed in a custom-built cradle within a 7 T magnetic resonance scanner (Varian Biomedical Systems, Yarnton, UK). Betweeen 10 and 11 contiguous cine-MR images (28-35 frames per cardiac cycle) were acquired of the heart in the short-axis orientation covering the entire heart using a quadrature high pass birdcage coil (RAPID Biomedical GmhB, Germany) as previously described in Section 2.3.5 [69].

5.3.6 *In vivo* Assessment of Metabolic Parameters using Dynamic Nuclear Polarization

Pyruvate dehydrogenase (PDH) flux was assessed *in vivo* at 4, 9 and 14 weeks post-surgical induction of left ventricular hypertrophy using [^{13}C]pyruvate labelled on the first carbon as previously described in Section 2.3. Male Sprague-Dawley rats were prepared as described in Section 2.3.1. Approximately 1 ml of hyperpolarized [1-^{13}C]pyruvate was infused over 10 seconds and 60 single scan spectra were acquired over a period of 60 seconds as previously described in Section 2.3.

5.3.7 *Ex vivo* Assessment of Glycolytic Flux in the Isolated Langendorff Perfused Heart

At 18 weeks post-surgery, hearts were isolated and perfused with Krebs-Heinsleit (KH) buffer containing 11 mM glucose, 0.4 mM palmitate and 0.5 μCi [5-^{3}H]glucose as previously described in Section 2.5. Following a 10 minute acclimatisation period, hearts were perfused for 20 minutes to obtain basal glycolytic rates prior to the addition of insulin (2048 pmol L^{-1}) and then hearts were perfused for a further 32 minutes as previously

described in Section 2.5.4.1. Hearts were washed for 4 minutes with fresh KH in the absence of radiotracers at the end of the perfusion protocol and rapidly freeze-clamped on the cannula and stored at -80 °C for subsequent analysis as previously described in Section 2.5.4.1. A sample (1 ml) of perfusate were taken every 4 minutes across the 52 minute perfusion period and stored at -20 °C as previously described in Section 2.5.5.

5.3.8 Measurement of the Rate of Lactate Efflux from the Langendorff Perfused Heart

The rate of lactate efflux was measured from aliquots of perfusate from hearts perfused via the Langendorff mode as previously described in Section 2.5.7.

5.3.9 Statistical Analysis

All data is presented as mean ± standard error of the mean (SEM). *In vivo* structural, functional and metabolic data was analysed using a one-way ANOVA with Sidak correction for multiple comparison. Perfusion data acquired at 18 weeks post-surgery was analysed using a two-way ANOVA with repeated measures taking insulin and hypertrophy as independent variables. All data was analysed using the GraphPad Prism 7 Software Package (GraphPad Softwares, California, USA).

5.4 Results

5.4.1 The Effect of Early and Late Dichloroacetate Treatment on Structural Remodelling in the Hypertrophic Heart

Changes in cardiac structure were assessed at 4, 9 and 14 weeks following the surgical induction of hypertrophy. At 4 weeks post-surgery, the Early Treatment group had received DCA treatment for 4 weeks and the Late Treatment group had not yet received treatment. Consistent with the presence of left ventricular (LV) hypertrophy, no difference in LV mass was observed in either the Early Treatment or Late Treatment groups when compared to the AC group ($p = 0.70$ *AC vs. Early Treatment*; $p > 0.99$ *AC vs. Late Treatment*). This was accompanied by a difference in LV mass to body weight ratio in both the Early Treatment and the Late Treatment relative to the AC group ($p = 0.83$ *AC vs. Early Treatment*; $p = 0.99$ *AC vs. Late Treatment*). No change in body weight was observed in either the Early Treatment or Late Treatment groups when compared to the AC group (Fig 5.2B; $p = 0.69$ *AC vs. Early Treatment*; $p = 0.87$ *AC vs. Late DCA Treatment*).

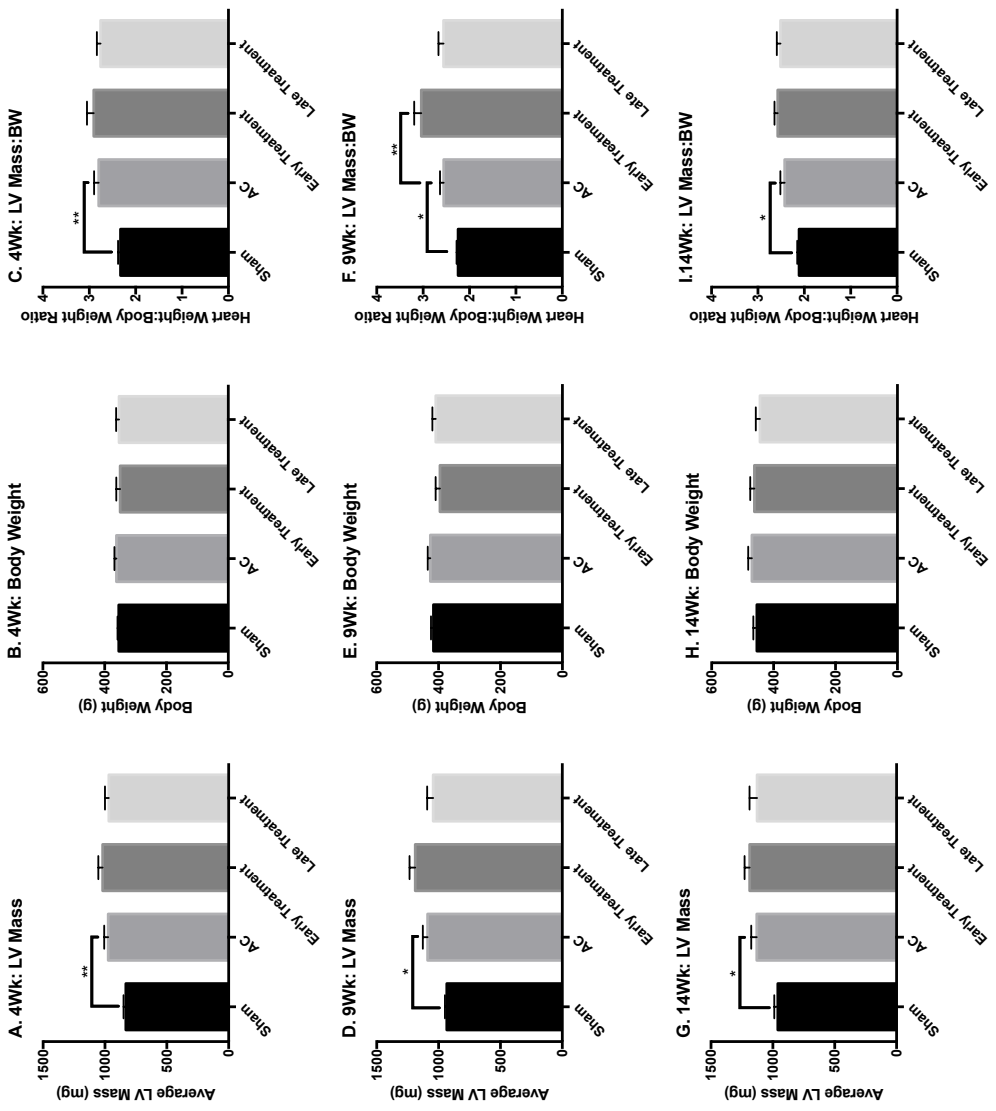


Figure 5.2: The Effect of Early and Late Dichloroacetate (DCA) Treatment on Structural Remodelling in the Hypertrophic Heart at 4, 9 and 14 Weeks Post- the Surgical Induction of Hypertrophy. A. Left Ventricular (LV) Mass at 4 Weeks Post-Surgery; B. Body Weight (BW) at 4 Weeks Post-Surgery; C. Left Ventricular Mass to Body Weight Ratio at 4 Weeks Post-Surgery; D. LV Mass at 9 Weeks Post-Surgery; E. BW at 9 Weeks Post-Surgery; F. LV Mass to BW Ratio at 9 Weeks Post-Surgery; G. LV Mass at 14 Weeks Post-Surgery; H. BW at 14 Weeks Post-Surgery; I. LV Mass to BW Ratio at 14 Weeks Post-Surgery. 4 Weeks: Sham: n = 18; AC: n = 23; Early Treatment: n = 13; Late Treatment: n = 20. 9 Weeks: Sham: n = 20; AC: n = 26; Early Treatment: n = 13; Late Treatment: n = 19; 14 Weeks: Sham: n = 18; AC: n = 23; Early Treatment: n = 8; Late Treatment: n = 17; * $p < 0.05$ *vs. AC* ** $p < 0.01$ *vs. AC*. *Mean* $\pm$ *SEM* One-Way ANOVA with Sidak Correction for Multiple Comparisons. AC: Aortic Constriction; Early Treatment: Early DCA Treatment; Late Treatment: Late DCA Treatment.

At 9 weeks post-surgery, the Early Treatment group had received 9 weeks of treatment with DCA whereas, the Late Treatment group had only received 5 weeks of DCA treatment. Hypertrophy was sustained in both the Early Treatment and Late Treatment groups represented by no difference in LV mass in either group when compared to the AC group at 9 weeks post-surgery (Fig 5.2D; *p = 0.23 AC vs. Early Treatment*; *p = 0.79 AC vs. Late Treatment*). In the Late Treatment group, this was supported by no difference in LV mass to body weight ratio when compared with the AC group (Fig 5.2F; *p >0.99 AC vs. Late Treatment*) however, an elevation in LV mass to body weight ratio was observed in the Late Treatment group when compared to the AC group (AC: 2.56 ± 0.08 Late Treatment: 2.56 ± 0.11; Fig 5.2F; *p = 0.01 AC vs. Late Treatment*). No change in body weight was observed in either the Early or Late DCA treatment groups vs. the AC group at 9 weeks post-surgery (Fig 5.2E; *p = 0.13 AC vs. Early Treatment*; *p = 0.49 AC vs. Late Treatment*).

Hypertrophic remodelling was further sustained at 14 weeks post-surgery in both the Early Treatment, following 14 weeks of DCA treatment and in the Late Treatment group following 10 weeks of DCA treatment. This was marked by no difference between the both treatment groups and when compared to the AC group (Fig 5.2G; *p = 0.86 AC vs. Early Treatment*; *p >0.99 AC vs. Late Treatment*). This was mirrored by no difference in LV mass to body weight ratio in both the Early and Late treatment groups relative to the AC group (Fig 5.2I; *p = 0.62 AC vs. Early Treatment*; *p = 0.76 AC vs. Late Treatment*). This was accompanied by no change in body weight in the Early or Late treatment groups relative to the AC group (Fig 5.2H; *p = 0.97 AC vs. Early Treatment*; *p = 0.33 AC vs. Late Treatment*).

5.4.2 The Effect of Early and Late Dichloroacetate Treatment on Functional Remodelling in the Hypertrophic Heart

The effect of DCA treatment on functional remodelling was assessed within the hypertrophied heart at 4, 9 and 14 weeks post-surgery. At 4 weeks post-surgery, the Early Treatment group had experienced 4 weeks of DCA treatment which was associated with

no change in cardiac output or heart rate when compared with the AC group (cardiac output: Fig 5.3A; $p = 0.99$ *AC vs. Early Treatment*; heart rate: Fig 5.3C; $p = 0.81$ *AC vs. Early Treatment*). However, a significant reduction in ejection fraction was observed in the Early Treatment group vs. the AC group (AC: 76 ± 1 %; Early Treatment: 64 ± 2 % Fig 5.3B; $p < 0.001$ *AC vs. Early Treatment*). The Late DCA Treatment group had not yet received DCA treatment at 4 weeks post-surgery and exhibited no evidence of functional remodelling when compared to the AC group (cardiac output: Fig 5.3A; $p = 0.68$ *AC vs. Late Treatment*; ejection fraction: Fig 5.3B; $p = 0.18$ *AC vs. Late Treatment*; heart rate: Fig 5.3C; $p = 0.75$ *AC vs. Late Treatment*).

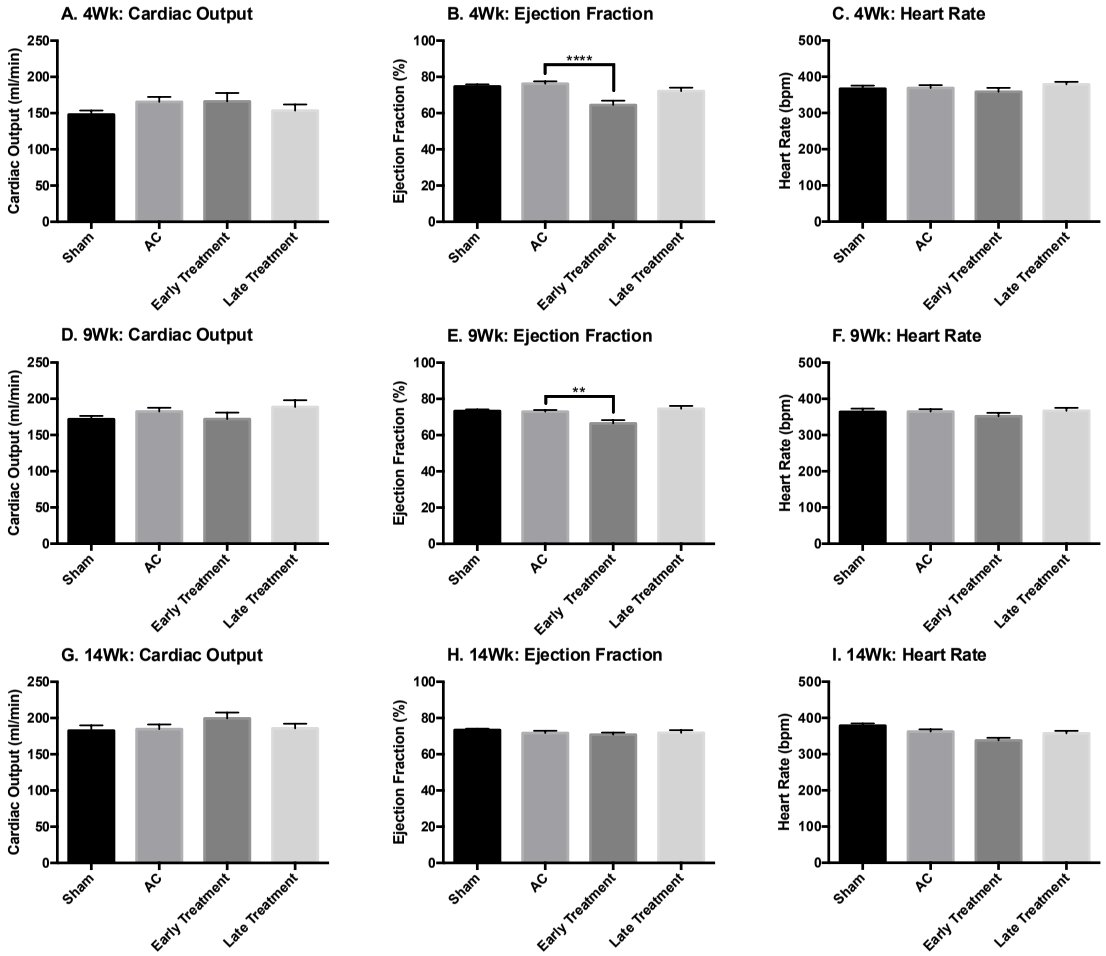


Figure 5.3: The Effect of Early and Late Dichloroacetate (DCA) Treatment on Functional Parameters in the Hypertrophic Heart at 4, 9 and 14 Weeks Post- the Surgical Induction of Hypertrophy. A. Cardiac Output at 4 Weeks Post-Surgery; B. Ejection Fraction at 4 Weeks Post-Surgery; C. Heart Rate at 4 Weeks Post-Surgery; D. Cardiac Output at 9 Weeks Post-Surgery; E. Ejection Fraction at 9 Weeks Post-Surgery; F. Heart Rate at 4 Weeks Post-Surgery; G. Cardiac Output at 14 Weeks Post-Surgery; H. Ejection Fraction at 14 Weeks Post-Surgery; I. Heart Rate at 14 Weeks Post-Surgery. 4 Weeks: Sham: n = 18; AC: n = 23; Early Treatment: n = 13; Late Treatment: n = 20; 9 Weeks: Sham: n = 20; AC: n = 26; Early Treatment: n = 13; Late Treatment: n = 19; 14 Weeks: Sham: n = 18; AC: n = 23; Early Treatment: n = 8; Late Treatment: n = 17. ** $p < 0.01$ *AC vs. Early Treatment* **** $p < 0.001$ *AC vs. Late Treatment* $Mean \pm SEM$ One-Way ANOVA with Sidak Correction for Multiple Comparisons. AC: Aortic Constriction; Early Treatment: Early DCA Treatment; Late Treatment: Late DCA Treatment.

Following 9 weeks of DCA treatment, a significant decrease in ejection fraction was sustained in the Early Treatment group vs. the AC group (AC: 74 ± 1 %; Early Treatment: 66 ± 1 %; Fig 5.3E; *p <0.001 AC vs. Early Treatment*). This was accompanied by no change in cardiac output (Fig 5.3D; *p = 0.67 AC vs. Early Treatment*) or heart rate (Fig 5.3F; *p = 0.67 AC vs. Early Treatment*) in the Early Treatment group vs. the AC group. No change in cardiac output (Fig 5.3G; *p = 0.87 AC vs. Late Treatment*), ejection fraction (Fig 5.3E; *p = 0.72 AC vs. Early Treatment*) or heart rate (Fig 5.3F; *p >0.99 AC vs. Late Treatment*) was observed in the Late Treatment group vs. the Ac group following 5 weeks of DCA treatment.

No change in cardiac output, ejection fraction or heart rate was observed in either the Early or Late Treatment groups relative to the AC group at 14 weeks post-surgery (cardiac output: Fig 5.3G; *p = 0.52 AC vs. Early Treatment*; *p >0.99 AC vs. Late Treatment*; ejection fraction: Fig 5.3H; *p = 0.95 AC vs. Early Treatment*; *p >0.99 AC vs. Late Treatment*; heart rate: Fig 5.3I; *p = 0.11 AC vs. Early Treatment*; *p = 0.93 AC vs. Late Treatment*).

At 4 weeks post-surgery no change in stroke volume or end diastolic volume (EDV) was observed in either the Early Treatment group, which had received 4 weeks of DCA treatment or the Late Treatment group, which had yet to receive DCA treatment when compared to the AC group (stroke volume: Fig 5.4A; *p = 0.58 AC vs. Early Treatment*; *p = 0.78 AC vs. Late Treatment*; EDV: Fig 5.4B; *p 0.61 AC vs. Early Treatment*; *p >0.99 AC vs. Late Treatment*). However, a significant increase in end systolic volume (ESV) was observed in the Early Treatment group vs. the AC group (ESV: AC: 148 ± 10 μl; Early Treatment: 232 ± 18 μl; Fig 5.4C; *p <0.001 AC vs. Early Treatment*).

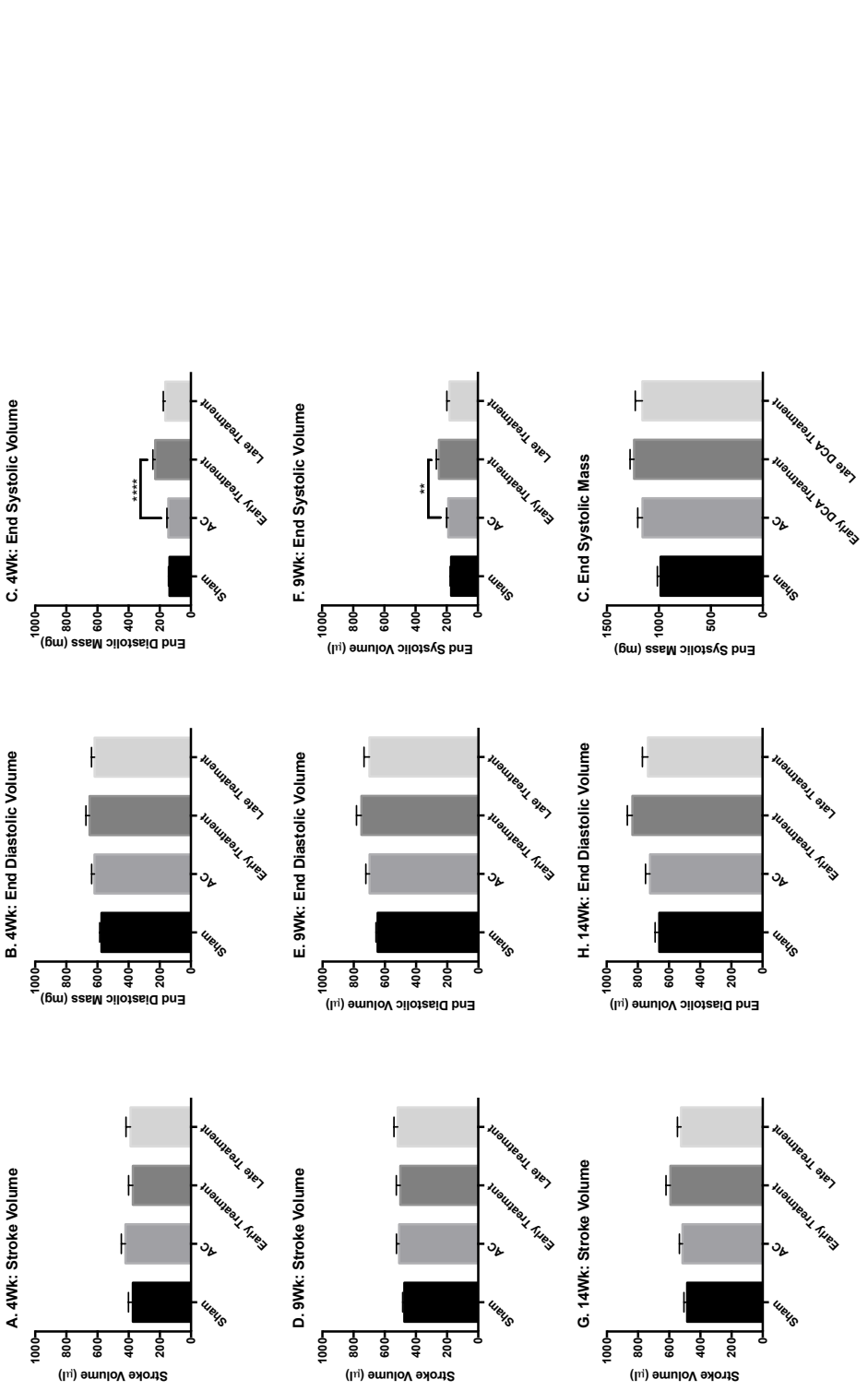


Figure 5.4: The Effect of Early and Late Dichloroacetate (DCA) Treatment on Structural and Functional Remodelling in the Hypertrophic Heart at 4, 9 and 14 Weeks Post-Surgery. A. Stroke Volume at 4 Weeks Post-Surgery; B. End Diastolic Volume at 4 Weeks Post-Surgery; C. End Systolic Volume at 4 Weeks Post-Surgery; D. Stroke Volume at 9 Weeks Post-Surgery; E. End Diastolic Volume at 9 Weeks Post-Surgery; F. End Systolic Volume at 9 Weeks Post-Surgery; G. Stroke Volume at 14 Weeks Post-Surgery; H. End Diastolic Volume at 14 Weeks Post-Surgery; C. End Systolic Volume at 14 Weeks Post-Surgery. 4 Weeks: Sham: n = 18; AC: n = 23; Early Treatment: n = 13; Late Treatment: n = 20; 9 Weeks: Sham: n = 20; AC: n = 26; Early Treatment: n = 13; Late Treatment: n = 19; 14 Weeks: Sham: n = 18; AC: n = 23; Early Treatment: n = 8; Late Treatment: n = 17. ** $p < 0.01$ *vs. AC* **** $p < 0.001$ *vs. AC*. $Mean \pm SEM$ One-Way ANOVA with Sidak Correction for Multiple Comparisons. AC: Aortic Constriction; Early Treatment: Early DCA Treatment; Late Treatment: Late DCA Treatment.

No change in end systolic volume was observed in the Late Treatment vs. the AC group, prior to treatment with DCA (ESV: Fig 5.4C; *p = 0.44 AC vs. Late Treatment*).

This was mirrored at 9 weeks post-surgery where no change in stroke volume or EDV was observed in the Early Treatment group relative to the AC group following 9 weeks of DCA treatment (stroke volume: Fig 5.4D; *p = 0.99 AC vs. Early Treatment*; EDV: Fig 5.4E; *p = 0.47 AC vs. Early Treatment*). However, a significant increase in ESV was observed in the Early Treatment group vs. the AC group at 9 weeks post-surgery (ESV: AC: 186 ± 10 μl; Early Treatment: 251 ± 11 μl; Fig 5.4F; *p <0.01 AC vs. Early Treatment*). No change in stroke volume, end diastolic or end systolic volume was observed in the Late Treatment group vs. the AC group following 5 weeks of DCA treatment (stroke volume: Fig 5.4D; *p = 0.98 AC vs. Late Treatment*; EDV: Fig 5.4E; *p >0.99 AC vs. Late Treatment*; ESV: Fig 5.4F; *p = 0.95 AC vs. Late Treatment*).

No change in stroke volume (Fig 5.4G; *p = 0.13 AC vs. Early Treatment*; *p = 0.98 AC vs. Late Treatment*), EDV (Fig 5.4H; *p = 0.11 AC vs. Early Treatment*; *p = 0.98 Sham vs. Late Treatment*) or ESV (Fig 5.4I; *p = 0.34 AC vs. Early Treatment*; *p = 0.99 AC vs. Late Treatment*) was observed in either the Early or Late Treatment groups at 14 weeks post-surgery, relative to the AC group following 14 and 10 weeks of DCA treatment respectively.

5.4.3 The Effect of Early and Late Dichloroacetate Treatment on Myocardial Metabolism *in vivo*

The effect of dichloroacetate (DCA) treatment on myocardial metabolism was assessed in the hypertrophied heart using hyperpolarised [1-^{13}C]labelled pyruvate following DCA treatment at 4, 9 and 14 weeks post-surgery.

Consistent with 4 weeks of DCA treatment, pyruvate dehydrogeanse (PDH) flux was elevated in the Early Treatment group vs. the AC group at 4 weeks post-surgery (AC: 0.0084 ± 0.0023 s^{-1}; Early Treatment: 0.0119 ± 0.0033 s^{-1}; Fig 5.5A; *p <0.01 AC vs. Early Treatment*). This was accompanied by no change in label incorporation into lactate (Fig 5.5B; *p = 0.39 AC vs. Early Treatment*) or alanine (Fig 5.5C; *p >0.99 AC vs. Early*

Treatment). No change in PDH flux (Fig 5.5A; $p = 0.87$ *AC vs. Late Treatment*) was observed in the Late Treatment group vs. the AC group accompanied by no change in label incorporation into lactate (Fig 5.5B; $p = 0.39$ *AC vs. Late Treatment*) or alanine (Fig 5.5C; $p > 0.99$ *AC vs. Late Treatment*) at 4 weeks post-surgery prior to treatment with DCA.

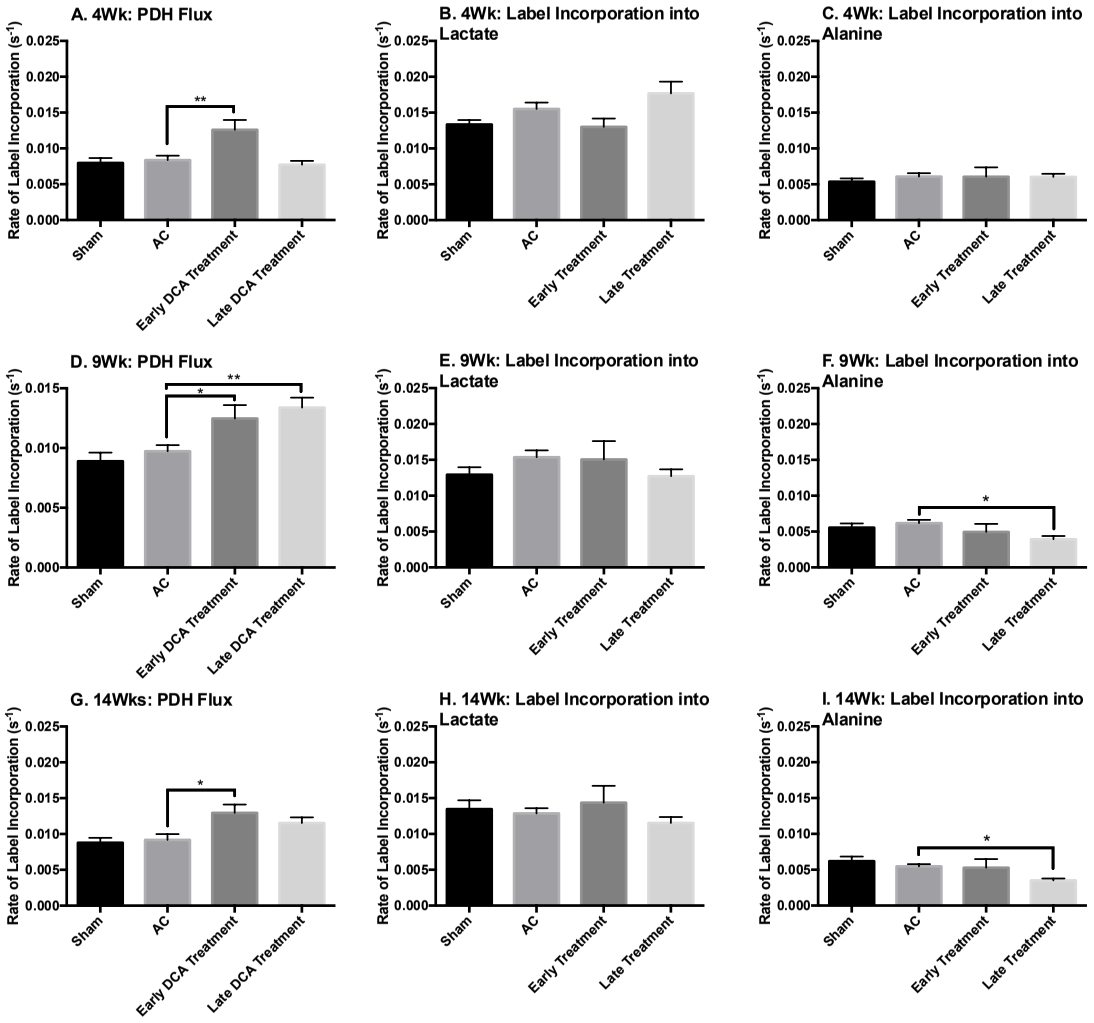


Figure 5.5: The Effect of Early and Late Dichloroacetate (DCA) Treatment on Myocardial Metabolism in the Hypertrophic Heart. A. PDH Flux at 4 Weeks Post-Surgery; B. Label Incorporation into Lactate at 4 Weeks Post-Surgery; C. Label Incorporation into Alanine at 4 Weeks Post-Surgery; D. PDH Flux at 9 Weeks Post-Surgery; E. Label Incorporation into Lactate at 9 Weeks Post-Surgery; F. Label Incorporation into Alanine at 9 Weeks Post-Surgery; G. PDH Flux at 14 Weeks Post-Surgery; H. Label Incorporation into Lactate at 14 Weeks Post-Surgery; I Label Incorporation into Alanine at 14 Weeks Post-Surgery. 4 Weeks: Sham: n = 18; AC: n = 22; Early Treatment: n = 9; Late Treatment: n = 19; 9 Weeks: Sham: n = 19; AC: n = 24; Early Treatment: n = 13; Late Treatment: n = 19; 14 Weeks: Sham: n = 18; AC: n = 23; Early Treatment: n = 8; Late Treatment: n = 19. * $p < 0.05$ *vs. AC* ** $p < 0.01$ *vs. AC. Mean* $\pm$ *SEM* One-Way ANOVA with Sidak Correction for Multiple Comparisons. AC: Aortic Constriction; Early Treatment: Early DCA Treatment; Late Treatment: Late DCA Treatment.

Following DCA treatment in both the Early and Late Treatment groups, a significant increase in PDH flux was observed when compared to the AC group at 9 weeks post-surgery (AC: $0.0097 \pm 0.0024\ s^{-1}$; Early Treatment: $0.0125 \pm 0.0035\ s^{-1}$; Late Treatment: $0.0127 \pm 0.0038\ s^{-1}$; Fig 5.5D; $p \leqslant 0.05$ *AC vs. Early Treatment*; $p < 0.01$ *AC vs. Late Treatment*). This was accompanied by no change in label incorporation into lactate (Fig 5.5E; $p > 0.99$ *AC vs. Early Treatment*) or alanine (Fig 5.5F; $p = 0.44$ *AC vs. Early Treatment*) in the Early Treatment group vs. the AC group. No change in label incorporation into lactate (Fig 5.5E; $p = 0.33$ *AC vs. Late Treatment*) was observed in the Late Treatment group vs. the AC group at 9 weeks post-surgery, however, an increase in PDH flux was accompanied by a significant reduction in label incorporation into alanine (AC: $0.0062 \pm 0.0016\ s^{-1}$; Late Treatment: $0.0039 \pm 0.0009\ s^{-1}$; Fig 5.5F; $p < 0.01$ *vs. AC*). Again, an elevation in label incorporation into lactate was observed in the AC group vs. the Sham group at 9 weeks post-surgery but this failed to reach statistical significance as described in Chapter 3 (Fig 5.5E; $p = 0.41$ *vs. Sham*).

At 14 weeks post-surgery, an elevation in PDH flux was sustained in both the Early Treatment group following 14 weeks when compared to the AC group (AC: $0.0092 \pm 0.0019\ s^{-1}$; Early Treatment: $0.0129 \pm 0.0046\ s^{-1}$; Fig 5.5G; $p = 0.05$ *AC vs. Early Treatment*). This was accompanied by no change in label incorporation into either lactate or alanine in the Early Treatment group vs. the AC group (lactate: Fig 5.5H; $p = 0.80$ *AC vs. Early Treatment*; alanine: Fig 5.5I; $p > 0.99$ *AC vs. Early Treatment*). An increase in PDH flux was also observed within the Late Treatment group when compared with AC group, however, this failed to reach statistical significance (Fig 5.5G; $p = 0.10$ *AC vs. Late Treatment group*). No change in label incorporation into lactate was observed in the Late Treatment groups vs. the AC group but a significant reduction in label incorporation into alanine was observed (lactate: Fig 5.5H; $p = 0.80$ *AC vs. Late Treatment*; alanine: AC: $0.0055 \pm 0.0012\ s^{-1}$; Late Treatment: $0.0035 \pm 0.0012\ s^{-1}$; Fig5.5I; $p < 0.05$ *AC vs. Late Treatment*).

5.4.4 The Effect of Early and Late Dichloroacetate Treatment on Myocardial Metabolism in the Langendorff-Perfused Heart

The presence of insulin resulted in a significant increase in glycolytic flux irrespective of dichloroacetate (DCA) treatment (Fig 5.6A; $p < 0.005$ *vs. Basal*). This was accompanied by a 25 % increase in glycolytic flux in the Early Treatment group (basal: 0.4849 ± 0.0746 s^{-1}; insulin: 0.6068 ± 0.0960 s^{-1}; Fig 5.6A) and a 17 % increase in the Late Treatment group at 18 weeks post-surgery (basal: 0.5086 ± 0.0350 s^{-1}; insulin: 0.5979 ± 0.0761 s^{-1}; Fig 5.6A). DCA treatment had no effect on glycolytic flux irrespective of insulin (Fig 5.6A; $p = 0.94$ *vs. Untreated*). DCA treatment had a significant effect on lactate efflux in the perfused heart (Fig 4.7B; $p = 0.05$ *vs. Untreated*) and the addition of insulin had a near significant effect (Fig 4.7B; $p = 0.07$ *vs. Basal*) on lactate efflux.

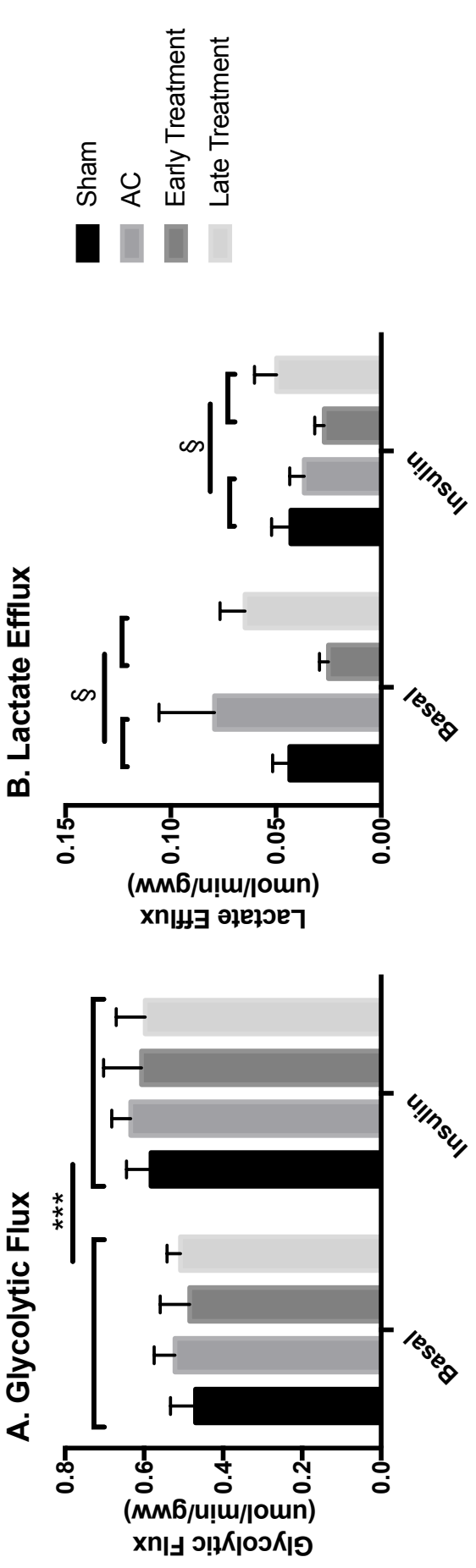


Figure 5.6: The Effects of Hypertrophy and Chronic DCA Treatment on the Glycolytic Flux in the Langendorff Perfused Heart at 18 Weeks Post- the Surgical Induction of Hypertrophy. A. Glycolytic Flux; B. Lactate Efflux. Glycolytic Flux: Sham: n = 11; AC: n =11; Early Treatment: n = 8; Late Treatment n = 9. Lactate Efflux: Sham: n = 10; AC: n = 6; Early Treatment: n = 8; Late Treatment: n = 4; *** $p < 0.005$ *vs. Basal* § $p = 0.05$ *vs. Untreated* Two-Way ANOVA with Repeated Measures. $Mean \pm SEM$. DCA: DCA Treatment. AC: Aortic Constriction.

Neither insulin ($p = 0.56$ *vs. Basal*) nor DCA treatment ($p = 0.23$ *vs. Untreated*) had an effect on rate pressure product (RPP) in either the Early Treatment or Late Treatment vs. the Sham group (Fig 5.7A). A significant reduction in left ventricular developed pressure was observed following the addition of insulin ($p < 0.05$ vs. Basal; Fig 4.8B). However, this was accompanied by a significant increase in heart rate following the addition of insulin ($p < 0.05$ *vs. Basal*; Fig 4.8B) and the overall maintenance of cardiac function as described by the RPP.

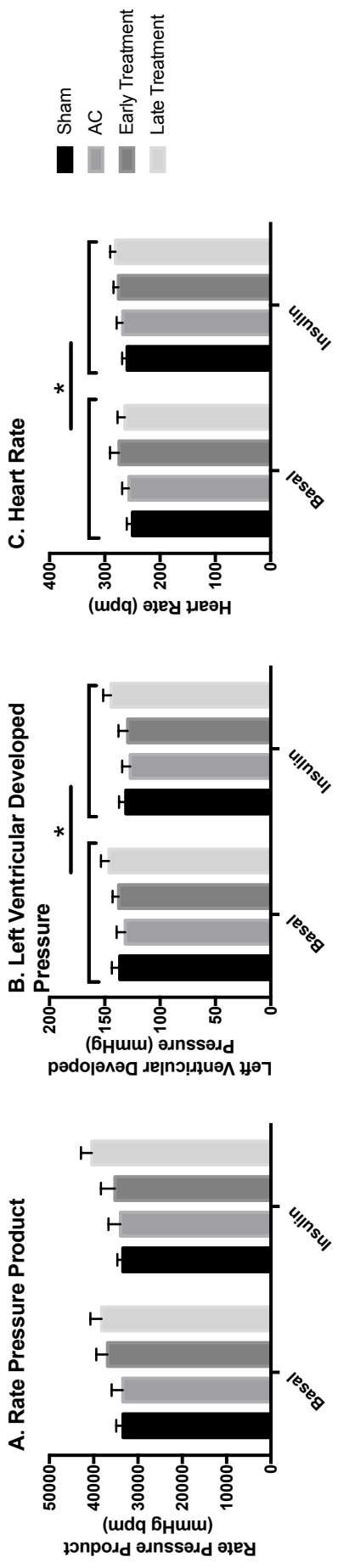


Figure 5.7: Functional Parameters in the Perfused at 18 Weeks Post-Surgery. A. Rate Pressure Product (RPP); B. Left Ventricular Developed Pressure (LVDP); C. Heart Rate (HR); Sham: n = 14; AC: n = 12; Early DCA Treatment: n = 8; Late DCA Treatment: n = 11. * $p < 0.05$ *vs. Basal.* Two-Way ANOVA with Repeated Measures. $Mean \pm SEM$. LV: Left Ventricular; DCA: DCA Treatment; AC: Aortic Constriction.

.

5.5 Discussion

5.5.1 Summary of Findings

5.5.1.1 The Effect of Early Dichloroacetate Treatment on Hypertrophic Function and Progression

Within the Early Treatment group, dichloroacetate (DCA) treatment was given immediately post-surgery for a total of 18 weeks. A significant increase in PDH flux was observed *in vivo* at 4, 9 and 14 weeks post-surgery consistent with DCA treatment and no elevation in lactate production was observed at 4 weeks post-surgery as noted in the AC and Late Treatment groups which had yet to receive treatment. This was accompanied by a significant increase in left ventricular (LV) mass and LV mass to body weight ratio at 4, 9 and 14 weeks post-surgery consistent with the presence of hypertrophy. Furthermore, Early DCA treatment was associated with a 23 % increase in LV mass relative to the Sham group at 4 weeks post-surgery, a 27 % increase in LV mass at 9 weeks post-surgery and a 24 % increase in LV mass at 14 weeks post-surgery compared with a consistent 17 % increase in LV mass in the AC group relative to the Sham group at 4, 9 and 14 weeks post-surgery suggesting that enhanced PDH activity may exacerbate hypertrophic remodelling. However, an sample size of 50 would be required to detect a difference of this size with an $\alpha = 0.05$ and a power of 80 %. This was accompanied by a significant reduction in ejection fraction at 4 and 9 weeks post-surgery consistent with the initial stages of functional decline. No evidence of reduced ejection fraction was observed at 14 weeks post-surgery, however, a significant reduction in heart rate was observed. This was accompanied by a significant increase in stroke volume, end diastolic volume and end systolic volume allowing maintenance of cardiac output. An increase in end diastolic and end systolic volume is suggestive of myocardial dilation and may represent the initial stages of cardiac dysfunction and failure.

5.5.1.2 The Effect of Late Dichloroacetate Treatment on Hypertrophic Function and Progression

Within the Late Treatment group, dichloroacetate (DCA) treatment was administered from 5 weeks post-surgery following the development of hypertrophy for a total of 13 weeks. The presence of hypertrophy was confirmed at 4 weeks post-surgery, prior to treatment with DCA, marked by a significant increase in left ventricular (LV) mass and LV mass to body weight ratio. This was accompanied by a significant increase in label incorporation into lactate representative of enhanced glycolytic flux as previously described in Chapter 3.

An elevation in PDH flux was confirmed at 9 and 14 weeks post-surgery following 4, and 9 weeks of DCA treatment respectively. At 9 weeks post-surgery, no difference in LV mass or LV mass to body weight ratio was observed when compared with the AC group. However, only 12 % increase in LV mass was observed between Sham group and the Late Treatment group compared with a 17 % increase in LV mass in the AC group suggesting the rate of hypertrophic development may be slowed in the Late Treatment group. Statistically, we are powered to see an effect size of 80 % between the Sham and AC groups with the sample size given, however, in comparison, we would require a sample size of over 40 to confirm the that the LV mass within the Late Treatment group is statistically lower than the AC group. In addition, no changein both LV mass or LV mass to body weight ratio was observed at 14 weeks post-surgery when compared to the AC group.

Converse to early treatment with DCA, no functional changes represented by cardiac output, ejection fraction, heart rate and stroke volume were observed within the Late DCA Treatment group at 4, 9 or 14 weeks post-surgery. This was accompanied by no evidence of myocardial dilation.

5.5.2 Dichloroacetate Treatment During the Initial Stages of Hypertrophic Remodelling Induces Functional Decline

Early dichloroacetate (DCA) treatment, given immediately post-surgery was associated with a reduction in ejection fraction representative of reduced myocardial function. The study summarised in Chapter 3 confirms that the initial stages of hypertrophic remodelling are associated with an increased dependence on glycolysis and is a concept widely supported within the literature [1, 5, 42, 50, 54]. Based on the work presented here we hypothesise that this is to sustain the increase in cardiac output observed whilst the heart is adapting to a chronic increase in blood pressure. In support of this, we have shown chronic DCA treatment, which we have previously shown reduces glycolytic flux (Chapter 4) induces functional decline within the heart suggesting that the enhanced glycolytic flux observed in the hypertrophied heart may be beneficial in maintaining cardiac output during the remodelling process. Interestingly, functional compensation is observed at 14 weeks post-surgery accompanied by an apparent slowing in the rate of hypertrophic development as depicted in Figure 5.8.

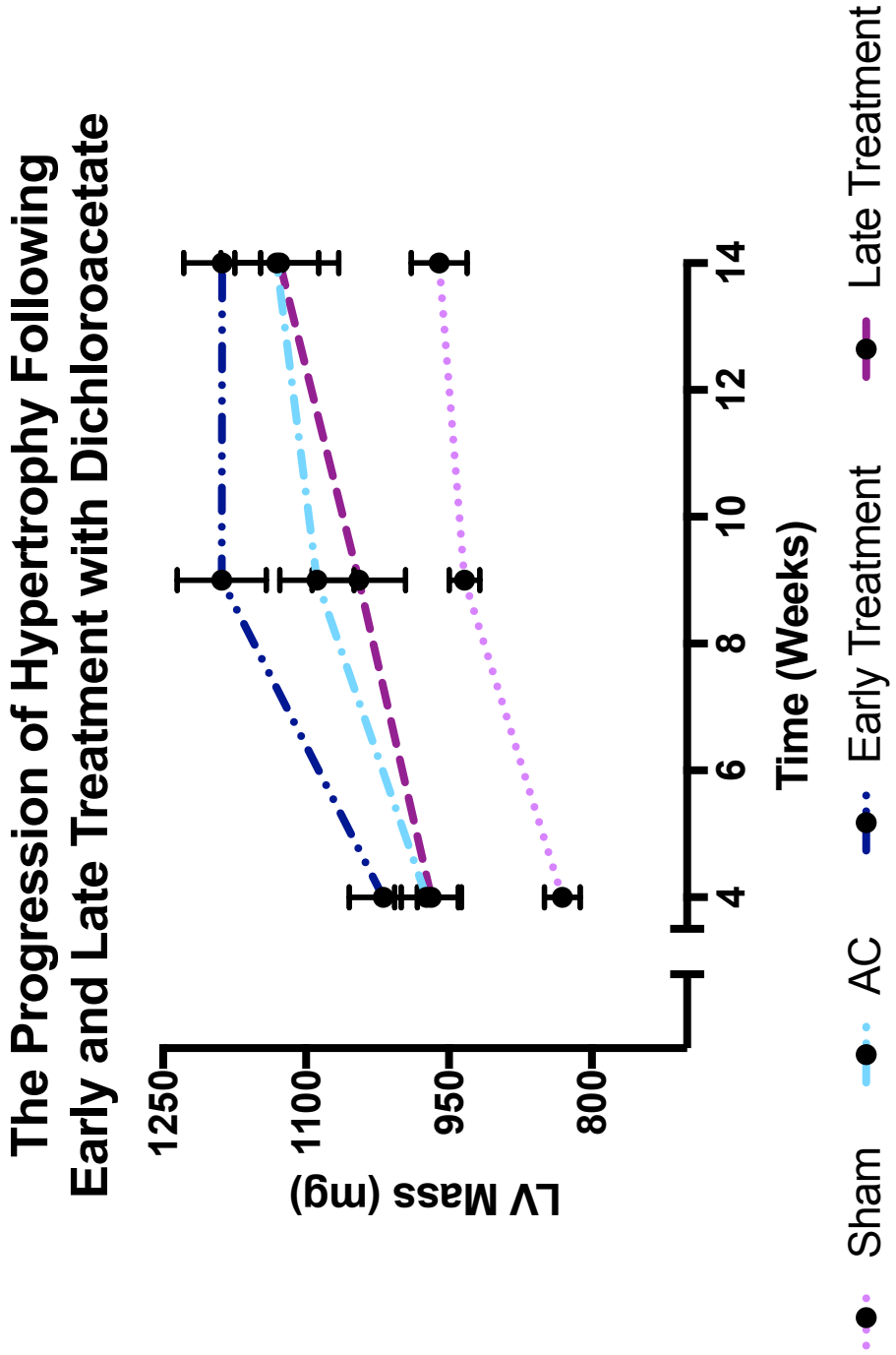


Figure 5.8: Hypertrophic Progression Following Treatment with Dichloroacetate. $Mean \pm SEM$

The left ventricle remains hypertrophied at 14 weeks post-surgery, however, a reduction in heart rate is accompanied by an increase in stroke volume which leads to overall maintenance of both cardiac output and ejection fraction. The work summarised in Chapter 3 suggests the heart reaches a compensated phase at 14 weeks post-surgery during which function is stabilised, represented by no change in cardiac output or ejection fraction, accompanied by no evidence of enhanced glycolytic flux. Interestingly, a significant reduction in heart rate is observed in the untreated hypertrophied heart (Chapter 3) similar to that noted in the Early Treatment group. We can speculate that the early treated hypertrophied heart may be starting to stabilise at the 14 week time point despite evidence of functional decline following DCA treatment at 4 and 9 weeks post-surgery however, the damage accrued by the heart still remains marked by myocardial dilation and cardiac hypertrophy.

Chronic DCA treatment was shown in Chapter 4 to reduce glycolytic flux but promote fatty acid oxidation which is supported by work by Sobrino *et al*, Clark *et al* and Anderson *et al* [133, 132, 134]. Given the hypertrophic heart is proposed to undergo a shift away from fatty acid oxidation as decribed by Akki *et al* amongst others [64], promoting fatty acid oxidation in the heart accompanied by a reduced glycolytic dependence may contribute to the negative effects of DCA treatment during the initial stages of hypertrophic development. However, as the hypertrophied heart is continually undergoing structural, functional and metabolic changes, it is possible an increase in fatty acid oxidation starts to convey a positive effect during the later compensatory phases, however, this is purely speculative. This is supported by work by Degens *et al* which identified no change in fatty acid oxidation at 4 weeks post-surgery in the abdominal aortic constriction model suggesting that treatment with DCA within the first 4 weeks of hypertrophic development preceeds a shift away from fatty acid oxidation towards glycolytic dependence [65]. We also identified no change in the glycolytic flux in either the DCA treated groups which may be due to both the stage and length of DCA treatment given which is longer than that described in Chapter 4. Furthermore, this study is limited to looking at the effects of DCA treatment during the early stages of hypertrophic development and the beginning

of compensation with no ability to assess whether in the long term, DCA treatment is associated with the prevention of the decline into heart failure in the longer term.

Interestingly, work by Le Page *et al* in an STZ-induced model of type II diabetes showed that chronic DCA treatment lead to normalisation of the myocardial substrate utilisation and reversed diastolic dysfunction [141]. This is contrary to what has been observed within the early stages of the AC model which may highlight the differential effects that metabolic modulation has in different disease states.

5.5.3 Dichloroacetate Treatment During the Later Stages of Hypertrophic Remodelling May Attenuate Hypertrophy

The presence of hypertrophy was characterised by a significant increase in LV mass and LV mass to body weight ratio at 4 weeks post-surgery following which dichloroacetate (DCA) treatment was administered for a total 9 weeks. DCA treatment was accompanied by an increase in pyruvate dehydrogenase (PDH) flux at 9 and 14 weeks post-surgery as expected. No significant difference in LV mass was observed between the AC group and Late DCA Treatment group at 9 weeks post-surgery, however, Figure 5.8 would suggest an attenuation of hypertrophic progression within the Late Treatment group accompanied by the presence of hypertrophy at 14 weeks post-surgery. Only a 17 % increase in LV mass relative to the Sham group is observed in the Late Treatment group at 4 and 14 weeks post-surgery in line with untreated hypertrophied heart which also exhibits a 17 % increase in LV mass relative to the Sham group. At 9 weeks post-surgery, only a 12 % increase in LV mass relative to the Sham group was observed in the Late Treatment group compared with a 17 % increase in the AC group. We can subsequently speculate that the heart may be undergoing an attenuation of hypertrophic progression between 5 and 14 weeks post-surgery following DCA treatment. Work by Atherton *et al*, have previously shown a regression in hypertrophy within the T3 model of hyperthyroid-induced LVH following one week of chronic DCA treatment [142] which hasn't been observed in the AC model as hypothesised. Similarly to the differential role of DCA in the type II diabetic model, the individual metabolic state of the disease may have a role in the efficacy of the

treatment used.

Interestingly, we saw a reduction in function at 4 and 9 weeks in the Early Treatment group following DCA treatment which we speculate was due to a reduction in glycolytic flux during this period stimulated by DCA Treatment (Section 5.5.2). However, no change in functional decline was observed at 9 weeks post-surgery in the Late Treatment group irrespective of DCA treatment. An increase in glycolytic flux was observed in the untreated hypertrophied heart at 9 weeks post-surgery (Chapter 3). The absence of functional decline in the Late Treatment group at the same stage may suggest that the heart is starting to stabilise at 9 weeks post-surgery, therefore a proposed reduction in glycolytic flux following DCA treatment may be sufficient to attenuate structural remodelling but the hypertrophic remodelling which has already occurred may be sufficient to maintain cardiac function.

At 14 weeks post-surgery, characterisation of the model in Chapter 3 identified no increase in glycolytic flux in the hypertrophied heart. Interestingly, this is correlated with evidence of hypertrophic remodelling in the Late Treatment group. Given that we have previously characterised a transition between hypertrophic development and cardiac stabilisation both metabolically and physically, this suggests that the metabolic changes induced by DCA previously described in Chapter 4 as reducing glycolytic flux and promoting fatty acid oxidation may have a differential effect on the hypertrophied heart at this stage.

5.5.4 The Effect of Dichloroacetate Treatment has a Differential Effect Dependent on the Stage of Hypertrophy

The work described in Chapter 3 highlights that hypertrophic remodelling is a dynamic process characterised by an increased glycolytic dependence in the initial stages of hypertrophy which normalises as structural remodelling starts to stabilise. This is highlighted by the differential effects of DCA treatment when given during hypertrophic development compared with when treatment is given during hypertrophic progression. The work conducted by Atherton *et al* and Le Page *et al* further demonstrates the differential effects of

DCA in different diseases with a metabolic basis [142, 141]. Within this study, when DCA is given immediately post-abdominal aortic constriction surgery, DCA treatment induces functional decline and myocardial dilation which persists past the developmental stage. Whereas, when DCA treatment is given following the development of hypertrophy, it may cause a mild attenuation in hypertrophic development with no associated functional decline.

This suggests that enhanced glycolytic dependence plays a compensatory role during the initial stages of hypertension and hypertrophic development. Allard *et al* amongst others suggest that this phase is also accompanied by a reduction in fatty acid oxidation [42, 4, 1]. Treatment with DCA, which we have also shown promotes fatty acid oxidation, has a deterimental effect on cardiac function during hypertrophic development, suggesting that reducing glycolytic flux and promoting fatty acid oxidation is not beneficial during hypertrophic development. However, following the inital stages of development, up to 5 weeks post-surgery, a reduction in glycolytic flux and increased fatty acid oxidation may convey a positive effect on hypertrophic remodelling and isn't associated with a negative effect. Furthermore, as this model is representative of compensated hypertrophy rather than directly of heart failure, we can not make any conclusions on whether DCA treatment prevents the eventual decline in function in the hypertrophied heart.

Metabolic modulation remains an attractive therapeutic target in the development of hypertrophy, however, the stage-specific effect of DCA suggests that caution should be exercised in when metabolic therapies are given.

5.6 Conclusions and Future Perspectives

From this study we can conclude that alteration of the metabolic profile using dichloroacetate (DCA) treatment during the initial stages of hypertrophic development promotes left ventricular remodelling, myocardial dilation and cardiac dysfunction suggesting that enhanced glycolytic dependence may convey a compensatory effect during hypertrophic development. Conversely, alteration of the myocardial metabolic profile in the later stages of hypertrophic development may have a beneficial effect and was associated with no adverse functional effects. This further highlights the complexity of metabolic remodelling within the hypertrophied heart.

This study is focused on the effects of DCA treatment and the alteration of myocardial glucose handling on structural changes during the development and progression of compensated hypertrophy. It would be interesting to assess the effect of hypertrophy and DCA treatment on fatty acid oxidation, especially as we have previously shown in Chapter 4 that chronic DCA treatment is associated with enhanced fatty acid oxidation. In addition, it would be interesting to assess whether DCA treatment during hypertrophic progression, as given in the Late Treatment group, would convey a beneficial effect in preventing the decline into heart failure. Alternatively, placing a stress on the heart, such as ischemia reperfusion, dobutamine treatment or high workload, would give some indication as to whether hypertrophied hearts treated with DCA during hypertrophic progression had a more sustained function than untreated hypertrophied hearts.

Chapter 6

The Effects of Ramipril Treatment on Myocardial Metabolism

6.1 Chapter Overview

Previous work by Linz *et al* and Boeteng *et al* suggests that the effectiveness of Ramipril as a preventative treatment for left ventricular hypertrophy (LVH) and heart failure are not limited to its anti-hypertensive effects alone [103, 143].

We propose that the efficacy of Ramipril may be enhanced, in part by the induction of beneficial metabolic changes within the heart. Pyruvate dehydrogenase (PDH) is a key metabolic regulator of myocardial metabolism and its activity tightly coupled to Ca^{2+} flux linking myocardial contraction to the energetic status of the cell [36]. Our previous work and the work presented in Chapter 3, amongst others, have previously shown that metabolic remodelling, characterised by a shift away from fatty acid oxidation towards increased glucose utilisation, occurs with the development of hypertension-induced hypertrophy in the abdominal aortic constriction (AC) model of LVH [50, 42, 4, 65]. The mechanism behind this metabolic switch is currently unclear, however, it is possible that it is linked to a SERCA mediated reduction in Ca^{2+} flux during hypertrophic development, which is restored following Ramipril treatment as suggested by Boetang *et al* [103].

Using dynamic nuclear polarization (DNP) and cine MRI we assessed the effects of a low dose (0.1 mg kg^{-1} day^{-1}) and a high dose (1 mg kg^{-1} day^{-1}) of Ramipril on myocardial remodelling following AC and the induction of hypertrophy to identify whether the positive effects of Ramipril treatment have a metabolic basis at 9 weeks post-surgery. Glycolytic flux and the ability of the Ramipril treated heart to recover from ischemia was further assessed at 10 weeks post-surgery in the Langendorff-perfused heart. In Chapter 3, we characterised the structural, functional and metabolic remodelling which occurs with the development of hypertrophy in the abdominal aortic constriction model. Therefore, this chapter focuses purely on the effects of Ramipril treatment on hypertrophic development.

6.2 Introduction

6.2.1 The Renin-Angiotensin-Aldosternone System and its Role in the Development of Cardiac Hypertrophy

6.2.1.1 The Classic Renin-Angiotensin-Aldosterone System

The primary role of the Renin-Angiotensin-Aldosterone (RAA) System is the homeostatic control of arteriole pressure, tissue perfusion and extracellular volume, the dysregulation of which plays a significant role in cardiovascular diseases such as chronic hypertension and heart failure [144, 145]. Although the action of the RAA system is largely systemic in nature, a local, tissue-specific system is also present in the heart as well as in the peripheral blood vessels, kidney and brain, amongst others. However, the regulation of these systems is thought to remain under the control of the systemic pathway [144].

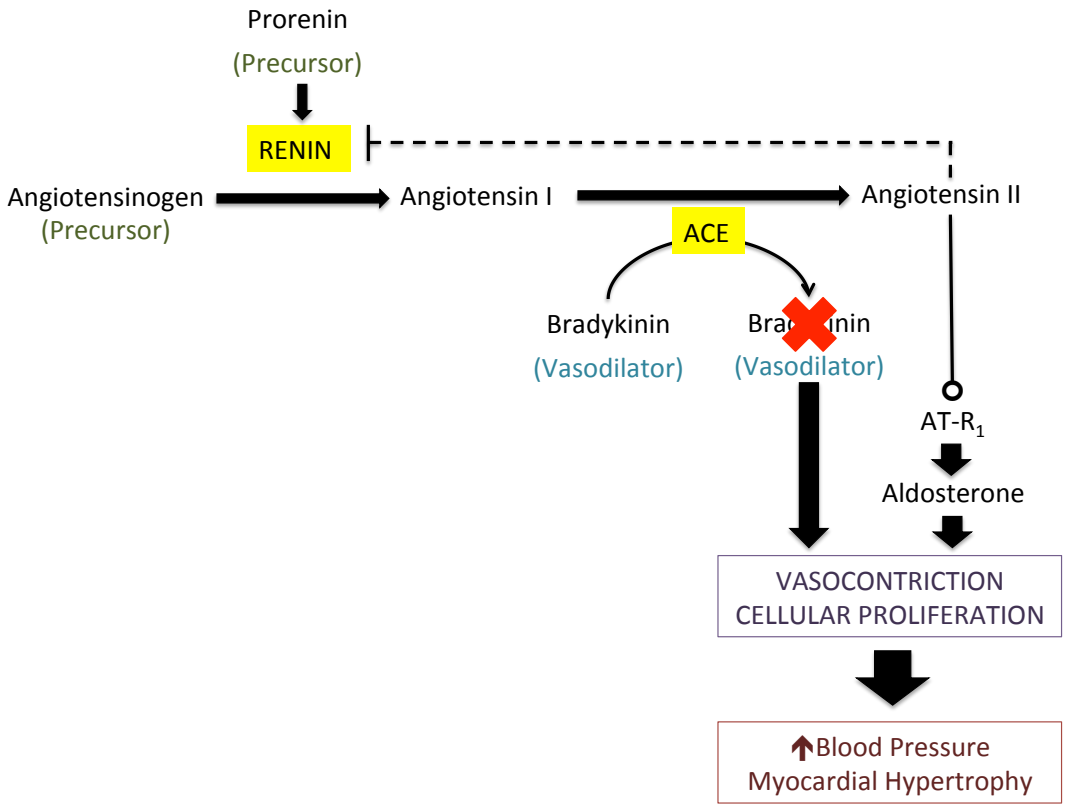


Figure 6.1: The Classic Renin-Angiotensin-Aldosterone (RAA) System. ACE: Angiotensin-Converting Enzyme; AT-R_1: Angiotensin receptor 1. Adapted from Atlas (2007) [144]

The classic RAA system is comprised of four major components; renin, angiotensin I (Ang I), angiotensin II (Ang II) and aldosterone as described in Figure 6.1. Renin converts angiotensinogen, an inactive precursor molecule secreted by the liver, into Ang I an inactive decapeptide. Ang I subsequently undergoes truncation of the C terminus to form the biologically active octomer, Ang II, a reaction catalysed by angiotensin-converting enzyme (ACE) [144, 145]. Within the classic system, Ang II binds to angiotensin receptor 1 (AT-R_1) leading to the production of aldosterone, which is responsible for a systemic increase in blood pressure mediated by the kidneys through alteration of the sodium-potassium balance and a resultant retention of water. In addition, local binding of Ang II to AT-R_1 within the cardiomyocyte induces vasoconstriction, increased cardiac contractility, inflammation and mediates cellular growth and proliferation leading to hypertrophic development [144].

Renin is secreted by the liver in response to a drop in blood pressure. As the enzyme which catalyses the initial conversion of angiotensinogen to Ang I (Fig 6.1), renin is considered the rate-limiting step within the RAA system [144, 146]. However, it is the activity of ACE which acutely determines the balance between vasoconstriction and vasodilation [147]. The binding of Ang II, the product of the cleavage of Ang I by ACE, to the AT-R_1 induces vasoconstriction. In addition, ACE favours the degradation of bradykinin, a potent vasodilator, over Ang I contributing to an increase in blood pressure [144, 147].

The majority of ACE is membrane bound on the vascular endothelium however, some ACE is found in the serum, although this is likely due to the clearance and recycling of ACE from the vascular endothelium. In addition, tissue specific ACE is found in the peripheral tissues including the heart [144]. Low concentrations of ACE are found within the healthy myocardium, localised to the right ventricle, endothelial layer and the valves [147]. Circulating renin and angiotensinogen are thought to be taken up by the cardiomyocytes where they are metabolised locally forming a local RAA system facilitating local maintenance of cellular balance and acute adaptation to an increase in blood pressure in conjunction with the global RAA system [145, 144, 146]. However, this concept has been challenged following evidence, albeit inconsistent, that renin mRNA has been found in

the heart. Despite this, evidence for the presence of a local system is still strong, characterised by the presence of cardiac-specific ACE as previously described [147, 146]. It is proposed that the local and systemic RAA systems work in concert together and as a result, disruption of both the cardiac and the systemic RAA system under pathological conditions such as chronic hypertension has potentially deleterious effects [146]. Elevated levels of cardiac ACE have been identified in hypertension, heart failure and Type II diabetes [147, 144, 145, 148]. Under these conditions, the up-regulation of tissue specific ACE in the assaulted myocardium is supplemented by the presence of macrophages which migrate to the cardiac tissue during inflammation and disease. Macrophages express a high level of ACE activity leading to the accumulation of Ang II and further perpetuation of the RAA system contributing to damage within the myocardium [147].

6.2.1.2 The Alternative Aspects of the Renin-Angiotensin-Aldosterone System

An alternative, opposing arm of the classic renin-angiotensin-aldosterone (RAA) system has been identified and is thought to play a role in tissue-specific self-regulation [146, 144]. Both Ang I and Ang II can undergo alternative fates mediated by angiotensin-converting enzyme 2 (ACE2). Ang II gets converted to Ang(1-7) through removal of the C-terminal phenylalanine and Ang I undergoes cleavage of the C-terminal residue to produce Ang(1-9) as shown in Figure 6.2 [146].

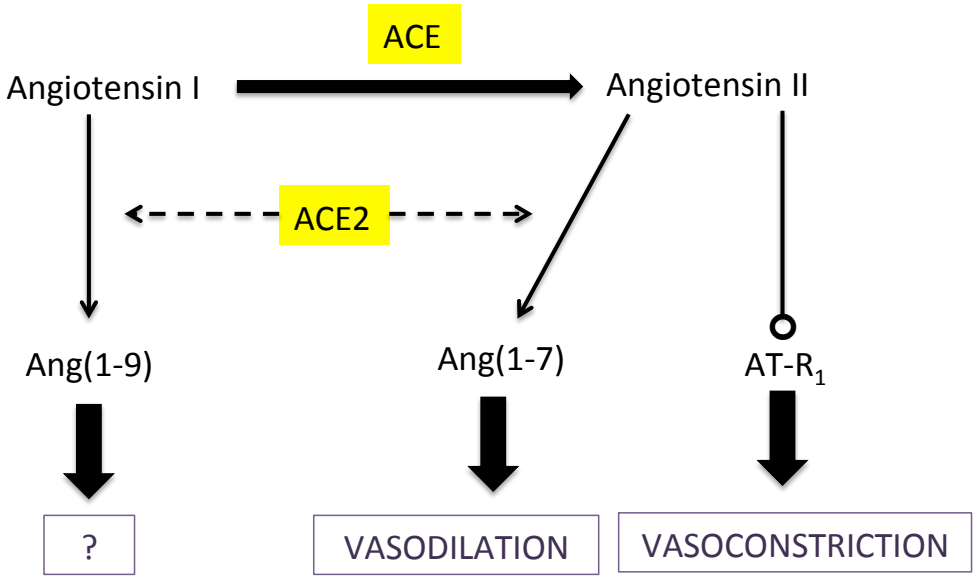


Figure 6.2: The Altenative Aspects of the Renin-Angiotensin-Aldosternone Pathway

The presence of Ang(1-7), Ang(1-9) and ACE2 within the RAA system are well characterised but their role and how they fit into the system remains unclear [146, 144]. Interestingly, Ang(1-7), an Ang II derivative has been shown to act as a vasodilator which may provide a means to counteract the tissue-specific effects of the RAA system. ACE2 is resistant to ACE inhibitors (ACEI) and is localised to the myocardial blood vessels and the tubular epithelia of the kidneys supporting the idea that it has a role in regulating the cardiac RAA system [146]. Further work has suggested that ACE2, which is thought to be localised to the X chromosome has a role in the genetic causes of hypertension, however, this remains controversial [146]. The role of ACE2, or the impairment of ACE2 in cardiovascular disease is supported by work by Crackower *et al* in ACE2 KO mice [149]. Although only a modest change in blood pressure was observed within this model, severe changes in cardiac contractility accompanied by an increase in local levels of Ang II and the induction of pathways involved in the mediation of hypoxic signalling were observed suggesting ACE2 plays a significant role in maintaining cardiac homoeostasis [149, 146]. Furthermore, Crackower *et al* showed a significant reduction in the expression of ACE2 in the salt-sensitive Sabra model of genetic hypertension supporting a role of ACE2 within the diseased myocardium [149].

It is possible that the positive attributes of ACE2 and the production of Ang(1-7)

may be enhanced within heart disease where the origin is not genetic. ACE2 function is unaffected by ACEI [146] and although the production of Ang II is reduced by the inhibition of ACE, the alternative pathways by which Ang II is produced are potentially unaffected. Chymase is known to produce Ang II but its role in the cardiac RAA system remains unclear. It is thought that chymase is localised to the mast cells [146] which infiltrate the myocardium in the diseased state. It has been widely postulated that ACEI work via multiple mechanisms aside from their role in the inhibition of ACE [93, 150, 151, 152, 145]. Further clarification of both the wider actions of ACEI and the role of ACE2 may identify a situation where the actions of Ang(1-7) as a vasodilator are promoted over ACE activity, however, this is pure speculation but we can conclude that ACE2 appears to play an important role in maintaining cardiac homoeostasis and potentially the onset of cardiovascular pathogenesis.

6.2.2 The Effects of Ramipril, an Angiotensin-Converting Enzyme Inhibitor

Ramipril is a widely prescribed and highly effective drug in the treatment of hypertension and heart failure [153, 144, 147]. It is a second generation angiotensin converting enzyme inhibitor. ACEI were originally identified when the peptides isolated from the venom of the Brazilian Arrowhead Viper were shown to inhibit an analogue of ACE [144]. This formed the basis of the design of modern ACEI and has been shown to be very effective in the treatment of hypertension and heart failure [145]. Classically Ramipril reduces vascular resistance and remodelling via the inhibition of angiotensin II (Ang II) production leading to the regression of left ventricular hypertrophy (LVH) and if prescribed early, the prevention of heart failure (Fig 6.3) [154].

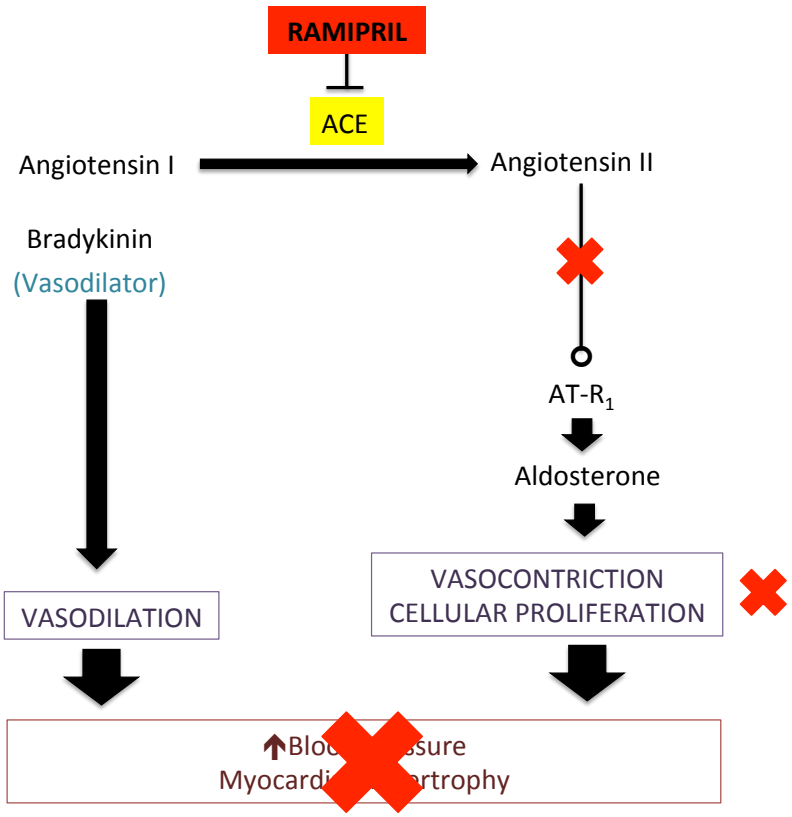


Figure 6.3: The Classic Mechanism by which Ramipril Acts. ACE: Angiotensin-Converting Enzyme; AT-R_1: Angiotensin receptor 1.

However, its positive effects potentially extend beyond that of its classical role on inhibiting Ang II-mediated vasocontriction. Several studies [151, 152, 143, 155, 103, 103, 156] have shown that even sub-antihypertensive doses of Ramipril have a beneficial effect on myocardial remodelling and ischemic injury during hypertrophy independent of its affect on blood pressure. Furthermore, studies into the alternative effects of Ramipril and other ACE inhibitors have helped clarify the role of ACE within the renin-angiotensin-aldosterone (RAA) pathway, with work conducted by Fleming *et al* suggesting that ACE adopts a role as a signalling molecule involved in regulating its own expression, in addition to its role in the production of Ang II and the degregation of bradykinin [147, 154].

6.2.3 The Alternative Routes via which Ramipril May Act to Improve Myocardial Viability during Hypertension and Hypertrophy

Linz *et al* conducted a study comparing the effects of an antihypertensive (1 mg kg^{-1} day^{-1}) and a sub-antihypertensive (10 μg kg^{-1} day^{-1}) dose of Ramipril on hypertrophic remodelling in the abdominal aortic constriction (AC) rat model of left ventricular hypertropht (LVH) [155] A reduction in myocardial fibrosis, LV mass, ACE activity and angiotensin II was observed in both Ramipril treated groups, however, no reduction in blood pressure was observed in the group which received the sub-antihypertensive dose of Ramipril suggesting the mechanism of Ramipril extends beyond that of the blood pressure-mediated pathway [155]. In addition, normalisation of the phosphocreatine to ATP ratio, a marker of decreased myocardial energy availability [11, 72], was observed in the Ramipril-treated groups suggestive of increased cardiomyocyte viability [155].

The effects of Ramipril treatment observed in rats with LVH were mirrored in hypertensive patients with LVH who were treated for 6 months with either an antihypertensive (5 mg kg^{-1} day^{-1}) or sub-antihypertensive (1.25 mg kg^{-1} day^{-1}) dose in a study conducted by Lievre *et al* [157]. A reduction in the LVH index was observed in both Ramipril treated groups irrespective of a reduction in blood pressure in the patients who received the sub-antihypertensive dose of Ramipril. This was suggested to be mediated through inhibition of angiotensin II production and a concomitant release in the inhibition of bradykinin production, a concept supported by Linz *et al* amongst others [143, 156, 158, 159, 145, 147]. This suggests that it is the balance between a reduction of angiotensin II, which reduces both systemic blood pressure and local cardiomyocyte remodelling and the production of bradykinin and the subsequent release of nitric oxide leading to increased vasorelaxation and perfusion of nutrients to the cardiomyocytes.

6.2.3.1 Ramipril Treatment Increases Bradykinin Release Improving Ischemia Reperfusion Recovery

The effects of bradykinin were assessed in a further study by Linz *et al* in isolated rat hearts perfused via the Langendorff mode [143, 151]. Hearts were subjected to ischemic injury and bradykinin infused during both the ischemic and reperfusion period. Even a low dose of bradykinin increased coronary flow and reduced the presence of ventricular fibrillation during the reperfusion period. This was accompanied by a reduction in lactate dehydrogenase (LDH) activity, lactate production and a reduction in the depletion of creatine kinase [143, 151]. Furthermore the combination of threshold levels of bradykinin and Ramipril, concentrations which are otherwise ineffective individually, demonstrated a cardioprotective role during ischemia and reperfusion. This was ablated by the introduction of the bradykinin agonist, (D-Arg)-hyp2 This5, D-Phekk, suggesting that it is the combination of ACE inhibition and the subsequent increase in bradykinin which is key to its cardioprotective role [143].

The presence of bradykinin has an additional metabolic role within the heart following reperfusion characterised by a reduction in LDH and lactate in the perfused rat heart suggestive of a reduction in glycolytic dependence during reperfusion [143]. A surge in glycolysis has previously been thought to underpin the damage caused during ischemia reperfusion [160], and the presence of bradykin may act to address that. In support of this, the infusion of bradykinin in dogs that have undergone ligation of the left descending coronary artery was associated with increased levels of glycogen within the infarcted region [156]. Given that ACE promotes bradykinin degradation over Ang I truncation and the production of Ang II [161], it is perhaps unsurprising that the presence of bradykinin plays such a cardioprotective role during ischemia reperfusion.

6.2.3.2 Ramipril Promotes Calcium Handling within the Hypertrophied Myocardium

Interestingly, these beneficial effects on the myocardium, aside from the lowering of blood pressure, only occur during treatment with Ramipril and do not occur in the presence of

other widely described ACE inhibitors. The actions of Ramipril may therefore work via a range of different interlinking biochemical mechanisms. Work conducted by Boateng *et al* suggests that a sub-antihypertensive dose (50 μg kg^{-1} day^{-1}) of Ramipril upregulate mRNA levels of the sarcoplasmic reticulum Ca^{2+} ATPase (SERCA) 2A and phospholambin B (PLB) in both control and hypertensive rats and enhances their translation in hypertensive rats [103]. Impaired Ca^{2+} handling has been shown to contribute to cardiac dysfuction in the development of heart failure [162, 163] and the reduction in mRNA levels of SERCA and PLB have been reported in the failing myocardium of patients with end-stage heart failure [106] leading to impaired cardiac function. Further work by Boetang *et al* shows that normalisation of SERCA levels following Ramipril treatment improves relaxation in isolated cardiomyocytes compared with untreated hypertrophied cardiomyocytes. This is accompanied by an increase in mRNA transcripts encoding the Na^+/Ca^{2+} exchanger in both treated control and hypertensive rats [150]. The Na^+/Ca^{2+} exchanger works in conjunction with SERCA to ensure efficient calcium handling and enhanced levels of its expression have been associated with preserved ejection fraction in patients with end-stage heart failure undergoing transplant [164]. Ramipril therefore appears to play a role in improved calcium handling and relaxation within the hypetrophied myocardium.

Calcium (Ca^{2+}) also acts to couple metabolism and contraction within the myocyte. Pyruvate dehydrogenase phosphatase (PDP), an enhancer of pyruvate dehydrogenase (PDH) activity, contains a Ca^{2+}-binding domain and when Ca^{2+} binds, it associates with the E2 subunit of the PDH complex enhancing its phosphatase activity [36, 165]. This promotes flux through PDH and the increased oxidation of glucose during periods of high energy demand. Therefore, impaired calcium handling within the hypertrophied cardiomyocyte may underpin metabolic dysfunction within the myocardium. Our previous work and the work reported in Chapter 3 identified an uncoupling between glycolysis and glucose oxidation within the hypertrophied myocardium of the abdominal aortic constriction (AC) rat model of LVH. This was driven by an increase in glycolytic flux with the development of hypertrophy but no change in PDH flux [50]. When coupled with the work conducted by Boeteng *et al* which report a reduction in the transcription and

expression of calcium handling machinery within the same model [103], this suggests that impaired contractility and metabolism may be a joint contributor to myocardial dysfunction following hypertrophic development. Ramipril may therefore provide an attractive treatment avenue to restore myocardial metabolism in the hypertrophied heart.

6.2.4 Chapter Aims

The work this chapter focuses on whether the positive effects of Ramipril extends beyond that of an anti-hypertensive and has a metabolic basis. Previous work by Linz *et al*, Boateng *et al* and Lievre *et al* suggests that Ramipril has a variety of targets given that even at sub-antihypertensive doses, treatment with Ramipril has cardioprotective effects [155, 103, 157]. Within this study, the metabolic effect of two different doses of Ramipril were considered, a low, sub-antihypertensive (0.1 mg kg^{-1} day^{-1}) and a high, antihypertensive (1 mg kg^{-1} day^{-1}) dose. These doses were selected based on the dose-response study conducted by Unger *et al* as previously discussed in Section 2.4.3 [99].

6.3 Methods

6.3.1 Study Overview

Hypertension and hypertrophy were surgically induced in male Sprague-Dawley rats via abdominal aortic constriction (AC). Hypertrophic development was assessed at 4 weeks post-surgery using cine MRI and myocardial metabolism assessed following an injection of either [1-^{13}C] or [2-^{13}C]labelled pyruvate. The presence of left ventricular hypertrophy (LVH) was confirmed within a subset of AC rats which were subsequently treated with either a low dose (0.1 mg kg^{-1} day^{-1}) or a high dose (1 mg kg $^{-1}$ day $^{-1}$) of Ramipril and cardiac structure function and metabolism further assessed at 9 weeks post-surgery.

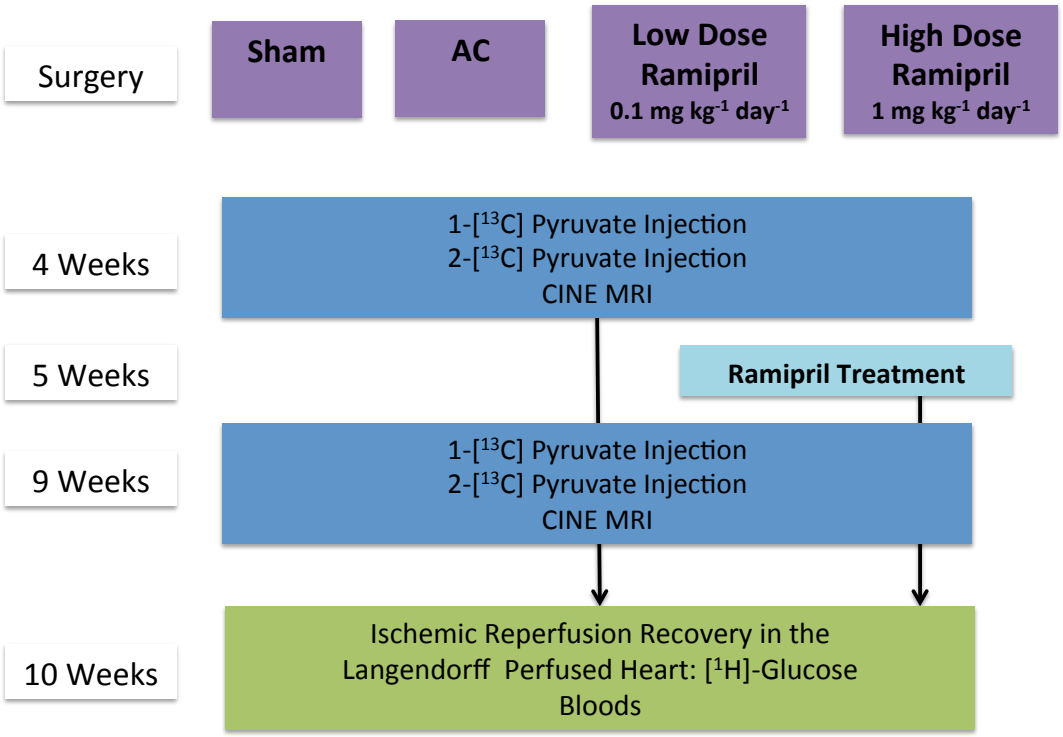


Figure 6.4: The Effects of Ramipril on Myocardial Metabolism - Study Overview

The effect of hypertrophy and Ramipril treatment on cardiac glucose utilisation and the ability of the heart to recover from low-flow ischemia (0.3 ml min^{-1} gww^{-1}) was assessed at 10 weeks post-surgery in the hearts perfused with [^{3}H]glucose via the Langendorff mode.

6.3.2 Animal Work

All animal experiments were conducted by a licensed individual in accordance with the Home Office Guidance on the Operation of Animals (Scienctific Procedures) Act of 1986 and to University of Oxford institutional guidelines.

Animals were housed in a dedicated facility (Biomedical Sciences Services, University of Oxford, UK) under a 12 hr light-dark cycle and maintained on a standard laboratory chow (Harlan Laboratories, Kent, UK) and standard laboratory water given *ad libtum* unless otherwise stated. All *in vivo* metabolic experiments were performed whilst animals were in the fed state (taken as between 6 am and 1 pm) unless otherwise stated.

6.3.3 Surgical Induction of Left Ventricular Hypertrophy

Male Sprague-Dawley rats (200-250 g; Harlan Laboratories, Kent, UK) underwent constriction of the abdominal aorta (AC; n = 28) between the two renal arteries under aseptic conditions as previously described in Section 2.2. Following a laparotomy whereby the abdominal aorta was exposed, a reproducible constriction was placed around the aorta between the two renal arteries. Sham animals (n = 11) received the same procedure but without constriction of the aorta.

6.3.4 Preparation and Administration of Ramipril Treatment

Ramipril treatment was administered to a subset of AC rats at 5 weeks post-surgery following the characterisation of hypertrophic development. One subset of AC rats (n = 9) received a low dose (0.1 mg kg^{-1} day^{-1}; Low Dose) of Ramipril and a further subset (n = 9) received a high dose (1 mg kg^{-1} day^{-1}; High Dose) both administered in drinking water. The Sham and AC groups were maintained on standard laboratory drinking water as previously described in Section 2.4.3.

The water and body weight of the Ramipril-treated groups was monitored daily for the first week of treatment and the volume adjusted accordingly to take into account increased

water intake due to side effects of Ramipril and to ensure that the rats received the correct dose. No change in body weight was observed in the Ramipril-treated groups when compared with the untreated groups. Following the first week, water weight was monitored a minimum of every 3 days and any adjustments in water volume made, however, following the first week of treatment, the volume of water consumed within the treated groups remained relatively consistent. Body weight was monitored a minimum of weekly but no difference in body weight was observed in the treated groups relative to the untreated groups.

The degree of cardiac hypertrophy, determined by the average heart weight to body weight ratio of the group, was matched between the AC, High Dose and Low Dose rats prior to treatment. Water intake within the High Dose and Low Dose groups was monitored in the cages containing rats on Ramipril treatment and the concentration of Ramipril within the drinking water adjusted based on the average weights of the rats within the cage and volume of water consumed to ensure an average dosage of either 0.1 mg kg^{-1} day^{-1} or 1 mg kg^{-1} day^{-1} in the Low and High Dose groups respectively. Treatment was monitored and replaced a minimum of every 2 days.

6.3.5 *In Vivo* Assessment of Cardiac Structure and Function

Cardiac structure and function was assessed at 4 and 9 weeks post-surgery using cine MRI as previously described in Section 2.3.5. Male Sprague-Dawley rats were anaesthetised as described in Section 2.3.1 and placed in a custom-built cradle within a 7 T magnetic resonance scanner (Varian Biomedical Systems, Yarnton, UK). Betweeen 10 and 11 contiguous cine-MR images (28-35 frames per cardiac cycle) were acquired of the heart in the short-axis orientation covering the entire heart [69] using a phase array 4-channel surface receive volume transmit coil (RAPID Biomedical GmhB, Germany) as previously described in Section 2.3.5.

6.3.6 *In vivo* Assessment of Metabolic Parameters using Dynamic Nuclear Polarization

The effects of Ramipril treatment on cardiac metabolism was assessed *in vivo* at 4 and 9 weeks post-surgical induction of left ventricular hypertrophy using [^{13}C]pyruvate labelled on the first or second prime carbon as previously described in Section 2.3. Male Sprague-Dawley rats were prepared as described in Section 2.3.1. Approximately 1 ml of hyperpolarized [^{13}C]pyruvate was infused over 10 seconds and 60 single scan spectra were acquired over a period of 60 seconds as previously described in Section 2.3.

6.3.7 Assessment of Glycolytic Flux and Ischemia Reperfusion Injury the Isolated Langendorff Perfused Heart

At 10 weeks post-surgery, hearts were isolated and perfused with Krebs-Heinsleit (KH) buffer containing 11 mM glucose, 0.4 mM palmitate, 2048 pmol L^{-1} insulin and 0.5 μCi [5-^{1}H]glucose as previously described in Section 2.5. Following a 10 minute acclimatisation period, pre-ischemic function and metabolism was assessed for a total of 20 minutes following which hearts received low flow ischemia (0.3 ml min^{-1} gww^{-1}) for a period of 30 minutes as previously described in Section 2.5.4.2. Normal flow was resumed for a further 20 minutes as described in Section 2.5.4.2. Hearts were washed for 4 minutes with fresh Krebs-Heinsleit (KH), free of radiotracer, at the end of the perfusion protocol and rapidly freeze-clamped on the cannula and stored at -80 °C for subsequent analysis as previously described in Section 2.5.4.2. A sample of perfusate (1 ml) was taken every 4 minutes over the 80 minute perfusion period and used to calculate myocardial glycolytic flux as previously described in Section 2.5.5.

6.3.8 Blood Sampling and Plasma Analysis

Terminal bloods were obtained as previously described in Section 2.6 and the plasma concentrations of glucose, lactate, triacylglycerides (TAG), low-density lipoprotein (LDL), cholesterol, high-density lipoprotein (HDL), and β-hydroxybutyrate were assessed using

an ABX Pentra 400 (Horiba ABX Diagnostics, California, USA) as previously described in Section 2.6.

6.3.9 Statistical Analysis

All data is presented as mean ± standard error of the mean (SEM). Data acquired at 4 weeks post-surgery was analysed using an unpaired, two-tailed Student's t test whereas *in vivo* structural, functional and metabolic data acquired at 9 weeks post-surgery was analysed using a one-way ANOVA with Sidak correction for multiple comparisons. Perfusion data acquired at 10 weeks post-surgery was also analysed using a one-way ANOVA with Sidak correction for multiple comparisons. All data was analysed using the GraphPad Prism 7 Software Package (GraphPad Softwares, California, USA).

6.4 Results

6.4.1 Characterisation of Hypertrophic Development at 4 Weeks Post-Surgery

Cardiac structure and function was assessed at 4 weeks post-surgery using cine MRI prior to treatment with Ramipril. Evidence of cardiac hypertrophy was confirmed in the Aortic Constriction (AC) group vs. Sham group at 4 weeks post-surgery marked by a significant increase in left ventricular (LV) mass in the AC group relative to the Sham group (Sham: 830 ± 27 mg; AC: 925 ± 22 mg; Fig 6.5A; $p < 0.05$ *vs. Sham*). This was accompanied by a significant increase in heart weight to body weight ratio within the AC group vs. Sham group (Sham: 2.26 ± 0.07; AC: 2.59 ± 0.05; Fig 6.5B; $p < 0.01$ *vs. Sham*) consistent with hypertrophic development.

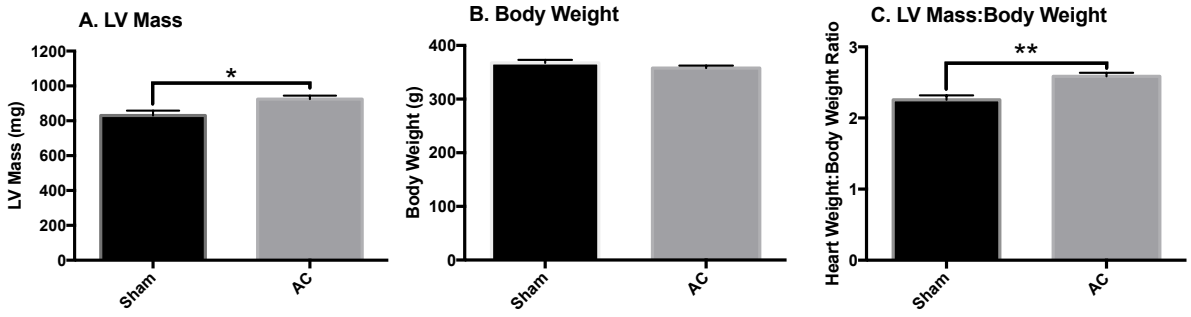


Figure 6.5: Characteristation of Cardiac Hypertrophy at 4 Weeks Post- the Surgical Induction of Hypertrophy. A. Left Ventricular (LV) Mass; B. Body Weight; C. Left ventricular (LV) Mass:Body Weight Ratio. Sham: n = 8; AC n = 28. * $p < 0.05$ *vs. Sham;* ** $p < 0.01$ *vs. Sham.* Unpaired Two-Tailed Student's t test. $Mean \pm SEM$, AC: Aortic Constriction.

No change in cardiac output was observed in the AC group vs. the Sham group (Fig 6.6A; $p = 0.96$ *vs. Sham*) at 4 weeks post-surgery, however, a significant reduction in ejection fraction was observed in the AC group vs. the Sham group (Sham: 74 ± 1 %; AC: 70 ± 1; Fig 6.6B; $p = 0.05$ *vs. Sham*). This was accompanied by no change in heart rate (Fig 6.6C; $p = 0.18$ *vs. Sham*) or stroke volume (Fig 6.7A; $p = 0.34$ *vs. Sham*) in the AC group vs. the Sham group.

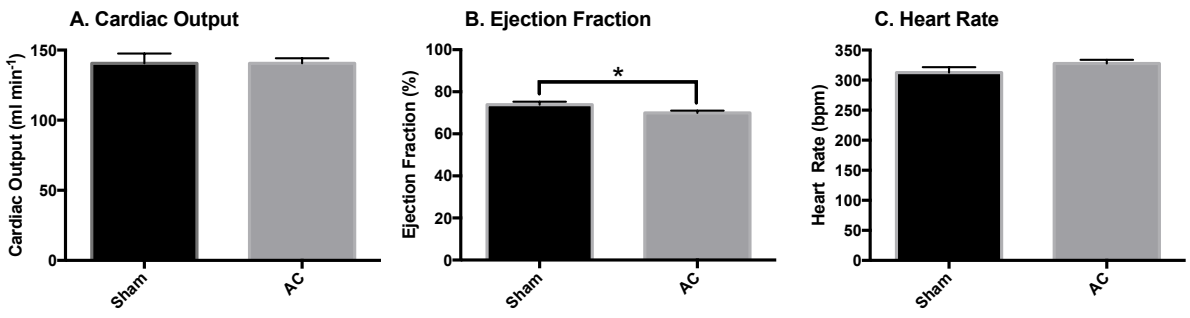


Figure 6.6: Functional Parameters Following the Development of Hypertrophy at 4 Weeks Post- the Surgical Induction of Hypertrophy. A. Cardiac Output. B. Ejection Fraction. C. Heart Rate. Sham: n = 11; AC: n = 28. * $p = 0.05$ *vs. Sham*. Unpaired Two-Tailed Student's t test. $Mean \pm SEM$. AC: Aortic Constriction.

No change in the end diastolic volume was observed in the AC group vs. the Sham group (Fig 6.7B; $p = 0.73$ *vs. Sham*). A slight increase in end systolic volume was observed in the AC group relative to the Sham group (Fig 6.6C; $p = 0.06$ *vs. Sham*) however, this failed to reach statistical significance.

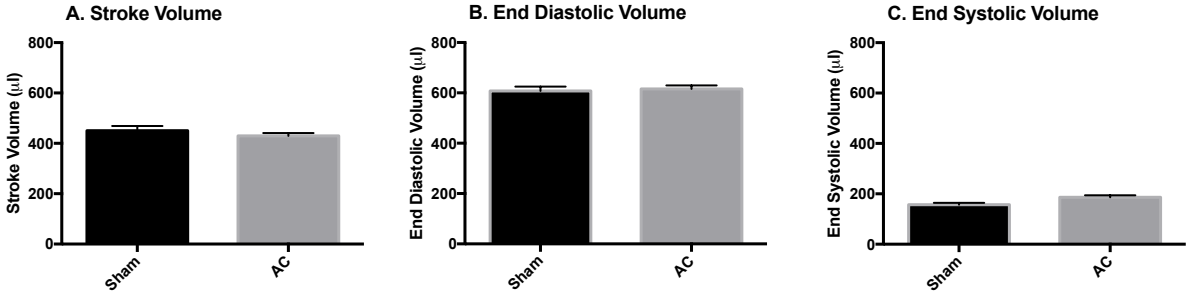


Figure 6.7: Further Functional Parameters Following the Development of Cardiac Hypertrophy at 4 Weeks Post- the Surgical Induction of Hypertrophy. A. Stroke Volume. B. End Diastolic Volume. C. End Systolic Volume. Sham: n = 11; AC: n = 28; Unpaired Two-Tailed Student's t Test. $Mean \pm SEM$. AC: Aortic Constriction.

6.4.2 Metabolic Characterisation of the Heart with the Development of Hypertrophy at 4 Weeks Post-Surgery

No change in flux through pyruvate dehydrogenase (PDH) was observed in the AC group vs. the Sham group (Fig 6.8A; $p = 0.39$ *vs. Sham*). This was accompanied by no change in label incorporation into either lactate (Fig 6.8B; $p = 0.95$ *vs. Sham*) or alanine (Fig

6.8C; $p = 0.63$ *vs. Sham*) in the AC group vs. the Sham group. A significant increase in label incorporation into lactate was previously observed in the AC group vs. the Sham group in Chapter 3. However, a smaller sample size is presented here which may account for the lack of difference observed.

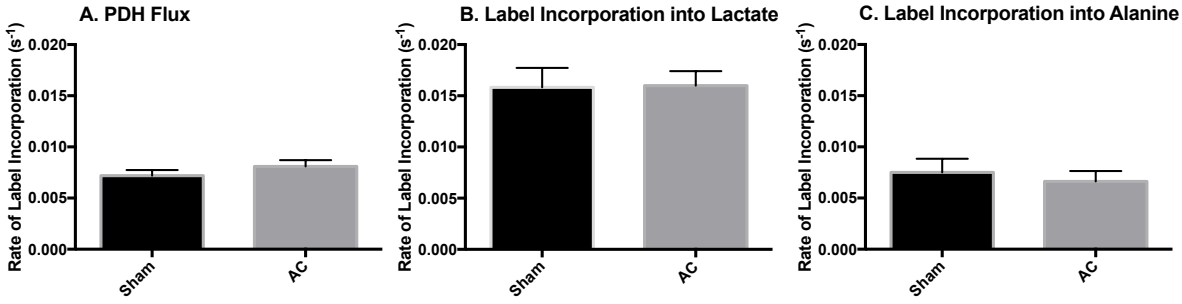


Figure 6.8: Pyruvate Dehydrogenase (PDH) Flux at 4 Weeks Post- the Surgical Induction of Hypertrophy. A. PDH Flux. B. Label Incorporation into Lactate. C. Label Incorporation into Alanine. Sham: n = 11; AC: n = 28. Unpaired Two-Tailed Student's t test. $Mean \pm SEM$. AC: Aortic Constriction.

An increase in label incorporation into glutamate, citrate and acetylcarnitine was observed in the AC group vs. the Sham group (Glutamate: Fig 6.9A; $p = 0.12$ *vs. Sham* Citrate: Fig 6.9B; $p = 0.10$ *vs. Sham*; Acetylcarnitine: 6.9C; $p = 0.06$ *vs. Sham*) but this failed to reach statistical significance. However, when normalised to the average PDH flux for the group, a significant increase into glutamate, citrate and acetylcarnitine was observed in the AC group vs. the Sham group (Glutamate: Sham: 1.32 ± 0.18 a.u.; AC: 3.63 ± 0.53 a.u.; Fig 6.9D; $p < 0.05$ *vs. Sham*; Citrate: Sham: 0.75 ± 0.05 a.u. AC: 1.84 ± 0.25 a.u.; Fig 6.9E; $p < 0.05$ *vs. Sham*; Acetylcarnitine: Sham: 3.14 ± 0.35 a.u. AC: 7.89 ± 1.14 a.u.; Fig 6.9F; $p < 0.05$ *vs. Sham*).

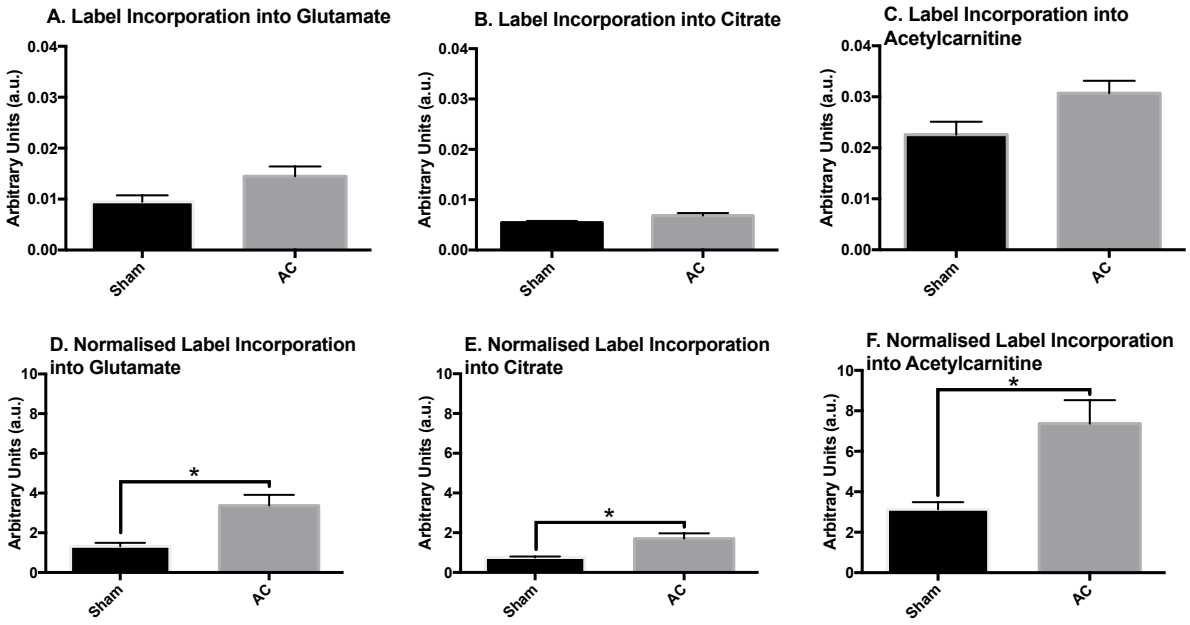


Figure 6.9: Label Incorporation into TCA Cycle Intermediates at 4 Weeks Post- the Surgical Induction of Hypertrophy. A. Label Incorporation into Glutamate; B. Label Incorporation into Citrate; C. Label Incorporation into Acetylcarnitine; D. Normalised Label Incorporation into Glutamate; E. Normalised Label Incorporation into Citrate; F. Normalised Label Incorporation into Acetylcarnitine. Sham: n = 8; AC: n = 17. * $p < 0.05$ *vs. Sham.* Unpaired Two-Tailed Student's t test. $Mean \pm SEM$; AC: Aortic Constriction.

6.4.3 The Effect of Ramipril Treatment on Hypertrophic Progression

The effects of 5 weeks of treatment with either a low dose of Rampril (Low Dose; 0.1 mg kg^{-1}) or a high dose of Ramipril (High Dose; 1 mg kg^{-1}) on cardiac structure and function was assessed at 9 weeks post the surgical induction of hypertrophy. The presence of hypertrophy was confirmed in the treated groups prior to the development of hypertrophy.

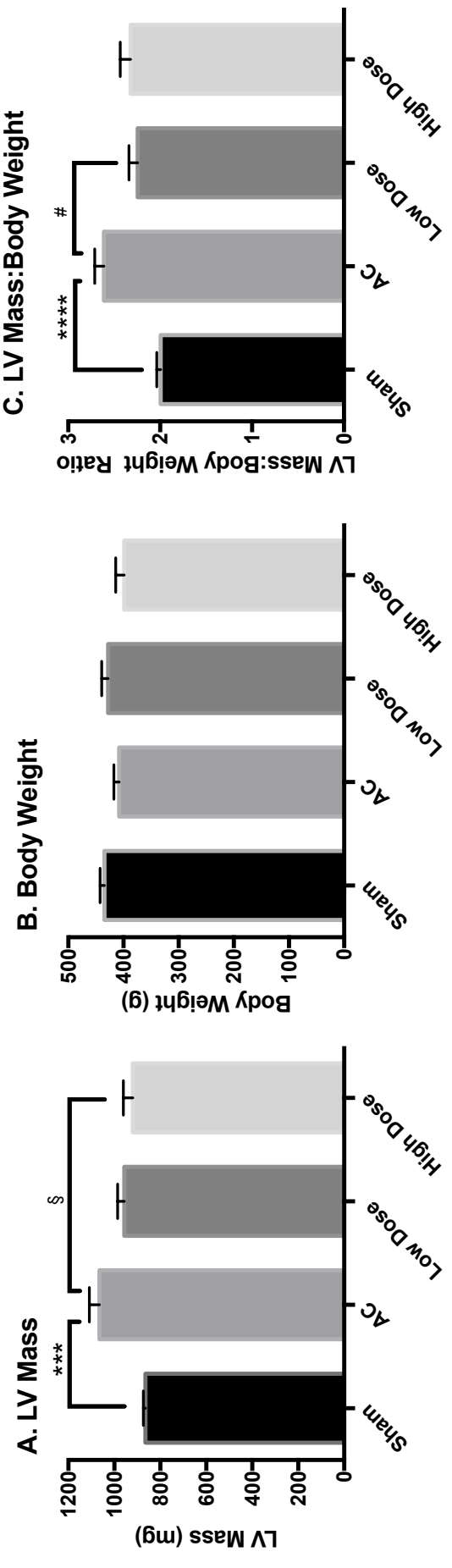


Figure 6.10: The Effects of Ramipril treatment on Myocardial Remodelling in the Hypertrophied Heart. A. Left Ventricular (LV) Mass. B. Body Weight. C. Left Ventricular (LV) Mass to Body Weight Ratio. Sham: n = 11; AC: n = 10; Low Dose: n = 9; High Dose: n = 9. *** $p < 0.005$ *vs. Sham*; **** $p < 0.001$ *vs. Sham*; § $p < 0.05$ *AC vs. High Dose*; # $p < 0.05$ *AC vs. Low Dose.* One-Way ANOVA with Sidak Correction for Multiple Comparisons. $Mean \pm SEM$. AC: Aortic Constriction; Low Dose: 0.1 mg kg^{-1} day^{-1} Ramipril Treatment. High Dose: 1 mg kg^{-1} day^{-1} Ramipril Treatment.

No increase in LV mass was observed within the Low Dose or High Dose groups relative to the Sham group (Fig 6.10A; *p = 0.25 Sham vs. Low Dose*; *p = 0.76 Sham vs. High Dose*). No significant difference in LV mass was observed in the Low Dose group vs. the AC group (Fig 6.10A; *p = 0.13 AC vs. Low Dose*) but a significant reduction in LV mass was observed in the High Dose group when compared with AC group (AC: 1066 ± 44 mg; High Dose; 920 ± 124 mg; Fig 6.10A; *p <0.05*) suggestive of hypertrophic regression in the High Dose group. No change in body weight was observed in either the Low Dose or High Dose groups when compared with the Sham group or AC group (Fig 6.10B; *p >0.99 Sham vs. Low Dose*; *p = 0.13 Sham vs. High Dose*; *p = 0.70 AC vs. Low Dose*; *p = 0.98 AC vs. High Dose*). No change in heart weight to body weight ratio was observed in the Low Dose group when compared with the Sham group (Fig 6.10C; *p = 0.24 Sham vs. Low Dose*) and a significant reduction in LV mass to body weight ratio was observed in the Low Dose group vs. the AC group (AC: 2.61 ± 0.10; Low Dose: 2.25 ± 0.10; Fig 6.10C; *p <0.05 AC vs. Low Dose*). No change in LV mass to body weight ratio was observed in the High Dose group relative to the Sham group (Fig 6.10C; *p = 0.06 Sham vs. High Dose*).

No changes in functional parameters were observed in the Ramipril treated groups relative to the Sham group. This was represented by no change in cardiac output, stroke volume, ejection fraction or heart rate in either the Low Dose or High Dose groups when compared with the Sham group (Cardiac Output: Fig 6.11A; *p = 0.89 Sham vs. Low Dose*; *p >0.99 Sham vs. High Dose*; Stroke Volume: Fig 6.12A; *p = 0.66 Sham vs. Low Dose*; *p = 0.98 Sham vs. High Dose*; Ejection Fraction: Fig 6.11B; *p >0.99 Sham vs. Low Dose*; *p = 0.83 Sham vs. High Dose*; Heart Rate: Fig 6.11C; *p = 0.97 Sham vs. Low Dose*; *p = 0.98 Sham vs. High Dose*).

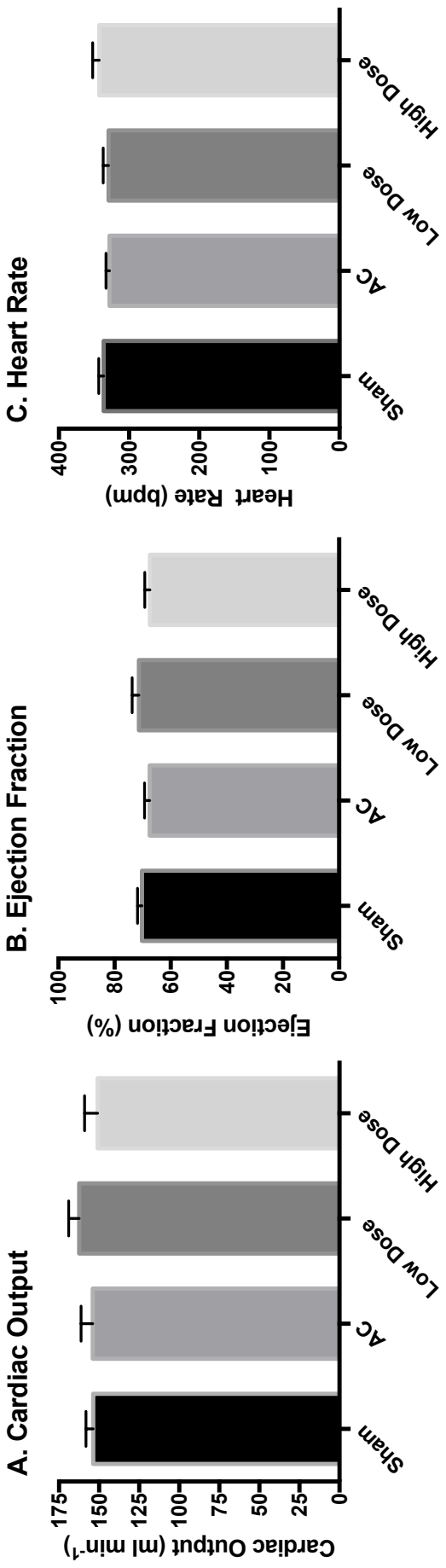


Figure 6.11: The Effects of Ramipril Treatment on Functional Parameters in the Hypertrophied Heart. A. Cardiac Output. B. Ejection Fraction. C. Heart Rate. Sham: n = 11; AC: n = 10; Low Dose: n = 9; High Dose: n = 9; One-Way ANOVA with Sidak Correction for Multiple Comparisons. $Mean \pm SEM$. AC: Aortic Constriction; Low Dose: 0.1 mg kg^{-1} day^{-1} Ramipril Treament. High Dose: 1 mg kg^{-1} day^{-1} Ramipril Treatment.

This was accompanied by no changes in functional parameters in the Low and High Dose groups when compared with the AC group (Cardiac Output: Fig 6.11A; $p = 0.91$ *AC vs. Low Dose*; $p > 0.99$ *AC vs. High Dose*; Stroke Volume: Fig 6.12A; $p = 0.90$ *AC vs. Low Dose*; $p = 0.87$ *AC vs. High Dose*; Ejection Fraction: Fig 6.11B; $p = 0.68$ *AC vs. Low Dose*; $p > 0.99$ *Sham vs. High Dose*; Heart Rate: Fig 6.11C; $p > 0.99$ *AC vs. Low Dose*; $p = 0.60$ *AC vs. High Dose*).

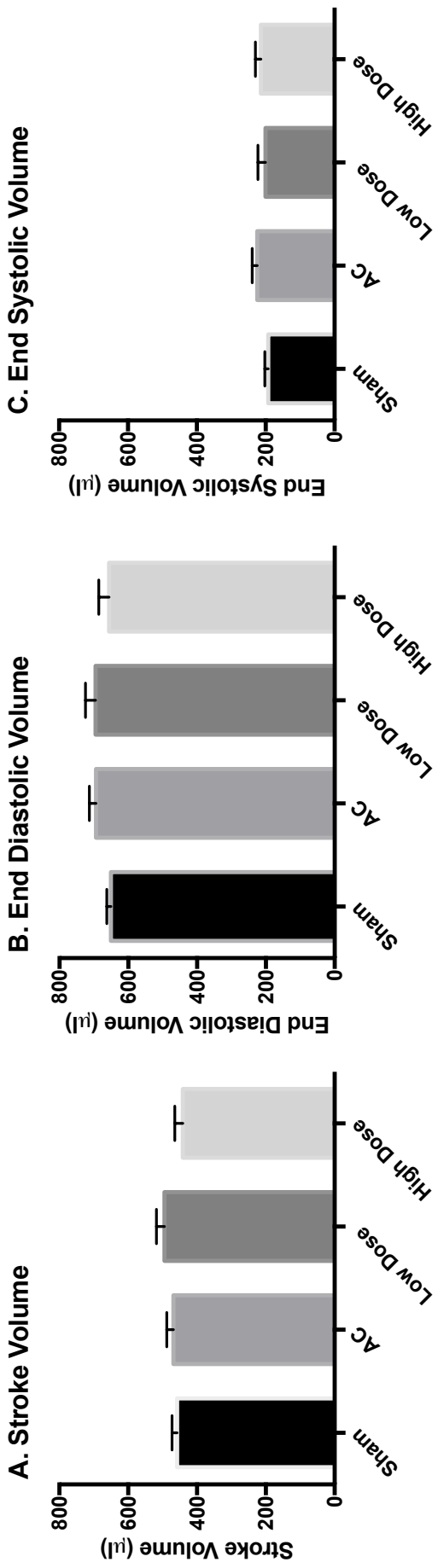


Figure 6.12: The Effects of Ramipril Treatment on Additional Functional Parameters in the Hypertrophied Heart. A. Stroke Volume. B. End Diastolic Volume. C. End Systolic Volume. Sham: n = 11; AC: n = 10; Low Dose: n = 9; High Dose: n = 9; One-Way ANOVA with Sidak Correction for Multiple Comparisons. $Mean \pm SEM$. AC: Aortic Constriction; Low Dose: 0.1 mg kg^{-1} day^{-1} Ramipril Treatment. High Dose: 1 mg kg^{-1} day^{-1} Ramipril Treatment.

No changes in end diastolic or end systolic volume was observed in either of the Ramipril treated groups vs. the Sham group accompanied by no change in stroke volume in the treated groups vs. the Sham group (End Diastolic Volume: Fig 6.12B; *p = 0.61 Sham vs. Low Dose*; *p >0.99 Sham vs Low Dose*; End Systolic Volume: Fig 6.12C; *p >0.99 Sham vs. Low Dose*; *p = 0.87 Sham vs. High Dose*; Stroke Volume: 6.12A; *p = 0.66 Sham vs. Low Dose*; *p = 0.98 Sham vs. High Dose*). This was accompanied by no change in either end diastolic volume or end systolic volume or stroke volume in the Ramipril treated groups when compared to the AC group (End Diastolic Volume: Fig 6.12B; *p >0.99 AC vs. Low Dose*; *p = 0.77 AC vs Low Dose*; End Systolic Volume: Fig 6.12C; *p = 0.82 AC vs. Low Dose*; *p >0.99 AC vs. High Dose*; Stroke Volume: 6.12A; *p = 0.90 AC vs. Low Dose*; *p = 0.87 AC vs. High Dose*)

6.4.4 The Effects of Ramipril Treatment on Myocardial Metabolism

No change in flux into pyruvate dehydrogenase (PDH) was observed in either the Low Dose or High Dose groups vs. the Sham group (Fig 6.13A; *p = 0.85 Sham vs. Low Dose*; *p = 0.85 Sham vs. High Dose*). This was accompanied by no change in label incorporation into lactate or alanine in either of the Ramipril treated groups vs. the Sham group (Lactate: Fig 6.13B; *p = 0.87 Sham vs. Low Dose*; *p = 0.81 Sham vs. High Dose*; Alanine: Fig 6.13C; *p = 0.99 Sham vs. Low Dose*; *p >0.99 Sham vs. High Dose*).

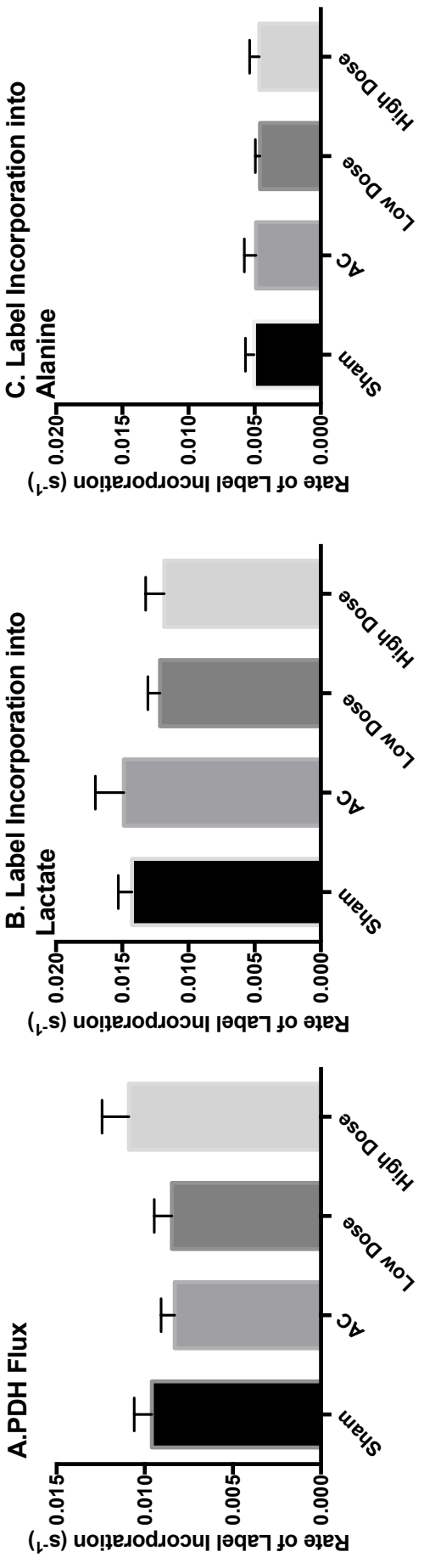


Figure 6.13: The Effect of Ramipril Treatment on Flux into Pyruvate Dehydrogenase in the Hypertrophied Heart. A. PDH Flux. B. Label Incorporation into Lactate. C. Label Incorporation into Alanine. Sham: n = 11; AC: n = 10; Low Dose: n = 9; High Dose: n = 9; AC: Aortic Constriction; One-Way ANOVA with Sidak Correction for Multiple Comparisons. $Mean \pm SEM$; Low Dose: 0.1 mg kg^{-1} day^{-1} Ramipril Treatment. High Dose: 1 mg kg^{-1} day^{-1} Ramipril Treatment.

No change in flux into glutamate, citrate or acetylcarnitine was observed in either the Low Dose or High Dose group at 9 weeks post-surgery (glutamate: Fig 6.14A; $p = 0.27$ *Sham vs. Low Dose*; $p = 0.85$ *Sham vs. High Dose*; citrate: Fig 6.14B; $p = 0.94$ *Sham vs. Low Dose*; $p = 0.98$ *Sham vs. High Dose*; acetylcarnitine: Fig 6.14C; $p = 0.57$ *Sham vs. Low Dose*; $p = 0.94$ *Sham vs. High Dose*). This was mirrored when the Low and High Dose groups were compared to the AC group (glutamate: Fig 6.14A; $p = 0.46$ *AC vs. Low Dose*; $p = 0.94$ *AC vs. High Dose*; citrate: Fig 6.14B; $p = 0.99$ *AC vs. Low Dose*; $p = 0.97$ *AC vs. High Dose*; acetylcarnitine: Fig 6.14C; $p = 0.68$ *AC vs. Low Dose*; $p = 0.96$ *Sham vs. High Dose*).

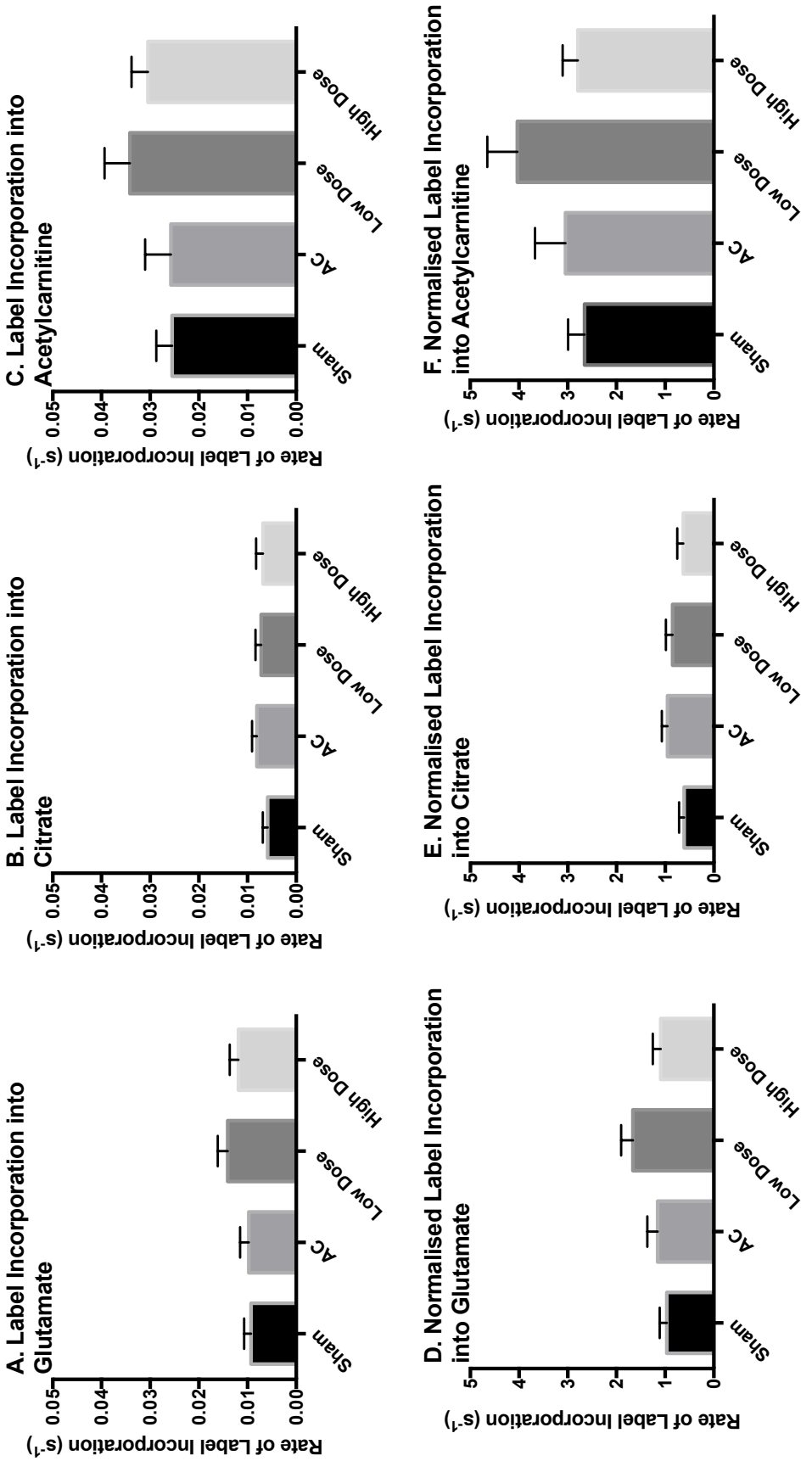


Figure 6.14: Label Incorporation into TCA Intermediates following Low and High Dose Ramipril Treatment at 9 Weeks Post-Surgery. A. Label Incorporation into Lactate; B. Label Incorporation into Alanine; C. Label Incorporation into Glutamate; D. Label Incorporation into Citrate; E. Label Incorporation into Acetylcarnitine. Sham: n = 9; AC: n = 6; Low Dose: n = 9; High Dose: n = 8; AC: Aortic Constriction; Low Dose: 0.1 mg kg^{-1} day^{-1} Ramipril. High Dose: 1 mg kg^{-1} day^{-1} Ramipril. One-Way ANOVA with Sidak Correction for Multiple Comparisons. $Mean \pm SEM$

However, when normalised to the average PDH flux for the group, an increase in flux into the glutamate in the Low Dose group vs. the Sham group was observed but this failed to reach statistical significance (Fig 6.14D; *p = 0.08 Sham vs. Low Dose*). This was accompanied by no change in label incorporation into citrate or acetylcarnitine in the Low Dose group when normalised to PDH flux (citrate: Fig 6.14E *p = 0.62 Sham vs. Low Dose*; acetylcarnitine: Fig 6.14F; *p = 0.22 Sham vs. Low Dose*). No change in label incorporation into glutamate, citrate or acetylcarnitine was observed in the High Dose group relative to the Sham group following normalisation to PDH flux (glutamate: Fig 6.14D; *p >0.99 Sham vs. High Dose*; citrate: Fig 6.14E; *p >0.99 Sham vs. High Dose*; acetylcarnitine: Fig 6.14F; *p >0.99 Sham vs. High Dose*).

6.4.4.1 The Effects of Ramipril Treatment on Glycolytic Flux in the Langendorff-Perfused Heart

No change in pre-ischemic, ischemic or post-ischemic glycolytic flux was observed in either the Low Dose or High Dose groups vs. the Sham group (pre-ischemic: Fig 6.15A; *p = 0.33 Sham vs. Low Dose*; *p >0.99 Sham vs. High Dose*; ischemia: Fig 6.15B; *p >0.99 Sham vs. Low Dose*; *p >0.99 Sham vs. High Dose*; post-ischemia: Fig 6.15A; *p = 0.99 Sham vs. Low Dose*; *p = 0.98 Sham vs. High Dose*) following 6 weeks of Ramipril treatment. When compared to the AC group, no further changes in glycolytic flux were observed in the Low Dose or High Dose groups in the pre-ischemic, ischemic or post-ischemic phase (pre-ischemic: Fig 6.15A; *p >0.99 AC vs. Low Dose*; *p = 0.15 AC vs. High Dose*). No significant increase in pre-ishemic glycolytic flux was observed in the AC group vs. the Sham group (Fig 6.15A; *p = 0.33 vs. Sham*) as previously described in Chapter 3. This is likely due to the reduced statistical power caused by the presence of other groups within this study.

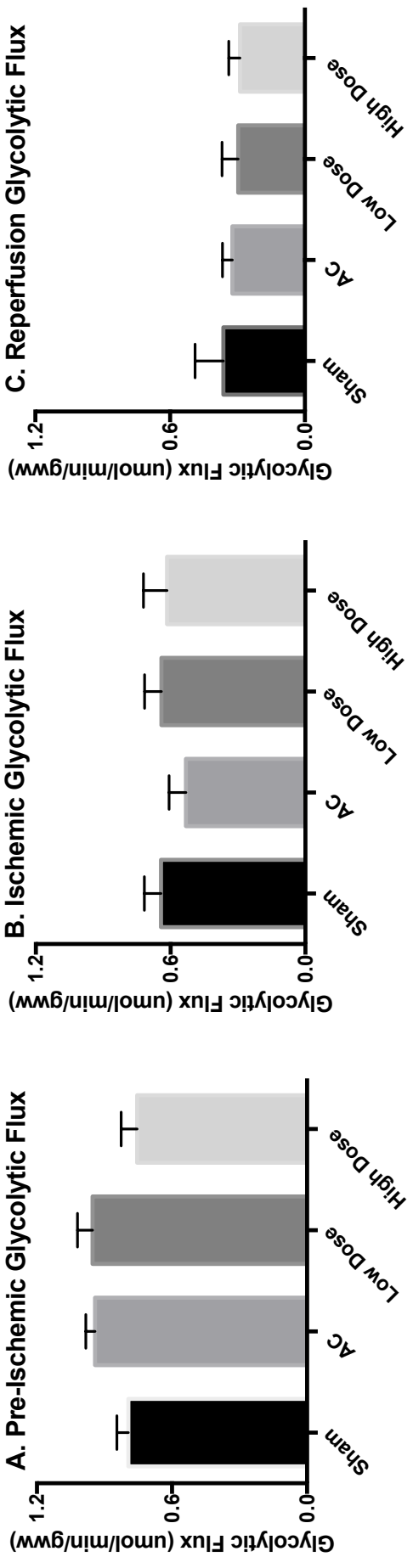


Figure 6.15: The Effects of Ramipril Treatment on Glycolytic Flux in the Hypertrophied Heart Perfused via the Langendorff Mode. A. Pre-Ischemic Glycolytic Flux. B. Ischemic Glycolytic Flux. C. Reperfusion Glycolytic Flux. Sham: n = 9; AC: n = 8; Low Dose: n = 9; High Dose: n = 9; AC: Aortic Constriction; Low Dose: 0.1 mg kg^{-1} day^{-1} Ramipril. High Dose: 1 mg kg^{-1} day^{-1} Ramipril One-Way ANOVA with Sidak Correction for Multiple Comparisons. $Mean \pm SEM$

6.4.5 The Impact of Ramipril Treatment on Ischemia Reperfusion Recovery in the Treated and Untreated Hypertrophied Heart

The effect of ischemia was assessed at 10 weeks post-surgery in the hypertrophied heart treated with either a low dose (0.1 mg kg^{-1} day^{-1}) or high dose of Ramipril (1 mg kg^{-1} day^{-1}) to assess whether Ramipril treatment played a role in protecting the heart from ischemic damage. Hearts perfused in the Langendorff mode received low flow ischemia (0.3 ml min^{-1} gww^{-1}) prior to reperfusion.

No difference in rate pressure product (RPP; Fig 6.16A), representative of cardiac function was observed in the Ramipril treated groups vs. the Sham group during the pre-ischemic or post-ischemic period (pre-ischemia: Fig 6.16B; $p > 0.99$ *Sham vs. Low Dose*; $p = 0.95$ *Sham vs. High Dose*; post-ischemia: Fig 6.16C; $p > 0.99$ *Sham vs. Low Dose*; $p > 0.99$ *Sham vs. High Dose*).

This was accompanied by no change in left ventricular developed pressure (LVDP; Fig 6.17) or heart rate (HR; Fig 6.18) in either the Ramipril treated groups vs. the Sham group pre- or post-ischemia (LVDP: pre-ischemia: Fig 6.17B; $p > 0.99$ *Sham vs. Low Dose*; $p = 0.97$ *Sham vs. High Dose*; post-ischemia: Fig 6.17C; $p = 0.78$ *Sham vs. Low Dose*; $p = 0.98$ *Sham vs. High Dose*; HR: pre-ischemia: Fig 6.18B; $p > 0.99$ *Sham vs. Low Dose*; $p > 0.99$ *Sham vs. High Dose*; post-ischemia: Fig 6.18C; $p = 0.19$ *Sham vs. Low Dose*; $p = 0.79$ *Sham vs. High Dose*).

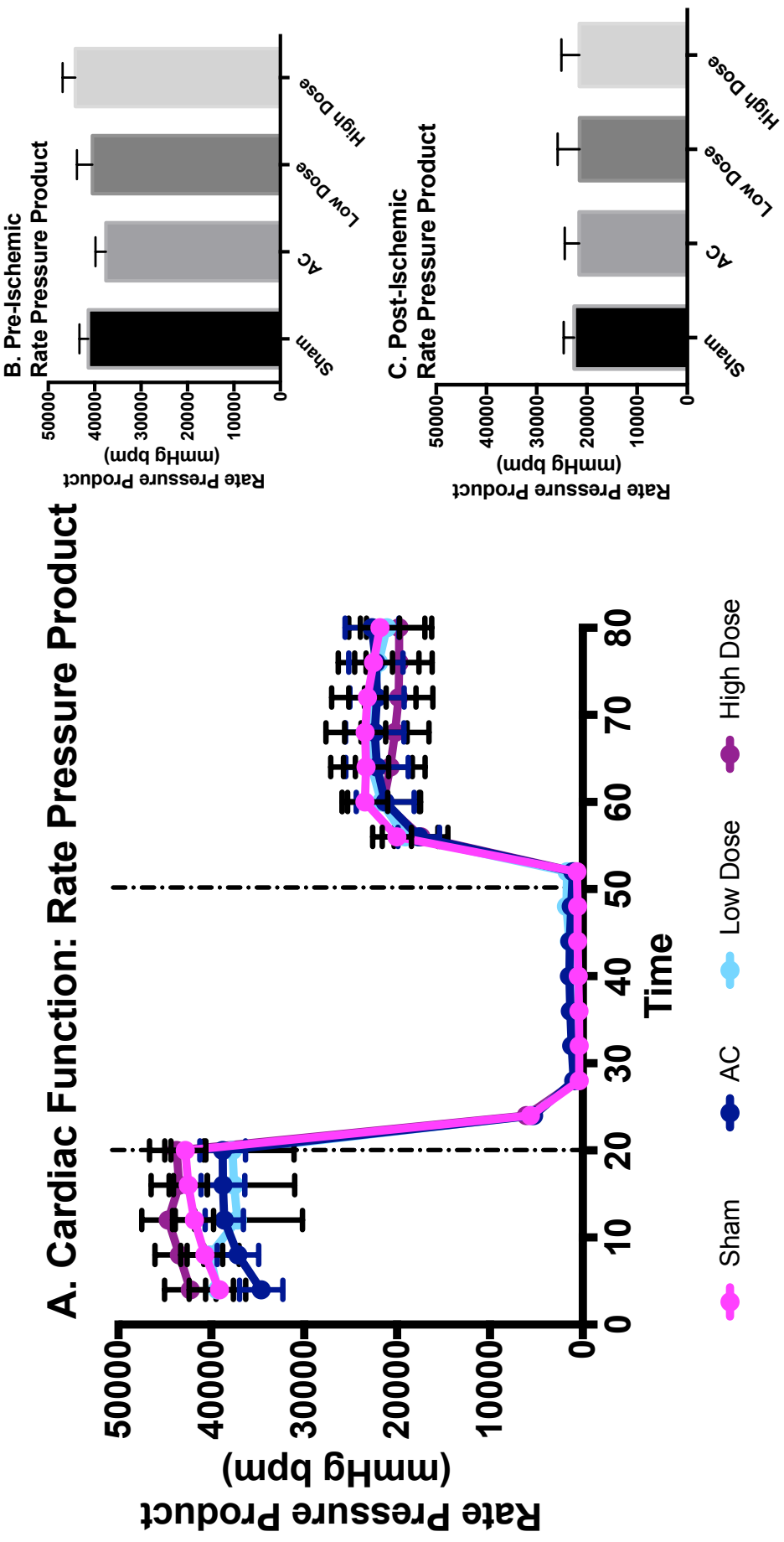


Figure 6.16: The Effects of Ischemia on Cardiac Function in the Ramipril-Treated Heart. A. Rate Pressure Product. B. Average Pre-Ischemic Rate Pressure Product. C.Average Post-Ischemic Rate Pressure Product. Sham: n = 9; AC: n = 10; Low Dose: n = 8; High Dose: n = 8; Unpaired Two Tailed Student's t test with Correction for Multiple Comparisons and One-Way ANOVA with Sidak Correction for Multiple Comparisons. $Mean \pm SEM$. AC: Aortic Constriction; Low Dose: 0.1 mg kg^{-1} day^{-1} Ramipril. High Dose: 1 mg kg^{-1} day^{-1} Ramipril.

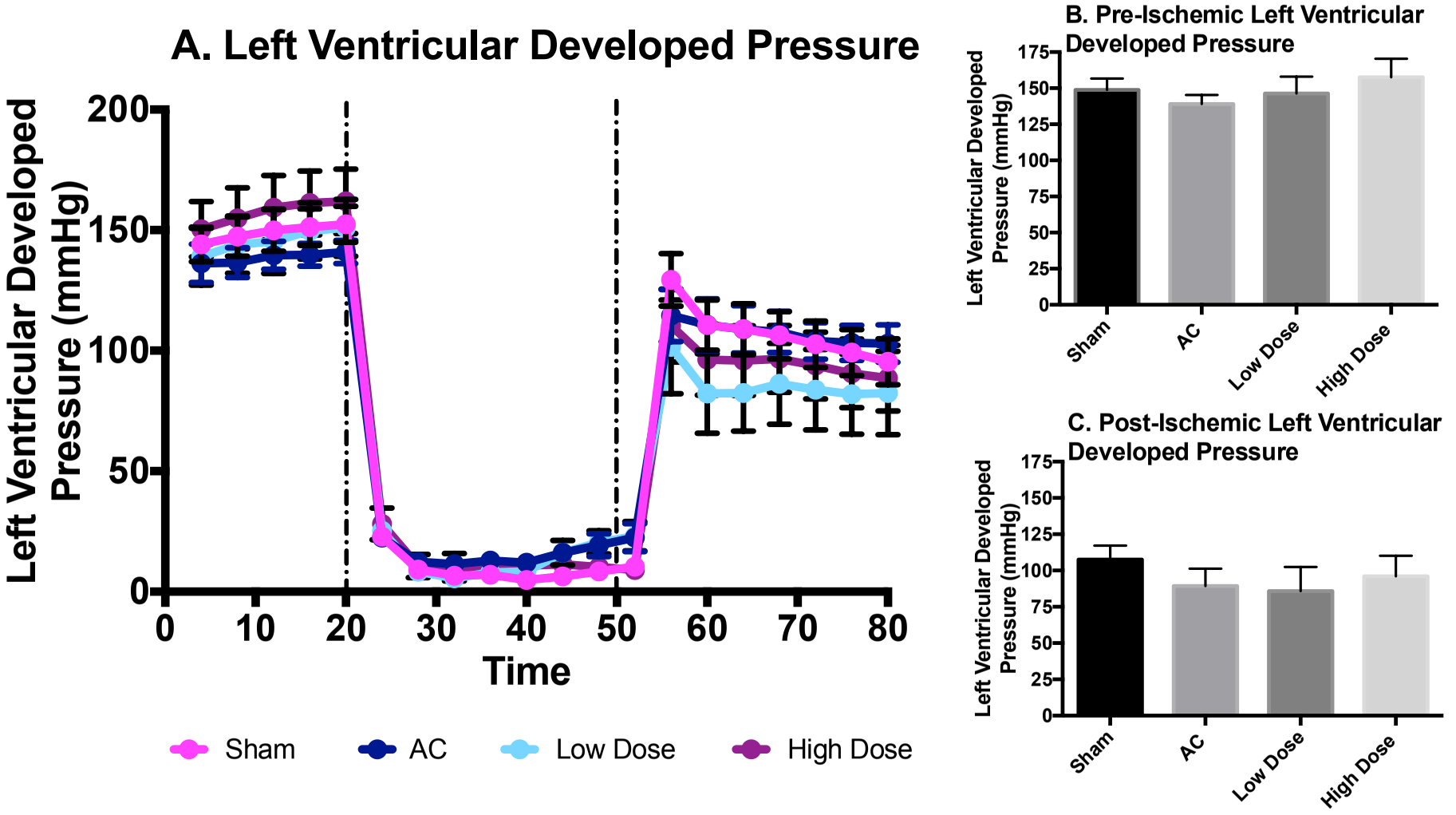


Figure 6.17: The Effects of Ischemia on Left Ventricular Developed Pressure in the Ramipril Treated Heart. A. Left Ventricular Developed Pressure. B. Average Pre-Ischemic Left Ventricular Developed Pressure. C. Post-Ischemic Left Ventricular Developed Pressure. Sham: n = 9; AC: n = 10; Low Dose: n = 8; High Dose: n = 8; Unpaired Two-Tailed Student's t test with Correction for Multiple Comparisons. and One-Way ANOVA with Sidak Correction for Multiple Comparisons. $Mean \pm SEM$. AC: Aortic Constriction; Low Dose: 0.1 mg kg^{-1} day^{-1} Ramipril. High Dose: 1 mg kg^{-1} day^{-1} Ramipril.

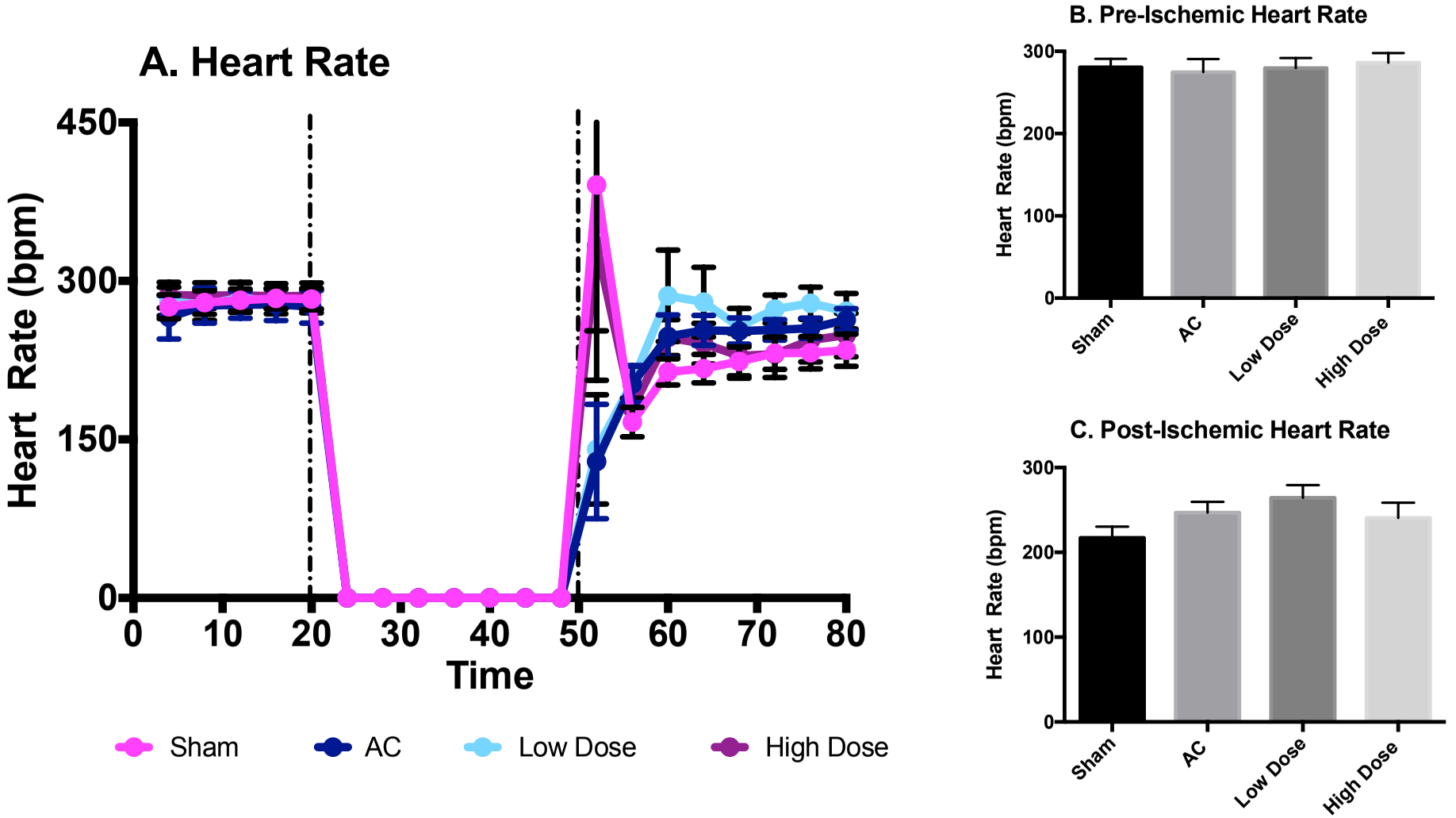


Figure 6.18: The Effects of Ischemia Reperfusion on Heart Rate in the Ramipril Treated Heart. A. Heart Rate. B. Average Pre-Ischemic Heart Rate. C. Average Post-Ischemic Heart. Sham: n = 9; AC: n = 10; Low Dose: n = 8; High Dose: n = 8; Unpaired Two-Tailed Student's t test with Correction for Multiple Comparisons and One-Way ANOVA with Sidak Correction for Multiple Comparisons. $Mean \pm SEM$. AC: Aortic Constriction; Low Dose: 0.1 mg kg^{-1} day^{-1} Ramipril. High Dose: 1 mg kg^{-1} day^{-1} Ramipril.

No change in end diastolic pressure was observed in the Ramipril treated groups vs. the Sham group pre-ischemia (pre-ischemia: Fig 6.19B; $p > 0.99$ *Sham vs. Low Dose*; $p > 0.99$ *Sham vs. High Dose*), during ischemia (ischemia: Fig 6.19C; $p = 0.49$ *Sham vs. Low Dose*; $p = 0.72$ *Sham vs. High Dose*) or following ischemia (ischemia: Fig 6.19D; $p = 0.97$ *Sham vs. Low Dose*; $p = 0.85$ *Sham vs. High Dose*).

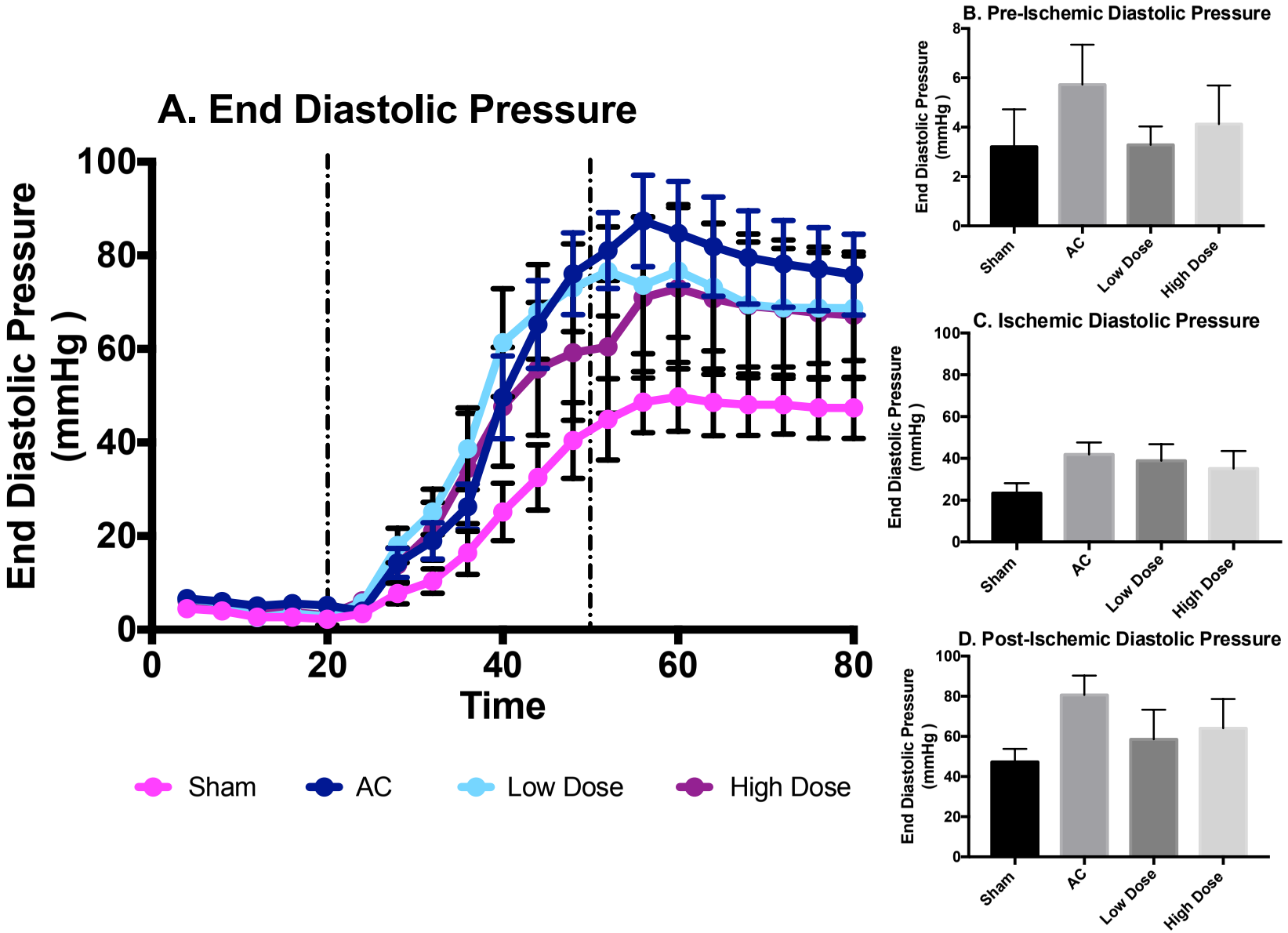


Figure 6.19: The Effects of Ischemia on the End Diastolic Pressure on the Ramipril Treated Heart Perfused via the Langendorff Mode. * $p < 0.05$ *Sham vs. AC* Sham: n = 9; AC: n = 10; Low Dose: n = 8; High Dose: n = 8; Unpaired Two-Tailed Student's t test with Correction for Multiple Comparisons and One-Way ANOVA with Sidak Correction for Multiple Comparisons. $Mean \pm SEM$. AC: Aortic Constriction; Low Dose: Low Dose: 0.1 mg kg^{-1} day^{-1} Ramipril. High Dose: 1 mg kg^{-1} day^{-1} Ramipril.

The ability of the heart to recover function following the ischemic period was assessed through calculation of the RRP, LVDP and HR at 1 minute post-reperfusion, 3 minutes post-reperfusion and at 30 minutes post-reperfusion (Fig 6.20). The percentage recovery of function was calculated relative to cardiac function at 1 minute prior to ischemia. No change in the RPP was observed in either the Low Dose or High Dose groups vs. the Sham group at 1, 3 or 30 minutes post-ischemia (1 minute: Fig 6.20A; $p = 0.98$ *Sham vs. Low Dose*; $p > 0.99$ *Sham vs. High Dose*; 3 minutes: Fig 6.20E; $p = 0.91$ *Sham vs. Low Dose*; $p > 0.99$ *Sham vs. High Dose*; 30 minutes: Fig 6.20I $p > 0.99$ *Sham vs. Low Dose*; $p > 0.99$ *Sham vs. High Dose*). No difference in the recovery of function was observed in the Ramipril treated groups vs. the Sham groups at 1 minute, 3 minute and 30 post-ischemia (1 minute: Fig 6.20D; $p = 0.98$ *Sham vs. Low Dose*; $p > 0.99$ *Sham vs. High Dose*; 3 minutes: Fig 6.20H; $p = 0.91$ *Sham vs. Low Dose*; $p > 0.99$ *Sham vs. High Dose*; 30 minutes: Fig 6.20K; $p = 0.31$ *Sham vs. Low Dose*; $p > 0.99$ *Sham vs. High Dose*). This was accompanied by no change in LVDP or HR in the Ramipril treated groups vs. the Sham group at 1, 3 or 30 minutes post-ischemia (LVDP: 1 minute: Fig 6.20B; $p = 0.62$ *Sham vs. Low Dose*; $p = 0.84$ *Sham vs. High Dose*; 3 minutes: Fig 6.20F; $p = 0.25$ *Sham vs. Low Dose*; $p = 0.64$ *Sham vs. High Dose*; 30 minutes: Fig 6.20J; $p > 0.99$ *Sham vs. Low Dose*; $p = 0.93$ *Sham vs. High Dose*; HR: 1 minute: Fig 6.20C; $p = 0.98$ *Sham vs. Low Dose*; $p > 0.99$ *Sham vs. High Dose*; 3 minutes: Fig 6.20G; $p = 0.87$ *Sham vs. Low Dose*; $p = 0.50$ *Sham vs. High Dose*; 30 minutes: Fig 6.20K; $p = 0.53$ *Sham vs. Low Dose*; $p > 0.99$ *Sham vs. High Dose*).

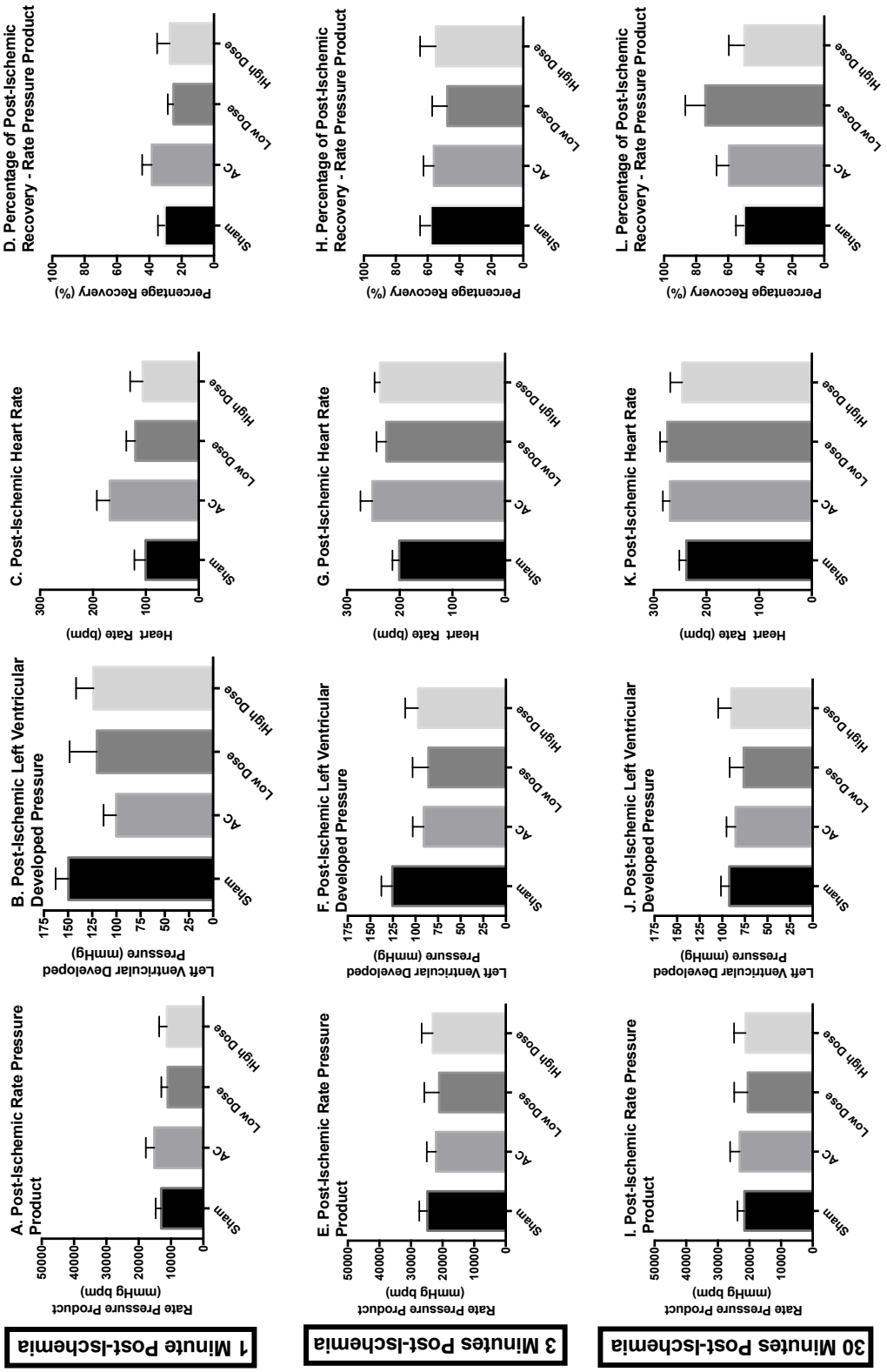


Figure 6.20: The Ability of the Ramipril Treated Heart tp Recover from Ischemia . A. Rate Pressure Product (1 minute Post-Ischemia). B. Left Ventricular Developed Pressure (1 minute Post-Ischemia). C. Heart Rate (1 minute Post-Ischemia). D. Percentage Recovery of Rate Pressure Product (1 minute Post-Ischemia). E. Rate Pressure Product (3 minutes Post-Ischemia). F. Left Ventricular Developed Pressure (3 minutes Post-Ischemia). G. Heart Rate (3 minutes Post-Ischemia). H. Percentage Recovery of Rate Pressure Product (3 minutes Post-Ischemia). I. Rate Pressure Product (30 minutes Post-Ischemia). J. Left Ventricular Developed Pressure (30 minutes Post-Ischemia). K. Heart Rate (30 minutes Post-Ischemia). L. Percentage Recovery of Rate Pressure Product (30 minutes Post-Ischemia). Percentage Recovery was determined by dividing the post-ischemic rate pressure product by the rate pressure product at 1 minute prior to ischemia. Sham: n = 9; AC: n = 10; Low Dose: n = 8; High Dose: n = 8; One-Way ANOVA with Sidak Correction for Multiple Comparisons. $Mean \pm SEM$. AC: Aortic Constriction; Low Dose: 0.1 mg kg^{-1} day^{-1} Ramipril. High Dose: 1 mg kg^{-1} day^{-1} Ramipril.

6.4.6 Further Biochemical Analysis

6.4.6.1 Plasma Analysis following Ramipril Treatment

No change in the plasma composition was observed in the Ramipril treated groups vs. the Sham group (glucose: Fig 6.21A; $p = 0.80$ *Sham vs. Low Dose*; $p > 0.99$ *Sham vs. High Dose*; lactate: Fig 6.21B; $p = 0.84$ *Sham vs. Low Dose*; $p = 0.98$ *Sham vs. High Dose*; β-hydroxybutyrate: Fig 6.21C; $p = 0.89$ *Sham vs. Low Dose*; $p = 0.98$ *Sham vs. High Dose*; NEFA: Fig 6.21D; $p = 0.57$ *Sham vs. Low Dose*; $p = 0.94$ *Sham vs. High Dose*; cholesterol: Fig 6.21E; $p < 0.99$ *Sham vs. Low Dose*; $p = 0.99$ *Sham vs. High Dose*; TAG: Fig 6.21F; $p = 0.92$ *Sham vs. Low Dose*; $p = 0.94$ *Sham vs. High Dose*).

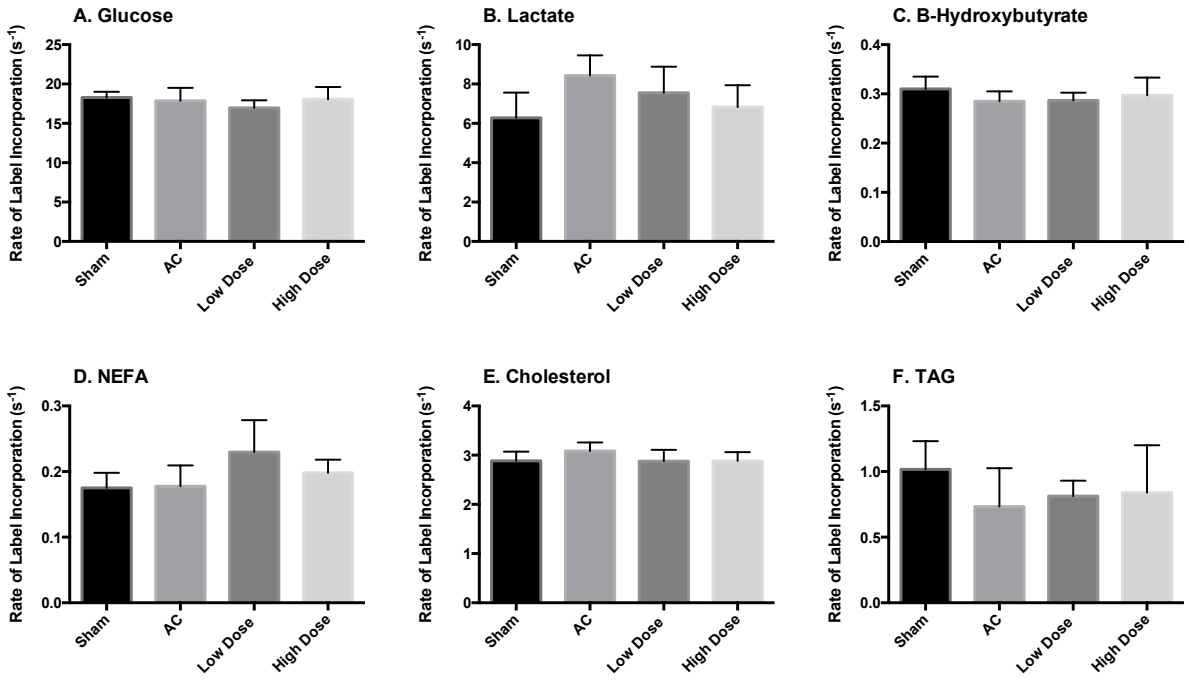


Figure 6.21: Terminal Plasma Analysis of Rats with Left Ventricular Hypertrophy either Treated or Untreated with Ramipril. A. Glucose. B. Lactate. C. β-Hydroxybutyrate. D. Non-esterified Fatty Acid (NEFA). E. Cholesterol. F. Triacylglyceride (TAG). Sham: n = 7; AC: n = 4; Low Dose: n = 6; High Dose: n = 6; AC: Aortic Constriction; Low Dose: Low Sub-antihypertensive Dose of Ramipril; High Dose: High Antihypertensive Dose of Ramipril. One-Way ANOVA with Sidak Correction for Multiple Comparisons. $Mean \pm SEM$.

6.5 Discussion

6.5.1 Summary of Findings

The presence of left ventricular (LV) hypertrophy was confirmed in the AC group prior to treatment with either a low dose (0.1 mg kg^{-1} day^{-1}) or a high dose (1 mg kg^{-1} day^{-1}) of Ramipril. This was represented by a significant increase in both LV mass and LV mass to body weight ratio in the AC group. A significant reduction in ejection fraction was observed within the AC group, which has not been noted previouly (Chapter 3). No accompanying reduction in cardiac output, stroke volume or heart rate was observed and no significant increase in end diastolic volume which is representative of myocardial dilation. This suggests that the reduction in ejection fraction observed was a result of the remodelling process prior to the establishment of the compensated phase of LV hypertrophy.

Following both Low Dose and High Dose Ramipril treatment, there was no significant increase in LV mass and a regression in LV mass was observed in the High Dose marked by a significant reduction in LV mass relative to the AC group. This was accompanied by no evidence of functional change within the Ramipril treated groups.

No significant changes in PDH flux or label incorporation into lactate, alanine, glutamate, citrate and acetylcarnitine were observed following either High Dose or Lose Dose Ramipril treatment. This was accompanied by no change in pre-ischemic, ischemic or post-ischemic glycolytic flux in either of the treatment groups and the High and Low dose groups showed no altered ability to recover from ischemia relative to the Sham group.

Although no significant metabolic changes were observed following Ramipril treatment, a high dose of Ramipril may be having a mild effect on glycolytic flux within the hypertrophied heart. In the absence of the Low Dose group, a one-way ANOVA with Sidak correction for multiple comparisons presents a p value of 0.05 and comparison between the AC and High Dose group presents a p value of 0.07. Power calculations suggest that we are currently underpowered to detect a difference of this size and a sample size of at least 18 per group would be required to see a statistically significant effect of 80 %. Furthermore, the sample size proposed is comparable to those presented in previous

studies within this thesis. However, given that within this sample size we are seeing a regression in LV mass with Ramipril treatment, it suggests that any metabolic changes induced by Ramipril are having a relatively small effect.

Ramipril hearts exhibited no reduction in pre-ischemic function or ability to recover following 30 minutes of ischemia when compared to the Sham hearts which also experienced ischemia reperfusion. It should be noted however, that all groups received the same flow rate whereas *in vivo*, the hypertrophied heart would receive a higher pressure. As a result, it may be difficult to distinguish any functional differences which may exist within the hypertrophied heart *in vivo*. However, consistent with the data obtained from the perfused heart, no functional changes were observed *in vivo*.

6.5.2 Ramipril Treatment Induces Hypertrophic Regression Independent of Dosage

The regression in hypertrophy observed following a high dose of Ramipril treatment is proposed to result from an inhibition of angiotensin converting enzyme (ACE). However, a reduction in LV mass was also observed in the low dose group which has previously been reported as sub-antihypertensive. This is supported by work by Linz *et al*, who identified both a regression in hypertrophy and a reduction in angiotensin II levels in aortic constriction model following daily treatment with 10 μl kg^{-1} Ramipril and may support a role for bradykinin and the alternative RAA system. This was accompanied by no change in systemic blood pressure, as reported by Linz *et al*, suggesting that treatment with Ramipril is not limited to a single target [155].

6.6 Conclusions and Future Perspectives

Our work suggests that both a Low and High dose of Ramipril treatment induces a regression in hypertrophy. Given that the low dose given here is proposed to be sub-antihypertensive, this supports the proposition that the actions of Ramipril are not limited to its role as an angiotensin converting enzyme inhibitor (ACEI). A high dose of Ramipril may be having a mild effect on myocardial metabolism, acting to normalise glycolytic flux within the hypertrophied heart. However, with the sample size presented, the study is underpowered to achieve statistical significant but the data presented is sufficient to warrant further investigation to confirm whether the tentative conclusions drawn are correct.

Further investigation into the molecular mechanisms associated with a reduction in glycolytic flux in the High Dose group would provide further insight into the mechanisms by which Ramipril may act. Linking this to the previous work by Boateng *et al* on calcium handling along with identification of the effects of Ramipril treatment on fatty acid oxidation would provide a fuller picture as to the role of Ramipril outside of its primary role as an ACEI.

Chapter 7

General Discussion

7.1 A Brief Overview

The work summarised in this thesis is focused around the changes in the balance between glycolysis and glucose oxidation with the development of hypertrophy. Hypertrophic development and the associated changes in glycolysis and glucose oxidation were characterised in the abdominal aortic constriction (AC) model of left ventricular hypertrophy (LVH), a physiologically relevant model of compensated hypertrophy [101]. Previous studies within this model have focused on a metabolic changes at individual stages of hypertrophic remodelling [166, 64, 42, 105], however, the stage of hypertrophy is often poorly characterised. Within the work presented here, we have characterised the pattern of structural, functional and metabolic remodelling *in vivo* in response to chronic hypertension using a novel combination of MRI and dynamic nuclear polarisation. We identified reduced coupling between glycolysis and glucose oxidation in the early stages of hypertrophic development which has been widely reported within the literature [1, 64, 5, 12, 50, 52, 91, 167] however, contrary to what has previously been published we have shown that the heart stablised and enter a fully compensated stage at 14 weeks post-surgery accompanied by normalised glycolytic flux.

The model was further used to assess the effects of two different therapeutic avenues. Dichloroactetate (DCA) is a well-known compound which has been proposed as a treatment for a range of diseases with a metabolic basis including cancer [118], hypertrophy [142], diabetes [141, 115] and hypercholesteremia [116, 117] but has yet to be successfully used clinically. It is well-known that DCA upregulates pyruvate dehydrogenase (PDH) activity [111, 119], however, prior to this study the wider effects of DCA on myocardial metabolism was not well clarified. The work presented in this thesis has assessed the effects of DCA treatment on cardiac metabolism which identified its additional role in reducing glycolytic flux and promoting fatty acid oxidation, highlighting its potential as a treatment of hypertrophy. Alternatively, we looked at the effects of Ramipril, a widely prescribed and highly sucessful angiotensing-converting enzyme inhibitor (ACEI) [168, 147]. Ramipril reduces systemic blood pressure via an ACEI mediated mechanism but it has also been shown to have beneficial effects on the heart at sub-antihypertensive

levels [155, 152, 151, 143, 93, 118, 156]. We proposed that this benefit was derived from the link between improved calcium handling and Ca^{2+} mediated up-regulation of PDH activity [36]. This section places in context the development of compensated LVH and the therapeutic angles taken.

7.2 Metabolic Changes with Hypertrophic Development in the Abdominal Aortic Constriction Model

The findings of this thesis are summarised in Figure 7.1. In Chapter 3 we characterised the metabolic and structural changes which occur with the development of hypertrophy in the abdominal aortic constriction (AC) model. The use of cine MRI and the novel technique, dynamic nuclear polarisation (DNP) allowed the longitudinal assessment of hypertrophic development *in vivo* which has otherwise rarely been observed. We identified a consistent 17 % increase in LV mass with the development of hypertrophy over 14 weeks which was confirmed using MRI, which has been shown to be more reproducible in small animal models when compared with 2D-echocardiography [169]. This is a considered a mild model of hypertrophy especially compared with thoracic aortic constriction (TAC) model which induces approximately a 40 % increase in heart weight at 7 days post-surgery however, the slow onset is considered to be of physiological relevanance [170, 101]. Hypertrophic development in the AC model as assessed here was accompanied by a significant increase in label incorporation into lactate during the first 9 weeks of hypertrophic development and a mild increase in cardiac output where the heart is compensating for an increase in systemic pressure. Interestingly, increased glycolytic dependence has been associated with the negative aspects of hypertrophic development [15]. However, when we administered DCA treatment, which we identified reduces glycolytic flux and promotes fatty acid oxidation (Chapter 4), in the initial stages of hypertrophic development, it was associated with a reduction in ejection fraction and myocardial dilation, a profile associated with heart failure rather than compensated hypertrophy (Chapter 5). This is contrary to previous studies which suggest that chronic DCA treatment has a positive effect on the heart in type II diabetes and hyperthyroid-induced hypertrophy [142, 141]. However, in pressure-overload hypertrophy, as investigated here, this suggests that increased glycolytic flux is integral to sustained cardiac output in the initial stages of hypertrophic development whilst the heart is adapting to increased systemic pressure.

One limitation of this model, unlike the TAC model, is that there is no evidence of

heart failure observed during the time frame studied [104]. Therefore, we can not identify whether either increased glycolytic dependence or DCA treatment has an impact on the decline into heart failure which has previously been observed at later time points [105]. More typically, an increase in glycolytic dependence has been associated with patients with end stage of heart failure and it is possible that the heart undergoes a number of transitions from the initial stages of hypertrophic development to end stage heart failure [1].

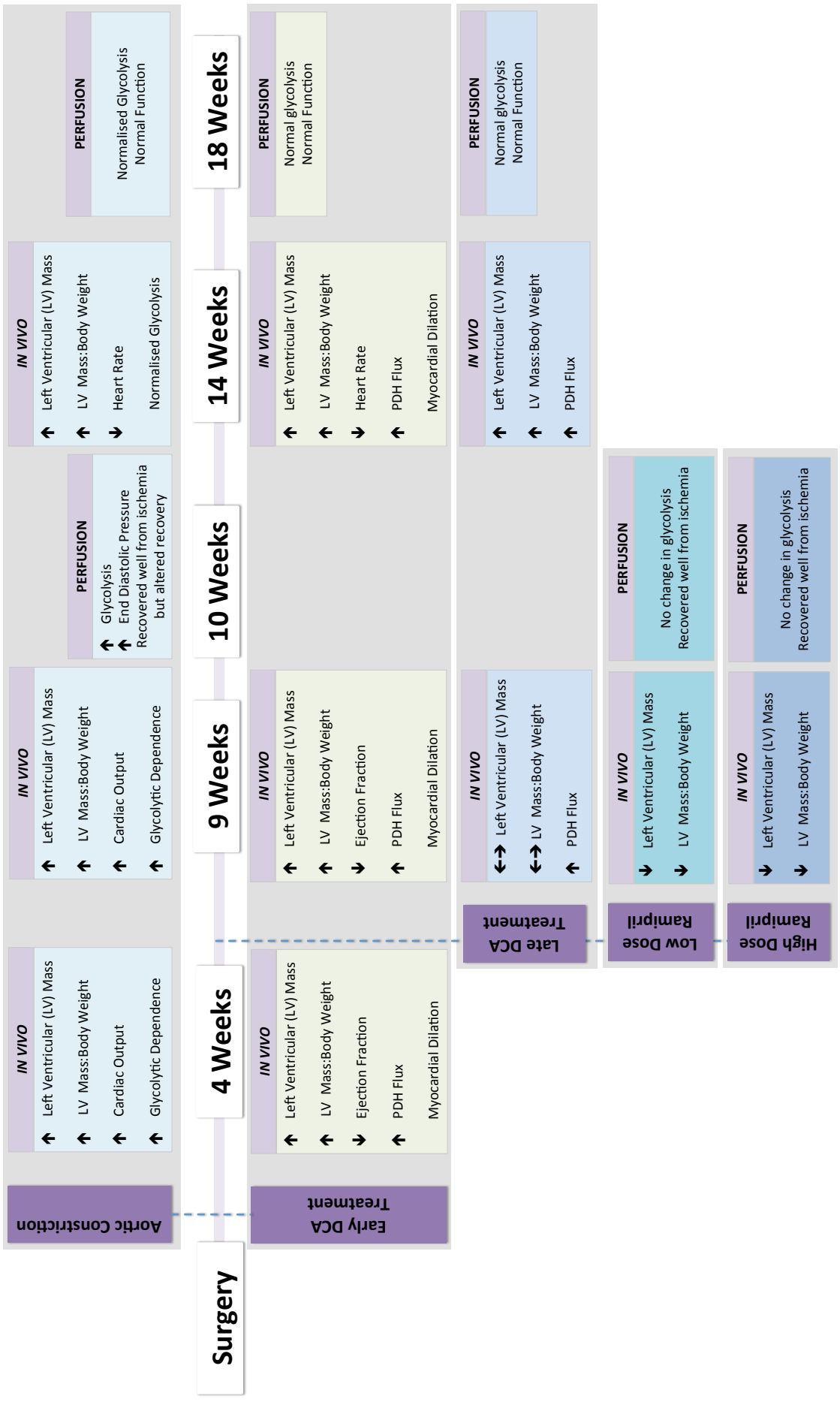


Figure 7.1: An Overview of the Structural, Functional and Metabolic Changes which occur in the Hypertrophied Heart and the Effect of Dichloroacetate (DCA) and Ramipril Treatments

Within the AC model, we start to see a stabilisation of both function and a normalisation of glycolysis at 14 weeks post-surgery and this was confirmed in the perfused heart at 18 weeks post-surgery. Interestingly, this is different to what we observed previously in the AC model, where no change in glycolysis was observed at 4 weeks post-surgery, but was evident at 9 and 14 weeks post-surgery (Appendix A,[50]). There was no difference in the degree of hypertrophy, represented by LV mass and LV mass to body weight ratio, observed between the two different studies and may be representative of the dyanamic nature of hypertrophic remodelling. We also didn't identify a significant increase in label incorporation into lactate at 4 weeks post-surgery in the Ramipril study, although an increase was present. The increase in label incorporation is subtle and the lack of a statistically significant effect may be due to the sample size used and a possible limitation in the sensitivity of dynamic nuclear polarization as a technique. However, it also allows the longitudinal assessment of metabolic flux in real time *in vivo* within the same animal, which is arguably a highly invaluable technique. Following characterisation of model, the metabolic effects of DCA treatment and Ramipril treatment were assessed.

7.3 The Use of Dichloroacetate Treatment and Ramipril Treatment in the Hypertrophied Heart in Elucidating the Role of Metabolism in Hypertrophied Development and Progression

As previously discussed, treatment with dichloroacetate (DCA) in the initial stages of myocardial adaptation to hypertension has a detrimental effect on the heart suggesting that glycolytic dependence plays an important role in hypertrophic development. Myocardial dilation and reduced function is extended up until 14 weeks post-surgery (Chapter 5). However, in the Late DCA Treatment group, where DCA is given following the establishment of hypertrophy, a mild attenuation in hypertrophic remodelling may occur. No significant difference in LV mass was observed in the Late DCA Treatment group when compared with the AC group however, only a 12 % increase in LV mass is still observed within the Late DCA Treatment group suggesting that DCA may induce a slowing of

hypertrophic progression rather than causing a regression in hypertrophy as observed in the T3 model of hyperthyroid induced hypertrophy [142]. The percentage increase in LV mass when compared to the Sham group is summarised for all groups in Figure 7.2.

Treatment Group	4 Weeks	9 Weeks	14 Weeks
AC	17%	17%	17%
Early DCA Treatment	23%	27%	24%
Late DCA Treatment	17%	12%	17%
Low Dose Ramipril	17%	1%	
High Dose Ramipril	17%	1%	

Untreated
Treated

Figure 7.2: The Percentage Increase in Left Ventricular (LV) Mass in the Aortic Constriction (AC), Dichloroacetate (DCA) and Ramipril treated Groups when compared to the Sham group.

From our characterisation of the model, from 4 to 10 weeks, we identified an increase in glycolytic dependence, however, we are experiencing differential effects within this time period based on when DCA treatment was given. As previously stated, chronic DCA treatment is associated with a reduced glycolytic flux, increased pyruvate dehydrogenase (PDH) flux and enhanced fatty acid oxidation (Chapter 4). This suggests that the metabolic remodelling during this period is more complex than presented in this study and may lie in the changes in fatty acid oxidation. Akki *et al* report a reduction in the levels of palmitate oxidation at 9 weeks post-surgery supported by work by Allard *et al* at 8 weeks post-surgery [4, 42]. This is the point at which we propose that DCA treatment is having a beneficial effect on hypertrophic remodelling represented by a mild attenuation. It may be that restoration of fatty acid oxidation, if that is what is occuring, is beneficial at this point in hypertrophic development. This is supported by work by Degens *et al*, who report no change in fatty acid oxidation at 4 weeks post-surgery in the AC model [65]. We have shown that DCA treatment, when given immediately post-surgery is detrimental at the 4 weeks post-surgery. Perhaps forcing fatty acid oxidation at that stages contributes to the negative effects reported.

We are also unable to determine the effects of chronic DCA treatment on the decline into heart failure which may provide some further insight into the longer term effects of treatment on cardiac viability. In work published by Allard *et al*, glucose metabolism was normalisation in the hypertrophied heart at higher work loads suggesting that stressing the heart induces a different metabolic profiles which would be interesting to assess here [42]. It may also provide some insight into whether DCA treatment is beneficial in the long term. A closer clarification of the molecular changes which occur between the induction of hypertrophy 4 and 9 weeks post-surgery such as the effects of hypertrophy and DCA treatment on glucose and fatty acid transport especially following the work presented by Perira *et al*, Abel *et al* and Razeghi *et al* on the possible role of GLUT 1 and GLUT 4 in the onset of hypertrophy and heart failure [54, 49, 171].

Treatment with both a low and high dose of Ramipril was associated with a regression in hypertrophy. However, in both the absence of myocyte isolation and blood pressure measurements we can't fully confirm this and especially further clarification of the antihypertensive effects of Ramipril treatment would benefit this study. The low dose of Ramipril (0.1 mg kg^{-1} day^{-1}) was previously reported to be sub-antihypertensive [99] and 1 mg kg^{-1} was reported to be anti-hypertensive. However, even sub-antihypertensive doses have been reported to induce a regression in hypertrophy and may be due to enhanced levels of bradykinin production [155], furthermore no evidence of metabolic remodelling was associated with a low dose of Ramipril which suggests that other mechanisms are responsible for hypertrophic regression with Ramipril treatment. Activation of the systemic renin-angiotensin-aldosterone (RAA) system induces an elevation in atrial natriuretic factor (ANP) and brain natriuretic factor (BNP), the recruitment of immune effector cells such as macrophages and fibroblasts. This induces the activation of the local RAA system, collegen secretion and the development of fibrosis in the later stages of hypertrophic remodelling [172]. This study doesn't address what additional effect Ramipril treatment, at either dosage, may have on the ventricular tissue.

A possible alteration in metabolic profile in the High Dose group may be present but this is purely speculative. However, we propose that the sample size used here is

underpowered to draw statistical significance (Chapter 6).

7.4 Final Conclusions and Future Perspectives

This work has highlighted a role for metabolic remodelling with the development of left ventricular hypertrophy (LVH). Following the characterisation of the abdominal aortic constriction (AC) model of LVH, we have combined the use of dichloroactetate (DCA) treatment, a known up-regulator of pyruvate dehydrogenase activity with Ramipril treatment which is a widely used treatment for hypertension and heart failure, to further elucidate the effects of metabolic modulation on hypertrophic development with a view to preventing the negative aspects of hypertrophy.

This study is limited to the effects of metabolic remodelling and the treatment of compensated hypertrophy. Extension of the model to assess the effect of both DCA treatment and Ramipril treatment on myocardial metabolism in the later stages of hypertrophy, prior to the development of heart failure, would provide further insight into whether these approaches have a beneficial effect long-term.

This work confirms the AC model as physiologically relevant and the work presented here has the potential for clinical translation. Through the use of *in vivo* techniques such as dynamic nuclear polarization (DNP), which is an emerging technique clinically and CINE MRI, which is widely used, we have characterised hypertrophic development within the AC model and identified the effects of different therapies including Ramipril which is an accepted treatment for hypertension. This highlights the potential of these techniques in the investigation of hypertension and heart disease in patient as well as their response to different therapeutic angles.

Bibliography

[1] W. C. Stanley. Myocardial Substrate Metabolism in the Normal and Failing Heart. *Physiological reviews* **2005**:*85*(3): 1093–1129.

[2] S. J. Pilkis and D. K. Granner. Molecular physiology of the regulation of hepatic gluconeogenesis and glycolysis. *Annual Review of Physiology* **1992**:*54*: 885–909.

[3] A. M. Seymour and J. C. Chatham. The effects of hypertrophy and diabetes on cardiac pyruvate dehydrogenase activity. *Journal of Molecular and Cellular Cardiology* **1997**:*29*(10): 2771–2778.

[4] A. Akki, K. Smith, and A. M. Seymour. Compensated cardiac hypertrophy is characterised by a decline in palmitate oxidation. *Molecular and cellular biochemistry* **2008**:*311*(1-2): 215–224.

[5] A. Akki and A. M. Seymour. Western diet impairs metabolic remodelling and contractile efficiency in cardiac hypertrophy. *Cardiovascular research* **2009**:*81*(3): 610–617.

[6] P. J. Randle, P. B. Garland, C. N. Hales, and E. A. Newsholme. The glucose fatty-acid cycle. Its role in insulin sensitivity and the metabolic disturbances of diabetes mellitus. *The Lancet* **1963**:*1*(7285): 785–789.

[7] S. P. Bessman and P. J. Geiger. Transport of energy in muscle: the phosphorylcreatine shuttle. *Science* **1981**:*211*(4481): 448–452.

[8] S. Neubauer. The failing heart–an engine out of fuel. *The New England journal of medicine* **2007**:*356*(11): 1140–1151.

[9] N. Sorokina, J. M. O'donnell, R. D. McKinney, K. M. Pound, G. Woldegiorgis, K. F. Lanoue, K. Ballal, H. Taegtmeyer, P. M. Buttrick, and E. D. Lewandowski. Recruitment of compensatory pathways to sustain oxidative flux with reduced carnitine palmitoyltransferase I activity characterizes inefficiency in energy metabolism in hypertrophied hearts. *Circulation* **2007**:*115*(15): 2033–2041.

[10] T. Wallimann, M. Wyss, D. Brdiczka, K. Nicolay, and H. M. Eppenberger. Intracellular compartmentation, structure and function of creatine kinase isoenzymes in tissues with high and fluctuating energy demands: the 'phosphocreatine circuit' for cellular energy homeostasis. *Biochemical Journal* **1992**:*281*(Pt 1): 21.

[11] S. Neubauer, M. Horn, M. Cramer, K. Harre, J. B. Newell, W. Peters, T. Pabst, G. Ertl, D. Hahn, J. S. Ingwall, and K. Kochsiek. Myocardial phosphocreatine-to-ATP ratio is a predictor of mortality in patients with dilated cardiomyopathy. *Circulation* **1997**:*96*(7): 2190–2196.

[12] A. T. Turer, C. R. Malloy, C. B. Newgard, and M. V. Podgoreanu. Energetics and metabolism in the failing heart: important but poorly understood. *Current opinion in clinical nutrition and metabolic care* **2010**:*13*(4): 458–465.

[13] W. C. Stanley, E. R. Dabkowski, R. F. Ribeiro, and K. A. O'Connell. Dietary Fat and Heart Failure: Moving From Lipotoxicity to Lipoprotection. *Circulation research* **2012**:*110*(5): 764–776.

[14] S. Neubauer, M. Horn, A. Naumann, R. Tian, K. Hu, M. Laser, J. Friedrich, P. Gaudron, K. Schnackerz, and J. S. Ingwall. Impairment of energy metabolism in intact residual myocardium of rat hearts with chronic myocardial infarction. *The Journal of clinical investigation* **1995**:*95*(3): 1092–1100.

[15] J. S. Ingwall. Energy metabolism in heart failure and remodelling. *Cardiovascular research* **2009**:*81*(3): 412–419.

[16] W. C. Stanley, G. D. Lopaschuk, J. L. Hall, and J. G. McCormack. Regulation of myocardial carbohydrate metabolism under normal and ischaemic conditions.

Potential for pharmacological interventions. *Cardiovascular research* **1997**:*33*(2): 243–257.

[17] H. Taegtmeyer and K. Ballal. No low-fat diet for the failing heart? *Circulation* **2006**:*114*(20): 2092–2093.

[18] B. E. Rupert, J. L. Segar, B. C. Schutte, and T. D. Scholz. Metabolic Adaptation of the Hypertrophied Heart: Role of the Malate/Aspartate and α -Glycerophosphate Shuttles. *Journal of Molecular and Cellular Cardiology* **2000**:*32*(12): 2287–2297.

[19] J. C. Chatham and M. E. Young. Metabolic Remodeling in the Hypertrophic Heart: Fuel for Thought. *Circulation research* **2012**:*111*(6): 666–668.

[20] R. D. Evans and L. C. Heather. Metabolic pathways and abnormalities. *Surgery* **2016**:pages 1–7.

[21] J. S. Jaswal, W. Keung, W. Wang, J. R. Ussher, and G. D. Lopaschuk. Targeting fatty acid and carbohydrate oxidation — A novel therapeutic intervention in the ischemic and failing heart, **2011**.

[22] J. R. Ussher and G. D. Lopaschuk. Targeting malonyl CoA inhibition of mitochondrial fatty acid uptake as an approach to treat cardiac ischemia/reperfusion. *Basic research in cardiology* **2009**:*104*(2): 203–210.

[23] P. J. Randle. Metabolic fuel selection: general integration at the whole-body level. *The Proceedings of the Nutrition Society* **1995**:*54*(1): 317–327.

[24] D. Granner and S. Pilkis. The genes of hepatic glucose metabolism. *Journal of Biological Chemistry* **1990**:*265*: 10173–10176.

[25] H. G. Hers and L. Nue. Gluconeogenesis and Related Aspects of Glycolysis, **1983**.

[26] L. Hue and M. H. Rider. Role of fructose 2,6-bisphosphate in the control of glycolysis in mammalian tissues. *Biochemical Journal* **1987**:*245*(2): 313.

[27] E. Van Schaftingen. Glycolysis revisited. *Diabetologia* **1993**:*36*: 581–588.

[28] R. T. Watson and P. J. E. Intracellular organization of insulin signaling and GLUT4 translocation. . *Recent Progress in Hormone Research* **2001**:(56): 175–193.

[29] G. D. Aquaro and L. Menichetti. Hyperpolarized 13C-Magnetic Resonance Spectroscopy: Are We Ready for Metabolic Imaging? *Circulation: Cardiovascular Imaging* **2014**:*7*(6): 854–856.

[30] K. Golman. Real-time metabolic imaging. *Proceedings of the National Academy of Sciences* **2006**:*103*(30): 11270–11275.

[31] L. R. Gray, S. C. Tompkins, and E. B. Taylor. Regulation of pyruvate metabolism and human disease. *Cellular and Molecular Life Sciences* **2014**:*71*: 2577–2604.

[32] P. Felig. Amino Acid Metabolism in Man. *Annual Review of Biochemistry* **1975**: pages 933–955.

[33] R. H. Cooper, P. J. Randle, and R. M. Denton. Stimulation of phosphorylation and inactivation of pyruvate dehydrogenase by physiological inhibitors of the pyruvate dehydrogenase reaction. *Nature* **1975**:*257*(5529): 808–809.

[34] K. T. Chambers, T. C. Leone, N. Sambandam, A. Kovacs, C. S. Wagg, G. D. Lopaschuk, B. N. Finck, and D. P. Kelly. Chronic inhibition of pyruvate dehydrogenase in heart triggers an adaptive metabolic response. *Journal of Biological Chemistry* **2011**:*286*(13): 11155–11162.

[35] A. L. Kerbey, P. J. Randle, R. H. Cooper, S. Whitehouse, H. T. Pask, and R. M. Denton. Regulation of pyruvate dehydrogenase in rat heart. Mechanism of regulation of proportions of dephosphorylated and phosphorylated enzyme by oxidation of fatty acids and ketone bodies and of effects of diabetes: role of coenzyme A, acetyl-coenzyme A and reduced and oxidized nicotinamide-adenine dinucleotide. *The Biochemical journal* **1976**:*154*(2): 327–348.

[36] B. Glancy and R. S. Balaban. Role of mitochondrial Ca2+ in the regulation of cellular energetics. *Biochemistry* **2012**:*51*(14): 2959–2973.

[37] P. C. Hinkle. P/O ratios of mitochondrial oxidative phosphorylation. *Biochimica et Biophysica Acta (BBA) - Bioenergetics* **2005**:*1706*(1-2): 1–11.

[38] G. D. Lopaschuk, D. D. Belke, J. Gamble, T. Itoi, and B. O. Schonekess. Regulation of fatty acid oxidation in the mammalian heart in health and disease. *Biochimica et biophysica acta* **1994**:*1213*(3): 263–276.

[39] D. P. Y. Koonen, J. F. C. Glatz, A. Bonen, and J. J. F. P. Luiken. Long-chain fatty acid uptake and FAT/CD36 translocation in heart and skeletal muscle. *Biochimica et Biophysica Acta (BBA) - Molecular and Cell Biology of Lipids* **2005**:*1736*(3): 163–180.

[40] M. S. R. Murthy and S. V. Pande. Malonyl-CoA binding site and the overt carnitine palmitoyltransferase activity reside on the opposite sides of the outer mitochondrial membrane, **1987**.

[41] J. L. Flanagan, P. A. Simmons, J. Vehige, M. D. P. Willcox, and Q. Garrett. Role of carnitine in disease. *Nutrition & Metabolism* **2010**:*7*: 30.

[42] M. F. Allard, B. O. Schonekess, S. L. Henning, D. R. English, and G. D. Lopaschuk. Contribution of oxidative metabolism and glycolysis to ATP production in hypertrophied hearts. *American Journal of Physiology – Legacy Content* **1994**:*267*(2 Pt 2): H742–50.

[43] S. J. Wakil and L. A. Abu-Elheiga. Fatty acid metabolism: target for metabolic syndrome. *The Journal of Lipid Research* **2008**:*50*(Supplement): S138–S143.

[44] D. W. Foster. Malonyl-CoA: the regulator of fatty acid synthesis and oxidation. *The Journal of clinical investigation* **2012**:*122*(6): 1958.

[45] L. A. Witters, T. D. Watts, D. L. Daniels, and J. L. Evans. Insulin stimulates the dephosphorylation and activation of acetyl-CoA carboxylase. *Proceedings of the National Academy of Sciences of the United States of America* **1988**:*85*(15): 5473.

[46] L. Hue and H. Taegtmeyer. The Randle cycle revisited: a new head for an old hat. *AJP: Endocrinology and Metabolism* **2009**:*297*(3): E578–E591.

[47] W. Nadruz. Myocardial remodeling in hypertension **2014**:*29*(1): 1–6.

[48] J. Heineke and J. D. Molkentin. Regulation of cardiac hypertrophy by intracellular signalling pathways. *Nature reviews. Molecular cell biology* **2006**:*7*(8): 589–600.

[49] E. D. Abel and T. Doenst. Mitochondrial adaptations to physiological vs. pathological cardiac hypertrophy. *Cardiovascular research* **2011**:*90*(2): 234–242.

[50] A.-M. L. Seymour, L. Giles, V. Ball, J. J. Miller, K. Clarke, C. A. Carr, and D. J. Tyler. In vivo assessment of cardiac metabolism and function in the abdominal aortic banding model of compensated cardiac hypertrophy. *Cardiovascular research* **2015**:*106*(2): 249–260.

[51] T. Doenst, T. D. Nguyen, and E. D. Abel. Cardiac Metabolism in Heart Failure. *Circulation research* **2013**:*113*: 709–724.

[52] T. Doenst, G. Pytel, A. Schrepper, P. Amorim, G. Farber, Y. Shingu, F. W. Mohr, and M. Schwarzer. Decreased rates of substrate oxidation ex vivo predict the onset of heart failure and contractile dysfunction in rats with pressure overload. *Cardiovascular research* **2010**:*86*(3): 461–470.

[53] S. R. Houser, K. B. Margulies, A. M. Murphy, F. G. Spinale, G. S. Francis, S. D. Prabhu, H. A. Rockman, D. A. Kass, J. D. Molkentin, M. A. Sussman, W. J. Koch, C. o. C. C. on behalf of the American Heart Association Council on Basic Cardiovascular Sciences, C. o. F. Genomics, and T. Biology. Animal Models of Heart Failure: A Scientific Statement From the American Heart Association. *Circulation research* **2012**:*111*(1): 131–150.

[54] R. O. Pereira, A. R. Wende, C. Olsen, J. Soto, T. Rawlings, Y. Zhu, C. Riehle, and E. D. Abel. GLUT1 deficiency in cardiomyocytes does not accelerate the transition from compensated hypertrophy to heart failure. *Journal of Molecular and Cellular Cardiology* **2014**:*72*(C): 95–103.

[55] T. L. Broderick, H. A. Quinney, and G. D. Lopaschuk. Carnitine stimulation of glucose oxidation in the fatty acid perfused isolated working rat heart. *The Journal of biological chemistry* **1992**:*267*: 3758–3763.

[56] M. A. Schroeder, H. J. Atherton, M. S. Dodd, P. Lee, L. E. Cochlin, G. K. Radda, K. Clarke, and D. J. Tyler. The Cycling of Acetyl-Coenzyme A Through Acetylcarnitine Buffers Cardiac Substrate Supply: A Hyperpolarized 13C Magnetic Resonance Study. *Circulation: Cardiovascular Imaging* **2012**:*5*(2): 201–209.

[57] B. O. Schonekess, M. F. Allard, and G. D. Lopaschuk. Propionyl L-carnitine improvement of hypertrophied heart function is accompanied by an increase in carbohydrate oxidation. *Circulation research* **1995**:*77*(4): 726–734.

[58] J. Heineke and J. D. Molkentin. Regulation of cardiac hypertrophy by intracellular signalling pathways. *Nature reviews. Molecular cell biology* **2006**:*7*(8): 589–600.

[59] M. Luo and M. E. Anderson. Mechanisms of Altered Ca2+ Handling in Heart Failure. *Circulation Research* **2013**:*113*: 690–708.

[60] A. G. Dawson. Oxidation of cytosolic NADH formed during aerobic metabolism in mammalian cells. *Trends in Biochemical Sciences* **1979**:*4*(8): 171–176.

[61] E. D. Abel, H. C. Kaulbach, R. Tian, J. C. A. Hopkins, J. Duffy, T. Doetschman, T. Minnemann, M.-E. Boers, E. Hadro, C. Oberste-Berghaus, W. Quist, B. B. Lowell, J. S. Ingwall, and B. B. Kahn. Cardiac hypertrophy with preserved contractile function after selective deletion of GLUT4 from the heart. *Journal of Clinical Investigation* **1999**:*104*(12): 1703–1714.

[62] P. Razeghi, M. E. Young, J. L. Alcorn, C. S. Moravec, O. H. Frazier, and H. Taegtmeyer. Metabolic gene expression in fetal and failing human heart. *Circulation* **2001**:*104*(24): 2923–2931.

[63] G. Y. Lee, N. H. Kim, Z.-S. Zhao, B. S. Cha, and Y. S. Kim. Peroxisomal-proliferator-activated receptor alpha activates transcription of the rat hepatic

malonyl-CoA decarboxylase gene: a key regulation of malonyl-CoA level. *Biochemical Journal* **2004**:*378*(3): 983–990.

[64] A. Akki, K. Smith, and A.-M. L. Seymour. Compensated cardiac hypertrophy is characterised by a decline in palmitate oxidation. *Molecular and cellular biochemistry* **2008**:*311*(1-2): 215–224.

[65] H. Degens, K. F. J. de Brouwer, A. J. Gilde, M. Lindhout, P. H. M. Willemsen, B. J. Janssen, G. J. van der Vusse, and M. van Bilsen. Cardiac fatty acid metabolism is preserved in the compensated hypertrophic rat heart. *Basic research in cardiology* **2005**:*101*(1): 17–26.

[66] D. B. Plewes and W. Kucharczyk. Physics of MRI: A Primer. *Journal of Magnetic Resonance Imaging* **2012**:*35*: 1038–1054.

[67] J. C. Chatham and S. J. Blackband. Nuclear Magnetic Resonance Spectroscopy and Imaging in Animal Research. *Journal of the Institute of Laboratory Animal Resources* **2001**:*43*: 189–208.

[68] J. Francis, M. D. Robson, and D. J. Tyler. Chapter 1 Understanding Cardiovascular Magnetic Resonance. In S. G. Myerson, J. Francis, and S. Neubauer, editors, *Cardiovascular Magnetic Resonance* (The Oxford University Press), **2010**:.

[69] D. J. Tyler, C. A. Lygate, J. E. Schneider, P. J. Cassidy, S. Neubauer, and K. Clarke. CINE-MR imaging of the normal and infarcted rat heart using an 11.7 T vertical bore MR system. *Journal of cardiovascular magnetic resonance : official journal of the Society for Cardiovascular Magnetic Resonance* **2006**:*8*(2): 327–333.

[70] J. E. Schneider, F. Wiesmann, C. A. Lygate, and S. Neubauer. How to perform an accurate assessment of cardiac function in mice using high-resolution magnetic resonance imaging. *Journal of cardiovascular magnetic resonance : official journal of the Society for Cardiovascular Magnetic Resonance* **2006**:*8*(5): 693–701.

[71] J. H. Ardenkjaer-Larsen, C. Laustsen, S. Bowen, and R. Rizi. Hyperpolarized H 2O MR angiography. *Magnetic Resonance in Medicine* **2013**:*71*(1): 50–56.

[72] M. A. Conway, J. Allis, R. Ouwerkerk, T. Niioka, B. Rajagopalan, and G. K. Radda. Detection of low phosphocreatine to ATP ratio in failing hypertrophied human myocardium by 31P magnetic resonance spectroscopy. *The Lancet* **1991**:*338*(8773): 973–976.

[73] C. S. Clendinen, B. Lee-McMullen, C. M. Williams, G. M. Stupp, K. Vandenborne, D. A. Hahn, G. A. Walter, and A. S. Edison. ^{13}C NMR Metabolomics: Applications at Natural Abundance. *Analytical Chemistry* **2014**:*86*: 1942–9250.

[74] J. H. Ardenkjaer-Larsen, B. Fridlund, A. Gram, G. Hansson, L. Hansson, M. H. Lerche, R. Servin, M. Thaning, and K. Golman. Increase in signal-to-noise ratio of >10,000 times in liquid-state NMR. *Proceedings of the National Academy of Sciences* **2003**:*100*(18): 10158–10163.

[75] M. A. Schroeder, K. Clarke, S. Neubauer, and D. J. Tyler. Hyperpolarized magnetic resonance: a novel technique for the in vivo assessment of cardiovascular disease. *Circulation* **2011**:*124*(14): 1580–1594.

[76] D. Mayer, Y.-F. Yen, S. Josan, J. M. Park, A. Pfefferbaum, R. E. Hurd, and D. M. Spielman. Application of hyperpolarized [1-13C]lactate for the in vivo investigation of cardiac metabolism. *NMR in biomedicine* **2012**:*25*(10): 1119–1124.

[77] A. P. Chen, J. Y. C. Lau, R. D. A. Alvares, and C. H. Cunningham. Using [1-13C]lactic acid for hyperpolarized 13C MR cardiac studies. *Magnetic Resonance in Medicine* **2014**:*73*(6): 2087–2093.

[78] D. R. Ball, B. Rowlands, M. S. Dodd, L. Le Page, V. Ball, C. A. Carr, K. Clarke, and D. J. Tyler. Hyperpolarized butyrate: A metabolic probe of short chain fatty acid metabolism in the heart. *Magnetic Resonance in Medicine* **2013**:*71*(5): 1663–1669.

[79] A. Flori, M. Liserani, F. Frijia, G. Giovannetti, V. Lionetti, V. Casieri, V. Positano, G. D. Aquaro, F. A. Recchia, M. F. Santarelli, L. Landini, J. H. Ardenkjaer-Larsen, and L. Menichetti. Real-time cardiac metabolism assessed with hyperpolarized [1-

13C]acetate in a large-animal model. *Contrast Media & Molecular Imaging* **2014**: *10*(3): 194–202.

[80] S. J. Nelson, J. Kurhanewicz, D. B. Vigneron, P. E. Z. Larson, A. L. Harzstark, M. Ferrone, M. van Criekinge, J. W. Chang, R. Bok, I. Park, G. Reed, L. Carvajal, E. J. Small, P. Munster, V. K. Weinberg, J. H. Ardenkjaer-Larsen, A. P. Chen, R. E. Hurd, L. I. Odegardstuen, F. J. Robb, J. Tropp, and J. A. Murray. Metabolic Imaging of Patients with Prostate Cancer Using Hyperpolarized [1-13C]Pyruvate. *Science Translational Medicine* **2013**:*5*(198): 198ra108–198ra108.

[81] D. J. Tyler. Cardiovascular Applications of Hyperpolarized MRI. *Current Cardiovascular Imaging Reports* **2011**:*4*(2): 108.

[82] A. Abragam and M. Goldman. Principles of dynamic nuclear polarisation. *Rep Prog Phys* **1978**:*41*(395): 395.

[83] M. S. Dodd, D. R. Ball, M. A. Schroeder, L. M. Le Page, H. J. Atherton, L. C. Heather, A.-M. Seymour, H. Ashrafian, H. Watkins, K. Clarke, and D. J. Tyler. In vivo alterations in cardiac metabolism and function in the spontaneously hypertensive rat heart. *Cardiovascular research* **2012**:*95*(1): 69–76.

[84] M. A. Schroeder, L. E. Cochlin, L. C. Heather, K. Clarke, G. K. Radda, and D. J. Tyler. In vivo assessment of pyruvate dehydrogenase flux in the heart using hyperpolarized carbon-13 magnetic resonance. *Proceedings of the National Academy of Sciences of the United States of America* **2008**:*105*(33): 12051–12056.

[85] M. S. Dodd, V. Ball, R. Bray, H. Ashrafian, H. Watkins, K. Clarke, and D. J. Tyler. In vivo mouse cardiac hyperpolarized magnetic resonance spectroscopy. *Journal of Cardiovascular Magnetic Resonance* **2013**:*15*: 19.

[86] A. Z. Lau, A. P. Chen, J. Barry, J. J. Graham, W. Dominguez-Viqueira, N. R. Ghugre, G. A. Wright, and C. H. Cunningham. Reproducibility study for free-breathing measurements of pyruvate metabolism using hyperpolarized 13C in the heart. *Magnetic Resonance in Medicine* **2013**:*69*(4): spcone–spcone.

[87] S. Obrzut, N. Jamshidi, A. Karimi, U. Birgersdotter-Green, and C. Hoh. Imaging and Modeling of Myocardial Metabolism. *Journal of Cardiovascular Translational Research* **2010**:*3*(4): 384–396.

[88] M. A. Schroeder, H. J. Atherton, D. R. Ball, M. A. Cole, L. C. Heather, J. L. Griffin, K. Clarke, G. K. Radda, and D. J. Tyler. Real-time assessment of Krebs cycle metabolism using hyperpolarized 13C magnetic resonance spectroscopy. *The FASEB Journal* **2009**:*23*(8): 2529–2538.

[89] T. B. Rodrigues, E. M. Serrao, B. W. C. Kennedy, D.-E. Hu, M. I. Kettunen, and K. M. Brindle. Magnetic resonance imaging of tumor glycolysis using hyperpolarized 13C-labeled glucose. *Nature medicine* **2013**:*20*(1): 93–97.

[90] K. N. Timm, J. Hartl, M. A. Keller, D.-E. Hu, M. I. Kettunen, T. B. Rodrigues, M. Ralser, and K. M. Brindle. Hyperpolarized [U- 2H, U- 13C]Glucose reports on glycolytic and pentose phosphate pathway activity in EL4 tumors and glycolytic activity in yeast cells. *Magnetic Resonance in Medicine* **2014**:*74*(6): 1543–1547.

[91] H. J. Atherton, M. S. Dodd, L. C. Heather, M. A. Schroeder, J. L. Griffin, G. K. Radda, K. Clarke, and D. J. Tyler. Role of pyruvate dehydrogenase inhibition in the development of hypertrophy in the hyperthyroid rat heart: a combined magnetic resonance imaging and hyperpolarized magnetic resonance spectroscopy study. *Circulation* **2011**:*123*(22): 2552–2561.

[92] O. J. Rider and D. J. Tyler. Clinical Implications of Cardiac Hyperpolarized Magnetic Resonance Imaging. *Journal of Cardiovascular Magnetic Resonance* **2013**: *15*(1): 93.

[93] S. Y. Boateng, A. M. Seymour, N. S. Bhutta, M. J. Dunn, M. H. Yacoub, and K. R. Boheler. Sub-antihypertensive doses of ramipril normalize sarcoplasmic reticulum calcium ATPase expression and function following cardiac hypertrophy in rats. . *J Mol Cell Cardiol* **1998**:*20*(12): 2683–2694.

[94] D. J. Tyler, L. E. Hudsmith, K. Clarke, S. Neubauer, and M. D. Robson. A comparison of cardiac (31)P MRS at 1.5 and 3 T. *NMR in biomedicine* **2008**:*21*(8): 793–798.

[95] A. Naressi, C. Couturier, I. Castang, R. de Beer, and D. Graveron-Demilly. Java-based graphical user interface for MRUI, a software package for quantitation of in vivo/medical magnetic resonance spectroscopy signals. *Computers in Biology and Medicine* **2001**:*31*(4): 269–286.

[96] M. L. Zierhut, Y.-F. Yen, A. P. Chen, R. Bok, M. J. Albers, V. Zhang, J. Tropp, I. Park, D. B. Vigneron, J. Kurhanewicz, R. E. Hurd, and S. J. Nelson. Kinetic modeling of hyperpolarized 13C1-pyruvate metabolism in normal rats and TRAMP mice. *Journal of magnetic resonance (San Diego, Calif. : 1997)* **2010**:*202*(1): 85–92.

[97] H. J. Atherton, M. A. Schroeder, M. S. Dodd, L. C. Heather, E. E. Carter, L. E. Cochlin, S. Nagel, N. R. Sibson, G. K. Radda, K. Clarke, and D. J. Tyler. Validation of the in vivo assessment of pyruvate dehydrogenase activity using hyperpolarised 13C MRS. *NMR in biomedicine* **2011**:*24*(2): 201–208.

[98] S. W. Rasband. Image J, **2016**. URL `http://imagej.nih.gov/ij/`.

[99] T. Unger, M. Moursi, D. Ganten, K. Hermann, and R. E. Lang. Antihypertensive action of the converting enzyme inhibitor perindopril (S9490-3) in spontaneously hypertensive rats: comparison with enalapril (MK421) and ramipril (Hoe298) . *J Cardiovasc Pharmacol* **1986**:*8*(2): 276–285.

[100] G. D. Lopaschuk and R. L. Barr. Measurements of fatty acid and carbohydrate metabolism in te isolated working rat heart. *Molecular and cellular biochemistry* **1997**:*172*(1/2): 137–147.

[101] R. D. Patten and M. R. Hall-Porter. Small Animal Models of Heart Failure: Development of Novel Therapies, Past and Present. *Circulation. Heart failure* **2009**: *2*(2): 138–144.

[102] S. E. Litwin, S. E. Katz, E. O. Weinberg, B. H. Lorell, G. P. Aurigemma, and P. S. Douglas. Serial Echocardiographic-Doppler Assessment of Left Ventricular Geometry and Function in Rats With Pressure-Overload Hypertrophy . *Circulation* **1995**:*91*(10): 2642–2654.

[103] S. Boateng, A.-M. Seymour, M. Dunn, M. Yacoub, and K. Boheler. Inhibition of Endogenous Cardiac Phosphatase Activity and Measurement of Sarcoplasmic Reticulum Calcium Uptake: A Possible Role of Phospholamban Phosphorylation in the Hypertrophied Myocardium. *Biochemical and Biophysical Research Communications* **1997**:*239*(3): 701–705.

[104] B. K. Kundu, M. Zhong, S. Sen, G. Davogustto, S. R. Keller, and H. Taegtmeyer. Remodeling of Glucose Metabolism Precedes Pressure Overload-Induced Left Ventricular Hypertrophy: Review of a Hypothesis. *Cardiology* **2015**:*130*(4): 211–220.

[105] M. I. Miyamoto, F. del Monte, U. Schmidt, T. S. DiSalvo, Z. B. Kang, T. Matsui, J. L. Guerrero, J. K. Gwathmey, A. Rosenzweig, and R. J. Hajjar. Adenoviral gene transfer of SERCA2a improves left-ventricular function in aortic-banded rats in transition to heart failure. *Proceedings of the National Academy of Sciences* **2000**: *97*(2): 793–798.

[106] M. Arai, N. R. Alpert, D. H. MacLennan, P. Barton, and M. Periasamy. Alterations in sarcoplasmic reticulum gene expression in human heart failure. A possible mechanism for alterations in systolic and diastolic properties of the failing myocardium. *Circulation research* **1993**:*72*(2): 463–469.

[107] N. Sambandam PhD, G. D. Lopaschuk PhD, R. W. Brownsey PhD, and M. F. Allard BSc MD. Energy Metabolism in the Hypertrophied Heart - Springer. *Heart Failure Reviews* **2002**:*7*(2): 161–173.

[108] L. Liu, W. Wang, X. Meng, J. Gao, H. Wu, P. Wang, W. Wu, L. Wang, L. Ma, and W. Zhang. Left ventricular hypertrophy induced by abdominal aortic banding and

its prevention by angiotensin receptor blocker telmisartan—a proteomic analysis **2010**:*66*(4): 329–338.

[109] M. J. Cunningham, C. S. Apstein, E. O. Weinberg, W. M. Vogel, and B. H. Lorell. Influence of glucose and insulin on the exaggerated diastolic and systolic dysfunction of hypertrophied rat hearts during hypoxia. *Circulation research* **1990**:*66*(2): 406–415.

[110] M. J. Sopel, N. L. Rosin, T. D. Lee, and J.-F. Légaré. Myocardial fibrosis in response to Angiotensin II is preceded by the recruitment of mesenchymal progenitor cells. *Laboratory Investigation* **2010**:*91*(4): 565–578.

[111] S. Whitehouse and P. J. Randle. Activation of pyruvate dehydrogenase in perfused rat heart by dichloroacetate (Short Communication). *The Biochemical journal* **1973**:*134*: 651–653.

[112] R. B. Wambolt, G. D. Lopaschuk, R. W. Brownsey, and M. F. Allard. Dichloroacetate improves postischemic function of hypertrophied rat hearts. *Journal of the American College of Cardiology* **2000**:*36*(4): 1378–1385.

[113] P. W. Stacpoole, N. V. Nagaraja, and A. D. Hutson. Efficacy of Dichloroacetate as a Lactate-Lowering Drug. *The Journal of Clinical Pharmacology* **2003**:*43*(7): 683–691.

[114] P. W. Stacpoole, A. C. Lorenz, R. G. Thomas, and E. M. Harman. Dichloroacetate in the treatment of lactic acidosis. - PubMed - NCBI. *Ann Intern Med* **1988**:*108*(1): 58–63.

[115] P. W. Stacpoole, G. W. Moore, and D. M. Kornhauser. Metabolic Effects of Dichloroacetate in Patients with Diabetes Mellitus and Hyperlipoproteinemia. *The New England journal of medicine* **1978**:*298*(10): 526–530.

[116] G. W. Moore, L. L. Swift, D. Rabinowitz, J. A. Crofford, J. A. Oates, and P. W. Stacpoole. Reduction of serum cholesterol in two patients with homozygous familial hypercholesterolemia by dichloroacetate **1979**:*33*: 285–93.

[117] D. W. Crabb, E. A. Yount, and R. A. Harris. The metabolic effects of dichloroacetate. *Metabolism* **1981**:*30*(10): 1024–1039.

[118] S. Bonnet, S. L. Archer, J. Allalunis-Turner, A. Haromy, C. Beaulieu, R. Thompson, C. T. Lee, G. D. Lopaschuk, L. Puttagunta, S. Bonnet, G. Harry, K. Hashimoto, C. J. Porter, M. A. Andrade, B. Thebaud, and E. D. Michelakis. A Mitochondria-K+ Channel Axis Is Suppressed in Cancer and Its Normalization Promotes Apoptosis and Inhibits Cancer Growth. *Cancer Cell* **2007**:*11*(1): 37–51.

[119] S. Whitehouse, R. H. Cooper, and P. J. Randle. Mechanism of activation of pyruvate dehydrogenase by dichloroacetate and other halogenated carboxylic acids. *The Biochemical journal* **1974**:*141*(3): 761–774.

[120] P. W. Stacpoole. The pharmacology of dichloroacetate. *Metabolism: clinical and experimental* **1989**:*38*(11): 1124–1144.

[121] M. Kato, J. Li, J. L. Chuang, and D. T. Chuang. Distinct Structural Mechanisms for Inhibition of Pyruvate Dehydrogenase Kinase Isoforms by AZD7545, Dichloroacetate, and Radicicol. *Structure* **2007**:*15*(8): 992.

[122] M. M. Bowker-Kinley, W. I. Davis, P. Wu, R. A. Harris, and K. M. Popov. Evidence for existence of tissue-specific regulation of the mammalian pyruvate dehydrogenase complex. *The Biochemical journal* **1998**:*329 (Pt 1)*: 191–196.

[123] T. L and V. Adam-Vizi. Alpha-ketoglutarate dehydrogenase: a target and generator of oxidative stress. *Philosophical Transactions of the Royal Society B: Biological Sciences* **2005**:*360*(1464): 2335.

[124] F. Demaugre, C. Cepanec, and J.-P. Leroux. Characterization of oxalate as a catabolite of dichloroacetate responsible for the inhibition of gluconeogenesis and pyruvate carboxylation in rat liver cells. *Biochemical and Biophysical Research Communications* **1978**:*85*(3): 1180–1185.

[125] M. L. Pratt and T. E. Roche. Mechanism of pyruvate inhibition of kidney pyruvate dehydrogenasea kinase and synergistic inhibition by pyruvate and ADP. *Journal of Biological Chemistry* **1979**:*254*(15): 7191–7196.

[126] O. B. Evans and P. W. Stacpoole. Prolonged hypolactatemia and increased total pyruvate dehydrogenase activity by dichloroacetate. *Biochemical Pharmacology* **1982**:*31*(7): 1295–1300.

[127] J. P. Backshear, A. P. Holloway, and G. K. Alberti. Metabolic interactions of dichloroacetate and insulin in experimental diabetic ketoacidosis. *Biochemical Journal* **1975**:*146*(2): 447.

[128] P. W. Stacpoole and Y. J. Greene. Dichloroacetate. *Diabetes Care* **1992**:*6*: 1038–1054.

[129] L. K Trofimova, W. L Araujo, A. A Strokina, A. R Fernie, L. Bettendorff, and V. I Bunik. Consequences of the α-Ketoglutarate Dehydrogenase Inhibition for Neuronal Metabolism and Survival: Implications for Neurodegenerative Diseases. *Current Medicinal Chemistry* **2012**:*19*(34): 5895–5906.

[130] P. W. Stacpoole, H. J. J. Harwood, D. F. Cameron, S. H. Curry, D. A. Samuelson, P. E. Cornwell, and H. E. Sauberlich. Chronic toxicity of dichloroacetate: possible relation to thiamine. *Fundamental and Applied Physiology* **1990**:*14*: 327–37.

[131] M. Lorini and M. Ciman. Hypoglycaemic action of DIISOpropylammonium salts in experimental diabetes. *Biochemical Pharmacology* **1962**:*11*(9): 823–827.

[132] A. S. Clark, W. E. Mitch, M. N. Goodman, J. M. Fagan, M. A. Goheer, and R. T. Curnow. Dichloroacetate inhibits glycolysis and augments insulin-stimulated glycogen synthesis in rat muscle. *The Journal of clinical investigation* **1987**:*79*(2): 588–594.

[133] F. Sobrino, A. Gualberto, and J. Gonzalez-Rivero. Regulation of fructose-2,6-bisphosphate and glycogen synthesis by dichloroacetate and phenazine methosulphate in rat adipose tissue. *Biochem Int* **1986**:*12*(5): 767–774.

[134] J. W. Anderson, D. Karounos, T. Yoneyama, and J. W. Hollingsworth. Dichloroacetate-induced changes in liver of normal and diabetic rats. *Proceedings of the Society for Experimental Biology and Medicine. Society for Experimental Biology and Medicine (New York, N.Y.)* **1975**:*149*(3): 814–821.

[135] P. W. Stacpoole, H. J. Harwood, Jr, and C. E. Varnado. Regulation of rat liver hydroxymethylglutaryl coenzyme A reductase by a new class of noncompetitive inhibitors. Effects of dichloroacetate and related carboxylic acids on enzyme activity. *The Journal of clinical investigation* **1983**:*72*(5): 1575–1585.

[136] L. Laffel. Ketone bodies: a review of physiology, pathophysiology and application of monitoring to diabetes. *Diabetes Metab Res Rev* **1999**:*15*(6): 412–426.

[137] A. S. Clark, W. E. Mitch, M. N. Goodman, J. M. Fagan, M. A. Goheer, and R. T. Curnow. Dichloroacetate inhibits glycolysis and augments insulin-stimulated glycogen synthesis in rat muscle. *The Journal of clinical investigation* **1987**:*79*(2): 588–594.

[138] S. C. Kolwicz and R. Tian. Glucose metabolism and cardiac hypertrophy. *Cardiovascular research* **2011**:*90*(2): 194–201.

[139] H. Taegtmeyer. Cardiac Metabolism as a Target for the Treatment of Heart Failure. *Circulation* **2004**:*110*(8): 894–896.

[140] L. H. Opie and J. Knuuti. The Adrenergic-Fatty Acid Load in Heart Failure. *Journal of the American College of Cardiology* **2009**:*54*(18): 1637–1646.

[141] L. M. Le Page, O. J. Rider, A. J. Lewis, V. Ball, K. Clarke, E. Johansson, C. A. Carr, L. C. Heather, and D. J. Tyler. Increasing Pyruvate Dehydrogenase Flux as a Treatment for Diabetic Cardiomyopathy: A Combined 13C Hyperpolarized Magnetic Resonance and Echocardiography Study. *Diabetes* **2015**:*64*(8): 2735–2743.

[142] H. J. Atherton, M. S. Dodd, L. C. Heather, M. A. Schroeder, J. L. Griffin, G. K. Radda, K. Clarke, and D. J. Tyler. Role of Pyruvate Dehydrogenase Inhibition in the

Development of Hypertrophy in the Hyperthyroid Rat Heart: A Combined Magnetic Resonance Imaging and Hyperpolarized Magnetic Resonance Spectroscopy Study. *Circulation* **2011**:*123*(22): 2552–2561.

[143] W. Linz, P. A. Martorna, and B. A. Scholkens. Local inhibition of bradykinin degradation in ischemic hearts. *J Cardiovasc Pharmacol* **1990**:*6*: S99–109.

[144] S. Atlas. The renin-angiotensin aldosterone system: pathophysiological role and pharmacologic inhibition. . *Journal of Managed Care Pharmacy* **2007**:*13*(8): S9–S20.

[145] M. M. Ibrahim. RAS inhibition in hypertension. *Journal of Human Hypertension* **2006**:*20*: 101–8.

[146] M. Paul, A. P. Mehr, and R. Kreutz. Physiology of local renin-angiotensin systems. . *Physiological reviews* **2006**:*86*(3): 747–803.

[147] P. Pagliaro and C. Penna. Rethinking the Renin-Angiotensin System and Its Role in Cardiovacular Regulation. *Cardiovascular Drugs and Therapy* **2005**:*19*: 77–87.

[148] M. Ruzicka, V. Skarda, and F. H. H. Leenen. Effects of ACE Inhibitors on Circulating Versus Cardiac Angiotensin II in Volume OverloadInduced Cardiac Hypertrophy in Rats. *Circulation* **1995**:*92*(12): 3568–3573.

[149] M. A. Crackower, R. Sarao, G. Y. Oudit, C. Yagil, I. Kozieradzki, S. E. Scanga, A. J. Oliveira-dos Santos, J. da Costa, L. Zhang, Y. Pei, J. Scholey, C. M. Ferrario, A. S. Manoukian, M. C. Chappell, P. H. Backx, Y. Yagil, and J. M. Penninger. Angiotensin-converting enzyme 2 is an essential regulator of heart function. *Nature* **2002**:*417*(6891): 822–828.

[150] S. Y. Boateng, R. U. Naqvi, M. U. Koban, M. H. Yacoub, K. T. MacLeod, and K. R. Boheler. Low-dose ramipril treatment improves relaxation and calcium cycling after established cardiac hypertrophy. *American Journal of Physiology - Heart and Circulatory Physiology* **2001**:*280*(3): H1029–H1038.

[151] W. Linz, B. A. Scholkens, and D. Ganten. Converting enzyme inhibition specifically prevents the development and induces regression of cardiac hypertrophy in rats. . *Clinical and experimental hypertension* **1989**:*7*(11): 1325–1350.

[152] W. Linz, B. A. Scholkens, and Y. F. Han. Beneficial effects of the converting enzyme inhibitor, ramipril, in ischemic rat hearts. . *J Cardiovasc Pharmacol* **1986**:*8*(Suppl 10): S91–9.

[153] Effects of an Angiotensin-Converting–Enzyme Inhibitor, Ramipril, on Cardiovascular Events in High-Risk Patients. *New England Journal of Medicine* **2000**:*342*(3): 145–153.

[154] K. Kohlstedt, R. Busse, and I. Fleming. Signaling via the Angiotensin-Converting Enzyme Enhances the Expression of Cyclooxygenase-2 in Endothelial Cells. *Hypertension* **2004**:*45*(1): 126–132.

[155] W. Linz, J. Schaper, G. Wiemer, U. Albus, and B. A. Scholkens. Ramipril prevents left ventricular hypertrophy with myocardial fibrosis without blood pressure reduction: a one year study in rats. *British Journal of Pharmacology* **1992**:*107*(4): 970.

[156] B. A. Scholkens, W. Linz, and P. A. Martorna. Experimental cardiovascular benefits of angiotensin-converting enzyme inhibitors: beyond blood pressure reduction. . *J Cardiovasc Pharmacol* **1991**:*18*(2): S26–30.

[157] M. Lievre, P. Gueret, C. Gayet, R. Roudaut, M. C. Haugh, S. Delair, and J. P. Boissel. Ramipril-Induced Regression of Left Ventricular Hypertrophy in Treated Hypertensive Individuals. *Hypertension* **1995**:*25*(1): 92–97.

[158] J. C. Hartman, T. M. Wall, T. G. Hullinger, and R. J. Shebuski. Reduction of myocardial infarct size in rabbits by ramiprilat: reversal by the bradykinin antagonist HOE 140. . *J Cardiovasc Pharmacol* **1993**:*21*(6): 996–1003.

[159] J. R. Parratt. Cardioprotection by angiotensin converting enzyme inhibitors - the experimental evidence. *Cardiovascular research* **1994**:*28*(2): 183–189.

[160] G. D. Lopaschuk and W. C. Stanley. Glucose Metabolism in the Ischemic Heart. *Circulation* **1997**:*95*(2): 313–315.

[161] V. Panagia, S. L. Lee, A. Singh, G. N. Pierce, G. Jasmin, and N. S. Dhalla. Impairment of mitochondrial and sarcoplasmic reticular functions during the development of heart failure in cardiomyopathic (UM-X7.1) hamsters. *The Canadian journal of cardiology* **1986**:*2*(4): 236–247.

[162] C. H. Davies, K. Davia, J. G. Bennett, J. R. Pepper, P. A. Poole-Wilson, and S. E. Harding. Reduced Contraction and Altered Frequency Response of Isolated Ventricular Myocytes From Patients With Heart Failure. *Circulation* **1995**:*92*(9): 2540–2549.

[163] D. J. Beuckelmann, M. Nabauer, and E. Erdmann. Intracellular calcium handling in isolated ventricular myocytes from patients with terminal heart failure. *Circulation* **1992**:*85*(3): 1046–1055.

[164] G. Hasenfuss, W. Schillinger, S. E. Lehnart, M. Preuss, B. Pieske, L. S. Maier, J. Prestle, K. Minami, and H. Just. Relationship Between Na+-Ca2+ Exchanger Protein Levels and Diastolic Function of Failing Human Myocardium. *Circulation* **1999**:*99*(5): 641–648.

[165] R. H. Cooper, P. J. Randle, and R. M. Denton. Regulation of heart muscle pyruvate dehydrogenase kinase. *The Biochemical journal* **1974**:*143*(3): 625–641.

[166] A. Akki and A.-M. L. Seymour. Western diet impairs metabolic remodelling and contractile efficiency in cardiac hypertrophy. *Cardiovascular research* **2008**:*81*(3): 610–617.

[167] S. C. Kolwicz and R. Tian. Glucose metabolism and cardiac hypertrophy. *Cardiovascular research* **2011**:*90*(2): 194–201.

[168] S. Atlas. The Renin-Angiotensin Aldosterone System: Pathophysiological Role and Pharmacologic Inhibition **2016**:pages 1–12.

[169] D. J. Stuckey, C. A. Carr, D. Tyler, and K. Clarke. Cine-MRI versus two-dimensional echocardiography to measure in vivo left ventricular function in rat heart. . *NMR in biomedicine* **2008**:*21*(7): 765–772.

[170] H. A. Rockman, R. S. Ross, A. N. Harris, K. U. Knowlton, M. E. Steinhelper, L. J. Field, J. Ross, and K. R. J. Chien. Segregation of atrial-specific and inducible expression of an atrial natriuretic factor transgene in an in vivo murine model of cardiac hypertrophy. *Proceedings of the National Academy of Sciences of the United States of America* **1991**:*88*(18): 8277.

[171] P. Razeghi, M. E. Young, J. Ying, C. Depre, I. P. Uray, J. Kolessar, G. J. Shipley, C. S. Moravec, P. J. Davies, O. H. Frazier, and H. Taegtmeyer. Downregulation of metabolic gene expression in failing human heart before and after mechanical unloading. . *Cardiology* **2002**:*97*(4): 203–209.

[172] M. G. S. J. Sutton and N. Sharpe. Left Ventricular Remodeling After Myocardial Infarction : Pathophysiology and Therapy. *Circulation* **2000**:*101*(25): 2981–2988.

Appendix A

In Vivo Assessment of Cardiac Metabolism and Function in the Abdominal Aortic Banding Model of Compensated Cardiac Hypertrophy

Cardiovascular Research (2015) **106**, 249–260
doi:10.1093/cvr/cvv101

In vivo assessment of cardiac metabolism and function in the abdominal aortic banding model of compensated cardiac hypertrophy

Anne-Marie L. Seymour[1†], Lucia Giles[2†], Vicky Ball[2], Jack J. Miller[2], Kieran Clarke[2], Carolyn A. Carr[2], and Damian J. Tyler[2*]

[1]School of Biological, Biomedical and Environmental Sciences, University of Hull, Hull HU6 7RX, UK; and [2]Department of Physiology, Anatomy and Genetics, University of Oxford, Sherrington Building, Parks Road, Oxford OX1 3PT, UK

Received 8 September 2014; revised 27 February 2015; accepted 2 March 2015; online publish-ahead-of-print 6 March 2015

Time for primary review: 38 days

Aims Left ventricular hypertrophy is an adaptive response of the heart to chronic mechanical overload and can lead to functional deterioration and heart failure. Changes in cardiac energy metabolism are considered as key to the hypertrophic remodelling process. The concurrence of obesity and hypertrophy has been associated with contractile dysfunction, and this work therefore aimed to investigate the *in vivo* structural, functional, and metabolic remodelling that occurs in the hypertrophied heart in the setting of a high-fat, high-sucrose, Western diet (WD).

Methods and results Following induction of cardiac hypertrophy through abdominal aortic banding, male Sprague Dawley rats were exposed to either a standard diet or a WD (containing 45% fat and 16% sucrose) for up to 14 weeks. Cardiac structural and functional characteristics were determined by CINE MRI, and *in vivo* metabolism was investigated using hyperpolarized ^{13}C-labelled pyruvate. Cardiac hypertrophy was observed at all time points, irrespective of dietary manipulation, with no evidence of cardiac dysfunction. Pyruvate dehydrogenase flux was unchanged in the hypertrophied animals at any time point, but increased incorporation of the ^{13}C label into lactate was observed by 9 weeks and maintained at 14 weeks, indicative of enhanced glycolysis.

Conclusion Hypertrophied hearts revealed little evidence of a switch towards increased glucose oxidation but rather an uncoupling of glycolytic metabolism from glucose oxidation. This was maintained under conditions of dietary stress provided by a WD but, at this compensated phase of hypertrophy, did not result in any contractile dysfunction.

Keywords Dynamic nuclear polarization • Cardiac hypertrophy • Metabolic remodelling • Pyruvate dehydrogenase • ^{13}C magnetic resonance spectroscopy

Downloaded from by guest on April 20, 2015

1. Introduction

Heart failure continues to be a major cause of death in the Western World. Despite current therapies, the prognosis is poor and patient care is often costly. Patients with heart failure often have pre-existing hypertension and hypertrophy, recognized as independent risk factors in the development of heart failure.[1] Left ventricular hypertrophy (LVH), the adaptive response of the heart to chronic overload, is characterized by cellular and structural remodelling,[2] which may underpin the transition from compensated hypertrophy to decompensated heart failure. Studies using ^{31}P phosphorus magnetic resonance spectroscopy (MRS) have demonstrated a marked reduction in the energy reserves in the hypertrophied heart, leading to the suggestion that the failing heart is energy depleted.[3] In particular, the hypertrophied heart undergoes significant metabolic remodelling, switching from dependence upon fatty acids for energy provision to reliance on carbohydrates.[4,5] This switch is underpinned by altered expression of key transcription factors including PPARα and PGC1α, which in turn cause decreased expression of the enzymes involved in fatty acid oxidation.[6]

* Corresponding author. Tel: +44 1865 282252; fax: +44 1865 282272, Email: damian.tyler@dpag.ox.ac.uk

† These authors contributed equally to this work.

© The Author 2015. Published by Oxford University Press on behalf of the European Society of Cardiology.
This is an Open Access article distributed under the terms of the Creative Commons Attribution License (http://creativecommons.org/licenses/by/4.0/), which permits unrestricted reuse, distribution, and reproduction in any medium, provided the original work is properly cited.

Obesity is a growing threat to health owing to its association with a number of cardiovascular risk factors including hypertension, insulin resistance, and dyslipidaemia (metabolic syndrome).[7] Exposure of the hypertrophied heart to surplus lipids and nutrients, as occurs in obesity, may result in further dysregulation of metabolism and energy provision.[8,9] Ultimately, the combination of hypertrophy and obesity may accelerate the onset of contractile dysfunction, cell death, and heart failure. Studies to date have generated conflicting data in that high-lipid diets have been both beneficial and deleterious to cardiac function. An extended study using a variety of dietary manipulations including a Western diet (WD), consisting of high saturated lipid and sucrose content, demonstrated the greatest reduction in cardiac power in the WD group, as well as obesity, whereas in the high fat, low carbohydrate group, obesity was comparable, but no reduction in cardiac power occurred.[10] However, the cellular mechanisms that underpin this deterioration in function in the heart confronted by lipid and carbohydrate overload in the setting of hypertrophy and failure are complex and incompletely understood.

Many of the experimental studies on metabolic alterations have used *in vitro* experimentation on isolated hearts, assessing metabolic fluxes with the use of ^{14}C or ^{13}C-labelled substrates.[11–13] The advent of hyperpolarized magnetic resonance (MR) spectroscopy provides a powerful means to enhance the sensitivity of ^{13}C MR investigations. In combination with the rapid dissolution of small ^{13}C-labelled hyperpolarized substrates, this gives a novel method with which to study metabolic flux *in vivo*.[14–16]

The aim of this study was therefore to investigate the *in vivo* structural, functional, and metabolic remodelling that occurs during the time course of cardiac hypertrophic development in the setting of excess nutrient supply. In particular, the impact of a WD on the structure, function, and metabolism of the *in vivo* heart exposed to abdominal aortic banding (AAB) was determined through the use of CINE MRI and hyperpolarized ^{13}C MRS to assess pyruvate dehydrogenase (PDH) flux and incorporation of pyruvate into the tricarboxylic acid (TCA) cycle. This study utilized the relatively mild model of physiological hypertrophy generated by AAB as it allowed us to explore the metabolic alterations that occurred over a period of time as hypertrophy developed. The AAB model was chosen over genetic models like the Spontaneously Hypertensive Rat (SHR), because the SHR has a loss of function mutation in the gene encoding for fatty acid translocase (FAT/CD36), a sarcolemmal fatty acid transporter that is crucial for the transport of long chain fatty acids (LCFA) across the plasma membrane. Such a mutation severely impacts the metabolic phenotype induced by cardiac hypertrophy. The AAB model was also chosen over more severe hypertrophy models, such as the transverse aortic constriction (TAC) model, as they can result in a very rapid onset of overt heart failure, which would have limited our ability to examine the metabolic changes that occur during the highly clinically relevant period of compensated hypertrophy.

2. Methods

[1-^{13}C] and [2-^{13}C]pyruvic acid were obtained from Sigma-Aldrich Company Ltd (Dorset, UK). Male Sprague Dawley rats (Body weight 200–250 g, $n = 48$) were obtained from Harlan UK. All animals were housed on a 12:12-h light–dark cycle and studies were performed between 7 a.m. and 1 p.m., during the early absorptive (fed) state. All investigations conformed to Home Office Guidance on the Operation of the Animals (Scientific Procedures) Act (HMSO) of 1986, to institutional guidelines and to the Directive 2010/63/EU of the European Parliament. A local University ethics review board also approved experiments.

2.1 Induction of cardiac hypertrophy

Cardiac hypertrophy was induced surgically in male Sprague Dawley rats ($n = 24$) via banding of the abdominal aorta as described previously.[11] Anaesthesia was induced using 3% isofluorane in 3 L/min of oxygen and maintained using 2.5% isofluorane per litre O_2. In brief, a laparotomy was performed and the aorta exposed at the level of the renal arteries. A reproducible band was placed using a 0.7 mm OD blunted needle and 3.0 mm suture where the needle was withdrawn leaving a ligature in place. Sham operated animals ($n = 24$) underwent the same procedure but without the ligation.

Animals were allowed to recover and 24–48 h post-surgery; experimental (AAB) and sham animals were divided into two groups, one that received a standard chow diet and the other that received a WD consisting of 45% saturated fat and 16% sucrose (*Table 1*). Animals were studied at 4, 9, and 14 weeks post-surgery using hyperpolarized ^{13}C MR spectroscopy and CINE MRI.

2.2 MR investigations

At 4, 9, and 14 weeks post-surgery, rats received an intravenous injection of either [1-^{13}C]pyruvate together with blood sampling from the saphenous vein or [2-^{13}C]pyruvate together with a CINE MRI investigation to determine cardiac morphology and function. Anaesthesia was induced by 2.5–3% isofluorane in oxygen and nitrous oxide (O_2:N_2O 4:1, total of 2 L/min). The adequacy of anaesthesia was initially assessed based on the loss of the pedal response and was then continuously monitored through the evaluation of the heart and respiration rates. Anaesthesia was maintained by means of 2% isofluorane delivered during the experiment (O_2:N_2O 4:1, total of 2 L/min). A tail vein cannulation for i.v. administration of hyperpolarized solutions was performed before the animals were subsequently placed in a home-built MR animal handling system.[17] The ECG, respiration rate, and body temperature were monitored throughout the experiment, and air heating was provided to maintain the body temperature at 37°C as previously described.[18] A home-built $^{1}H/^{13}C$ butterfly surface coil (loop diameter, 20 mm) was placed over the rat chest, localizing the signal from the heart due to the high local sensitivity of the surface coil and the high metabolic rate of the heart (*Figure 1*). The animal was positioned with the heart at isocentre in a horizontal bore 7 T MR scanner interfaced to a direct-drive console (Varian Inc., Yarnton, UK) and correct positioning was confirmed by the acquisition of an axial proton fast low-angle shot (FLASH) image. An ECG-gated shim was used to reduce the proton line width to ~120 Hz.[16] Animals were allowed to recover fully from anaesthesia for serial MR investigations.

Table 1 Dietary composition of standard and WDs

	Calorie composition (%)	
	Standard chow	WD[a]
Carbohydrates	69	35
Total protein	19	20
Total fat	11	45
Saturated fat	6	16
Monounsaturated fat	4	20
Total polyunsaturated fat	1	8

[a]Contains carbohydrate from sucrose (16%), rice, and starch.

Downloaded from by guest on April 20, 2015

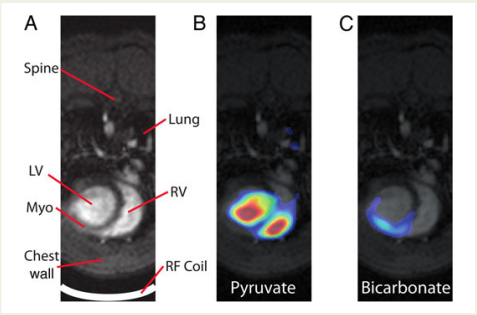


Figure 1 Cardiac hyperpolarized ^{13}C signal localization is achieved via the high local sensitivity of the RF surface coil used and the high metabolic rate of the heart relative to other organs/tissues within the sensitive region of the coil (*A*, LV, left ventricular lumen; RV, right ventricular lumen; myo, myocardial tissue). This figure, acquired with a 3D spectral-spatial, echo planar spectroscopic imaging sequence [matrix: 32 × 32 × 12, field of view: 64 × 64 × 45.5 mm^3, acquired resolution: 2 × 2 × 4 mm^3, echo time (TE): 16.3 ms, repetition time (TR): 1RR interval (≈150 ms); flip angle: 17° pyruvate/61°bicarbonate], demonstrates that the pyruvate signal (*B*) originates primarily from the blood in the chambers of the heart, while the downstream metabolic signals, in this example bicarbonate (*C*), are originating from the front wall of the left ventricle.

2.3 *In vivo* assessment of pyruvate dehydrogenase flux and oxidative metabolism

PDH flux was determined using hyperpolarized [1-^{13}C]pyruvate and incorporation of pyruvate into the TCA cycle evaluated using hyperpolarized [2-^{13}C]pyruvate. Hyperpolarized pyruvate was generated using ~40 mg of either [1-^{13}C]pyruvic acid or [2-^{13}C]pyruvic acid doped with 15 mM trityl radical (OXO63, Oxford Instruments, Abingdon, UK) and 3 μL Dotarem (1:50 dilution, Guerbet, Birmingham, UK) in a prototype polarizer system, with 45 min of microwave irradiation as previously described.[19] The sample was subsequently dissolved in a pressurized and heated alkaline solution, containing 2.4 g/L sodium hydroxide and 100 mg/L EDTA dipotassium salt (Sigma-Aldrich), to yield a solution of 80 mM hyperpolarized sodium [1-^{13}C]pyruvate or [2-^{13}C]pyruvate with a polarization of ~30 or ~20%, respectively, and at physiological temperature and pH.[16]

Immediately following dissolution, 1 mL of the ^{13}C hyperpolarized substrate was injected intravenously into the anaesthetised animal over 10 s. Sixty individual ECG-gated ^{13}C MR pulse-acquire cardiac spectra were acquired over 1 min after injection (repetition time, 1 s; excitation flip angle, 5°; sweep width, 13 593 Hz; acquired points, 2048).[16]

All cardiac ^{13}C spectra were analysed using the AMARES algorithm in the jMRUI software package.[20] Spectra were direct current offset corrected based on the last half of acquired points. For data acquired following the injection of hyperpolarized [1-^{13}C]pyruvate, the peak areas of [1-^{13}C]pyruvate, [1-^{13}C]lactate, [1-^{13}C]alanine, [^{13}C]carbon dioxide ($^{13}CO_2$), and [^{13}C]bicarbonate were quantified at each time point and used as input data for a kinetic model.[21] The kinetic model developed for the analysis of hyperpolarized [1-^{13}C]pyruvate MRS data was based on a model initially developed by Zierhut *et al.*[22] and further developed by Atherton *et al.*[21] The spectra acquired following injection of hyperpolarized [2-^{13}C]pyruvate were summed for the first 30 s following appearance of [2-^{13}C]pyruvate, to increase the sensitivity of measurements because of low signal to noise ratio. The peak areas of [1-^{13}C]acetylcarnitine, [1-^{13}C]citrate, and [5-^{13}C]glutamate were quantified in the summed spectra and normalized to the peak area of [2-^{13}C]pyruvate.

2.4 CINE MRI

Cardiac structure and function were determined *in vivo* by CINE MRI at 4, 9, and 14 weeks post-surgery.[23] A 72 mm quadrature birdcage transmit/receive radio frequency coil was used to obtain MR images (Rapid Biomedical, Rimpar, Germany). Long- and short-axis scout images were acquired so that true short-axis images could be planned using a segmented, ECG-triggered FLASH sequence.[24] CINE-MR images, consisting of 28–35 frames per heart cycle, were acquired in 7–10 contiguous slices in the short-axis orientation covering the entire heart.[18] The imaging parameters were as follows: field of view = 51.2 × 51.2 mm, matrix size = 256 × 256, slice thickness = 1.6 mm, TE/TR = 1.43/4.6 ms, 0.5 ms/17.5° Gaussian RF excitation pulse, and 6 averages. The total experimental time was ~50 min per animal. Heart rate remained stable throughout the procedure. End-diastolic (ED) and end-systolic (ES) frames were selected as those with the largest and smallest cavity volumes, respectively. Epicardial and endocardial borders were outlined using the freehand drawing function of ImageJ (National Institutes of Health, USA). Measurements from all slices were summed to calculate ED volume (EDV), ES volume (ESV), stroke volume (SV = EDV − ESV), ejection fraction (EF = SV/EDV), cardiac output (CO = SV × heart rate), and cardiac index (CO/body weight). LV mass was calculated as myocardial area × slice thickness × myocardial specific gravity (1.05).[18]

2.5 Serum analyses

Blood samples were collected from the saphenous vein at all time points immediately prior to [1-^{13}C]pyruvate hyperpolarization studies. Whole blood was centrifuged to obtain plasma (15 600 g for 10 min at 4°C) and analysed for plasma metabolites [glucose, lactate, triglycerides (TAGs), low-density lipoproteins (LDLs), high-density lipoproteins (HDLs), cholesterol, and β-hydroxybutyrate] using an ABX Pentra 400 (Horiba ABX Diagnostics). At the 14-week time point, plasma insulin levels were assessed on post mortem plasma using an insulin ELISA kit (Mercodia, Sweden).

2.6 Tissue metabolite analyses

After the MR investigations at 14 weeks post-surgery, animals were euthanized with an overdose of isoflurane (5% isoflurane with 2 L/min oxygen), and heart tissue, abdominal fat tissue, and kidneys were harvested, weighed, and, where appropriate, freeze clamped with Wollenberger tongs cooled in liquid nitrogen. Tissues were stored at −80°C until further analysis. Tissues were then ground into a fine powder using a liquid nitrogen cooled pestle and mortar, extracted as appropriate for the assay and analysed as described below.

2.7 Cardiac TAG assay

TAG was extracted from ~25–50 mg of powdered cardiac tissue following mixing and overnight suspension in 8 mL of Folch Solution ($CHCl_3$:MeOH; 2:1) and 2 mL of distilled water. The aqueous phase was subsequently removed leaving the organic layer, which was evaporated to dryness and re-suspended in 1 mL of cold ethanol to form the sample solution. Approximately 100 μL of the sample solution was evaporated to dryness overnight and the sample re-suspended in 20 μL of cold ethanol from which the TAG concentration was measured spectrophotometrically using a Randox triglyceride assay kit (Randox Laboratories Ltd).

2.8 Western blotting

Frozen tissue was crushed and lysis buffer added before tissue was homogenized, a protein assay established the protein concentration of each lysate. The same concentration of protein from each sample was loaded on to 12.5% SDS–PAGE gels and separated by electrophoresis.[25] A primary antibody for PDH kinase 4 (PDK4) was kindly donated by Prof. Mary Sugden

Downloaded from by guest on April 20, 2015

(Queen Mary's, University of London, UK). Even protein loading and transfer were confirmed by Ponceau staining (0.1% w/v in 5% v/v acetic acid, Sigma-Aldrich). Bands were quantified using the UN-SCAN-IT gel software (Silk Scientific, USA) and normalized to a loading control (Cyclophilin B, Abcam). All samples were run in duplicate on separate gels to confirm results.

2.9 Statistical analysis

All data are presented as mean ± SD. Statistical significance of the effects of AAB and diet on the acquired data were assessed using a two-way ANOVA at each individual time point. In cases where the interaction term was significant, the differences were evaluated in more detail by separately analysing the effects of AAB and diet using a Bonferroni corrected, two-sample unpaired *t*-test assuming equal variances. Statistical significance was considered at the $P \leq 0.05$ level.

3. Results

3.1 Structural remodelling

In vivo CINE MRI was used to study the extent of structural remodelling in hearts of animals subjected to AAB over time. *Figure 2* shows representative images of hypertrophied and control hearts in systole and diastole after 14 weeks of exposure to standard chow (*Figure 2A* and *B*) or WD (*Figure 2C* and *D*) with evident enlargement of the ventricle in AAB hearts independent of any dietary modification. Quantitatively, left ventricular mass (LVM) was markedly augmented in the AAB group compared with its respective control by 4 weeks post surgery (17%) and this increase was maintained over 9 (14%) and 14 weeks (14%), irrespective of dietary manipulation (*Figure 3A*). This was further reflected in the hypertrophic index of LVM to body weight ratio (*Figure 3B*), indicating that the hypertrophy occurred primarily as a result of the hypertension induced by aortic banding rather than any effect of the diet.

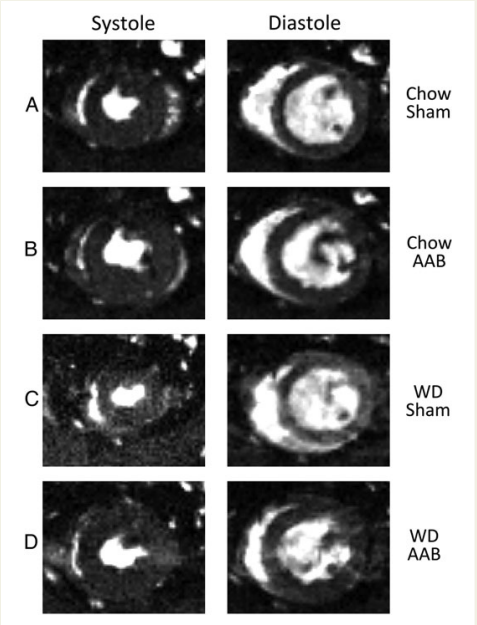


Figure 2 Representative *in vivo* CINE MR images of sham and AAB hearts at 14 weeks post-surgical induction of cardiac hypertrophy during systole and diastole, (*A* and *B*) on standard chow diet, (*C* and *D*) on WD.

In terms of body weight, there was no significant difference between AAB and control animals at 4 or 9 weeks irrespective of diet (*Table 2*). However by 14 weeks, both WD fed groups showed a significantly greater body weight than their standard chow counterparts (WD 480 ± 40 g vs. chow 440 ± 30 g), with signs of increased adiposity evidenced by larger abdominal fat deposits. This weight gain was independent of the hypertrophy present in the AAB group.

Initially systolic and diastolic volumes were enlarged in AAB groups at 4 weeks post induction of hypertrophy (*Figure 3*), which resulted in a reduction in ejection fraction (*Figure 4*). However by 14 weeks, these alterations had resolved, indicating a transition from an initial acute phase of hypertrophic induction to a more compensated stage. End-systolic volumes were reduced in the WD-fed animals at the 4-week time point, resulting in an elevated ejection fraction; however, this also resolved with time and no structural differences were seen between chow and WD-fed animals at 14 weeks (*Figures 3* and *4*).

3.2 Functional remodelling

Functional assessment *in vivo* using MRI permitted the study of individual animals serially over the 14-week time course, which showed no indication of cardiac dysfunction in the AAB groups at any stage as reflected by the cardiac index (*Figure 4*). In addition, no effect of AAB was observed on the stroke volume or cardiac output at any time point (*Figure 4*), suggesting an enlarged yet still compliant heart in the AAB groups. Heart rate remained stable at all stages of hypertrophic development (*Table 2*) and did not differ from the sham groups, and at no stage over the time course of the experiment did the AAB animals show any signs of heart failure (breathlessness or fatigue).

In contrast, a small elevation in cardiac output was observed in both WD fed groups at 4 and 14 weeks compared with standard chow counterparts, with a trend towards increased cardiac output also visible at 9 weeks ($P = 0.07$, *Figure 4*). When normalized to body weight to generate the cardiac index (*Figure 4*), this significant elevation only remained at 4 weeks, suggesting that this was in some way related to the weight gain seen in these animals. In addition, dietary modification had no impact on heart rate (*Table 2*).

3.3 Metabolic remodelling

3.3.1 *In vivo* assessment of PDH flux

PDH flux was determined *in vivo* through incorporation of the hyperpolarized ^{13}C label from [1-^{13}C]pyruvate into bicarbonate as previously demonstrated[21] (*Figure 5*). Rates of ^{13}C label incorporation into bicarbonate in AAB groups at the different time points were not significantly different from their respective controls (*Figure 6A*), implying little effect of AAB on PDH flux *in vivo* and thus glucose oxidation over the time course of hypertrophic development. At all time points however, dietary manipulation resulted in a marked reduction in ^{13}C label incorporation into bicarbonate, indicating that PDH flux was reduced in the WD groups compared with their respective standard chow groups as would be predicted from the Randle cycle.[26]

Label incorporation into alanine was unaffected by either AAB or dietary manipulation (data not shown). However, the rate of ^{13}C label incorporation into lactate was markedly enhanced in AAB

Downloaded from by guest on April 20, 2015

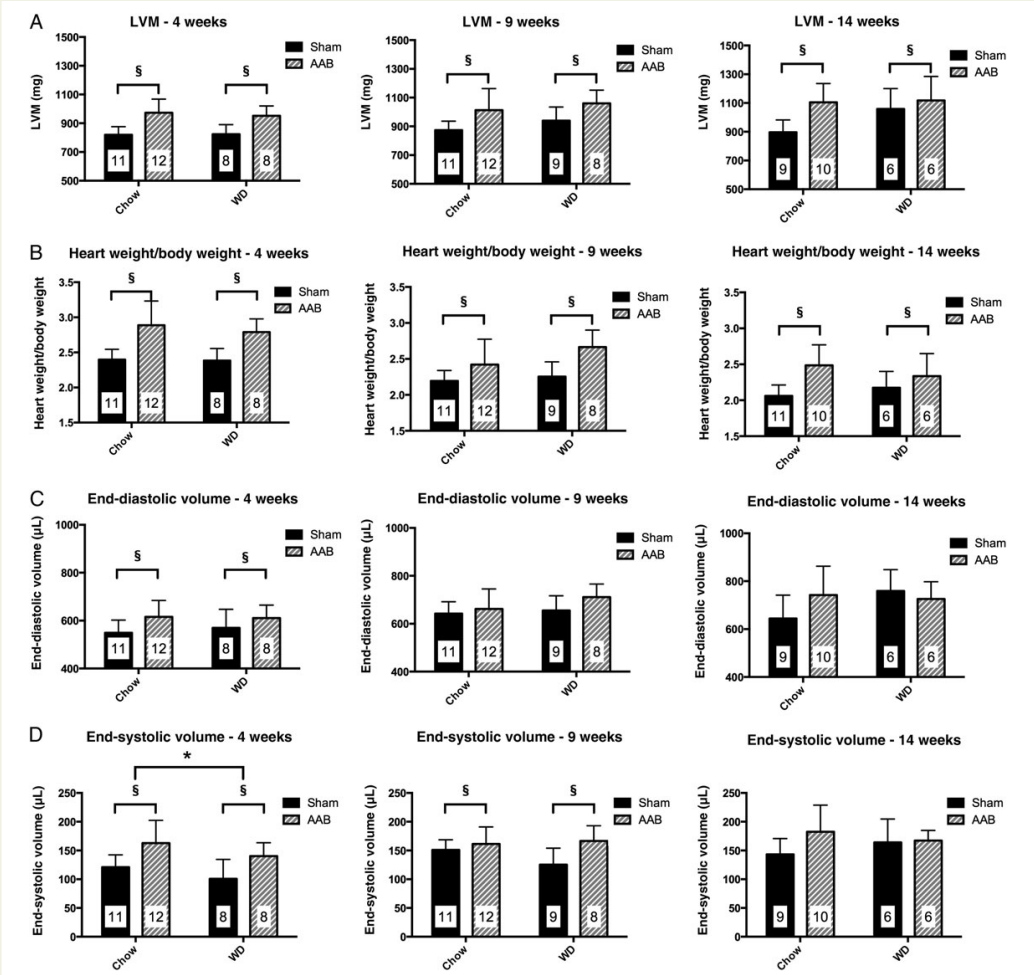


Figure 3 Cardiac structural parameters assessed in control and AAB animals at 4, 9, and 14 weeks post-surgical induction of cardiac hypertrophy. (*A*) LVM, (*B*) heart weight to body weight ratio, (*C*) end-diastolic volume, and (*D*) end-systolic volume. *$P < 0.05$ in WD groups compared with standard chow groups and $^{§}P < 0.05$ in AAB groups compared with sham control groups. Group sizes as indicated on individual bars.

groups by 9 weeks and sustained by 14 weeks (*Figure* 6*B*), independent of diet. These findings highlight that metabolic remodelling during the progression of cardiac hypertrophy is a continuous process with an increase in glycolytic metabolism as compensated hypertrophy develops.

3.3.2 *In vivo* assessment of TCA cycle metabolites

Hyperpolarized [2-^{13}C]pyruvate was used to determine incorporation of pyruvate into TCA cycle intermediates. Within the AAB groups, there was no change in the [^{13}C]metabolite:[2-^{13}C]pyruvate ratio for either citrate or glutamate, independent of diet (*Figure* 7*A* and *B*). Given that PDH flux was unaltered in the hypertrophied hearts, these observations would indicate that there was no increase in the flux of glucose into the TCA cycle during this phase of hypertrophic development. These findings are thus suggestive of a compensatory phase of cardiac hypertrophy with no adverse impact from the high-fat, high-sucrose content of the WD.

However, there was a substantial reduction in the ratio of [1-^{13}C] acetylcarnitine/[2-^{13}C]pyruvate within the WD-fed groups (*Figure* 7*C*). Previous findings have proposed a role for glycolytically derived acetylcarnitine to sustain and buffer the mitochondrial pool of acetyl-CoA, and therefore, a reduction in ^{13}C label incorporation may indicate a reduced buffering capacity driven by enhanced utilization of the available carnitine for mitochondrial fatty acid transport.[27]

Downloaded from by guest on April 20, 2015

Table 2 ***In vivo*** **structural and functional characteristics of hearts from control and abdominal aortic banded animals at 4, 9, and 14 weeks post induction of cardiac hypertrophy**

	Sham—Chow	Sham—WD	AAB—Chow	AAB—WD
	4 Weeks			
n	11	8	10	8
Body weight/g	340 ± 20	350 ± 20	340 ± 20	340 ± 20
End-diastolic volume/μL	550 ± 50	570 ± 80	620 ± 70§	610 ± 50§
End-systolic volume/μL	120 ± 20	100 ± 30*	160 ± 40§§§	140 ± 20*§§§
Ejection fraction/%	78 ± 4	83 ± 5**	74 ± 5§§	77 ± 3**§§
Stroke volume/μL	430 ± 50	470 ± 50	450 ± 60	470 ± 50
Heart rate/bpm	350 ± 20	360 ± 40	360 ± 30	360 ± 30
Cardiac output/mL min^{-1}	150 ± 20	170 ± 20*	160 ± 20	170 ± 20*
	9 Weeks			
n	11	9	10	8
Body weight/g	400 ± 30	420 ± 30	420 ± 20	400 ± 40
End-diastolic volume/μL	640 ± 50	660 ± 60	660 ± 80	710 ± 60
End-systolic volume/μL	150 ± 20	130 ± 30	160 ± 30§§	170 ± 30§§
Ejection fraction/%	76 ± 4	81 ± 3*	75 ± 5§	77 ± 4*§
Stroke volume/μL	490 ± 60	530 ± 40*	500 ± 80	550 ± 60*
Heart rate/bpm	350 ± 40	380 ± 30	360 ± 30	350 ± 40
Cardiac output/mL min^{-1}	170 ± 30	190 ± 30	180 ± 30	190 ± 30
	14 Weeks			
n	9	6	8	6
Body weight/g	440 ± 30	490 ± 40**	450 ± 30	480 ± 40**
End-diastolic volume/μL	640 ± 100	760 ± 90	740 ± 120	730 ± 70
End-systolic volume/μL	140 ± 30	160 ± 40	180 ± 50	170 ± 20
Ejection fraction/%	78 ± 2	79 ± 4	75 ± 5	77 ± 4
Stroke volume/μL	500 ± 70	600 ± 70	560 ± 110	560 ± 70
Heart rate/bpm	350 ± 30	350 ± 30	360 ± 40	380 ± 30
Cardiac output/mL min^{-1}	180 ± 20	210 ± 20*	200 ± 30	210 ± 30*

Data expressed as mean ± SD.
*$P < 0.05$ for effect of diet.
**$P < 0.01$ for effect of diet.
***$P < 0.001$ for effect of diet.
$^{\S}P < 0.05$ for effect of AAB.
$^{\S\S}P < 0.01$ for effect of AAB.
$^{\S\S\S}P < 0.001$ for effect of AAB.

3.4 Serum metabolite levels

Serum metabolite concentrations are summarized in *Table 3*. Few differences were observed between AAB and their respective control groups at 4, 9, or 14 weeks, identifying the fact that AAB and its associated hypertension *per se* does not influence serum nutrient levels. However, as might be anticipated, dietary manipulation did have a significant impact, with animals subjected to WD feeding repeatedly exhibiting elevated plasma TAG and LDL levels and reduced plasma lactate levels. Plasma insulin levels were also assessed at the 14-week time point (*Table 3*) and showed a significant elevation in the WD-fed groups irrespective of AAB, indicating a level of insulin resistance induced by the WD.

3.5 PDK4 expression and cardiac TAG concentrations

In vitro analysis of the expression of the key inhibitory enzyme PDK4 at the 14-week time point reflected the *in vivo* hyperpolarized ^{13}C MR findings with no alteration in expression in AAB or control groups within the same dietary group but a marked elevation of PDK4 expression in WD groups (*Figure 8A*). *In vitro* analysis of cardiac TAG levels demonstrated that they were unaffected by either AAB or the WD (*Figure 8B*), indicating no elevated deposition of lipids in the cardiac tissue.

4. Discussion

Using the novel, non-invasive technique of hyperpolarized MRS, this *in vivo* study has investigated the temporal metabolic, structural, and functional changes that are associated with the development of cardiac hypertrophy in the setting of excess nutrient supply. AAB caused a mild hypertrophic response in the heart without any functional detriment, a response that was unaffected by dietary manipulation. Although there was clear evidence of structural remodelling as early as 4 weeks post surgical induction of cardiac hypertrophy, the metabolic alterations that developed with the progression of hypertrophy determined by hyperpolarized ^{13}C MR were not observed until 9 weeks and highlighted a switch towards increased glycolytic metabolism rather than towards enhanced glucose oxidation.

Downloaded from by guest on April 20, 2015

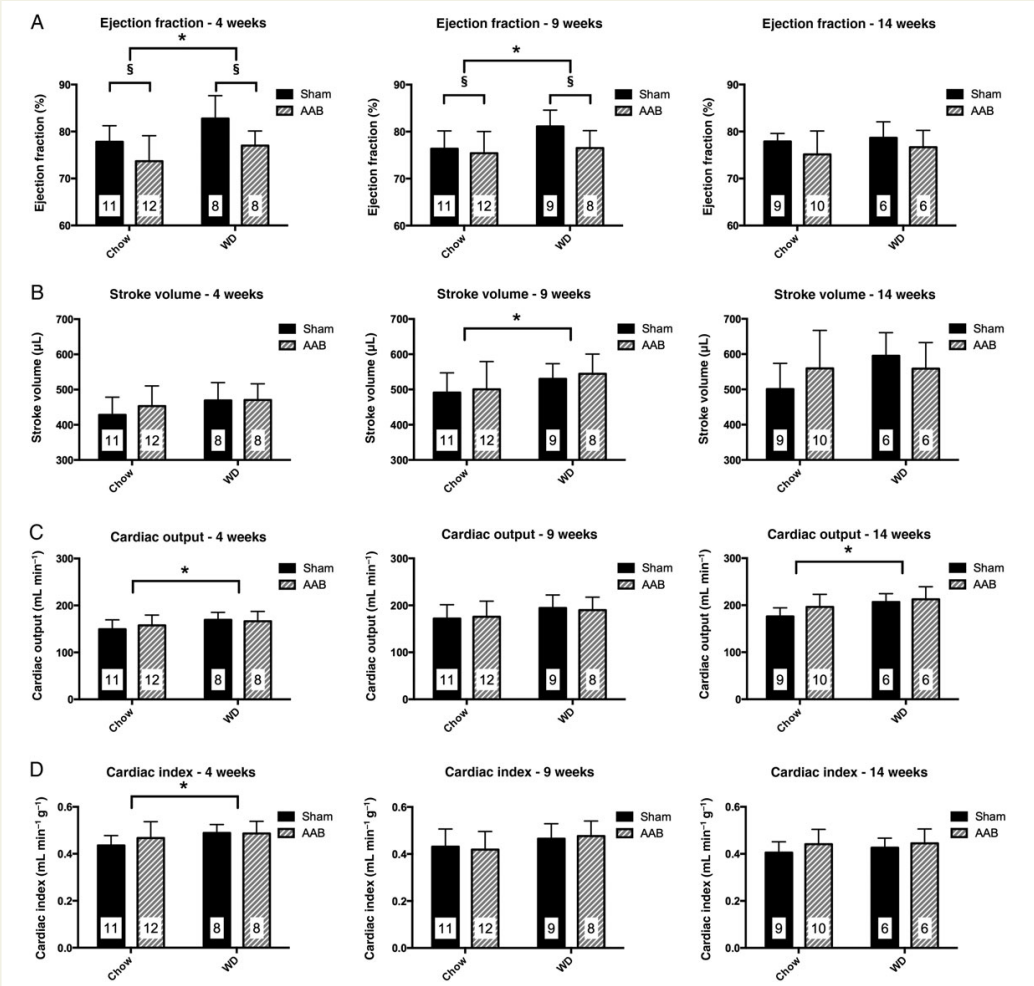


Figure 4 Functional characteristics of control and AAB hearts *in vivo*. (*A*) Ejection Fraction, (*B*) stroke volume, (*C*) cardiac output, and (*D*) cardiac index in sham and AAB animals at 4, 9, or 14 weeks post-surgical induction of cardiac hypertrophy, exposed to standard chow or WD. $^{*}P < 0.05$ in WD groups compared with standard chow groups and $^{\S}P < 0.05$ in AAB groups compared with sham control groups. Group sizes as indicated on individual bars.

4.1 Structural and functional impact of AAB

CINE MRI is a dynamic technique that allows measurement of both structural remodelling and cardiac function *in vivo*. The findings have clearly shown significant structural alterations in the left ventricle of AAB hearts. In line with the aim of this work to explore the structural, functional, and metabolic remodelling that occurs during the time course of cardiac hypertrophic development, the degree of hypertrophy induced in this model (14–17%) was smaller than that produced by the more severe ascending aortic constriction (30–45%),[28,29] TAC (33%),[30] and SHR (56%)[15] models of cardiac hypertrophy, which more rapidly progress to heart failure but the degree of hypertrophy was clearly evident both in the increased cardiac mass as well as the initially enlarged ventricular volumes and was consistent with previous studies employing this model.[11,31] The development of hypertrophy did not appear to be affected by the alteration in diet, although the animals maintained on the WD did show a greater weight gain by 14 weeks. This was primarily a result of increased fat mass, but the weight gain was small and could not be considered as representative of an obese model.

Although there was an increase in both end-systolic and end-diastolic dimensions in the AAB group at 4 weeks post surgery, resulting in a reduced ejection fraction, this appeared to be a transient event. These alterations may reflect the acute response of the heart to the

Downloaded from by guest on April 20, 2015

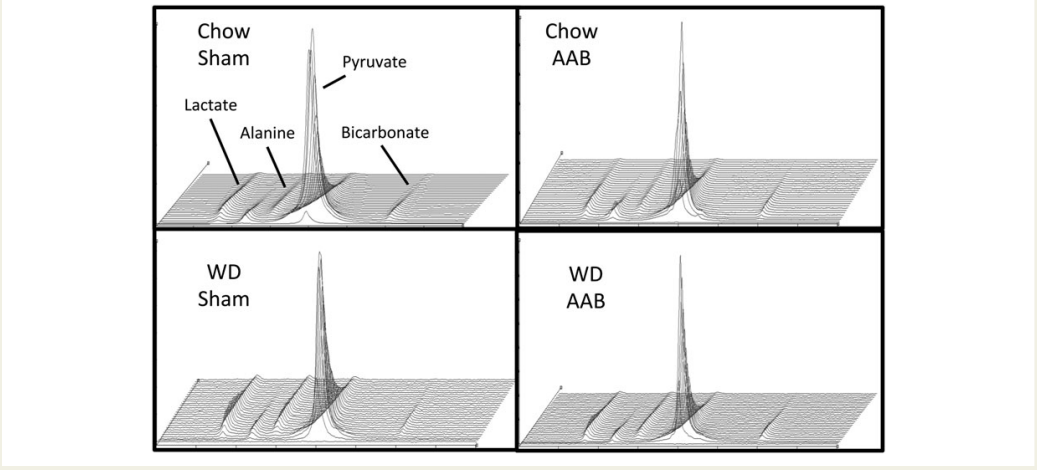


Figure 5 Representative *in vivo* ^{13}C spectra of hearts following injection of hyperpolarized [1-^{13}C] pyruvate in sham control and AAB animals at 14 weeks post-surgical induction of cardiac hypertrophy exposed to either standard chow or a WD.

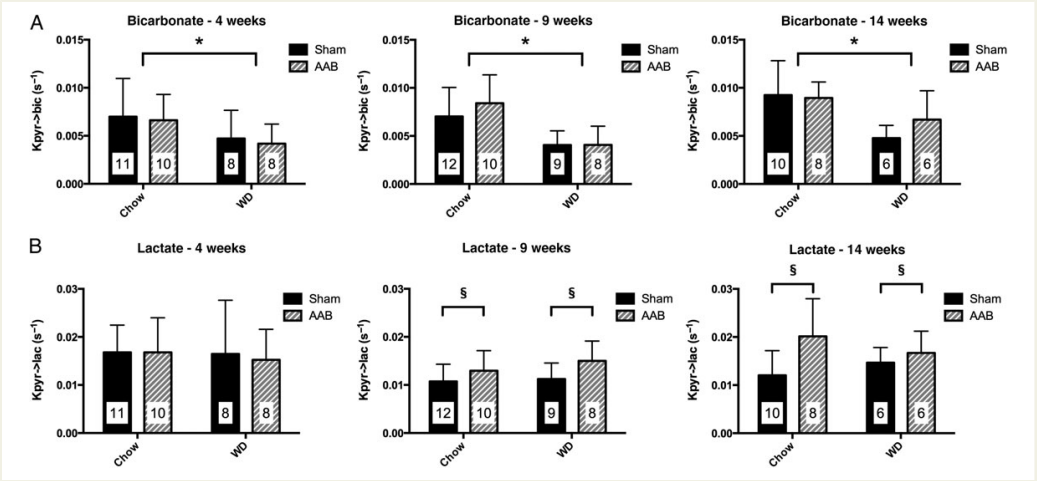


Figure 6 *In vivo* rates of incorporation of hyperpolarized [1-^{13}C]pyruvate into (*A*) bicarbonate (pyruvate dehydrogenase flux) and (*B*) lactate at 4, 9, and 14 weeks post-surgical induction of cardiac hypertrophy and exposure to standard chow or WD. *$P < 0.05$ in WD groups vs. standard chow and $^{§}P < 0.05$ in AAB groups vs. respective sham controls. Group sizes as indicated on individual bars.

hypertrophic pressure overload stimulus, which resolved into a compensated phase over the subsequent 10 weeks. *In vitro* studies of this model have shown early expression of ANF, a marker of hypertrophy, within a week of AAB but no evidence of heart failure at this phase.[31] Over time, there is little evidence of functional impairment in the AAB groups suggesting development of a compensated model of LVH by 14 weeks. This does not preclude the possibility of diastolic dysfunction, which we were unable to assess in this study. It is possible that the study of alterations in diastolic function may offer a more sensitive way to explore the effects of AAB within the setting of excess nutrient supply.

4.2 Metabolic remodelling with the development of hypertrophy

Metabolic remodelling is a frequently observed feature of cardiac hypertrophy and heart failure. Many studies have identified a switch from fatty

Downloaded from by guest on April 20, 2015

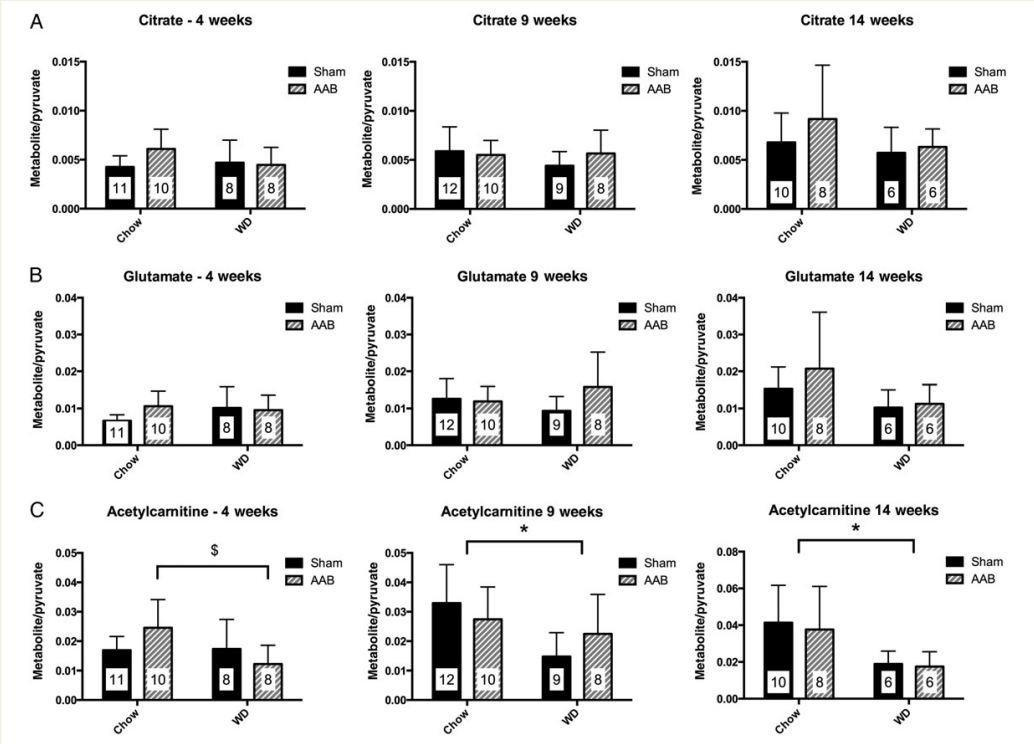


Figure 7 Ratio of (*A*) citrate, (*B*) glutamate, and (*C*) acetylcarnitine to injected hyperpolarized [2-^{13}C]pyruvate at 4, 9, and 14 weeks post-surgical induction of cardiac hypertrophy and exposure to standard chow or WD. $^{\$}P < 0.05$ WD AAB group compared with chow AAB group and $^{*}P < 0.05$ WD groups compared with standard chow groups. Group sizes as indicated on individual bars.

acid oxidation towards a reliance on glucose metabolism for energy generation in the hypertrophied and failing heart.[11,31–33] However, the majority of these studies have used *in vitro* systems in the isolated perfused heart with defined substrate concentrations in crystalloid buffers. In this *in vivo* study, the heart has been exposed to the natural composition of metabolites within the blood—giving a more biologically relevant picture of metabolic remodelling and the functional consequences.

Here we have used the novel *in vivo* method of hyperpolarized MRS to probe the remodelling of pyruvate metabolism in the hypertrophied heart exposed to a nutrient-rich environment over time. Our findings have identified an apparent uncoupling of glucose metabolism as an early event in hypertrophic development. Throughout the time course of the experiment, no change in flux through PDH was observed, which is in contrast to single time point studies on the SHR model where an 85% increase in PDH flux was observed.[15] The studies on the SHR model have shown a marked increase in PDH flux, supported by *in vitro* assay measurements of PDH activity. In part, the differences observed between these models could be due to a lesser degree of hypertrophic remodelling in the AAB model here compared with the SHR model or may imply that the increased reliance on glucose oxidation is a later event in the progression of hypertrophy. In addition, the SHR model is known to have multiple genetic mutations that contribute to the hypertensive phenotype.[15] A major mutation is a loss of the sarcolemmal fatty acid transporter, FAT/CD36, which is likely to lead to a reduction in fatty acid oxidation and a consequential increase in glucose oxidation and PDH flux. It is therefore highly likely that the metabolic alterations seen in the previously study[15] were impacted by this lack of FAT/CD36 and the ability to draw conclusions on the balance between the cause and effect of the hypertension in the light of these genetic changes is extremely challenging.

Previous studies measuring PDH activity in tissue extracts from the AAB model have identified a 69% reduction in the percentage of PDH in the active fraction.[34] However, the hyperpolarized MRS method is unique in measuring *in vivo* flux through PDH in contrast to *in vitro* assay systems, which only assess the proportion of enzyme in the active form.

Although there was no alteration in PDH flux *in vivo*, we have observed an elevation in glycolytic flux by 9 weeks as detected by greater incorporation of the hyperpolarized ^{13}C label into lactate. The level of enhanced label incorporation into lactate (26% at 9 weeks and 30% at 14 weeks) was smaller than that seen in previous hyperpolarized MRS studies investigating cancer treatment (lactate signal levels 50% higher

Downloaded from by guest on April 20, 2015

Table 3 Profile of serum metabolites from control and abdominal aortic banded animals at 4, 9, and 14 weeks post induction of cardiac hypertrophy

	Sham—Chow	Sham—WD	AAB—Chow	AAB—WD
	4 Weeks			
n	10	9	8	10
Glucose/mM	12 ± 2	12 ± 2	13 ± 3	12 ± 4
Lactate/mM	2.0 ± 0.5	1.7 ± 0.4**	2.2 ± 0.3	1.6 ± 0.4**
TAG/mM	1.2 ± 0.4	2.0 ± 0.5****	1.2 ± 0.3	2.0 ± 0.7****
LDL/mM	0.4 ± 0.1	0.5 ± 0.1**	0.4 ± 0.1	0.6 ± 0.1**
HDL/mM	0.8 ± 0.2	0.9 ± 0.1	0.8 ± 0.1	0.9 ± 0.1
Cholesterol/mM	2.2 ± 0.3	2.5 ± 0.5	2.4 ± 0.4	2.7 ± 0.6
β-Hydroxybutyrate/mM	0.07 ± 0.04	0.07 ± 0.04	0.09 ± 0.05	0.1 ± 0.1
	9 Weeks			
n	8	6	8	7
Glucose/mM	16 ± 1	16 ± 1	16 ± 2	17 ± 3
Lactate/mM	2.2 ± 0.5	2.0 ± 0.5	2.3 ± 0.4	2.2 ± 0.6
TAG/mM	1.6 ± 0.6	1.9 ± 0.5*	1.5 ± 0.3	1.8 ± 0.3*
LDL/mM	0.4 ± 0.1	0.4 ± 0.2	0.4 ± 0.1	0.5 ± 0.2
HDL/mM	0.8 ± 0.2	0.8 ± 0.1	0.9 ± 0.2	0.9 ± 0.2
Cholesterol/mM	3.1 ± 0.4	3.1 ± 0.1	3.2 ± 0.3	3.4 ± 0.4
β-Hydroxybutyrate/mM	0.05 ± 0.01	0.07 ± 0.04	0.06 ± 0.02	0.07 ± 0.04
	14 Weeks			
n	8	6	7	8
Glucose/mM	14 ± 4	14 ± 3	15 ± 3	13.6 ± 0.7
Lactate/mM	2.4 ± 0.4	1.9 ± 0.5*	2.3 ± 0.3	1.8 ± 0.3*
TAG/mM	1.4 ± 0.2	1.5 ± 0.5	1.3 ± 0.4	1.7 ± 0.2
LDL/mM	0.43 ± 0.06	0.6 ± 0.2**	0.5 ± 0.1	0.7 ± 0.1**
HDL/mM	0.9 ± 0.2	0.9 ± 0.2	0.9 ± 0.2	1.03 ± 0.06
Cholesterol/mM	3.0 ± 0.8	2.7 ± 0.6	3.3 ± 0.7	3.1 ± 0.3
β-Hydroxybutyrate/mM	0.07 ± 0.02	0.08 ± 0.04	0.08 ± 0.03	0.08 ± 0.04
Insulin/μg mL^{-1}	16 ± 2	30 ± 10**	15 ± 3	50 ± 30**

Data expressed as mean ± SD.
*$P < 0.05$ for effect of diet.
**$P < 0.01$ for effect of diet.
****$P < 0.0001$ for effect of diet.

in untreated vs. treated tumours)[35] or acute ischaemia (lactate signal levels 138% higher in ischaemic hearts vs. control hearts)[36] but when combined with the lack of alteration in PDH flux, it would suggest that, beyond the initial acute response to the hypertrophic stimulus, there was a degree of uncoupling of glucose oxidation from glycolysis. Lopaschuk and colleagues[37] have suggested that this may occur as a compensatory response under conditions such as ischaemia or more chronic situations such as hypertrophy. Enhanced [1-^{13}C]lactate generation was still observed at the 14-week time point suggesting, in the absence of any functional deterioration, that the observed level of glycolytic uncoupling was not a significantly deleterious adaptation. However, this does not preclude this uncoupling from becoming a detrimental factor as the LVH progresses into heart failure.

4.3 The effects of dietary modification

The application of a WD appears to have had little impact on cardiac structure, suggesting that, unlike other studies,[10,38,39] exposure to a WD for this time period does not induce hypertrophy. Functionally, the WD led to a small but significant increase in stroke volume and cardiac output. Therefore, at this stage, the WD does not cause any cardiac dysfunction but rather a small degree of hyperfunction.

Further, the combination of cardiac hypertrophy with dietary manipulation using a WD does not appear to have caused any functional deterioration, consistent with other studies employing high-fat/high-sugar diets.[40,41] However, controversy exists in this area, as augmenting the percentage of saturated fats in the diet without affecting the sugar content does appear to result in functional impairment. In these instances, studies have used up to 60% fat rather than the 45% used here. The excess supply of fat under conditions where fatty acid oxidation may be reduced, as in LVH, could result in lipotoxicity with inappropriate accumulation of lipids within the heart and cell death. Some evidence exists for this from work on isolated cardiomyocytes, which demonstrated that when palmitate was included as the fatty acid substrate it resulted in enhanced cell death as opposed to oleate that protected against apoptosis and lipotoxicity.[42]

Dietary manipulation had a major impact on PDH flux *in vivo* with an increased fat and carbohydrate composition in the diet, leading to a significant reduction in the utilization of glycolytically derived pyruvate.

Downloaded from by guest on April 20, 2015

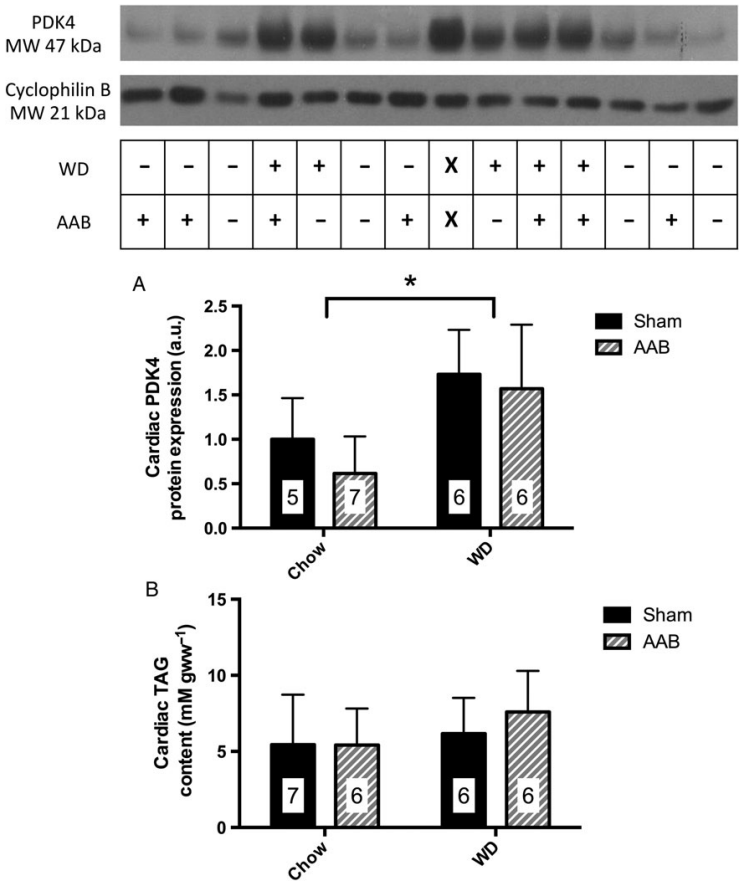


Figure 8 (*A*) Cardiac PDK4 protein expression and (*B*) cardiac TAG content at 14 weeks post-surgical induction of cardiac hypertrophy (AAB) and exposure to standard chow or WD. *$P < 0.05$ WD groups compared with standard chow groups. Group sizes as indicated on individual bars. X represents an internal standard on the western blot.

Although predicted from *in vitro* experimentation,[26] hyperpolarized MRS offers a unique way to visualize this effect *in vivo*. No concomitant change in [1-^{13}C]lactate production was observed with the dietary-induced decrease in PDH flux. Elevated insulin levels were observed in the WD-fed groups at the 14-week time point, which when coupled with the unaltered glucose levels, indicates a degree of insulin resistance induced by the high-fat, high-sugar diet.

Label incorporation into acetylcarnitine was markedly reduced in the WD-fed animals from 4 weeks onwards providing early evidence of the effect of dietary composition on substrate metabolism and storage. Given the role of carnitine as a co-factor in mitochondrial fatty acid transport,[32] this suggests that carnitine availability has become limiting following enhanced fatty acid utilization promoted by an increase in dietary fatty acid availability. The implications of a reduction in the buffering of pyruvate-derived acetyl-CoA into acetylcarnitine remains unclear at this point but does not appear to affect the development of hypertrophy nor have any deleterious effect on normal function.

5. Conclusions

This *in vivo* study examining the metabolic alterations that occur during the development of compensatory hypertrophy suggests a switch towards increased glycolytic metabolism rather than enhanced glucose oxidation as previously described. This appears to be irrespective of dietary manipulation with a WD, which despite causing a significant reduction in flux through PDH and evidence suggesting promoted fatty acid utilization, did not correlate with any structural or functional deterioration in the heart.

Conflict of interest: none declared.

Downloaded from by guest on April 20, 2015

Funding

This work was supported by the British Heart Foundation in the form of an Intermediate Basic Science Research Fellowship (FS/10/002/28078), a Senior Basic Science Research Fellowship (FS/14/17/30634) and a 4-year PhD Studentship. This work was also supported by EPSRC in the form of a 4-year PhD studentship, and GE Healthcare in the form of equipment support. Funding to pay the Open Access publication charges for this article was provided by the British Heart Foundation.

References

1. Opie LH, Commerford PJ, Gersh BJ, Pfeffer MA. Controversies in ventricular remodelling. *Lancet* 2006;**367**:356–367.
2. Heineke J, Molkentin JD. Regulation of cardiac hypertrophy by intracellular signalling pathways. *Nat Rev Mol Cell Bio* 2006;**7**:589–600.
3. Neubauer S. The failing heart--an engine out of fuel. *New Engl J Med* 2007;**356**:1140–1151.
4. Doenst T, Pytel G, Schrepper A, Amorim P, Farber G, Shingu Y, Mohr FW, Schwarzer M. Decreased rates of substrate oxidation ex vivo predict the onset of heart failure and contractile dysfunction in rats with pressure overload. *Cardiovasc Res* 2010;**86**:461–470.
5. Fillmore N, Lopaschuk GD. Targeting mitochondrial oxidative metabolism as an approach to treat heart failure. *Biochim Biophys Acta* 2013;**1833**:857–865.
6. Madrazo JA, Kelly DP. The PPAR trio: regulators of myocardial energy metabolism in health and disease. *J Mol Cell Cardiol* 2008;**44**:968–975.
7. Lopaschuk GD, Folmes CD, Stanley WC. Cardiac energy metabolism in obesity. *Circ Res* 2007;**101**:335–347.
8. Boudina S, Sena S, O'Neill BT, Tathireddy P, Young ME, Abel ED. Reduced mitochondrial oxidative capacity and increased mitochondrial uncoupling impair myocardial energetics in obesity. *Circulation* 2005;**112**:2686–2695.
9. Chiu HC, Kovacs A, Ford DA, Hsu FF, Garcia R, Herrero P, Saffitz JE, Schaffer JE. A novel mouse model of lipotoxic cardiomyopathy. *J Clin Invest* 2001;**107**:813–822.
10. Wilson CR, Tran MK, Salazar KL, Young ME, Taegtmeyer H. Western diet, but not high fat diet, causes derangements of fatty acid metabolism and contractile dysfunction in the heart of Wistar rats. *Biochem J* 2007;**406**:457–467.
11. Akki A, Seymour AM. Western diet impairs metabolic remodelling and contractile efficiency in cardiac hypertrophy. *Cardiovasc Res* 2009;**81**:610–617.
12. Allard MF, Schonekess BO, Henning SL, English DR, Lopaschuk GD. Contribution of oxidative metabolism and glycolysis to ATP production in hypertrophied hearts. *Am J Physiol* 1994;**267**:H742–H750.
13. Chatham JC, Seymour AM. Cardiac carbohydrate metabolism in Zucker diabetic fatty rats. *Cardiovasc Res* 2002;**55**:104–112.
14. Atherton HJ, Dodd MS, Heather LC, Schroeder MA, Griffin JL, Radda GK, Clarke K, Tyler DJ. Role of pyruvate dehydrogenase inhibition in the development of hypertrophy in the hyperthyroid rat heart: a combined magnetic resonance imaging and hyperpolarized magnetic resonance spectroscopy study. *Circulation* 2011;**123**:2552–2561.
15. Dodd MS, Ball DR, Schroeder MA, Le Page LM, Atherton HJ, Heather LC, Seymour A-M, Ashrafian H, Watkins H, Clarke K, Tyler DJ. *In vivo* alterations in cardiac metabolism and function in the spontaneously hypertensive rat heart. *Cardiovasc Res* 2012;**95**:69–76.
16. Schroeder MA, Cochlin LE, Heather LC, Clarke K, Radda GK, Tyler DJ. *In vivo* assessment of pyruvate dehydrogenase flux in the heart using hyperpolarized carbon-13 magnetic resonance. *Proc Natl Acad Sci USA* 2008;**105**:12051–12056.
17. Cassidy PJ, Schneider JE, Grieve SM, Lygate C, Neubauer S, Clarke K. Assessment of motion gating strategies for mouse magnetic resonance at high magnetic fields. *J Magn Reson Imaging* 2004;**19**:229–237.
18. Tyler DJ, Lygate CA, Schneider JE, Cassidy PJ, Neubauer S, Clarke K. CINE-MR imaging of the normal and infarcted rat heart using an 11.7 T vertical bore MR system. *J Cardiov Magn Reson* 2006;**8**:327–333.
19. Ardenkjaer-Larsen JH, Fridlund B, Gram A, Hansson G, Hansson L, Lerche MH, Servin R, Thaning M, Golman K. Increase in signal-to-noise ratio of >10,000 times in liquid-state NMR. *Proc Natl Acad Sci USA* 2003;**100**:10158–10163.
20. Naressi A, Couturier C, Castang I, de Beer R, Graveron-Demilly D. Java-based graphical user interface for MRUI, a software package for quantitation of in vivo/medical magnetic resonance spectroscopy signals. *Comput Biol Med* 2001;**31**:269–286.
21. Atherton HJ, Schroeder MA, Dodd MS, Heather LC, Carter EE, Cochlin LE, Nagel S, Sibson NR, Radda GK, Clarke K, Tyler DJ. Validation of the in vivo assessment of pyruvate dehydrogenase activity using hyperpolarised 13C MRS. *NMR Biomed* 2011;**24**:201–208.
22. Zierhut ML, Yen YF, Chen AP, Bok R, Albers MJ, Zhang V, Tropp J, Park I, Vigneron DB, Kurhanewicz J, Hurd RE, Nelson SJ. Kinetic modeling of hyperpolarized 13C1-pyruvate metabolism in normal rats and TRAMP mice. *J Magn Reson* 2010;**202**:85–92.
23. Schneider JE, Cassidy PJ, Lygate C, Tyler DJ, Wiesmann F, Grieve SM, Hulbert K, Clarke K, Neubauer S. Fast, high-resolution in vivo cine magnetic resonance imaging in normal and failing mouse hearts on a vertical 11.7 T system. *J Magn Reson Imaging* 2003;**18**:691–701.
24. Schneider JE, Wiesmann F, Lygate CA, Neubauer S. How to perform an accurate assessment of cardiac function in mice using high-resolution magnetic resonance imaging. *J Cardiov Magn Reson* 2006;**8**:693–701.
25. Boehm EA, Jones BE, Radda GK, Veech RL, Clarke K. Increased uncoupling proteins and decreased efficiency in palmitate-perfused hyperthyroid rat heart. *Am J Physiol Heart C* 2001;**280**:H977–H983.
26. Randle PJ, Garland PB, Hales CN, Newsholme EA. The glucose fatty-acid cycle. Its role in insulin sensitivity and the metabolic disturbances of diabetes mellitus. *Lancet* 1963;**1**:785–789.
27. Schroeder MA, Atherton HJ, Dodd MS, Lee P, Cochlin LE, Radda GK, Clarke K, Tyler DJ. The cycling of acetyl-coenzyme A through acetylcarnitine buffers cardiac substrate supply: a hyperpolarized 13C magnetic resonance study. *Circ Cardiovasc Imaging* 2012;**5**:201–209.
28. Schunkert H, Dzau VJ, Tang SS, Hirsch AT, Apstein CS, Lorell BH. Increased rat cardiac angiotensin converting enzyme activity and mRNA expression in pressure overload left ventricular hypertrophy. Effects on coronary resistance, contractility, and relaxation. *J Clin Invest* 1990;**86**:1913–1920.
29. Weinberg EO, Schoen FJ, George D, Kagaya Y, Douglas PS, Litwin SE, Schunkert H, Benedict CR, Lorell BH. Angiotensin-converting enzyme inhibition prolongs survival and modifies the transition to heart failure in rats with pressure overload hypertrophy due to ascending aortic stenosis. *Circulation* 1994;**90**:1410–1422.
30. Rockman HA, Ross RS, Harris AN, Knowlton KU, Steinhelper ME, Field LJ, Ross J Jr, Chien KR. Segregation of atrial-specific and inducible expression of an atrial natriuretic factor transgene in an in vivo murine model of cardiac hypertrophy. *Proc Natl Acad Sci USA* 1991;**88**:8277–8281.
31. Akki A, Smith K, Seymour AM. Compensated cardiac hypertrophy is characterised by a decline in palmitate oxidation. *Mol Cell Biochem* 2008;**311**:215–224.
32. Stanley WC, Recchia FA, Lopaschuk GD. Myocardial substrate metabolism in the normal and failing heart. *Physiol Rev* 2005;**85**:1093–1129.
33. Turer AT, Malloy CR, Newgard CB, Podgoreanu MV. Energetics and metabolism in the failing heart: important but poorly understood. *Curr Opin Clin Nutr* 2010;**13**:458–465.
34. Seymour AM, Chatham JC. The effects of hypertrophy and diabetes on cardiac pyruvate dehydrogenase activity. *J Mol Cell Cardiol* 1997;**29**:2771–2778.
35. Day SE, Kettunen MI, Gallagher FA, Hu DE, Lerche M, Wolber J, Golman K, Ardenkjaer-Larsen JH, Brindle KM. Detecting tumor response to treatment using hyperpolarized 13C magnetic resonance imaging and spectroscopy. *Nat Med* 2007;**13**:1382–1387.
36. Schroeder MA, Atherton HJ, Ball DR, Cole MA, Heather LC, Griffin JL, Clarke K, Radda GK, Tyler DJ. Real-time assessment of Krebs cycle metabolism using hyperpolarized 13C magnetic resonance spectroscopy. *FASEB J* 2009;**23**:2529–2538.
37. Lopaschuk GD, Wambolt RB, Barr RL. An imbalance between glycolysis and glucose oxidation is a possible explanation for the detrimental effects of high levels of fatty acids during aerobic reperfusion of ischemic hearts. *J Pharmacol Exp Ther* 1993;**264**:135–144.
38. Qin F, Siwik DA, Luptak I, Hou X, Wang L, Higuchi A, Weisbrod RM, Ouchi N, Tu VH, Calamaras TD, Miller EJ, Verbeuren TJ, Walsh K, Cohen RA, Colucci WS. The polyphenols resveratrol and S17834 prevent the structural and functional sequelae of diet-induced metabolic heart disease in mice. *Circulation* 2012;**125**:1757–1764, S1751–1756.
39. Vasanji Z, Cantor EJ, Juric D, Moyen M, Netticadan T. Alterations in cardiac contractile performance and sarcoplasmic reticulum function in sucrose-fed rats is associated with insulin resistance. *Am J Physiol Cell Ph* 2006;**291**:C772–C780.
40. Okere IC, Young ME, McElfresh TA, Chess DJ, Sharov VG, Sabbah HN, Hoit BD, Ernsberger P, Chandler MP, Stanley WC. Low carbohydrate/high-fat diet attenuates cardiac hypertrophy, remodeling, and altered gene expression in hypertension. *Hypertension* 2006;**48**:1116–1123.
41. Rennison JH, McElfresh TA, Okere IC, Vazquez EJ, Patel HV, Foster AB, Patel KK, Chen Q, Hoit BD, Tserng KY, Hassan MO, Hoppel CL, Chandler MP. High-fat diet postinfarction enhances mitochondrial function and does not exacerbate left ventricular dysfunction. *Am J Physiol Heart C* 2007;**292**:H1498–H1506.
42. Listenberger LL, Han X, Lewis SE, Cases S, Farese RV Jr, Ory DS, Schaffer JE. Triglyceride accumulation protects against fatty acid-induced lipotoxicity. *Proc Natl Acad Sci USA* 2003;**100**:3077–3082.

Downloaded from by guest on April 20, 2015